
Theses and Dissertations

Summer 2012

Advances In light-induced polymerizations: I. Shadow cure in free radical photopolymerizations, II. Experimental and modeling studies of photoinitiator systems for effective polymerizations with LEDs

Hajime Kitano
University of Iowa

Follow this and additional works at: <https://ir.uiowa.edu/etd>

 Part of the [Chemical Engineering Commons](#)


Copyright 2012 Hajime Kitano

This dissertation is available at Iowa Research Online: <https://ir.uiowa.edu/etd/4866>

Recommended Citation

Kitano, Hajime. "Advances In light-induced polymerizations: I. Shadow cure in free radical photopolymerizations, II. Experimental and modeling studies of photoinitiator systems for effective polymerizations with LEDs." PhD (Doctor of Philosophy) thesis, University of Iowa, 2012.
<https://doi.org/10.17077/etd.12fsduuz>

Follow this and additional works at: <https://ir.uiowa.edu/etd>

 Part of the [Chemical Engineering Commons](#)

ADVANCES IN LIGHT-INDUCED POLYMERIZATIONS:

- I. SHADOW CURE IN FREE RADICAL PHOTOPOLYMERIZATIONS
- II. EXPERIMENTAL AND MODELING STUDIES OF PHOTOINITIATOR SYSTEMS FOR EFFECTIVE POLYMERIZATIONS WITH LEDS

by

Hajime Kitano

An Abstract

Of a thesis submitted in partial fulfillment
of the requirements for the Doctor of Philosophy
degree in Chemical and Biochemical Engineering
in the Graduate College of
The University of Iowa

July 2012

Thesis Supervisor: Professor Alec B. Scranton

ABSTRACT

Photopolymerization has become the standard for many coating and printing applications that require rapid curing at room temperature due to its potential to reduce volatile organic compound (VOC) emissions while providing a means for efficient manufacturing processes. These advantages could be useful in a variety of emerging applications, such as anisotropic conductive films (ACF) if photopolymerization could extend into relatively narrow shadow regions which are not directly illuminated, and if visible wavelengths that are not absorbed by polyimide films could be used to trigger the reaction. The broad objectives of this research are i) to examine the factors that determine the attainable extent of shadow cure in free radical polymerizations, and ii) to develop initiator systems effective for polymerization using visible light and light emitting diode (LED) lamps.

Part I: Shadow Cure in Free Radical Photopolymerizations

In this aspect of the research, the extent of shadow cure in visible-light-induced free radical photopolymerization was investigated. A number of methods including specialized additives, reflective stages, and increased light intensity are considered. In addition, the use of fluorescent dyes in multi-component photoinitiator systems is proved to be very effective for shadow cure since the fluorescent light emitted from the dye could illuminate the shadow region.

The high viscosities associated with industrially relevant reaction systems (mixtures of oligomers and monomers) reduce the effectiveness of multi-component photoinitiator systems since a diffusion-controlled molecular encounter is required during a short excited state lifetime. Therefore, a new single-component organo-metallic visible-light-induced photoinitiator system was characterized. This innovative photoinitiator system resulted in high conversions in the shadow regions of the viscous oligomer-containing mixtures.

Part II: Experimental and Modeling Studies of Photoinitiator Systems for Effective Polymerizations with LEDs

In this second aspect of the research, various LED photocuring systems were investigated and characterized. LEDs are very energy efficient, however, the light intensities of LEDs are reduced as the peak emission wavelength is decreased. Therefore, to identify conditions for effective LED curing, the effect of both the light intensity and the emission spectrum of the lamp must be considered. Photopolymerization using four representative UV photoinitiators with different LEDs are investigated experimentally and theoretically. The effective light source is dependent on the photoinitiators and several LEDs demonstrate high thin cure ability. The calculated results from a theoretical model display good qualitative correspondence with the experimental results, and provide insight into effective operating conditions. For example, the commercialization of 355 nm LEDs is predicted to achieve superior photopolymerization compared to other currently available LED lamps.

Abstract Approved: _____
Thesis Supervisor

Title and Department

Date

ADVANCES IN LIGHT-INDUCED POLYMERIZATIONS:

- I. SHADOW CURE IN FREE RADICAL PHOTOPOLYMERIZATIONS
- II. EXPERIMENTAL AND MODELING STUDIES OF PHOTOINITIATOR SYSTEMS FOR EFFECTIVE POLYMERIZATIONS WITH LEDS

by

Hajime Kitano

A thesis submitted in partial fulfillment of the requirements for the Doctor of Philosophy degree in Chemical and Biochemical Engineering in the Graduate College of The University of Iowa

July 2012

Thesis Supervisor: Professor Alec B. Scranton

Graduate College
The University of Iowa
Iowa City, Iowa

CERTIFICATE OF APPROVAL

PH.D. THESIS

This is to certify that the Ph.D. thesis of

Hajime Kitano

has been approved by the Examining Committee
for the thesis requirement for the Doctor of Philosophy degree
in Chemical and Biochemical Engineering at the July 2012 graduation.

Thesis Committee:

Alec B. Scranton, Thesis Supervisor

C. Allan Guymon

Julie L. P. Jessop

Eric Nuxoll

Ned B. Bowden

ACKNOWLEDGEMENTS

This research was shaped by many people. I would like to express my sincere appreciation to a few who have been most influential. I would like to begin by giving my thanks to my advisor, Dr. Alec Scranton, whose enthusiasm in photopolymerization research inspired Bridgestone Corporation, in which I work, to investigate photopolymerization in greater detail. His attractive suggestions about photopolymerization research written in this thesis provided me with this unique opportunity. I would also like to thank my professors who have taught me valuable lessons both through class work and as living examples. A special thanks to Dr. Allan Guymon, Dr. Julie Jessop, Dr. Eric Nuxoll, and Dr. Ned Bowden who served on my committee. I would also like to acknowledge Linda Wheatley and Natalie Porter, whose resources and knowledge of the inner university workings proved priceless over the years.

I am grateful to the past graduate students, Cindy Hoppe and Sarah Winterton, who helped me through the day-to-day research work. I would also like to thank Briana Knoll, whose proof-reading definitely helped to improve this thesis. My heartfelt thanks go to all of my undergraduate assistants, Brandon Robson, Mike Baker, and Karthik Ramachandran, whose hard work and dedication were immensely helpful in completing this research. They are dear friends of mine, and I was very fortunate to meet them during my studies at the University of Iowa.

I am also indebted to the many excellent researchers working in Dr. Guymon's and Dr. Jessop's laboratory. They inspired me through our enthusiastic discussions on science and through their sincere attitude toward their own research. In addition, I would like to acknowledge the Photopolymerization Industry/University Cooperative Research

Center. The LED project in this research was made possible by their funding and made better by their suggestions. I wish to thank the individual representatives of these companies who mentored me over the years.

Additionally, I would like to thank Shuyo Akama, my friend, philosopher, and guide at Bridgestone, for encouraging me to pursue graduate studies at the University of Iowa. I would like to utilize what I have learned at Iowa to develop unprecedented products that will prove to be attractive and beneficial in the world at Bridgestone Corporation.

Finally, I would like to express my gratitude to my wife, Yuka, who has always been next to me during my stay in the United States and made this work possible. I cannot thank you enough.

TABLE OF CONTENTS

LIST OF TABLES	viii
LIST OF FIGURES	x
CHAPTER 1. BACKGROUND.....	1
1.1. Photopolymerization	1
1.2. Anisotropic Conductive Film (ACF).....	3
1.3. Visible-Light-Induced Free Radical Photoinitiator systems	6
1.4. Shadow Cure	6
1.5. LEDs for Photopolymerization	7
CHAPTER 2. OBJECTIVES OF THE PROPOSED RESEARCH	10
2.1. Part I: Shadow Cure in Free Radical Photopolymerizations.....	10
2.2. Part II: Experimental and Modeling Studies of Photoinitiator Systems for Effective Polymerizations with LEDs	11
CHAPTER 3. INVESTIGATION OF VISIBLE-LIGHT-INDUCED FREE RADICAL PHOTOINITIATOR SYSTEMS	13
3.1. Introduction	13
3.2. Screening Study of Visible-Light-Induced Free Radical Photoinitiator systems.....	14
3.2.1. Materials and Methods.....	14
3.2.2. Results	16
3.3. Characterization of EYss/MDEA Visible-Light-Induced Photoinitiator system	19
3.3.1. Photopolymerization Study of EYss-MDEA Two-Component and EYss-MDEA-DPI Three-Component Systems.....	19
3.3.2. Study of Heat Effects for EYss-MDEA Two-Component and EYss-MDEA-DPI Three-Component Systems	25
3.3.3. A Solution to Achieve High Photopolymerization and Long Shelf Life for EYss/MDEA/DPI Three-Component System	27
3.4. Conclusion.....	28
CHAPTER 4. EXTENT OF FREE-RADICAL SHADOW CURE	30
4.1. Introduction	30
4.2. Experimental	32
4.2.1. Materials.....	32
4.2.2. Shadow Cure via Photopolymerization.....	34
4.2.3. Characterization of Shadow Cure	35
4.3. Results and Discussion.....	36
4.3.1. Shadow Cure with Dye/Amine Photoinitiator Systems.....	36
4.3.2. Shadow Cure with Dye/Amine/DPI Photoinitiator Systems	42
4.3.3. Extent of Shadow Cure to Polymerize Wide Shadow Regions	44
4.4. Conclusions	45

CHAPTER 5.	SHADOW CURE IN SHORT CURE TIME	46
5.1.	Introduction	46
5.2.	Conversion Profiles under PET-FPC with UV Light.....	46
5.2.1.	Materials and Methods.....	47
5.2.2.	Results and Discussion.....	48
5.3.	Effect of Decreasing Dissolved Oxygen in Shadow Cure for Type 1 Photoinitiator	50
5.3.1.	Materials and Methods.....	52
5.3.2.	Results and Discussion.....	52
5.4.	Conversion Profiles under PI-FPC with Visible Light.....	54
5.4.1.	Materials and Methods.....	55
5.4.2.	Results and Discussion.....	55
5.5.	Optimization of Visible-Light Induced Photoinitiating Systems for Fast Shadow Cure	57
5.5.1.	Effect of the Third Component, Diphenyliodonium Chloride (DPI)	57
5.5.2.	Effect of Process Configuration: Two Types of Bottom Stage	58
5.5.3.	Effect of Additives	60
5.5.4.	Effect of Light Intensity	61
5.6.	Conclusion.....	63
CHAPTER 6.	EXTENT OF SHADOW CURE TO POLYMERIZE OLIGOMER-CONTAINING FORMULATION	64
6.1.	Introduction	64
6.2.	Comparison of Photopolymerization between Type I and Type II Photoinitiator for Oligomer-Containing Composition.....	64
6.2.1.	Materials and Methods.....	64
6.2.2.	Results and Discussion.....	66
6.3.	Comparison of Shadow Cure between Type I and Type II Photoinitiator Systems for Oligomer-Containing Formulation	68
6.3.1.	Methods.....	68
6.3.2.	Results and discussion	68
6.4.	Visible-Light-Induced Type I Photoinitiator: Bis(cyclopentadienyl) bis[2,6-difluoro-3-(1-pyrryl)phenyl]titanium (Ti-PI)	70
6.4.1.	Characteristics of Ti-PI Photopolymerization: Effect of Light Intensity and Additives	72
6.4.2.	Comparison between Ti-PI (Type 1) and Type II Photoinitiator Systems for Oligomer-Containing Composition Using Visible Light	75
6.5.	Shadow Cure for Oligomer-Containing Formulation with Visible Light	76
6.6.	Conclusion.....	78
CHAPTER 7.	EXPERIMENTAL AND MODELING STUDIES OF PHOTOINITIATOR SYSTEMS FOR EFFECTIVE POLYMERIZATIONS WITH UV LEDS.....	79
7.1.	Introduction	79
7.2.	Investigation of a Commercial LED System.....	80
7.2.1.	Light Emission Profiles.....	80

7.2.2.	Comparison of the Energy Consumption and Irradiation of Light Sources	85
7.3.	Simulation Analysis and Experimental Studies for Thick Cure	87
7.3.1.	Methods.....	87
7.3.2.	Results.....	93
7.3.3.	Heat Effect Analysis of Thick Cure.....	96
7.4.	Simulation Analysis and Experimental Studies for Thin Cure	105
7.4.1.	Methods.....	105
7.4.2.	Condition 1: Same Light Intensity.....	107
7.4.3.	Condition 2: Same Configuration	112
7.4.4.	Validity of the Modeling for Thin Cure.....	116
7.5.	Numerical Calculation for Thin Cure with Various LEDs.....	117
7.5.1.	Condition 1: Same Light Intensity.....	118
7.5.2.	Condition 2: Same Configuration	121
7.6.	Conclusion.....	123
CHAPTER 8.	STUDIES OF PHOTOINITIATOR SYSTEMS FOR EFFECTIVE POLYMERIZATIONS WITH VISIBLE LEDs: CHARACTERIZATION OF VISIBLE-LIGHT-INDUCED PHOTOPOLYMERIZATION USING THE TITANOCENE PHOTOINITIATOR BIS(CYCLOPENTADIENYL) BIS[2,6-DIFLUORO-3-(1-PYRRYL)PHENYL]TITANIUM.....	125
8.1.	Introduction	125
8.2.	Experimental	127
8.2.1.	Materials.....	127
8.2.2.	Methods.....	129
8.3.	Results and Discussion	129
8.3.1.	Effect of a Protonic Acid on the Photopolymerization Rate Using Ti-PI as a Visible Light Initiator.....	129
8.3.2.	Origin of the Effect of Acid on the Polymerization Rate.....	133
8.3.3.	Effect of Light Intensity and Photoinitiator Concentration on the Photopolymerization Rate and Conversion of Monomer	136
8.3.4.	Comparison of Ti-PI to a 3-Component Visible Light Photoinitiator system	141
8.4.	Conclusion.....	142
CHAPTER 9.	CONCLUSIONS AND RECOMMENDATIONS.....	144
9.1.	Part I: Shadow Cure in Free Radical Photopolymerizations.....	144
9.1.1.	Summary of Research	144
9.1.2.	Recommendations for Future Work.....	145
9.2.	Part II: Experimental and Modeling Studies of Photoinitiator Systems for Effective Polymerizations with LEDs	146
9.2.1.	Summary of Research	146
9.2.2.	Recommendations for Future Work.....	147
APPENDIX A.	FEASIBILITY STUDY FOR THE CANDIDATES OF VISIBLE-LIGHT-INDUCED PHOTOINITIATOR SYSTEM WITH FLUORESCENT ADDITIVE.....	153
A-1.	Materials and Methods	154
A-2.	Results and Discussions	155

APPENDIX B.	CHARACTERIZATION OF EYSS/DABCO/DPI AND EYSS/EDMAB/DPI THREE-COMPONENT SYSTEMS	158
B-1.	Photopolymerization of EYSS/DABCO/DPI Three- Component System	158
B-2.	Shelf Life of EYss/DABCO/DPI Three-Component System	162
B-3.	Photopolymerization of EYSS/EDMAB/DPI Three- Component System	166
B-4.	Shelf Life of EYss/EDMAB/DPI Three-Component System	167
B-5.	Summary of Shelf Lives Study for Various Amines in Three- Component System	169
APPENDIX C.	DEPENDENCY OF ABSORBANCE ON XHANTENE DYE CONCENTRATIONS	170
APPENDIX D.	IMPACT OF STAGE REFLECTION ON SHADOW CURE	172
APPENDIX E.	SUPPLEMENTAL STUDY ABOUT SINGLET-OXYGEN- GENERATOR/SINGLET-OXYGEN-TRAPPER SYSTEMS	174
E-1.	Measurement of Dissolved Oxygen Concentration in Various Formulations	174
E-2.	Light Intensity Effect	175
E-3.	Shelf life of ST in formulations	176
APPENDIX F.	SUPPLEMENTAL STUDY OF PHOTOPOLYMERIZATION WITH TI-PI	179
F-1.	Effect of Light Intensity and Photoinitiator Concentration on the Photopolymerization Rate and Conversion with a Xenon Lamp	179
F-2.	Shelf Life of HEA Monomer Containing Ti-PI and a Protonic Acid Additive	181
F-3.	Investigation of Ti-PI Photoinitiation Reaction Mechanism Using Styrene Monomer	182
F-4.	Investigation of Photopolymerization with Ti-PI for Various Monomers and Oligomers	186
REFERENCES	190

LIST OF TABLES

Table 1-1: List of commercial photocuring LED irradiation systems	8
Table 3-1: Screened photosensitizers and final conversions for concentration combinations.....	17
Table 3-2: Screened photosensitizers and final conversions for concentration combinations.....	18
Table 3-3: Two-component system and three-component system formulas studied.....	21
Table 4-1: Molar concentration of components in the photoinitiator systems under investigation.....	34
Table 6-1: Compositions of studied photoinitiator systems	65
Table 6-2: T_g , viscosity and final conversions for four photoinitiator systems of monomer-oligomer mixtures.....	66
Table 6-3: Compositions of studied photoinitiator systems and irradiated light conditions.....	69
Table 6-4: Compositions of studied photoinitiator systems	73
Table 6-5: Compositions of studied photoinitiator systems	75
Table 6-6: Compositions of studied photoinitiator systems and irradiated light conditions.....	77
Table 7-1: Consumed electric power and emitted light power of a 400 nm LED (Firefly, Phoseon), 100 W mercury (Hg) lamp (Acticure, EXFO), and a 150 W xenon (Xe) lamp (Max-150, Asahi).....	86
Table 8-1: Ultimate conversions of photopolymerization profiles in Figure 8-2 after 6 minutes of illumination.....	131
Table 8-2: Ultimate conversions of photopolymerization profiles in Figure 8-7	138
Table A- 1: Studied compositions and light conditions for EYss/MB/MDEA.	154
Table A- 2: Studied compositions and light conditions for EYss/FL/MDEA	155
Table B- 1: Two-component system and three-component system formulas studied for EYss/DABCO/DPI system.	159
Table B- 2: Three-component systems' formulas studied.....	162
Table B- 3: Two-component system and three-component system formulas studied.....	166
Table B- 4: EYss/EDMAB/DPI three-component systems' formulas studied.....	168
Table E- 1: Dissolved Oxygen Concentration in different formulations	175

Table E- 2: Compositions of studied samples.....	177
Table F- 1: Studied photoinitiator compositions and light conditions in styrene monomer	183
Table F- 2: Studied photoinitiator compositions and light conditions in styrene monomer	185
Table F- 3: Total exothermic energies and conversions in Figure F- 6.....	186

LIST OF FIGURES

Figure 1-1: ACF used for bonding between a display and circuit.....	4
Figure 1-2: Transmittance of polyimide film.....	5
Figure 1-3: Conventional heat process with ACF between FPC.....	5
Figure 3-1: Spectral light intensity of a 150 W xenon (Xe) lamp (MAX-150, Asahi Spectra).....	15
Figure 3-2: Absorbance and fluorescence of photosensitizers: (A) Fluorescein (FL), (B) eosin Y, (C) eosin Y spirit soluble (EYss), (D) erythrocin B, (E) rose bengal, (F) methylene blue.	17
Figure 3-3: Chemical structure of EYss (eosin Y spirit soluble), MDEA (N-methyldiethanolamine) and DPI (diphenyliodonium chloride).....	20
Figure 3-4: Reaction mechanism of EYss/MDEA two-component photoinitiator system. ¹⁷	20
Figure 3-5: Reaction mechanism of EYss/MDEA/DPI three-component system. ¹⁷	21
Figure 3-6: Light spectra of a 150 W xenon lamp (MAX-150, Asahi Spectra) emitted through no filter, polyimide film and 520 nm bandpass filter.....	22
Figure 3-7: Conversion vs. time of two-component systems and a three-component system for three different incident lights: (A) EYss/MDEA two-component system, (B) EYss/DPI two-component system, (C) EYss/MDEA/DPI three-component system. Monomer: HEA. Incident lights: a 150 W xenon lamp with no filter (89 mW/cm ²), a polyimide film (39 mW/cm ²) and a 520 nm bandpass filter (2.4 mW/cm ²).	23
Figure 3-8: Time dependence of the EYss/MDEA two-component system conversion profiles: (A) with 520 nm bandpass filter (light intensity: 2.4 mW/cm ²) and (B) without bandpass filter of a 150 W Xe lamp (light intensity: 89mW/cm ²). Monomer: HEA.....	24
Figure 3-9: Time dependence of the EYss/MDEA/DPI three-component system conversion profiles: (A) with 520 nm bandpass filter (light intensity: 2.4 mW/cm ²) and (B) without bandpass filter of a 150 W Xe lamp (light intensity: 89 mW/cm ²). Monomer: HEA.....	25
Figure 3-10: DSC heat flow (with the second run subtracted from the first run) as a function of temperature for HEA with EYss, MDEA, DPI, EYss-MDEA, EYss-DPI, MDEA-DPI, EYss-MDEA-DPI, or without species. [EYss] = 0.00115 M, [MDEA] = 0.32 M, [DPI] = 0.0023 M.....	26
Figure 3-11: Suggested reaction scheme between MEDA and DPI.....	27
Figure 3-12: Evaluation of photopolymerization and shelf life for various concentration combinations of EYss/MDEA/DPI three-component system. [EYss] = 0.00115 M.....	28

Figure 3-13: Stable time dependence of EYss/MDEA/DPI three-component systems conversion profiles achieved by controlling concentration combinations. Light source: 520 nm LED, light intensity: 4 mW/cm ² . (A) EYss = 0.00115 M, MDEA = 0.096 M, DPI = 0.023 M. (B) EYss = 0.00115 M, MDEA = 0.096 M, DPI = 0.0115 M.	28
Figure 4-1: Chemical structures of (A) fluorescein (FL), (B) eosin Y spirit soluble (EYss), (C) benzophenone (BP) (D) N-methyldiethanolamine (MDEA), (E) diphenyl iodonium chloride (DPI).	33
Figure 4-2: Absorbance and fluorescence emission spectra of (A) fluorescein (FL) and (B) eosin Y spirit soluble (EYss).	33
Figure 4-3: Schematic of the experimental geometry for the shadow cure studies. The mask was a 500 μm thick steel plate with a 6 mm diameter hole through which the monomer mixture was illuminated from above. After illumination of the prescribed duration, Raman microscopy was used to collect line (x-direction) and depth (z-direction) conversion profiles through the quartz cover slip on the bottom of the sample.	35
Figure 4-4: Shadow cure conversion profiles (x-direction) resulting from four different dye/amine photoinitiator systems. Negative values of x correspond to the illuminated region, while positive values of x correspond to the masked region. Light source: a 150 W xenon lamp, light intensity: 89 mW/cm ² , irradiation time: 15 minutes.	39
Figure 4-5: The effect of the incident light intensity on the conversion profiles (x-direction) observed for three different dye/amine systems; (A) BP/MDEA, (B) FL/MDEA, (C) EYss/MDEA. Light source: a 150 W xenon lamp, irradiation time: 15 minutes.	40
Figure 4-6: The dependency of the conversion profiles (x-direction) on irradiation time observed for three different dye/amine systems; (A) BP/MDEA, (B) FL/MDEA, (C) EYss/MDEA. Light source: a 150 W xenon lamp, light intensity: 1000 mW/cm ²	41
Figure 4-7: Effect of the addition of DPI on the shadow cure conversion profiles (x-direction) observed for FL and EYss dye/amine photoinitiator systems. Light source: a 150 W xenon lamp, light intensity: 89 mW/cm ² , irradiation time: 15 minutes.	43
Figure 4-8: Schematic representation of the reaction mechanism for three-component photoinitiator systems containing FL or EYss, MDEA, and DPI. (A) photo-reduction of the FL or EYss dye by MDEA and (B) photo-oxidation of the FL or EYss dye by DPI.	43
Figure 4-9: Shadow cure conversion profiles (x-direction) resulting from three different dye/amine photoinitiator systems containing DPI. Light source: a 150 W xenon lamp with a polyimide film, light intensity: 39 mW/cm ² , irradiation time: 15 minutes.	44
Figure 5-1: Designed PET-FPC film	47

Figure 5-2: Measurement of shadow cure with PET-FPC in x-direction. (A) Scanned area behind an electrode and (B) its conversion profile (X-direction) for 1 phr HCPK at the electrode surface of the $100 \times 100 \mu\text{m}$ line and space PET-FPC film. Monomer: HEA, UV light intensity: 1948 mW/cm^2 , Total UV light energy: 2.575 J/cm^2	48
Figure 5-3: Conversion profile (X-direction) for 1 phr HCPK at electrodes' surface of the $500 \times 500 \mu\text{m}$ line and space PET-FPC film. Monomer: HEA, UV light intensity: 1948 mW/cm^2 , total UV light energy: 2.575 J/cm^2	49
Figure 5-4: Measurement of shadow cure with PET-FPC in z-direction. (A) Scanned depth profiles behind an electrode and (B) depth profiles (Z-direction) for HCPK in the shadow region behind the electrode of the $500 \times 500 \mu\text{m}$ line and space PET-FPC film. Monomer: HEA, UV light intensity: 1948 mW/cm^2 , Total UV light energy: 2.575 J/cm^2	50
Figure 5-5: Chemical structure of Zinc 2,9,16,23-tetra-tert-butyl-29H,31H-phthalocyanine (Zn-ttp) and 9,10-dimethylanthracene (DMA)	51
Figure 5-6: Proposed mechanism of the singlet oxygen generation and trapping process.....	51
Figure 5-7: Comparison of conversion profile (X-direction) for the system without additives and with additives (0.00002M Zn-ttp and 0.002M DMA) at electrodes' surface of the $500 \times 500 \mu\text{m}$ line and space PET-FPC film. The system with the additives was pre-irradiated by a Xe lamp with 670 nm bandpass filter (light intensity: 19.6 mW/cm^2 , irradiation time 300 seconds). Monomer: HEA; UV light source: Fusion lamp; UV light intensity: 1948 mW/cm^2 , Total UV light energy: 2.575 J/cm^2	53
Figure 5-8: Measurement of shadow cure with PET-FPC in z-direction. (A) Scanned depth profiles behind an electrode and (B) depth profiles (Z-direction) for the system with additives (0.00002M Zn-ttp and 0.002M DMA) in the shadow region behind the electrode of the $500 \times 500 \mu\text{m}$ line and space PET-FPC film. The sample was pre-irradiated by a Xe lamp with 670 nm bandpass filter (light intensity: 19.6 mW/cm^2 , irradiation time 300 seconds). Monomer: HEA; UV light source: Fusion lamp, UV light intensity: 1948 mW/cm^2 , Total UV light energy: 2.575 J/cm^2	54
Figure 5-9: Designed PI-FPC film.....	54
Figure 5-10: Measurement of shadow cure with PI-FPC in x-direction. (A) Scanned area behind an electrode and (B) its conversion profile (X-direction) for EYss/MDEA visible-light-induced photoinitiator system at the electrode surface of the $500 \times 500 \mu\text{m}$ line and space PI-FPC film. Monomer: HEA; Visible light source: a 150 W Xe lamp, visible light intensity: 89 mW/cm^2 , irradiation time: 900 seconds.....	56

Figure 5-11: Measurement of shadow cure with PI-FPC in z-direction. (A) Scanned depth profiles behind an electrode and (B) depth profiles (Z-direction) for EY _{ss} /MDEA visible-light-induced photoinitiator system in the shadow region behind the electrode of the 500 × 500 μm line and space PI-FPC film. Visible light source: a 150 W Xe lamp, visible light intensity: 89 mW/cm ² , irradiation time: 900 seconds. [EY _{ss}] = 0.00115 M, [MDEA] = 0.32 M in HEA monomer.....	57
Figure 5-12: Comparison of conversion at the electrode's center surface of the 500 × 500 μm line and space PI-FPC film between the EY _{ss} /MDEA two-component photoinitiator system and EY _{ss} /MDEA/DPI three-component photoinitiator system. The both samples are cured with a black stage. Monomer: HEA, Visible light source: a 150 W Xe lamp; visible light intensity: 89 mW/cm ² , irradiation time: 10 seconds. [EY _{ss}] = 0.00115 M, [MDEA] = 0.32 M, [DPI] = 0.0023M.....	58
Figure 5-13: Comparison of conversion at the electrode's center surface of the 500 × 500 μm line and space PI-FPC film between black substrate and white substrate for the EY _{ss} /MDEA two-component photoinitiator system and EY _{ss} /MDEA/DPI three-component photoinitiator system. Monomer: HEA; Visible light source: a 150 W Xe lamp, visible light intensity: 89 mW/cm ² , irradiation time: 10 seconds. [EY _{ss}] = 0.00115 M, [MDEA] = 0.32 M, [DPI] = 0.0023M.	59
Figure 5-14: Chemical structure of pentaerythritol tetrakis(2-mercaptoacetate) (PEMP).....	60
Figure 5-15: Effect of adding FL (0.00115 M), DMA (0.002 M) and PEMP (the thiol/acrylate ratio is 0.05, which is molar ratios of functional groups.) upon shadow cure conversion for the EY _{ss} /MDEA/DPI three-component photoinitiator system. Top substrate: PI-FPC, Measurement Point: the electrode's center surface of the 500 × 500 μm line and space; Monomer: HEA; Visible light source: a 150 W Xe lamp, visible light intensity: 89 mW/cm ² , irradiation time: 10 seconds. [EY _{ss}] = 0.00115 M, [MDEA] = 0.32 M, [DPI] = 0.0023M.	61
Figure 5-16: Effect of light intensity on the shadow cure conversion for photoinitiator systems: EY _{ss} /MDEA, EY _{ss} /MDEA/DPI, EY _{ss} /MDEA/DPI/FL. The all samples were cured with a white stage. Top substrate: PI-FPC; Measurement Point: the electrode's center surface of the 500 × 500 μm line and space, Monomer: HEA; Visible light source: a 150 W Xe lamp, irradiation time: 10 seconds. [EY _{ss}] = 0.00115 M, [MDEA] = 0.32 M, [DPI] = 0.0023M, [FL] = 0.00115 M.	62
Figure 6-1: Chemical structure of BAPO and HCPK.....	65
Figure 6-2: Correlation between UV-light-induced Type I photoinitiator systems' (HCPK, BAPO) final conversions and: (A) T _g , (B) viscosity.....	67
Figure 6-3: Correlation between visible-light-induced Type II photoinitiator systems' (EY _{ss} /MDEA, EY _{ss} /MDEA/DPI) final conversions and: (A) T _g , (B) viscosity.....	67

Figure 6-4: Conversion profile (X-direction) for three different photoinitiator systems at electrodes' surface of the 500 × 500 μm line and space PET-FPC film. Resin: HEA/CN9002 (30/70 in mass ratio).	69
Figure 6-5: (A) Chemical structure of Ti-PI and (B) Napierian molar absorptivity of the photoinitiator and its photolysis product.	70
Figure 6-6: Suggested photoinitiation and photopolymerization mechanism for Ti-PI in acrylates.	71
Figure 6-7: Chemical structure of 2-carboxyethyl acrylate (CEA) and phosphoric acid 2-hydroxyethyl methacrylate ester (PhMA).	73
Figure 6-8: Comparison of the three different photoinitiator systems for photopolymerization conversion profiles. Monomer: HEA. (A) A 150W Xe lamp with 89 mW/cm ² light intensity, (B) the Xe lamp attaching a 520 nm bandpass filter with 2.4 mW/cm ² light intensity.	74
Figure 6-9: Comparison of the three different photoinitiator systems for photopolymerization conversion profiles. Resin: HEA/CN9002 (30/70 in mass ratio); Light source: a Xe lamp with a 520 nm bandpass filter, light intensity: 2.4 mW/cm ²	76
Figure 6-10: Conversion profile (X-direction) for three different photoinitiator systems at electrodes' surface of the 500 × 500 μm line and space PI-FPC film. Resin: HEA/CN9002 (30/70 in mass ratio).	78
Figure 7-1: Spectral light intensities of LEDs and conventional UV light (provided by Integration Technology .LTD) ⁶⁸	80
Figure 7-2: Shape of 400 nm LED light source (Firefly; Phoseon Technology, Inc.) indicating the five measurement points used for spectral light intensity.	81
Figure 7-3: Normalized light spectral intensity of 400 nm LED at each of the five measurement positions.	81
Figure 7-4: Correlation between light intensities at five measurement positions and measured distance.	82
Figure 7-5: Shape of 365nm and 385 nm LED light sources (LED zero Solidcure; Integration Technology, LTD.) indicating the five measurement points used for spectral light intensity.	83
Figure 7-6: Normalized light spectral intensity LEDs at each of the fifteen measurement positions. (A) 365 nm LED, (B) 385 nm LED.	84
Figure 7-7: Correlation between light intensities at fifteen measurement positions and measured distance. (A) 365 nm LED, (B) 385 nm LED	84
Figure 7-8: Comparison of 365 nm, 385 nm, and 400 nm LEDs; (A) Correlation between light intensities at center position and measured distance, (B) Spectral light intensities at 8cm distance, measured at center position.	85

Figure 7-9 : Energy efficiency of 400 nm LED (Firefly, Phoseon), 100 W mercury (Hg) lamp (Acticure, EXFO), and a 150 W xenon (Xe) lamp (Max-150, Asahi).	86
Figure 7-10: Chemical structure of the photoinitiators: BAPO (bis(2,4,6-trimethylbenzoyl)-phenylphosphine oxide), BDMB (2-benzyl-2-(dimethylamino)-1-[4-(4-morpholinyl)phenyl]-1-butanone), DMPA (2,2-dimethoxy-2-phenylacetophenone), and TPO (diphenyl(2,4,6-trimethylbenzoyl)-phosphine oxide).	87
Figure 7-11 : Normalized spectral light intensities of a Hg(-Xe) lamp and a 400 nm LED lamp	88
Figure 7-12: Napierian molar absorptivities of BAPO, DMPA, BDMP, and TPO and their photolysis products.....	92
Figure 7-13: Calculated photoinitiation rates of a system initiated with TPO using either a Hg(-Xe) lamp or a 400 nm LED lamp over time (light intensity: 41 mW/cm ² , photoinitiator concentration: 0.0167 M).	92
Figure 7-14: Comparison of two light sources for photopolymerizations of thick HDDA systems containing four different initiators: (A) BAPO ₃ , (B), BDMB, (C) DMPA, and (D) TPO. Light intensity: 41 mW/cm ² ; Photoinitiator concentration: 0.0167 M. (a) Experimental conversion measured as a function of time, and (b) simulation results for photoinitiation rate at 0.5 cm depth as a function of time.....	95
Figure 7-15: Final conversion profiles of thick cure samples with either BAPO, BDMB, DMPB, or TPO irradiated with a 400 nm LED (Firefly, Phoseon) for 20 minutes. Light intensity: 41 mW/cm ²	98
Figure 7-16: Temperature measured by an IR thermometer as a function of time at various heights of the cuvette during irradiation with a 400 nm LED (Firefly, Phoseon) for thick HDDA systems containing four different initiators: (A) BAPO ₃ , (B) BDMB, (C) DMPA, and (D)TPO. Light intensity: 41 mW/cm ² ; Photoinitiator concentration: 0.0167 M.	100
Figure 7-17: Percent conversion as a function of time at 23°C, 50°C, or 80°C for HDDA with (A) BAPO, (B) BDMB, (C) DMPA, and (D) TPO when cured with a 400 nm LED lamp (Firefly, Phoseon) (light intensity: 6.8 mW/cm ²).	102
Figure 7-18: DSC heat flow (with the second run subtracted from the first run) as a function of temperature for HDDA with BAPO, BDMB, DMPA, TPO, or without photoinitiator.....	103
Figure 7-19: Calculated time and depth dependence of the light intensity for 4.0 cm thick systems containing different photoinitiators: (A) DMPA, (B)TPO. The systems were irradiated by the 400 nm LED (light intensity: 41 mW/cm ² , photoinitiator concentration: 0.0167 M).	105
Figure 7-20: Normalized spectral light intensities of a Hg(-Xe) lamp, a 365 nm LED lamp, a 385 nm LED lamp, a 400 nm LED lamp, and a Xe lamp with a 400 nm bandpass filter (BPF).....	108

Figure 7-21: Comparison of five light sources for photopolymerization conversion profiles of thin HDDA systems containing four different initiators: (A) BAPO, (B), BDMB, (C) DMPA, and (D) TPO. Light intensity: 6.8 mW/cm ² , photoinitiator concentration: 0.0167 M. (a) Experimental, (b) simulation.	110
Figure 7-22: Spectral light intensities of a 365 nm LED lamp, a 385 nm LED lamp, and a 400 nm LED lamp, measured at 22.5 cm distance.	113
Figure 7-23: Comparison between a 365nm LED lamp (light intensity: 1.3 mW/cm ²), a 385 nm LED lamp (light intensity: 2.2 mW/cm ²) and a 400 nm LED lamp (light intensity: 6.8 mW/cm ²) for photopolymerization conversion profiles of thin HDDA systems containing four different initiators: (A) BAPO, (B), BDMB, (C) DMPA, and (D) TPO. Light intensity: 6.8 mW/cm ² , photoinitiator concentration: 0.0167 M. (a) Experimental, (b) simulation. The irradiation distances are all set to 22.5 cm.	114
Figure 7-24: Calculated conversion vs. experimental conversion at 40 seconds	117
Figure 7-25: Spectral light intensities of 335, 345, 355, 365, 375, 385, 400, 410, and 420 nm LED lamps.....	118
Figure 7-26: Comparison of seven LEDs for calculated photopolymerization conversion profiles of thin HDDA systems containing four different initiators: (A) BAPO, (B), BDMB, (C) DMPA, and (D) TPO. Light intensity: 6.8 mW/cm ² , photoinitiator concentration: 0.0167 M.....	120
Figure 7-27: Calculated time required to attain 60% conversion as a function of the LED wavelength for four different photoinitiators. Light intensity: 6.8 mW/cm ² , photoinitiator concentration: 0.0167 M. Dotted lines demonstrate the time required for a Hg(-Xe) lamp with 6.8 mW/cm ² light intensity to achieve 60% conversion.....	121
Figure 7-28: Spectral light intensities of 365, 375, 385, 400, 410, and 420 nm LED lamps.	122
Figure 7-29: Calculated time required to attain 60% conversion as a function of the LED wavelength for four different photoinitiators. Photoinitiator concentration: 0.0167 M. Light intensities: 1.3 mW/cm ² for a 365 nm LED, 2.2 mW/cm ² for a 385 nm LED, 6.8 mW/cm ² for 400 nm, 410 nm, and 420 nm LEDs. Here irradiation distances are assumed as same.	123
Figure 8-1: Chemical structures of the reaction components: (A) bis(cyclopentadienyl) bis[2,6-difluoro-3-(1-pyrryl)phenyl]titanium (Ti-PI), (B) 2-hydroxyethyl acrylate (HEA), (C) 2-carboxyethyl acrylate (CEA), (D) phosphoric acid 2-hydroxyethyl methacrylate ester (PhMA), and (E) p-toluenesulfonic acid (PTSA).....	128

Figure 8-2: HEA photopolymerization conversion profiles in the presence of various additives: 1.0 wt % (0.053 M) PTSA (○); 1.5 wt % (0.067 M) PhMA (▲); 1.5 wt % (0.105 M) CEA (■); no additives (◆); 1.0 wt % (0.053 M) PTSA plus 1.0 wt % (0.100 M) TEA (*). All samples contain 2.6 wt % (0.050 M) Ti-PI. Light intensity: 2 mW/cm ²	131
Figure 8-3: HEA photopolymerization conversion profiles for eight different concentrations of the protonic acid PhMA. All samples contain 2.6 wt % (0.050 M) Ti-PI. Light intensity: 2 mW/cm ²	132
Figure 8-4: Absorbance spectra with and without the acid additives in ethyl acetate. For all samples, Ti-PI = 0.01 wt %, PhMA = 0.006 wt %, PTSA = 0.005 wt %, TEA = 0.01 wt %.	133
Figure 8-5: The products of the light activated decomposition of a) diphenyltitanocene differ from those of b) perfluorodiphenyltitanocene.	135
Figure 8-6: Photodecomposition reactions of Ti-PI. a) When Ti-PI is not protonated by external acid, the degradation products resemble those from diphenyltitanocene. b) In the presence of an acid to protonate the nitrogen on Ti-PI, the degradation products change and resemble those of perfluorodiphenyltitanocene.	136
Figure 8-7: HEA photopolymerization conversion profiles for seven different light intensities: 2 mW/cm ² (◆), 4 mW/cm ² (■), 8 mW/cm ² (▲), 11 mW/cm ² (○), 18 mW/cm ² (*), 30 mW/cm ² (●), 40 mW/cm ² (+), 49 mW/cm ² (—). For all systems Ti-PI = 2.6 wt % (0.050 M), PhMA = 1.5 wt % (0.067 M).	138
Figure 8-8: HEA photopolymerization conversion profiles for three different Ti-PI/PhMA concentrations and two different light intensities: (a) 8 mW/cm ² and (b) 30 mW/cm ²	140
Figure 8-9: Photopolymerization conversion profiles for Ti-PI/PhMA photoinitiator system (Ti-PI = 2.6 wt %, PhMA = 1.5 wt %) and EYss/MDEA/DPI photoinitiator system (EYss = 0.074 wt %, MDEA = 3.77 wt %, DPI = 0.072 wt %) for two different monomer systems: (a) neat HEA monomer, (b) high viscosity urethane acrylate/HEA mixture (urethane acrylate = 70 wt %, HEA = 30 wt %). Light intensity: 2 mW/cm ²	142
Figure 9-1: Comparison of shadow cure conversion profiles (x-direction) between HEA(50)/HDDA(50) monomer mixture and CN9002(70)/HEA(30) oligomer-monomer mixture. Negative values of x correspond to the illuminated region, while positive values of x correspond to the masked region. Photoinitiator system: Ti-PI 2.7 wt%, PhMA; 1.5 wt %. Light source: a 150 W xenon lamp with 520 nm bandpass filter, light intensity: 24 mW/cm ² , irradiation time: 15 minutes.	146
Figure 9-2: Quenched dissolved oxygen as a function of illumination time. Monomer: HDDA. [Zntpp] = 2×10 ⁻⁵ M, [DMA] = 2×10 ⁻³ M. Light source: a 520 nm LED, light intensity 322 mW/cm ²	148

Figure 9-3: Comparison of RT-FTIR conversion profiles as a function of time in HDDA monomer in four different combinations of initiator, SG/ST, and light sources. Irradiation conditions: (A) 365 nm LED with 6.8 mW/cm ² light intensity, (B) 400 nm LED with 6.8 mW/cm ² light intensity. [DMPA] = 0.0167 M, [Zntpp] = 2×10 ⁻⁵ M, [DMA] = 2×10 ⁻³ M. A 520 nm LED with 322 mW/cm ² light intensity was used to scavenge dissolved oxygen.	149
Figure 9-4: Quenched dissolved oxygen as a function of illumination time. Monomer: HDDA. [DMA] = 1×10 ⁻⁴ M, [Zn-ttp] = 2×10 ⁻⁵ M. Light source: a Xe lamp with a polyimide film, light intensity 322 mW/cm ²	150
Figure 9-5: Comparison of RT-FTIR conversion profiles as a function of time in HDDA monomer in four different combinations of initiator, SG/ST, and light sources. Irradiation conditions: (A) 365 nm LED with 6.8 mW/cm ² light intensity, (B) 400 nm LED with 6.8 mW/cm ² light intensity. [DMPA] = 0.0167 M, [Zntpp] = 2×10 ⁻⁵ M, [DMA] = 2×10 ⁻³ M. A Xe lamp with a polyimide film (54 mW/cm ² light intensity) was used to scavenge dissolved oxygen.	151
Figure A- 1: Chemical structures of EYss, MB, FL, and MDEA.....	154
Figure A- 2: Conversion vs. time of HEA monomer with EYss, MB, MDEA irradiated by 520 nm wavelength light.....	156
Figure A- 3: Reaction schemes of (A) EYss/MDEA and (B) MB/MDEA photoinitiator systems.....	156
Figure A- 4: Conversion vs. time of HEA monomer with EYss, FL, MDEA irradiated by 450 nm wavelength light.....	157
Figure A- 5: Reaction schemes of (A) EYss/MDEA and (B) FL/MDEA photoinitiator syste	157
Figure B- 1 Chemical structures of 1, 4-diazabicyclo [2.2.2] octane, 1-azabicyclo [2.2.2] octane (DABCO) and ethyl 4-(dimethylamino)benzoate (EDMAB).....	158
Figure B- 2: Conversion vs. time of two-component systems and a three-component system for three different incident lights: (A) EYss/DABCO two-component system, (B) EYss/DPI two-component system, (C) EYss/DABCO/DPI three-component system. Monomer: HEA. Incident lights: a 150 W xenon lamp with no filter (89 mW/cm ²), a polyimide film (39 mW/cm ²) and a 520 nm bandpass filter (2.4 mW/cm ²).	160
Figure B- 3: Reaction mechanism of two-component systems. (A) EYss/DABCO (B) EYss/DPI.....	161
Figure B- 4: Reaction mechanism in an EYss/DABCO/DPI three-component system. (C) photo-reduction of EYss by DABCO and (D) photo-oxidation of EYss by DPI.....	161

Figure B- 5: The comparison of time dependence for conversion profiles. (A) EY _{ss} /MDEA/DPI three-component system and (B) EY _{ss} /DABCO/DPI three-component system. Light source: a Xe lamp with a 520 nm bandpass filter (light intensity: 2.4 mW/cm ²). Monomer: HEA.	163
Figure B- 6: DSC heat flow (with the second run subtracted from the first run) as a function of temperature for HEA with EY _{ss} , DABCO, DPI, EY _{ss} -DABCO, EY _{ss} -DPI, DABCO-DPI, EY _{ss} -DABCO-DPI, or without species. [EY _{ss}] = 0.00115 M, [DABCO] = 0.32 M, [DPI] = 0.0023 M.	164
Figure B- 7: DSC heat flow (with the second run subtracted from the first run) as a function of temperature for HEA with MDEA-DPI, EY _{ss} -MDEA-DPI, DABCO-DPI, EY _{ss} -DABCO-DPI. [EY _{ss}] = 0.00115 M, [MDEA] = 0.32 M, [DABCO] = 0.32 M, [DPI] = 0.0023 M.	165
Figure B- 8: Suggested reaction scheme between DABCO (DH) and DPI.....	165
Figure B- 10: Conversion vs. time of two-component systems and a three-component system. Monomer: HEA. Incident lights: a 520 nm LED (4 mW/cm ²).	166
Figure B- 11: HEA photopolymerization conversion profiles for seven different light intensities. For all systems EY _{ss} = 0.00115 M, EDMAB = 0.16 M, DPI = 0.0023 M. Light source: 520 nm LED.....	167
Figure B- 12: The comparison of time dependence for conversion profiles. (A) EY _{ss} /MDEA/DPI three-component system and (B) EY _{ss} /DABCO/DPI three-component system. Light source: a Xe lamp with a 520 nm bandpass filter (light intensity: 2.4 mW/cm ²). Monomer: HEA.	168
Figure B- 13: Conversion at 3 minutes irradiation vs. time. Light source: 520 nm lamp. Light intensity: 2~4 mW/cm ² . EY _{ss} = 0.00115 M, DPI = 0.0023 M for all systems. MDEA = DABCO = 0.32 M, EDMAB = 0.16 M.	169
Figure C- 1: Dependence of absorption on fluorescein (FL) concentration in methanol. (A) Napierian molar absorptivities (B) Normalized absorption.	171
Figure C- 2: Dependence of absorption on eosin Y spirit soluble (EY _{ss}) concentration in methanol. (A) Napierian molar absorptivities (B) Normalized absorption.	171
Figure D- 1: Four different stage substrates	172
Figure D- 2: The effect of the bottom substrate on the conversion profiles (x-direction) observed for EY _{ss} /MDEA system. Light source: a 150 W xenon lamp, light intensity: 89 mW/cm ² , irradiation time: 15 minutes.	173
Figure E- 1: Chemical structures of zinc 2,9,16,23-tetra-tert-butyl-29H,31H-phthalocyanine (Zn-ttp), 5,10,15,20-Tetraphenyl-21H23H-porphine zinc (Zn-tp), and 9,10-dimethylantracene (DMA).....	174

Figure E- 2: Quenched dissolved oxygen as a function of illumination time for different light intensities. Monomer: HDDA. $[Zntpp] = 2 \times 10^{-5} \text{ M}$, $[DMA] = 2 \times 10^{-3} \text{ M}$	176
Figure E- 3: Time dependence of the DMA/Zn-ttp UV-Visible spectrum profiles. Monomer: HDDA.....	177
Figure E- 4: Time dependence of DMA concentrations for DMA and DMA/Zn-ttp. Monomer: HDDA.....	178
Figure F- 1: HEA photopolymerization conversion profiles for seven different light intensities: (A) Ti-PI = 2.6 wt % (0.050 M), PhMA = 1.5 wt % (0.067 M), (B) Ti-PI = 0.5 wt % (0.0095 M), PhMA = 0.3 wt % (0.0133 M), (C) Ti-PI = 0.1 wt % (0.00019 M), PhMA = 0.06 wt % (0.00027 M).....	180
Figure F- 2: Ultimate conversions of photopolymerization profiles in Figure F- 1.	180
Figure F- 3: Time to reach 90 % of its ultimate conversion (T90) in Figure F- 1.....	181
Figure F- 4: The comparison of time dependence for conversion profiles: (A) 1.0 wt % (0.053 M) PTSA; (B) 1.5 wt % (0.067 M) PhMA. All samples contain 2.6 wt % (0.050 M) Ti-PI. Light source: a Xe lamp with a 520 nm bandpass filter (light intensity: 2.4 mW/cm^2). Monomer: HEA.	182
Figure F- 5: Percent conversion as a function of time at 70°C for styrene with four different photoinitiating systems.	184
Figure F- 6: Heat flow profiles for the photopolymerizations of styrene for four different photoinitiating systems at 40°C	186
Figure F- 7: Comparison of two light sources, a 150W Xe lamp with 89 mW/cm^2 light intensity (blue line) and the Xe lamp attaching a 520 nm bandpass filter with 2 mW/cm^2 light intensity (red line), for photopolymerization conversion profiles. Monomer: HEA. Photoinitiator: (A) Ti-PI, (B)Ti-PI + PhMA.....	187
Figure F- 8: Comparison of two light sources, a 150W Xe lamp with 89 mW/cm^2 light intensity (blue line) and the Xe lamp attaching a 520 nm bandpass filter with 2 mW/cm^2 light intensity (red line), for photopolymerization conversion profiles. Monomer: HDDA. Photoinitiator: (A) Ti-PI, (B)Ti-PI + PhMA.	188
Figure F- 9: Comparison of two light sources, a 150W Xe lamp with 89 mW/cm^2 light intensity (blue line) and the Xe lamp attaching a 520 nm bandpass filter with 2 mW/cm^2 light intensity (red line), for photopolymerization conversion profiles. Monomer: HEMA. Photoinitiator: (A) Ti-PI, (B)Ti-PI + PhMA.	188
Figure F- 10: Photopolymerization conversion profiles for different light intensities. Monomer/oligomer mixture: HEA(30)/CN9002(70). Light source: a 520 nm LED. Photoinitiator: (A) Ti-PI, (B) Ti-PI + PhMA.	189

CHAPTER 1. BACKGROUND

1.1. Photopolymerization

Photopolymerization technology recently has received considerable attention due to its environmental and manufacturing advantages.¹ Compared to the traditional thermal polymerization process, it has the potential to reduce VOC emissions, lower energy requirements and shorten cure times, thus, leading to a more efficient manufacturing process. Furthermore, photopolymerization processes do not require a drying step, so smaller space is required. Therefore, the photopolymerization technology can be used not only for the replacement of the conventional thermal process but also for new markets. Due to these advantages, photopolymerization technology has been employed for various applications including coatings, adhesives, printings, stereolithography and photoresists.

Photopolymerization formulations are basically composed of oligomers and monomers with a small amount of a photoinitiator. Light exposure causes the generation of active centers, which are the reactive species, via the photoinitiator. Oligomers and monomers in the formulation then quickly polymerize and/or crosslink because the chain polymerization reaction starts from the active centers. The polymerization process comprises three main steps: initiation by active centers, propagation and termination. The oligomer determines the basic polymer properties such as adhesion, stress-strain properties and glass transition. The monomer controls the viscosity, wetting property, elasticity, crosslink, and adhesion properties. The proportion of the photoinitiator in the formulation is very small compared to that of the oligomer and the monomer; the percentage of the photoinitiator in the formulation is usually between 0.1 wt% and 5 wt%. The photoinitiator determines the wavelengths active for active center generation. Although single component photoinitiator systems are more common, multi-component systems are employed as well for visible light induced photopolymerization.

The photopolymerization process is designed using a combination of light sources and photoinitiator systems. UV lights are commonly (or widely) used in the photopolymerization processes owing to the high energy of photons at these wavelengths. Therefore, many kinds of photoinitiators excited by UV wavelengths have been developed in the industry. Regarding a visible wavelength, photoinitiation under visible light exposure has been investigated for the last two decades. However, only a few industries (e.g. coatings, dental materials)²⁻⁵ use visible light induced photoinitiator systems, because visible light photons have a much lower energy compared to UV light photons.

Active centers for chain photopolymerization reactions may either be free radicals or cations.¹ Since a variety of radical photopolymerization materials including (meth)acrylate monomers and oligomers have been commercialized, free radical photopolymerization systems dominate the photopolymerization market. However, cationic photopolymerization systems are being eagerly investigated as the use of cationic photocuring rises. Compared to cationic photopolymerization, radical photopolymerization offers a higher polymerization rate so that short cure time processes can be developed.

Regarding radical photoinitiator systems, as described above, single component photoinitiator systems (Type I photoinitiators) are more common and mainly used with UV light. A type I photoinitiator is cleaved by absorbing photons, which is called α -cleavage, and generates several free radicals. Alternatively, multi-components radical photoinitiator systems (Type II photoinitiators) are employed, especially for visible light induced photopolymerization. A Type II photoinitiator is composed of a photosensitizer and a coinitiator that undergo a bimolecular reaction where the excited state of the photosensitizer interacts with the coinitiator to generate free radicals.

Although radical photopolymerization systems offer many advantages, oxygen inhibition of the system remains one of the biggest issues. The dissolved oxygen from

the air deactivates active centers and forms inactive peroxy radicals, thereby inhibiting photoinitiation. Therefore, a drop in the polymerization speed and a lowered final conversion in free-radical photopolymerization due to the presence of oxygen are often reported.⁶⁻⁸ Several methods have been applied to overcome oxygen inhibition in radical photopolymerization systems. An increase in photoinitiator concentration or the use of a high intensity light source to multiply the production of primary radicals is a solution to this problem in industry. Other physical methods are using an inert gas such as nitrogen to replace oxygen and lamination to prevent air exposure. O'Brien and Bowman⁸ show the clear influence of light intensity and inert gas on photopolymerization reaction by measuring the conversion of acrylates. There are also several chemical methods such as the addition of thiols and amines to reduce oxygen inhibition.^{9,10}

1.2. Anisotropic Conductive Film (ACF)

Anisotropic conductive films were first introduced in 1984 as adhesives for liquid crystal display (LCD) circuits and as a replacement for lead-containing solders.¹¹ In the past 25 years, they have been widely used in displays and large scale integration industries (Figure 1-1). Due to the recent market growth of display panels including LCDs, plasma displays and electric papers in the world, the market for ACF is dramatically increasing.

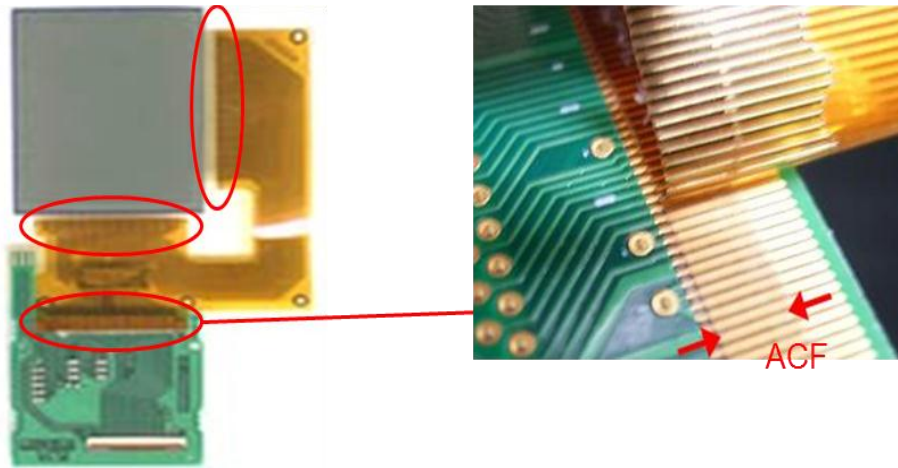


Figure 1-1: ACF used for bonding between a display and circuit.

ACFs contain fine electrically conductive particles in an insulating adhesive resin with solvents designed to provide electrical interconnection only at planned sites in which the particles come into contact with an electrode.¹² ACFs make electrical and mechanical connections between driver circuits and display panels using FPCs (flexible printed circuits). The FPC is usually composed of a polyimide film (rarely PET film is used instead) and micron-order pitch embedded electrodes.

Figure 1-2 shows a typical spectrum of a polyimide film. As shown in the graph, the polyimide film absorbs UV wavelengths but transmits only visible wavelengths. The ACF bonding process usually applies a thermal cure process as shown in Figure 1-3.¹³ First, the ACF is laminated between two (typically FPC) substrates in which the electrodes are designed. Finally, thermal energy is used to cure the adhesive for bonding these two substrates while applying pressure on them.

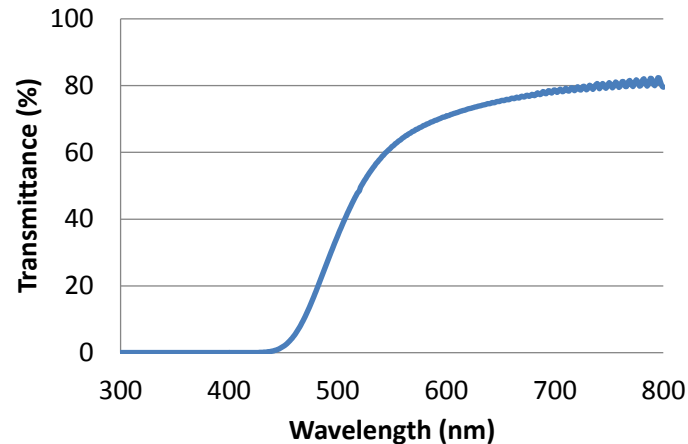


Figure 1-2: Transmittance of polyimide film.

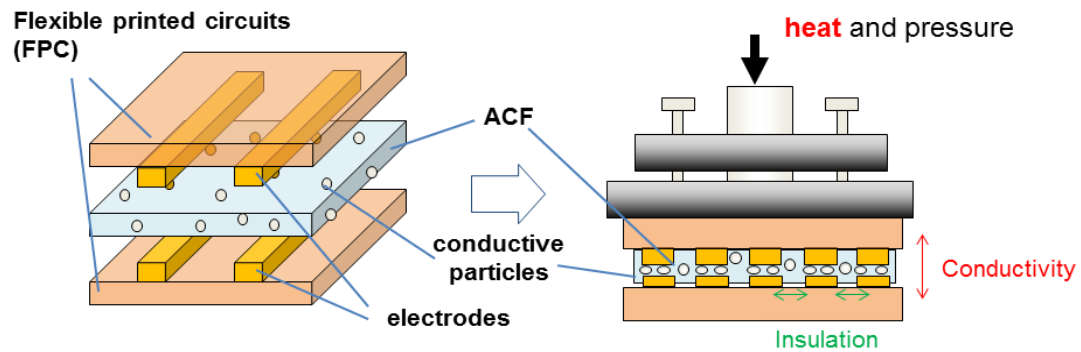


Figure 1-3: Conventional heat process with ACF between FPC.

Although this ACF technology offers many advantages such as lead-free adhesion and precise conductivity controls, some issues still need to be addressed such as the containment of volatile organic compounds (VOCs), requirement of a high temperature process, and relatively low cure speed. The emission of VOCs is a source of atmospheric pollution, and the high temperature process with slow speeds demands a high energy cost. Moreover, the recent use of plastics instead of glass for display manufacture precludes a high temperature process since the plastic will lose its dimensional stability. Photopolymerization technologies, especially Visible-light-induced

photopolymerization technologies, have a huge potential to offer reduced VOC, lower temperature and energy demands, and promise a faster cure speed.

1.3. Visible-Light-Induced Free Radical Photoinitiator systems

Since the energy of a photon in the UV region is higher than the energy of a covalent bond in a photoinitiator, the photoscission of the photoinitiator is so easy that radicals can be generated by UV irradiance. On the other hand, the energy of a photon in the visible region of the spectrum is generally less than the bond dissociation energy of most organic molecules. Therefore, visible-light-induced photoinitiator systems are typically two-component photoinitiator systems in which the active centers are produced via an electron transfer followed by a proton transfer from the electron donor (typically an amine) to the excited photosensitizer. Many dyes and other compounds that absorb in the visible range have been used as the photosensitizer in this type of system, including camphorquinone, (thio)xanthone derivatives, (thio)xanthene derivatives and ketocoumarin derivatives.^{3, 14} In order to enhance the electron transfer system besides adding other reaction schemes into these two-component photoinitiator systems, three-component photoinitiator systems have also been developed and investigated.¹⁵⁻²⁰

1.4. Shadow Cure

As previously mentioned, owing to its many advantages, photopolymerization technology has been employed for various applications including coatings, adhesives, printings, stereolithography and photoresists. On the other hand, one of the issues is its inability to cure optically shadowed regions and this results in a limitation of its application. If this disadvantage is overcome, the applications (e.g. three-dimensional adhesives²¹, optical impact films²², solar-light-induced coatings) will be greatly expanded. Although a process using UV light could be acceptable, the use of visible light is more preferable from the view of safety and cost.

The dual polymerization system combining photoinitiators with thermal initiators for thick shadow cure is well known^{23, 24}. However, the method using photoinitiators alone has only been reported in a paper by Ficek *et al.*²⁵ These authors studied thick shadow cure systems using cationic photoinitiators. The research achieved an almost 1 cm thick shadow cure, which was confirmed by its gelation and measurement of its physical properties. Only cationic photoinitiators were used as initiators in the experiments so that the polymerization was only caused by UV light. Although this method can be applied to various systems, there are some barriers to generalizing this system due to the limited varieties of cationic polymers, its slower cure speed compared to general radical systems, and its corrosiveness, especially to electronic devices. Therefore, investigation into radical shadow cure systems is required. Free-radical active centers have significantly shorter lifetimes than cationic active centers, and tend to terminate immediately upon the cessation of illumination. Thus, achieving shadow cure using radical photoinitiator systems is challenging and other innovative means must be developed.

1.5. LEDs for Photopolymerization

Various light sources are used for photopolymerization processes¹. Mercury lamps, metallic halide lamps and xenon lamps are well known as both UV and visible light sources. Recent laser sources offer many possibilities in wavelength selection from UV to near IR. For instance, excimer lasers can emit short wavelength (e.g., 193, 248 nm) and argon-ion lasers can emit 363, 488, and 514 nm light. LEDs (Light Emitting Diodes) are recently attracting attention as new photocuring light sources due to their many advantages including low energy consumption, low power requirements, long lifetimes, small size, fast switching, non-toxicity, and the lack of stray IR emissions^{26, 27}. Apart from visible LEDs, UV-LEDs have been developed as well and are being applied

in photocuring applications. To be useful for photocuring, the absorbance spectrum of the photoinitiator systems must match the light emission spectrum of the lamp.

Representative LED suppliers that are specifically developing light sources for photocuring are summarized in Table 1-1. As the table illustrates, the current suppliers are primarily American start-up companies and large Japanese corporations that are focusing on the lower energy consumption and long lifetimes of LED systems. Motivated by these advantages, the companies are developing UV LED irradiation systems as substitutes for conventional UV lamps such as high pressure mercury lamps, Xe lamps, and electrodeless UV lamps. To achieve a performance comparable to that of conventional UV lamps, each company is developing LEDs in the UV region (365-420nm) with high a light intensity. Furthermore, Clearstone and Digital light labs are developing LEDs in the visible region of the spectrum as well.

Table 1-1: List of commercial photocuring LED irradiation systems

Company	Country	Representative product name	Wavelength (nm)		Light Intensity (mW/cm ²)	Standard LED array dimensions	
			UV	Visible		Surface (mm × mm)	Linear (mm)
Phoseon Technology	USA	Fireline	b/w 380–420		8000 (surface)	From 25 × 25 to 75 × 50	25–1500
Clearstone	USA	AL432-365 E	365,390	470,505, 530,590, 615,630	135 (at 50 cm)	From 19 × 38 to 160 × 300	
HAMAMATSU	Japan	LC-L3	365,385		250 (at 30 mm)	12 mm dia.	
Panasonic Electric Works Co.	Japan	Aircure UD80	385		4000 (at 10 mm)	4 mm dia.	750
Digital Light Lab	USA	AccuCure	365–400	400–730	Up to a few thousands	Few mm ² – several m ²	
OMRON	Japan	ZUV-C30H	365		8100 (at 15 mm)	3–12 mm dia.	

Phoseon Technology (Hillsboro, OR) offers UV LED systems centered at 400 nm in a wide variety of sizes. Specific applications that they have targeted include the following: UV adhesives for micro-speakers which require a narrow spot size for the UV light, UV light sources which can illuminate a wide area for curing wood coatings and UV LED printing systems for CD/DVDs. Clearstone, which is located in Minneapolis, utilizes a proprietary lens array technology in their LED systems to achieve the desired illumination distribution, including long distance irradiance with uniform high intensity. HAMAMATSU offers a highly uniform irradiation from their UV LED light systems which maintain a uniform light level throughout the LED life of up to 20,000 hours. Panasonic Electric Works Co. LTD has developed a high power UV LED curing system for UV ink.

The UV LED curing system may be used to illuminate large areas. LED systems from Digital Light Lab (Knoxville, TN) can operate as low as a few mW/cm^2 up to a few W/cm^2 based on configuration, and can cure areas as small as a few mm^2 to several m^2 . In addition, the Digital Light Lab's products can be configured in UV, Visible, and NIR regions. OMRON supplies spot UV LED systems that are eight times smaller than conventional UV lamp systems. The OMRON Company has enhanced their value by their ultra cooling head systems that have industry-leading long life and illuminating stability because of their effective dissipation of heat.

CHAPTER 2. OBJECTIVES OF THE PROPOSED RESEARCH

2.1. Part I: Shadow Cure in Free Radical Photopolymerizations

As mentioned in chapter 1, it is obvious that photopolymerization technologies exhibit considerable potential to provide new ACF processes instead of the conventional thermal processes. The purpose of this research is to provide fundamental studies on advanced free radical photoinitiator systems which allow shadow cure, especially for initiation with visible light. These fundamental studies could find application for the replacement of thermal cure processes with photopolymerizable ACFs, thereby offering shorter cure times and lower energy consumption without using solvents. The elimination of heat sources required for thermal processes results in significant energy savings and substantial capital savings because light sources are relatively inexpensive, especially in the visible light spectrum. Furthermore, light-induced polymerization leads to shorter cure times compared to conventional thermal polymerization and higher cure rates without the use of solvents, thereby minimizing the emission of VOCs and reducing the need for solvent vapor handling systems. However, there are some challenges that need to be overcome for this process to fully replace conventional methods. One primary challenge is to attain full polymerization in unilluminated regions behind electrodes and around conductive particles. These regions are shaded from the initiating light source, and these shadow regions must be cured to an acceptable conversion. Secondly, illumination through polyimide and/or PET films is required, and since the polyimide film absorbs wavelengths below 450 nm, an effective initiating system and light source in the visible-light region has to be found.

The broad objective of this research is to examine the factors that determine the attainable extent of shadow cure using free radical polymerization. This shadow cure system can also be applied to various industrial processes other than ACF, including the polymerization of a surface layer containing carbon fillers of elastic conductive rollers in

copy machines. In addition, the system may be employed for photocuring black matrix layers for electronic papers and impact adhesive films used in display panels. This study addresses the development of unprecedented photoinitiator systems in which photocuring processes can be used for ACFs, thus enabling a new ACF bonding process using a photoinitiator system with visible light. The research is composed of two stages, namely (1) investigating visible-light-induced cure systems and (2) characterizing the experimental variables that affect the attainable shadow cure distance. Specific objectives of this research are:

- i. to identify photoinitiator systems which are active in the visible light region and achieve high polymerization rates;
- ii. to evaluate the extent of shadow cure with UV-light-induced and visible-light-induced photoinitiator systems;
- iii. to characterize the effect of oxygen inhibition on free radical lifetime, mobility, and shadow cure;
- iv. to develop a means for overcoming oxygen inhibition to extend the free radical lifetime and, thereby, enhance the shadow cure;
- v. to investigate the effect of illumination within shadow regions by emission from fluorescent additives;
- vi. to optimize the combination of photoinitiators, additives, their concentrations and light conditions.

2.2. Part II: Experimental and Modeling Studies of Photoinitiator

Systems for Effective Polymerizations with LEDs

As described in section 1.5, LED photocuring systems provide many advantages compared to conventional lamps including mercury lamps and xenon lamps. In order to use LED photocuring systems properly, optimized combinations between photoinitiator systems and LED light sources must be investigated. However, except for dental material

process research, especially around 450 nm LED lamps, ^{e.g.28-32} only a few researchers³³⁻³⁵ have published findings regarding the combination between photoinitiator systems and LEDs. Fundamental research of photopolymerization through LED photocuring systems is imperative if LEDs are to be used in practical photopolymerization processes, and optimized curing procedures must be developed for replacement of conventional lamps with LEDs.

The goal of this research is to provide a comprehensive characterization (with both experimental and modeling studies) of the photoinitiation efficiency of commercially available photoinitiators illuminated with LED lamps ranging from the near UV/blue region up to the red region of the visible spectrum with respect to both thick and thin cure processes. In addition, a strategy for minimizing oxygen inhibition and creating additional active centers will be investigated for photoinitiator/lamp combinations which require this enhancement. Specific objectives of this research are:

- i. to investigate current LED photocuring system characteristics including the light intensity, uniformity, and light spectra;
- ii. to develop a computer model to predict photopolymerization using LEDs;
- iii. to have experimental studies in order to verify the simulation results,
- iv. to investigate the photopolymerization with LEDs,
- v. to specify optimum combinations of photoinitiator systems and LEDs.

CHAPTER 3. INVESTIGATION OF VISIBLE-LIGHT-INDUCED FREE RADICAL PHOTOINITIATOR SYSTEMS

3.1. Introduction

The specific application of this shadow cure research is ACF (anisotropic conductive film) which is typically used to bond FPCs (flexible printed circuits). The FPC is usually composed of a polyimide film and micron-order pitch embedded electrodes. The polyimide film absorbs UV wavelengths but transmits visible wavelengths. Therefore, visible-light-induced photopolymerization technologies have a huge potential to offer unprecedented innovative cure processes of ACF instead of using of heat.

The energy of a photon in the visible spectrum of light is generally less than the bond dissociation energy of most organic molecules. Therefore, visible-light-induced photoinitiator systems are primarily two-component photoinitiator systems in which the active centers are produced via an electron transfer followed by a proton transfer from the electron donor (typically an amine) to the excited photosensitizer. Many dyes and other compounds that absorb in the visible range have been used as photosensitizers in this type of a system, including camphorquinone, (thio)xanthone derivatives, (thio)xanthene derivatives and ketocoumarin derivatives.^{3, 14} In order to enhance the electron transfer system besides adding other reaction schemes into these two-component photoinitiator systems, three-component photoinitiator systems have been developed and investigated as well.¹⁵⁻²⁰

In this chapter, various multi-component radical photoinitiator systems that utilize visible wavelengths of light were investigated. These systems must achieve high polymerization rates when illuminated through a polyimide film that blocks wavelengths below 450 nm. Apart from the ACF curing process, the visible-light-induced free radical photoinitiator systems established in this research can be practically applied to various

other industrial visible-light curing processes that include printings, pigments containing coatings, and colored particle photopolymerization for electronic paper.

3.2. Screening Study of Visible-Light-Induced Free Radical

Photoinitiator systems

Unlike typical UV photoinitiators, visible-light-induced photoinitiator systems are generally bimolecular photoinitiator systems (Type II photoinitiators) in which the active centers are produced via electron transfer followed by proton transfer from the electron donor to the excited photosensitizer.^{14, 15} In order to find visible-light-induced photoinitiator systems that can achieve high polymerization rates and conversion, screening experiments were performed using the same monomer resin and electron donor. Hence, various dyes, used as photosensitizers, were tested in these screening experiments.

3.2.1. Materials and Methods

To study polymerization rate, a monomer 2-hydroxyethyl acrylate (HEA, Sigma Aldrich) was chosen as the resin due to the high solubility of dyes and its common use in the industry. The electron donor was N-methyldiethanolamine (MDEA) and fourteen dyes were studied (See Table 3-1). All chemicals were purchased from Sigma Aldrich. For each photoinitiator system, the overall conversion of HEA films was measured using Real-Time Fourier transform infrared spectroscopy (RT-FTIR) with a modified Bruker 88 FTIR spectrometer designed to accommodate a horizontal sample. The RT-FTIR used a 150 W xenon (Xe) lamp (MAX-150, Asahi Spectra) to irradiate the samples. The light spectrum of the lamp, measured by an Ocean Optics USB 4000 fiber optic spectrometer, is shown in Figure 3-1 and the total light intensity emitted was 89 mW/cm².

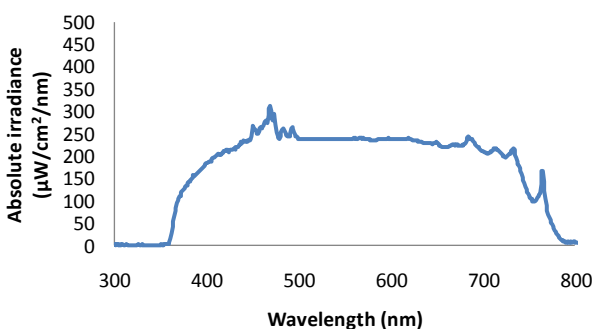


Figure 3-1: Spectral light intensity of a 150 W xenon (Xe) lamp (MAX-150, Asahi Spectra)

In this study, three combinations of photosensitizers (dyes) and electron donor (MDEA) concentrations were tested as follows: (i) photosensitizer 0.00115 M, MDEA 0.32 M, (ii) photosensitizer 0.00115 M, MDEA 0.16 M, (iii) photosensitizer 0.0023 M, MDEA 0.32 M. These concentration combinations were narrowed down by DOE (design of experiments) for EYss and MDEA. The samples were prepared by placing a droplet of resin between two rectangular IR grade sodium chloride salt crystals and 15 μm Teflon beads were placed between the crystals to serve as spacers. The sample was irradiated by the Xe lamp for three minutes and infrared absorption spectra were obtained. The carbon-carbon double bond infrared absorbance peak at 812 cm^{-1} , associated with an out-of-plane vibration, was monitored during the reaction to determine the acrylate conversion. The conversion was calculated using the ratio of current peak height to the peak height prior to polymerization. Equation 3-1 represents how the conversion was calculated:

$$\% \text{ Conversion} = \left[\frac{A_0 - A_t}{A_0} \right] \times 100 \quad \text{Equation 3-1}$$

where A_0 is the absorbance at 812 cm^{-1} before irradiation, and A_t is the absorbance at time t .

In chapter 4, the combination of dyes is investigated to achieve polymerization in the distant shadow region. To select the proper combination, information on absorbance and fluorescence spectra of each dye was required. So absorbance and fluorescence of the dyes were monitored using an 8453 UV-Visible spectrophotometer (Agilent Technologies) and a fluorescence spectrometer (Perkin Elmer). In these measurements, the solvent was methanol. Dye concentrations in the solvent were adjusted between 0.01 wt% and 0.00001 wt% to acquire unsaturated clear signals.

3.2.2. Results

Table 3-1 summarizes the screened dyes used as photosensitizer, the chemical types, wavelength of maximum absorption, and the final conversions for concentration combinations. Dyes that attain high conversions are all xanthene dyes, including fluorescein (FL)¹⁹, eosin Y, eosin Y spirit soluble (EYss)¹⁷, erythrosin B, and rose bengal¹⁹. Methylene blue^{9, 16, 18, 36} achieved relatively higher conversions compared to other non-xanthene dyes. Absorbance and fluorescence emission of these dyes are shown in Figure 3-2. The measurement conditions are illustrated in Table 3-2. As shown in the graphs, the individual fluorescence spectrum has a symmetrical shape compared to its absorbance spectrum.³⁷

From the results, the most promising photoinitiator system for visible cure is EYss due to its highest conversion among the photosensitizers and minimal overlapping of its absorbance with polyimide filter (see Figure 1-2). Therefore, this system can polymerize a resin using visible light through a polyimide film.

Table 3-1: Screened photosensitizers and final conversions for concentration combinations.

	Chemical Type	λ_{max} * (nm)	Dye 0.00115M MDEA 0.32M	Dye 0.00115M MDEA 0.16M	Dye 0.0023M MDEA 0.32M
Malachite Green Carbinol base	Triphenylmethane dye	446	0.0	1.0	0.6
Camphorquinone (CQ)	Quinone	450	4.2	6.3	3.2
Orange II	Naphthol dye	483	2.4	1.5	0.8
Fluorescein (FL)	Xanthene dye	496	94.8	93.5	94.4
Eosin Y (EY)	Xanthene dye	514	90.0	91.1	92.8
Eosin Y spirit soluble (EYss)	Xanthene dye	521	93.8	95.1	93.6
Erythrosin B (EB)	Xanthene dye	525	85.1	85.2	84.5
Neutral Red	Diazine dye	540	8.4	6.5	4.9
Rose Bengal (RB)	Xanthene dye	548	90.2	89.4	89.1
Crystal Violet	Triphenylmethane dye	590	4.7	6.5	7.9
Thymol Blue	Triphenylmethane dye	594	0.0	1.0	3.0
Erioglucine	Triphenylmethane dye	625	0.0	0.0	0.0
Disperse Blue	Anthraquinone dye	640	2.1	2.0	2.6
Methylene Blue (MB)	Thiazine	661	14.7	17.8	15.8

*Wavelength of maximum absorption (Sigma-Aldrich catalogue)

Monomer: HEA; Light source: 150W Xe-lamp, light intensity: 89 mW/cm²;
irradiation time: 3 minutes

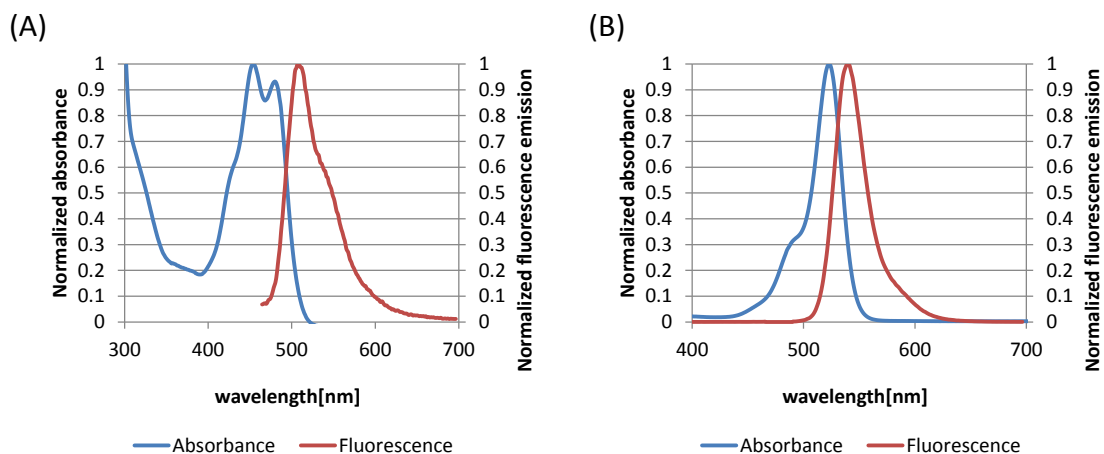


Figure 3-2: Absorbance and fluorescence of photosensitizers: (A) Fluorescein (FL), (B) eosin Y, (C) eosin Y spirit soluble (EYss), (D) erythrocin B, (E) rose bengal, (F) methylene blue.

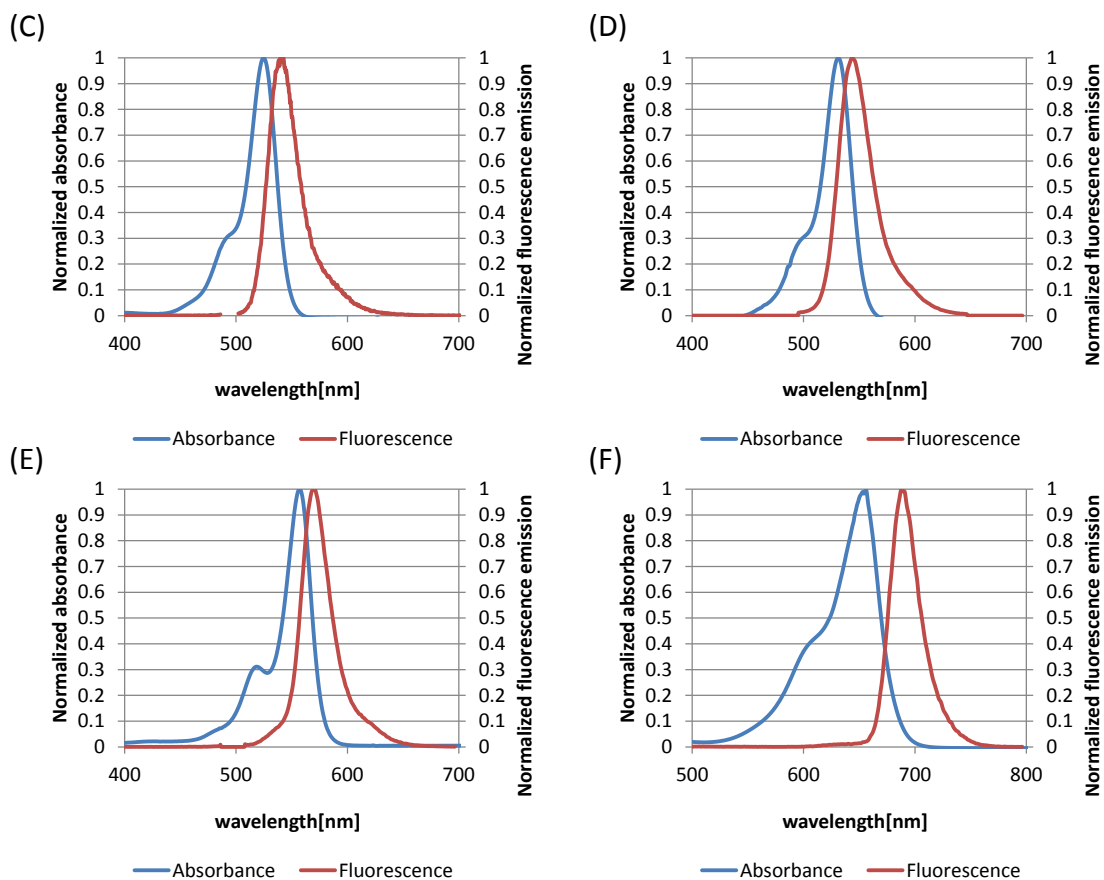


Figure 3-2 continued.

Table 3-2: Screened photosensitizers and final conversions for concentration combinations.

	Condition of UV-Vis		Condition of fluorescence spectroscopy	
	Concentration	Concentration	Excitation wavelength	
	wt %	wt %	λ_{ex} (nm)	
Fluorescein (Fl)	0.01	0.001	400	
Eosin Y	0.001	0.00005	480	
Eosin Y spirit soluble (EYss)	0.001	0.00001	500	
Erythrocin B	0.001	0.0002	490	
Rose bengal	0.001	0.001	500	
Methylene Blue (MB)	0.001	0.001	660	

Monomer: HEA; Light source: 150W Xe-lamp, light intensity: 89 mW/cm²; irradiation time: 3 minutes.

3.3. Characterization of EYss/MDEA Visible-Light-Induced

Photoinitiator system

As a result of the study in section 3.2, two-component systems containing EYss and MDEA can be considered as a main visible-light-induced photoinitiator system. In this section, this photoinitiator system is characterized, including the effect of the third component additive, its shelf life, and the dependency on its irradiated light.

3.3.1. Photopolymerization Study of EYss-MDEA Two-Component and EYss-MDEA-DPI Three-Component Systems

The electron-transfer/proton-transfer reaction between two-component systems containing EYss and MDEA and three-component systems composed of EYss, MDEA and diphenyliodonium chloride (DPI) has been investigated by Padon et al.¹⁷ These chemical structures are shown in Figure 3-3. They have clarified the mechanism of both two-component and three-component systems as shown in Figure 3-4 and Figure 3-5. Here, D-H represents the electron donor MDEA which can provide hydrogen H. In Figure 3-4, the amine active center, D^\bullet , is produced via electron transfer followed by proton transfer from MDEA to the excited EYss. In addition to this two component reaction, the third component DPI generates another active center, a phenyl radical, via electron transfer with the triplet state EYss, $EYss^*$. Furthermore, D^\bullet may also be generated through the reaction between EYss cationic radical $EYss^{+\bullet}$ and MDEA (D-H). Here, $EYss^{+\bullet}$ is generated by $EYss^*$ -DPI reaction, as shown in Figure 3-5. Hence, three-component photoinitiator systems enhance the effectiveness of the two-component electron transfer initiating system.

Regarding photocurable ACF application, which is the main application target of this shadow cure study, ionic species may be undesirable due to the possible corrosive effects of the salt on the conductive elements of the flexible printed circuit. In particular, chloride ions are well known as the cause of corrosion. However, it is worthwhile to

study the effect of the third component for shadow cure, because this shadow cure system could be applied to various applications other than ACF. In this study, the trends of the two-component and three-component photoinitiator systems are investigated.

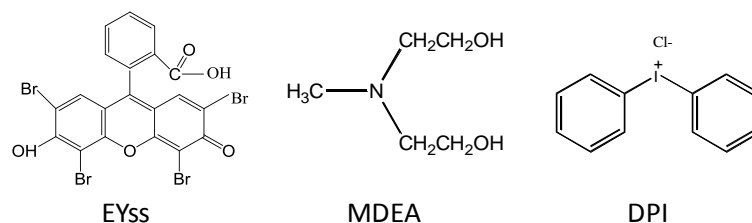


Figure 3-3: Chemical structure of EYss (eosin Y spirit soluble), MDEA (N-methyldiethanolamine) and DPI (diphenyliodonium chloride).

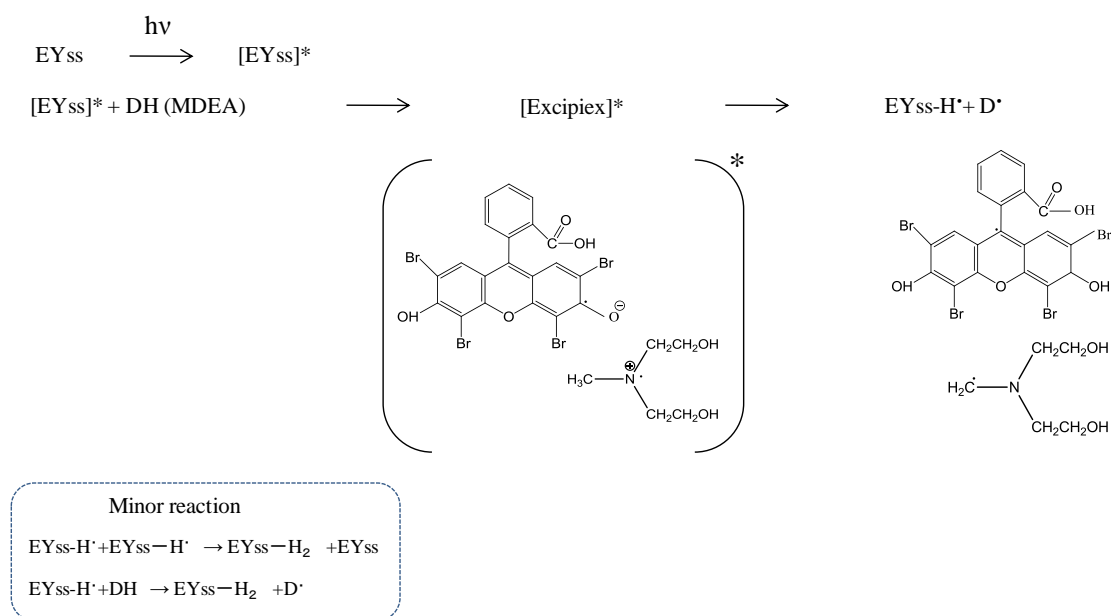


Figure 3-4: Reaction mechanism of EYss/MDEA two-component photoinitiator system.¹⁷

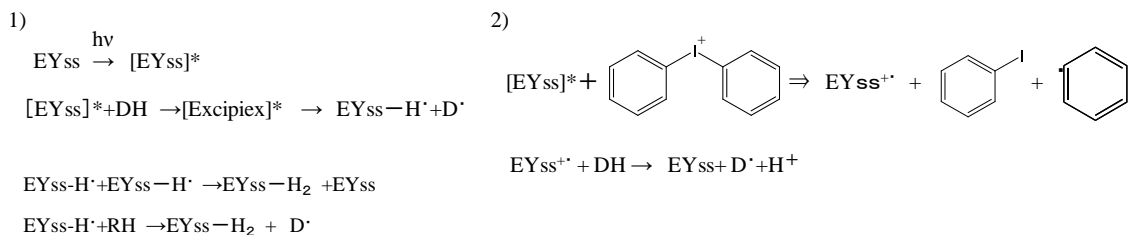


Figure 3-5: Reaction mechanism of EYss/MDEA/DPI three-component system.¹⁷

3.3.1.1. Materials and Methods

HEA monomer was used as the resin. The formulations of two types of two-component systems (EYss/MDEA, EYss/DPI) and a three-component system (EYss/MDEA/DPI) studied are shown in Table 3-3. All chemicals were acquired from Sigma Aldrich. The overall conversion of HEA films was measured using RT-FTIR with the method indicated in section 3.2.1. The sample was irradiated by a 150 W Xe lamp (MAX-150, Asahi Spectra) with no filter, a polyimide film, and a 520 nm bandpass filter. Normally, the xenon lamp emits an 89 mW/cm² total light intensity with a broad wavelength. However, with the polyimide film it emitted a 39 mW/cm² total light intensity due to the attenuation of light especially in low wavelength regions. With the bandpass filter, the lamp emitted a 2.4 mW/cm² total light intensity with 520 nm single wavelength. The light spectra of the three conditions are shown in Figure 3-6.

Table 3-3: Two-component system and three-component system formulas studied

		Two-component system		Three-component system
		EYss/MDEA	EYss/DPI	EYss/MDEA/DPI
EYss	[M]	0.00115	0.00115	0.00115
MDEA	[M]	0.32	-	0.32
DPI	[M]	-	0.0023	0.0023

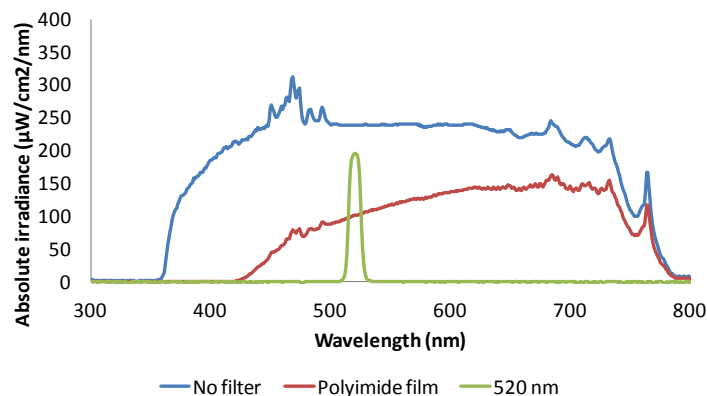


Figure 3-6: Light spectra of a 150 W xenon lamp (MAX-150, Asahi Spectra) emitted through no filter, polyimide film and 520 nm bandpass filter.

3.3.1.2. Results and Discussion

Figure 3-7 illustrates the conversion as a function of time for the two-component systems and three-component system. Obviously, the photopolymerization rates and final conversions of the three-component system are higher compared to that of the two-component systems in the all light conditions. However, when comparing the effective light in each system, very different trends are observed. In the EYss/MDEA two-component system, the lamp without filter can achieve higher polymerization because of its higher light intensity. On the contrary, in the EYss/DPI two-component system, in spite of its lower light intensity and narrower light spectra, the light with the 520 nm bandpass filter achieves faster cure and higher final conversion than the light without the bandpass filter. The lamp with polyimide film demonstrates the second best polymerization rate and final conversion in the both two-component systems. These trends imply that higher light intensity is more effective for the photoinitiation reaction in the EYss/MDEA photoinitiator system while too high a light intensity inhibits the photoinitiation reaction in the EYss/DPI photoinitiator system. Finally, the best performance of polymerization in the EYss/MDEA/DPI three-component system was achieved by the lamp with the polyimide film.

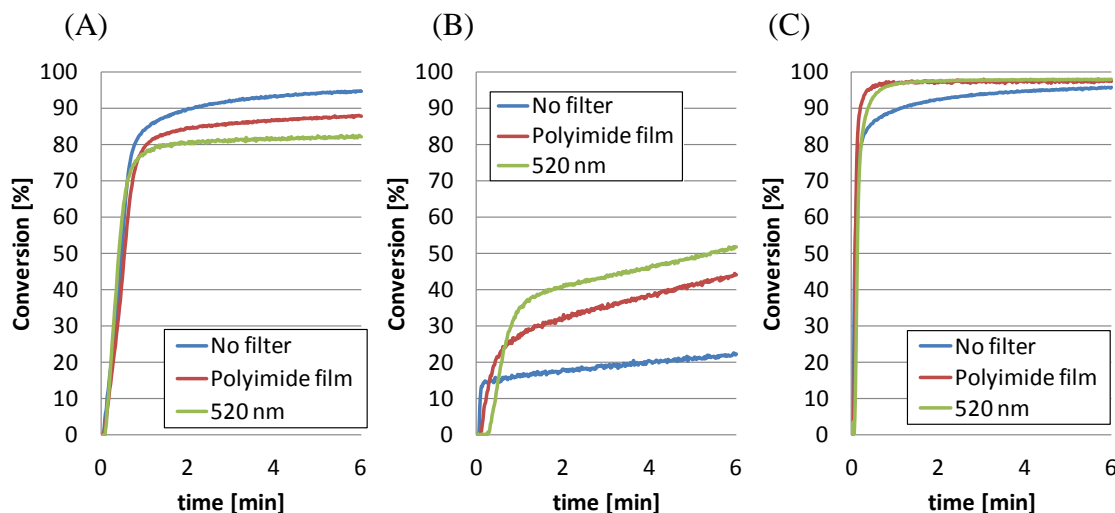


Figure 3-7: Conversion vs. time of two-component systems and a three-component system for three different incident lights: (A) EYss/MDEA two-component system, (B) EYss/DPI two-component system, (C) EYss/MDEA/DPI three-component system. Monomer: HEA. Incident lights: a 150 W xenon lamp with no filter (89 mW/cm^2), a polyimide film (39 mW/cm^2) and a 520 nm bandpass filter (2.4 mW/cm^2).

The shelf life of the EYss/MDEA two-component system and the EYss/MDEA/DPI three-component system was investigated. These samples were made on day zero. Then they were stored in a dark environment at room temperature and their polymerization was studied on successive days using RT-FTIR spectroscopy to investigate their shelf life. Figure 3-8 and Figure 3-9 show the time dependence study of both the two-component system and three-component system using the Xe lamp with and without a 520 nm bandpass filter. Regarding the two-component system, despite the change in initial conversions with the passage of time, the conversion profiles over several days of study are not so different. Therefore, it can be concluded that the shelf life of this system is longer than two months at room temperature. As for the three-component system, a dramatic change of conversion profiles occurs by day 7, especially when illuminated by 520 nm light. Hence, the shelf life of this three-component system cannot be guaranteed longer than one week at room temperature.

In order to extend this shelf life, electron donors, such as 1, 4-diazabicyclo [2.2.2] octane, 1-azabicyclo [2.2.2] octane and N, N-diisopropyl-3-pentylamine, were introduced in a previous study³⁸ due to proton-transfer inhibition. However, through the study of this system, which is described in APPENDIX 2, it was concluded that the use of 1, 4-diazabicyclo [2.2.2] octane instead of MDEA does not achieve a longer shelf life. In fact, the shelf life got worse compared to the EYss-MDEA-DPI three-component system. On the other hand, if ethyl 4-(dimethylamino)benzoate was used instead of MDEA, though photopolymerization became slow, the shelf life became longer (APPENDIX 2). Therefore, the selection of electron donor (amine) is one of the important keys for three-component systems to achieve high photopolymerization and long shelf life.

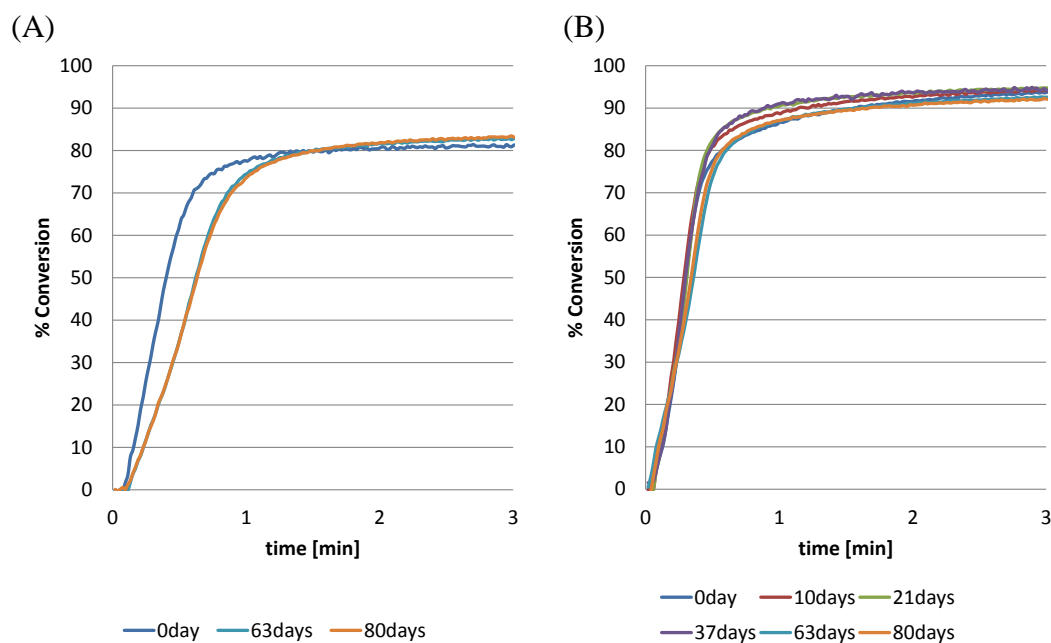


Figure 3-8: Time dependence of the EYss/MDEA two-component system conversion profiles: (A) with 520 nm bandpass filter (light intensity: 2.4 mW/cm²) and (B) without bandpass filter of a 150 W Xe lamp (light intensity: 89mW/cm²). Monomer: HEA.

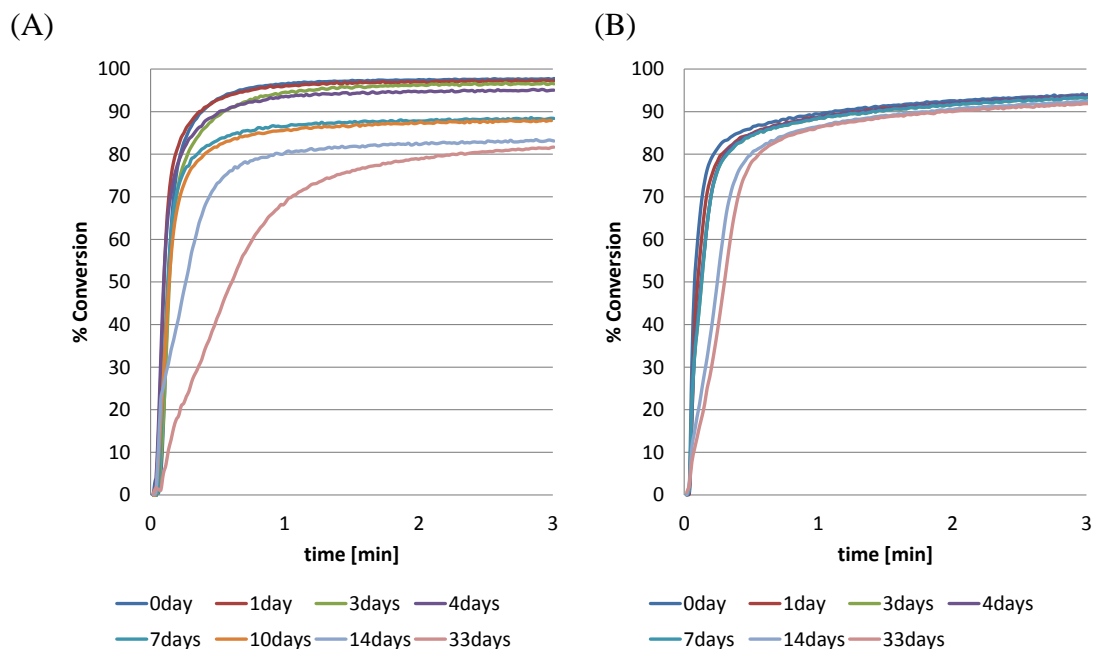


Figure 3-9: Time dependence of the EYss/MDEA/DPI three-component system conversion profiles: (A) with 520 nm bandpass filter (light intensity: 2.4 mW/cm^2) and (B) without bandpass filter of a 150 W Xe lamp (light intensity: 89 mW/cm^2). Monomer: HEA.

3.3.2. Study of Heat Effects for EYss-MDEA Two-Component and EYss-MDEA-DPI Three-Component Systems

To investigate the reactions under the dark condition that result in a shorter shelf life time for the three-component system, differential scanning calorimetry (DSC) (DSC-7, PerkinElmer) was used to characterize the stability as a function of temperature for the HEA monomer with and without the components under dark conditions. Using an experimental heat flow program that had a heating rate of $2^\circ\text{C}/\text{min}$ over a temperature range of $25\text{--}100^\circ\text{C}$, two consecutive DSC scans were obtained for each sample. For each measurement, a characteristic heat flow profile was obtained by subtracting the profile of the second run from the profile of the first run. If thermally-induced polymerization begins to occur, the heat flow profile exhibits exothermic heat flow as a function of temperature.

Figure 3-10 shows the heat flow profiles as a function of temperature for the HEA monomer with zero-, single-, two-, and three-component systems respectively. Obviously, only formulations containing MDEA-DPI (orange and gray lines) cause polymerization in this temperature range because other species demonstrate a similar trend that results in no reaction. Therefore, it can be assumed that the combination of MDEA and DPI in the three-component system causes a reaction under dark condition. As a result, the MDEA/DPI shortens the shelf life compared to the EYss/MDEA two-component system. This thermal reaction is assumed as in Figure 3-11. In the reaction, MDEA transfers an electron to DPI and releases a proton subsequently, thus generating an active center D^\bullet . At the same time, the reaction of DPI involves electron transfer from MDEA to an iodonium cation, followed by rapid decomposition of a neutral iodonium radical, which is also an active radical. It is worth noting that, if this three-component photoinitiator system is employed in thick cure systems such as 3 mm thick samples³⁹, the reaction between MDEA and DPI is not negligible because the temperature rises sharply during polymerization due the heat evolved in its polymerization.

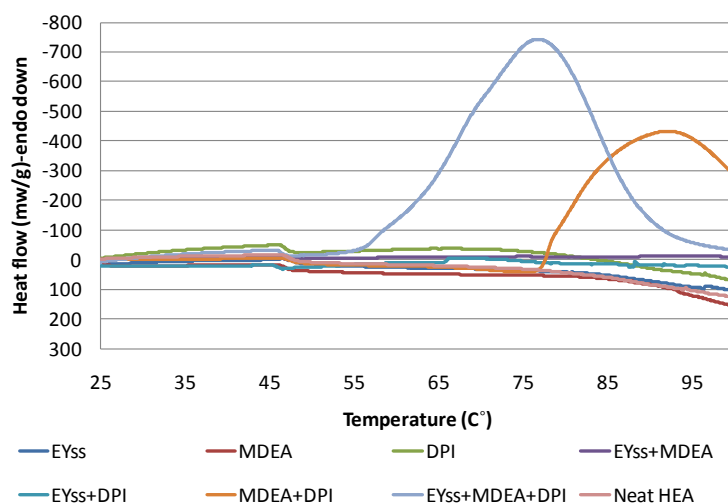


Figure 3-10: DSC heat flow (with the second run subtracted from the first run) as a function of temperature for HEA with EYss, MDEA, DPI, EYss-MDEA, EYss-DPI, MDEA-DPI, EYss-MDEA-DPI, or without species. [EYss] = 0.00115 M, [MDEA] = 0.32 M, [DPI] = 0.0023 M.

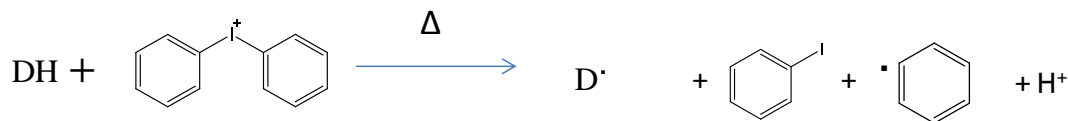


Figure 3-11: Suggested reaction scheme between MEDA and DPI.

3.3.3. A Solution to Achieve High Photopolymerization and Long Shelf Life for EYss/MDEA/DPI Three-Component System

Recently, we found a solution to achieve high photopolymerization and long shelf life at the same time with the EYss/MDEA/DPI three-component system. Figure 3-12 demonstrates the relatively evaluated score of photopolymerization (column “Cure” in the figure) and shelf life (column “Life” in the figure) for various MDEA and DPI concentration combinations, where the concentration of EYss is constant (0.00115 M). As shown in the figure, it is obvious that the concentration balance between MDEA and DPI is important to achieve high photopolymerization and long shelf life at the same time. Finally, two EYss/MDEA/DPI systems which show high photopolymerization reactivity and a long shelf life after two months of storage in the dark were found as shown in Figure 3-13. One of the significant reasons for the short shelf life of three component systems should be the consumption of DPI or MDEA during storage. Relatively low concentrations of DPI (or MDEA) can be consumed in the dark by the reaction between DPI and MDEA that results in too low a concentration of DPI (or MDEA) to achieve effective photopolymerization after storage. However, still the mechanism of this relationship between photopolymerization and shelf life is unclear. Therefore, further study is desired to clarify the mechanism to design three-component systems which achieve both high photopolymerization and long shelf life.

		MDEA									
		0		0.008		0.032		0.096		0.32	
DPI	0	1	5			2	5			3	5
	0.00115					2					
	0.0023	2	5			4				5	2
	0.0115					5	4	5	5		
	0.023	3		3		5	3	5	5		
		Cure	Life	Cure	Life	Cure	Life	Cure	Life	Cure	Life

Score	
Excellent	5
Good	4
Fair	3
Bad	2
Fail	1

Figure 3-12: Evaluation of photopolymerization and shelf life for various concentration combinations of EYss/MDEA/DPI three-component system. [EYss] = 0.00115 M.

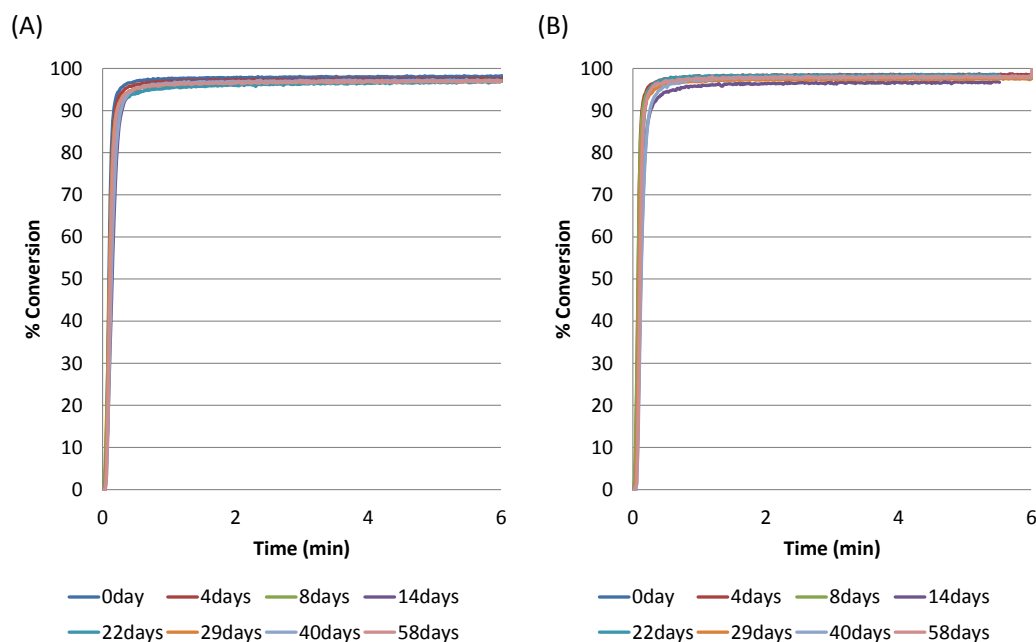


Figure 3-13: Stable time dependence of EYss/MDEA/DPI three-component systems conversion profiles achieved by controlling concentration combinations. Light source: 520 nm LED, light intensity: 4 mW/cm². (A) EYss = 0.00115 M, MDEA = 0.096 M, DPI = 0.023 M. (B) EYss = 0.00115 M, MDEA = 0.096 M, DPI = 0.0115 M.

3.4. Conclusion

In this contribution, various two-component systems with a fixed electron donor, MDEA, and dyes were screened to find effective visible-light induced photoinitiator systems. As a result, dyes that attain high conversions are all xanthenes, including

EYss. Therefore, EYss containing photoinitiator systems were focused on. Namely, the EYss/MDEA two-component system and EYss/MDEA/DPI three-component system were characterized using RT-IR and DSC for photopolymerization behavior and stability. Although three-component systems demonstrated better photopolymerization ability compared to two-component systems, their shelf life was much shorter due to the thermal reaction between MDEA and DPI. However, by optimizing the concentration of MDEA and DPI, both high photopolymerization and long shelf life (more than two months) with EYss/MDEA/DPI three-component system was achieved.

CHAPTER 4. EXTENT OF FREE-RADICAL SHADOW CURE

4.1. Introduction

Photopolymerization has received considerable attention due to its environmental and processing advantages^{1, 40}. Compared to traditional thermal polymerization processes, light-induced polymerization offers reduced volatile organic compound emissions, lower energy requirements, and shorter cure times. Furthermore, light sources are generally much more compact than ovens and autoclaves that are used for thermal cure. For these reasons, photopolymerization can be used not only for the replacement of conventional thermal processes but also for new systems and applications. In addition, the recent development of initiators for visible-light-induced photopolymerization enables processes based upon inexpensive light sources and lower energy photons which are not damaging to biological tissues and cells. Due to these advantages, visible-light-induced photopolymerization has been employed for various applications including coatings, adhesives, and printing. Despite these advantages, the inability to cure shaded regions which are inaccessible to the initiating light is a limitation for many applications. If this disadvantage is overcome a number of new applications of photopolymerization could emerge, such as three-dimensional adhesives²¹, optical impact films²², solar-light-induced coatings, and pigmented systems.

In photopolymerization systems, the term “shadow cure” may be defined as polymerization which extends into regions which are not illuminated by the incident initiating light source. Dual-cure systems containing both photoinitiators and thermal initiators for thick shadow cure are well known^{23, 24}; however, shadow cure in systems containing only photoinitiators has only recently been reported by Ficek *et al*²⁵. These authors demonstrated cationic photopolymerizations of thick systems in which polymerization could occur in shadow regions due to the mobility of the long-lived cationic active centers. Although this method could be attractive for some systems and

applications, it has a number of limitations. It may only be applied to cationically polymerizable monomers, exhibits relatively slow cure rates compared to free radical systems, and the photo-generated protons may be corrosive to electronic devices. Therefore, in this contribution, shadow cure in free radical photopolymerizations initiated using two-component and three-component photoinitiators is investigated.

Multi-component photoinitiator systems are commonly employed for visible-light-induced photopolymerization. The energy of a visible photon is generally lower than the bond dissociation energy of most organic molecules; therefore, visible-light-induced photoinitiator systems are primarily two-component photoinitiator systems in which the active centers are produced via an electron transfer followed by a proton transfer from the electron donor (typically an amine) to the excited photosensitizer.¹ Many dyes and other compounds that absorb in the visible range have been used as the photosensitizer in this type of a system, including camphorquinone, (thio)xanthone derivatives, (thio)xanthene derivatives and ketocoumarin derivatives.^{14, 41-45} In order to enhance the electron transfer system by adding other reaction schemes including diphenyl iodonium chloride (DPI) into these two-component photoinitiator systems, three-component photoinitiator systems have been developed and investigated as well.^{3, 16-20, 46-48}

The objective of this study is to evaluate the use of fluorescent additives for polymerization in masked regions that are unilluminated by the incident initiating light. In this method, the absorption of light by fluorescent additives leads to emission of fluorescent light at longer wavelengths in all directions. Therefore, careful selection of the combination of the incident wavelength, the fluorescent additive, and the photosensitizer can lead to effective illumination and polymerization in shaded regions that are inaccessible to the incident light source. In this study, two different fluorescent dyes are investigated: fluorescein (FL) and eosin Y spirit soluble (EYss). Each of these dyes may form free radical active centers in two-component initiator systems containing N-methyldiethanolamine (MDEA), or three component initiator systems containing

MDEA and DPI. A systematic series of studies was performed to characterize the effects of fluorescence intensity, the incident light intensity, and the presence of a diphenyl iodonium salt on the observed degree of shadow cure.

4.2. Experimental

4.2.1. Materials

A monomer mixture of 50wt% 2-hydroxyethyl acrylate (Sigma-Aldrich) and 50 wt% 1,6-hexanediol diacrylate (Sartomer) was used in these experiments. This monomer mixture was selected because it dissolves photoinitiators well and leads to a rigid, highly crosslinked polymer. The multi-component photoinitiator system materials FL, EYss, benzophenone (BP), MDEA, and DPI were obtained from Sigma-Aldrich. The molecular structures are displayed in Figure 4-1. The absorbance and fluorescence emission spectra of EYss and FL dyes are illustrated in Figure 4-2. The dyes chosen for this study have potential for fluorescence-derived shadow cure since there is overlap between the absorbance and emission spectra. For example, the fluorescein absorbance and emission spectra overlap at wavelengths between 475 nm and 510 nm, and the eosin Y absorbance and emission spectra overlap at wavelengths between 500 nm and 550 nm. At dye concentrations higher than 10^{-5} M, the dyes exist primarily as dimers, and the dimer formation is evident from the UV-visible absorption spectrum. For example, in the spectrum of fluorescein, the unassociated dye exhibits its maximum absorbance at a wavelength of 480 nm, and the formation of the associated dye (dimer) leads to appearance of a blue-shift with a maximum absorbance at 451 nm⁴⁹. Similarly, in the spectrum of eosin Y, the unassociated dye exhibits its maximum absorbance at a wavelength of 533 nm, and the formation of the associated dye (dimer) leads to appearance of a minor blue-shifted contribution at 495 nm⁴⁹⁻⁵¹. At the concentration used for the shadow cure experiments (1.15×10^3 M), the maximum molar absorption coefficients (Napierian molar absorptivity) are 1,144 L/mol-cm at 451 nm wavelength for

FL, and 28,918 L/mol-cm at 533 nm wavelength for EYss. Benzophenone has relatively low absorptivity above 300 nm wavelength and its molar absorption coefficient at 350 nm wavelength is 232 L/mol-cm. Note that the MDEA and DPI absorb only in the deep ultraviolet region of the spectrum and do not affect the absorption profile for wavelengths above 300 nm.

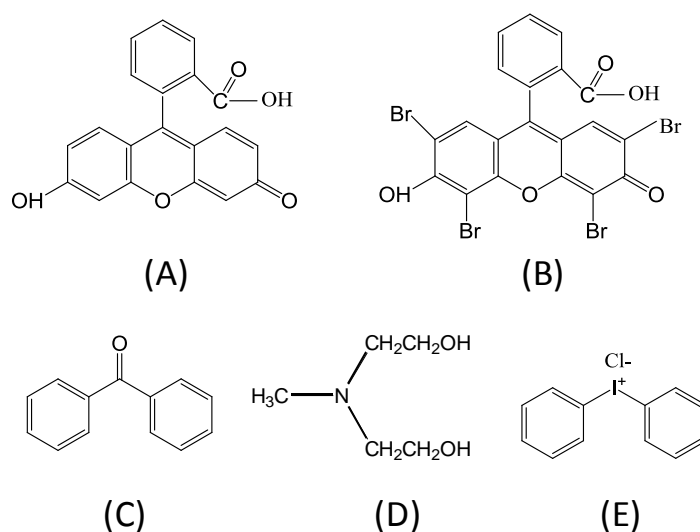


Figure 4-1: Chemical structures of (A) fluorescein (FL), (B) eosin Y spirit soluble (EYss), (C) benzophenone (BP) (D) N-methyldiethanolamine (MDEA), (E) diphenyl iodonium chloride (DPI).

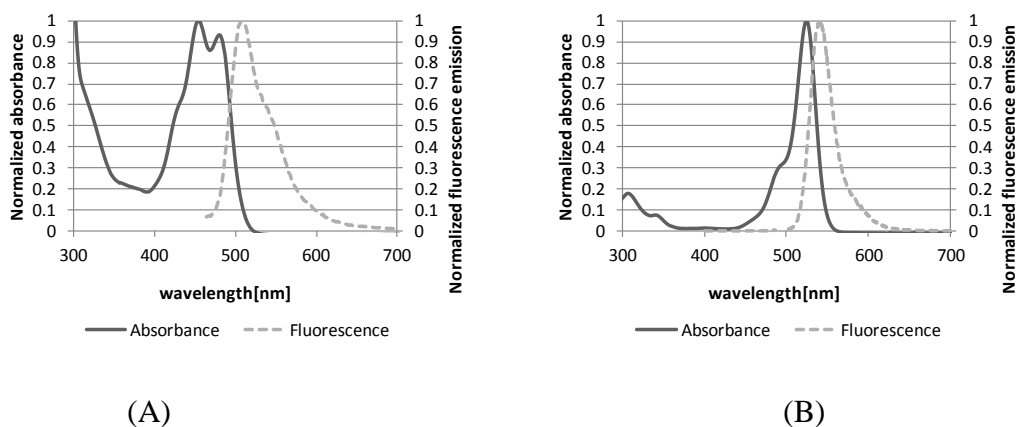


Figure 4-2: Absorbance and fluorescence emission spectra of (A) fluorescein (FL) and (B) eosin Y spirit soluble (EYss).

4.2.2. Shadow Cure via Photopolymerization

Shadow cure experiments were performed in the simple reaction geometry shown in Figure 4-3. The mask was a 500 μm thick steel plate with a 6 mm diameter hole through which the HEA-HDDA monomer mixture was illuminated using a 150 W xenon lamp (MAX-150, Asahi Spectra). Various multi-component photoinitiator systems including dye/amine systems and dye/amine/DPI systems were used to photopolymerize 100 μm thick HEA-HDDA monomer films. The compositions of the photoinitiator systems are summarized in Table 4-1. The monomer mixture containing the photoinitiator was sandwiched between the steel plate on the top surface and a quartz cover slip on the bottom surface. A 100 μm thick spacer (PET film) was used to ensure a uniform film thickness for all experiments. The hole in the steel plate was capped by a 37 μm thick PET film to avoid the influence of oxygen inhibition. Finally, the entire system was placed on a black stage to prevent reflection from the bottom and was illuminated from the top-down for fifteen minutes. The xenon lamp emits in a broad region between 350 nm and 760 nm, and the total incident light intensity at the surface of a sample was measured by a USB 4000 UV-VIS fiber optic spectrometer (Ocean Optics).

Table 4-1: Molar concentration of components in the photoinitiator systems under investigation

Systems	Dyes			Amine	Iodonium salt
	BP (M)	FL (M)	EY _{ss} (M)	MDEA (M)	DPI (M)
BP/MDEA	0.00115	-	-	0.32	-
FL/MDEA	-	0.00115	-	0.32	-
EY _{ss} /MDEA	-	-	0.00115	0.32	-
FL/EY _{ss} /MDEA	-	0.00115	0.00115	0.32	-
FL/MDEA/DPI	-	0.00115	-	0.32	0.0023
EY _{ss} /MDEA/DPI	-	-	0.00115	0.32	0.0023

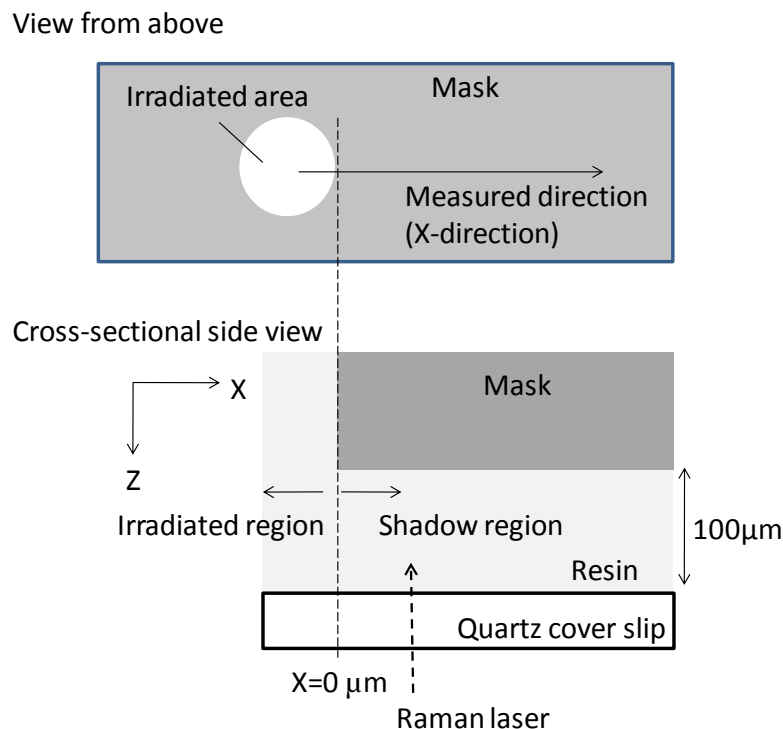


Figure 4-3: Schematic of the experimental geometry for the shadow cure studies. The mask was a 500 μm thick steel plate with a 6 mm diameter hole through which the monomer mixture was illuminated from above. After illumination of the prescribed duration, Raman microscopy was used to collect line (x-direction) and depth (z-direction) conversion profiles through the quartz cover slip on the bottom of the sample.

4.2.3. Characterization of Shadow Cure

The monomer conversion in the shadow regions behind the steel plate were investigated through a quartz cover slip. As shown in Figure 4-3, the line (x-direction) and depth (z-direction) conversion profiles of the cured samples were measured using Raman microscopy. Raman spectra of the samples were collected using a Leica DMLP optical microscope with confocal optics attached to the modular Raman spectrograph (HoloLab 5000R, Kaiser Optical Systems, Inc.) equipped with a 785 nm laser⁵²⁻⁵⁴. Note that the 785 nm laser does not cause photopolymerization for all samples. A combination of a 785 nm single mode excitation fiber, 100 μm collection fiber, and 100 \times objective with numerical aperture equal to 0.9 was employed in the measurement. The laser

intensity through the 100× lens was 7–12 mW/cm², measured by a laser power meter. For each measurement, the exposure time was set to 20–60 seconds with one accumulation in order to optimize the signal-to-noise ratio. The reactive C=C peak at 1640 cm⁻¹ and an unchanging reference peak at 1720 cm⁻¹ (attributed to the C=O carbonyl stretch) were monitored to determine the acrylate conversion. The conversion was calculated using the ratio of reactive (A_{rxn}) peak and internal reference (A_{ref}) peak areas:

$$\% \text{ Conversion} = \left[1 - \frac{A_{\text{rxn}}(\text{p})/A_{\text{ref}}(\text{p})}{A_{\text{rxn}}(\text{u})/A_{\text{ref}}(\text{u})} \right] \times 100 \quad \text{Equation 4-1}$$

where “u” refers to unpolymerized and “p” to polymerized resin.

The conversion profiles in the x-direction, perpendicular to the edge of the illuminated region, were measured by performing a line scan. The conversion profile beginning in the illuminated region and extending into the shadow region was characterized by taking measurements at 40 μm increments for distances up to 5,000 μm from the illuminated edge. The precision of the conversion measurements was generally ±3%. Confocal Raman spectroscopy was used to verify that the conversion was uniform across the thickness of the sample (the z-direction). This result is not surprising due to the relatively small thickness of this illuminated region. Therefore, only the line profiles in the x-direction, perpendicular to the edge of the illuminated region, will be considered in the remainder of this chapter.

4.3. Results and Discussion

4.3.1. Shadow Cure with Dye/Amine Photoinitiator Systems

Figure 4-4 contains plots of the conversion profiles in the x-direction, perpendicular to the edge of the illuminated region for four different photoinitiator systems: BP/MDEA, FL/MDEA, EYss/MDEA, and FL/EYss/MDEA. In this figure, the origin occurs at the illuminated edge; therefore, negative values of the abscissa correspond to the illuminated region. The conversion in the illuminated region was

relatively constant; therefore, only the first 200 μm are shown in the figure. For all four initiator systems, the conversion in the illuminated region is above 70%. The figure illustrates that, as the scanned position moves away from the boundary ($x=0$), the conversion decreases at a rate that depends upon the initiator system. For example, the conversion of the BP/MDEA system decreases to a value of zero in approximately 500 μm , while at 500 μm the FL/MDEA and EYss/MDEA systems exhibit conversions of 40% and 64%, respectively. The data in Figure 4-4 illustrate that the photoinitiator system used for the experiment has a marked effect on the observed degree of shadow cure, and that the systems exhibit the following trend: BP/MDEA < FL/MDEA < EYss/MDEA < FL/EYss/MDEA. Note that for the EYss/MDEA, even at the distance of 1,000 μm from the illuminated edge, the conversion is approximately 60%.

The shadow cure in the masked region illustrated in Figure 4-4 could arise from a number of effects, including scattering of the incident light, reflection from the quartz cover slip at the bottom surface, or diffusion of active centers into the shadow region. The shadow cure observed for the BP/MDEA system likely arises only from these effects since BP emits negligible fluorescence. For systems containing fluorescein or eosin Y spirit soluble, fluorescence light from the dyes may also enhance the shadow cure since dye molecules that absorb light in the illuminated region will fluoresce in all directions. Absorption of this fluorescent light by dye molecules in the shadow region may lead to active center generation. The dyes chosen for this study have potential for fluorescence-derived shadow cure since there is overlap between the absorbance and emission spectra. For example, the fluorescein absorbance and emission spectra overlap at wavelengths between 475 nm and 510 nm (see Figure 4-2), and the emission spectrum of fluorescein overlaps with the absorbance spectrum of eosin Y at wavelengths between 475 nm and 550 nm. Similarly, the eosin Y absorbance and emission spectra overlap at wavelengths between 500 nm and 550 nm.

The shadow cure trends illustrated in Figure 4-4 are consistent with the hypothesis that fluorescent light from the dyes leads to active center generation in the shadow region. Benzophenone exhibits negligible fluorescence, and, thus, the profile obtained for the BP/MDEA system provides a “control” experiment to which the fluorescent systems can be compared. Interestingly, other fluorescence-free photoinitiators such as bis(2,4,6-trimethylbenzoyl)-phenylphosphine oxide and 1-hydroxy-cyclohexyl-phenyl-ketone yielded similar conversion profiles. For the FL/MDEA and EYss/MDEA systems, the total intensity of fluorescent light was calculated from first principles^{55, 56} based upon the concentration of the dye, sample thickness, the intensity and spectrum of the incident light, the absorbance spectra of the respective dyes, and the fluorescence quantum yield. Note that the dyes exist primarily as associated dimers at the concentration used for the shadow cure experiments (1.15×10^3 M). Therefore, the molar absorptivity coefficients of the dimers must be used.⁴⁹⁻⁵¹ This calculation revealed that the fluorescent light generated by eosin Y was 7.8 times more intense than the fluorescent light generated by fluorescein. Despite the high fluorescence quantum yield of fluorescein (0.83⁵⁵), the fluorescence emission into the shadow region for the FL/MDEA system is low compared to that of EYss/MDEA due to the low molar absorption coefficient of fluorescein. Note that, for the FL/EYss/MDEA system containing both dyes, the data in Figure 4-4 illustrate that there is a small enhancement of the observed shadow cure compared to the EYss/MDEA system. This implies that FL can work not only as a multi-component photoinitiator with MDEA but also as a photon carrier which excites EYss in the shadow region by virtue of its fluorescence emission.

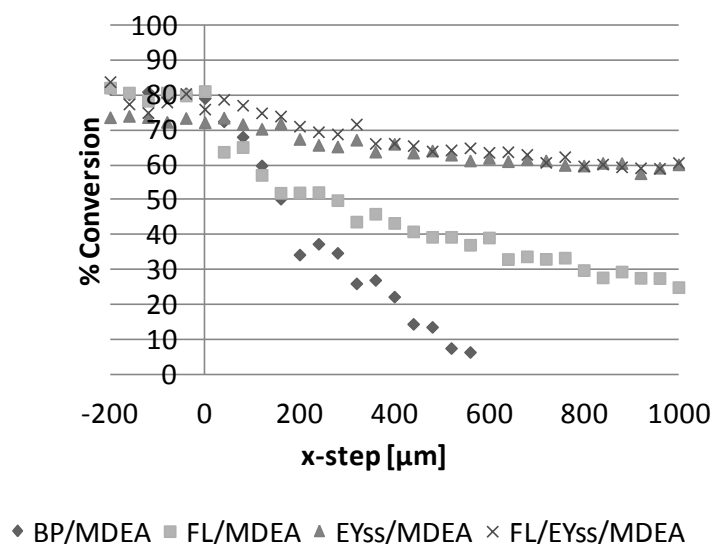


Figure 4-4: Shadow cure conversion profiles (x-direction) resulting from four different dye/amine photoinitiator systems. Negative values of x correspond to the illuminated region, while positive values of x correspond to the masked region. Light source: a 150 W xenon lamp, light intensity: 89 mW/cm^2 , irradiation time: 15 minutes.

Figure 4-5 illustrates the effect of the incident light intensity on the conversion profiles and the observed extent of shadow cure for three different photoinitiator systems: BP/MDEA, FL/MDEA, and EYss/MDEA. The figure illustrates that the extent of shadow cure for the system that does not contain a fluorescent dye (BP/MDEA, Figure 4-5A) does not show any appreciable difference when the light intensity is increased. In contrast, the extent of shadow cure is significantly enhanced for the systems containing the fluorescent dyes (FL/MDEA and EYss/MDEA in Figure 4-5B and C, respectively). In both cases, for the high light intensity (1.0 W/cm^2), the cure in the shadow region is nearly equivalent to that in the illuminated region. It is worth noting that oxygen inhibition is small in these systems because they are not exposed to the atmosphere, and the initially dissolved oxygen is consumed by MDEA active centers through a well-known cyclic reaction⁹. These results suggest that the increased incident light intensity

leads to increased fluorescence intensity, thereby resulting in increased shadow cure for the systems containing the fluorescent dye.

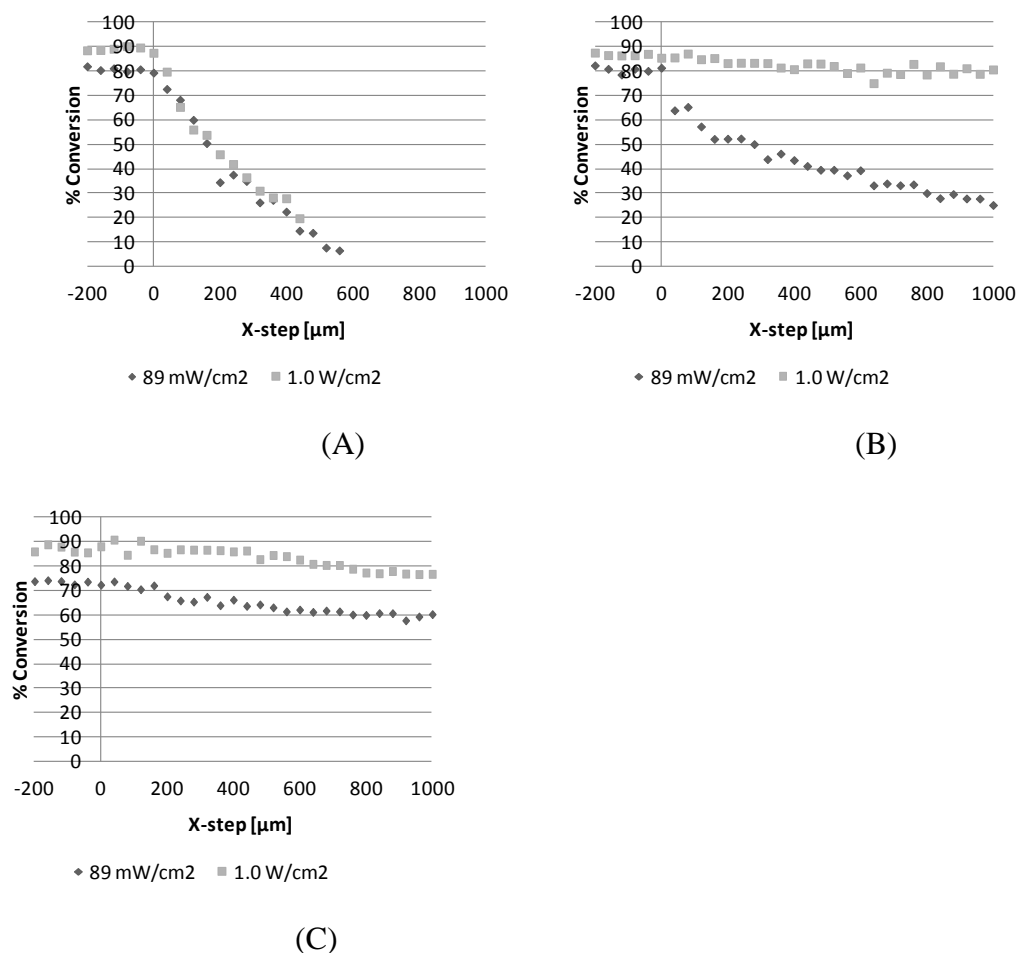


Figure 4-5: The effect of the incident light intensity on the conversion profiles (x-direction) observed for three different dye/amine systems; (A) BP/MDEA, (B) FL/MDEA, (C) EYss/MDEA. Light source: a 150 W xenon lamp, irradiation time: 15 minutes

Figure 4-6 illustrates the dependency of conversion profiles on irradiation time and the observed extent of shadow cure under the Xe lamp exposure with a 1.0 W/cm² light intensity for three different photoinitiator systems: BP/MDEA, FL/MDEA, and EYss/MDEA. The figure shows that the extent of shadow cure for the system that does not contain a fluorescent dye (BP/MDEA, Figure 4-6A) does not show any appreciable

difference after 81 seconds exposure. In contrast, the extent of shadow cure is still enhanced for the systems containing the fluorescent dyes (FL/MDEA and EY_{ss}/MDEA in Figure 4-6B and C, respectively) as the irradiation time increases after 81 seconds exposure. In both cases, by irradiating for enough time (900 seconds), the cure in the shadow region is nearly equivalent to that in the illuminated region. These results suggest that, due to the presence of fluorescent dyes, the shadow region is cured as the fluoresced light is able to reach deeper and deeper into the shadow region with the passage of time, where light from the lamp is unable to.

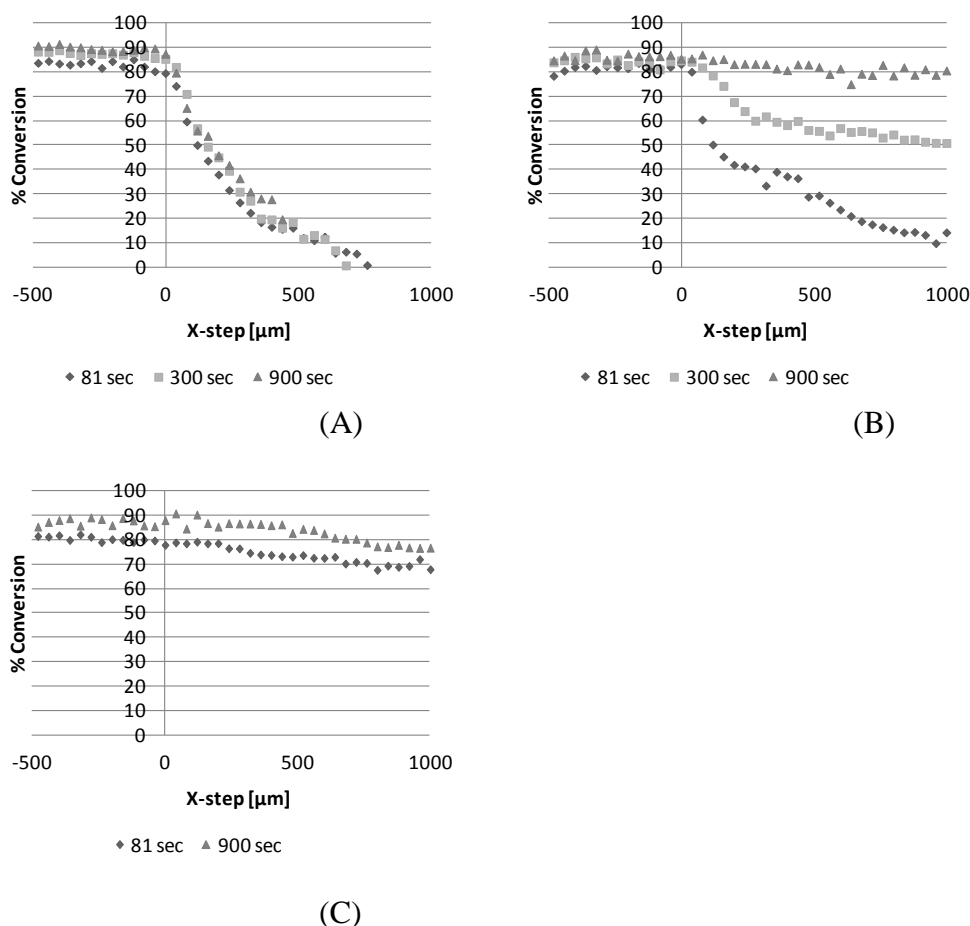


Figure 4-6: The dependency of the conversion profiles (x-direction) on irradiation time observed for three different dye/amine systems; (A) BP/MDEA, (B) FL/MDEA, (C) EY_{ss}/MDEA. Light source: a 150 W xenon lamp, light intensity: 1000 mW/cm².

4.3.2. Shadow Cure with Dye/Amine/DPI Photoinitiator Systems

A series of experiments was performed to investigate the effect of the addition of diphenyl iodonium chloride (DPI) on the shadow cure observed for systems containing MDEA and FL or EYss. Figure 4-7 contains the conversion profiles obtained for the two-component initiator systems (FL/MDEA and EYss/MDEA) and the corresponding three-component photoinitiator systems (EYss/MDEA/DPI and FL/MDEA/DPI). The figure illustrates that the addition of DPI leads to a significant enhancement in the shadow cure observed for both dyes. In both cases, the shadow cure conversion in the shadow region exhibits a relatively high and uniform value for a distance of 1500 μm from the illuminated edge. For the three-component initiator systems, the conversion of a few millimeters into the shadow region is nearly the same as that of the illuminated region.

To explain the effect of DPI on the observed degree of shadow cure, it is useful to consider the reaction mechanism which has been reported in the literature as shown in Figure 4-8^{17, 19}. In this photoinitiator system, the dye in its excited state may react with either MDEA or DPI in the parallel reactions shown in Figure 4-8. As shown in Figure 4-8A, free radical active centers ($\text{D}\bullet$) are produced by the electron transfer reaction from the MDEA (DH) to the excited state of the dye. As shown in Figure 4-8B, DPI oxidizes an excited dye molecule in a reaction that produces two active centers (an MDEA radical and a phenyl radical ($\Phi\bullet$)). Also, the DPI may oxidize nearly any radical species, such as an immobile radical that is trapped in the crosslinked polymer network to produce a mobile active phenyl radical. Finally, as shown in Figure 4-8B, the oxidized dye ($\text{DY}^{+\bullet}$) may be reduced by MDEA to regenerate the dyes – this would enhance the fluorescence effect and produce mobile initiating radicals. In addition, the DPI can enhance the number of effective active centers (free radicals capable of propagating) from the amine/dye reactions by irreversibly oxidizing the $\text{DY}\bullet$ radical, and thereby preventing the back-electron transfer reaction shown in Figure 4-8A. The reduced DPI will, in turn,

dissociate to produce an active phenyl radical. This can be significant since the DY^{\bullet} radical is generally not active for propagation. Therefore, the large impact of DPI on the observed extent of shadow cure likely arises from the effect of DPI increasing both the number of active centers and the mobility of the active centers.

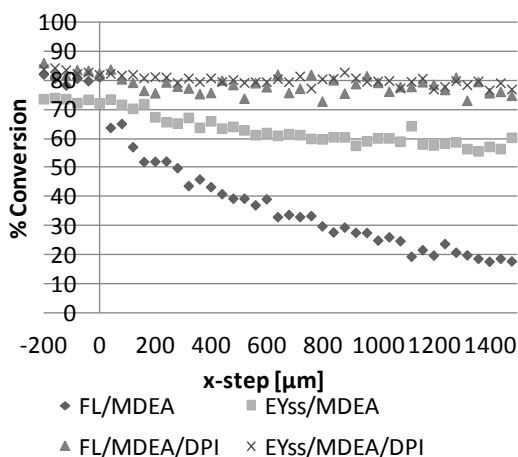


Figure 4-7: Effect of the addition of DPI on the shadow cure conversion profiles (x-direction) observed for FL and EYss dye/amine photoinitiator systems. Light source: a 150 W xenon lamp, light intensity: 89 mW/cm^2 , irradiation time: 15 minutes.

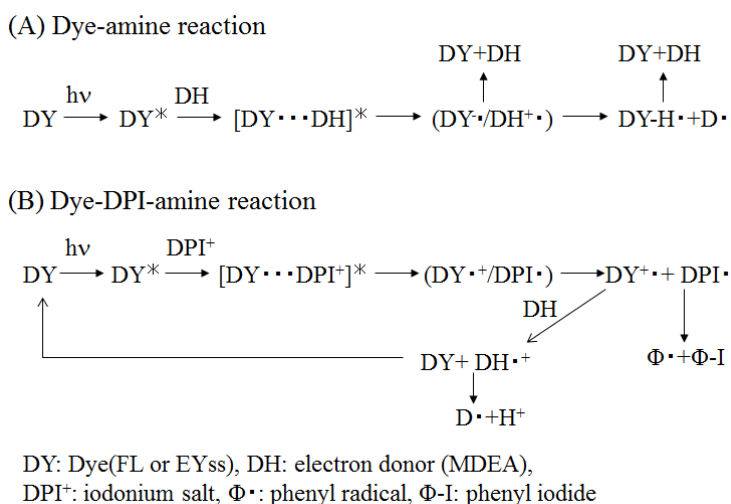


Figure 4-8: Schematic representation of the reaction mechanism for three-component photoinitiator systems containing FL or EYss, MDEA, and DPI. (A) photo-reduction of the FL or EYss dye by MDEA and (B) photo-oxidation of the FL or EYss dye by DPI.

4.3.3. Extent of Shadow Cure to Polymerize Wide Shadow Regions

A series of experiments were performed to investigate the effect of combining DPI and a photon carrier dye (FL) that can excite another dye (EYss) on the shadow cure observed for systems containing MDEA and EYss. Figure 4-9 contains the conversion profiles obtained for the three-component photoinitiator systems (EYss/MDEA/DPI and FL/MDEA/DPI) and the four-component photoinitiator system (FL/EYss/MDEA/DPI). These samples were irradiated for fifteen minutes by the xenon lamp (with a polyimide film attached to it) which emitted a light intensity of 39 mW/cm^2 (see Figure 3-6). As illustrated in Figure 4-9, the addition of FL to the three-component system, EYss/MDEA/DPI, greatly enhanced the observed shadow cure. The new four-component system was able to achieve a conversion of 5 millimeters into the shadow region which is nearly the same as that of the illuminated region, and the three-component systems (FL/MDEA/DPI, EYss/MDEA/DPI) showed a decrease of conversion in the shadow regions at around 3 millimeters.

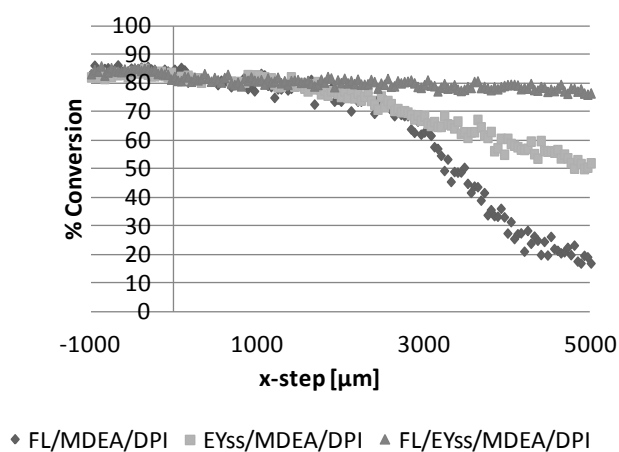


Figure 4-9: Shadow cure conversion profiles (x-direction) resulting from three different dye/amine photoinitiator systems containing DPI. Light source: a 150 W xenon lamp with a polyimide film, light intensity: 39 mW/cm^2 , irradiation time: 15 minutes.

4.4. Conclusions

The experimental results reported in this contribution demonstrate that shadow cure in free radical photopolymerizations of masked systems can be enhanced with the use of fluorescent additives in two- or three-component initiator systems. In this method, the absorption of light by the fluorescent additive leads to emission of fluorescent light at a longer wavelength in all directions, including into the shadow region. Enhanced shadow cure was observed if one or more fluorescent compounds emitted fluorescent light at wavelengths absorbed by the dye in a two- or three-component photoinitiator system as illustrated by the following shadow cure trend: BP/MDEA < FL/MDEA < EYss/MDEA < FL/EYss/MDEA. The addition of DPI to the two-component systems containing MDEA and FL or EYss led to a significant enhancement in the observed shadow cure. This result was attributed to the fact that DPI will increase both the number of active centers and the mobility of the active centers as a result of the electron transfer reactions in which it participates. For example, DPI may oxidize an excited dye molecule in a reaction that produces two active centers; the oxidized dye may be reduced by MDEA to regenerate the dye (thereby enhancing the fluorescence); and DPI may oxidize immobile radicals that are trapped in the crosslinked polymer network to produce mobile active phenyl radicals.

CHAPTER 5. SHADOW CURE IN SHORT CURE TIME

5.1. Introduction

In this chapter, the extent of shadow cure under electrodes of FPCs (flexible printed circuits) for the ACF (anisotropic conductive film) application is investigated. First, using a conventional UV radical photoinitiator 1-hydroxycyclohexyl phenyl ketone (HCPK) which generates radicals via photolysis (Type I photoinitiator), the photocuring potential in shadow regions was evaluated with electrode-embedded polyethylene terephthalate films. In the ACF bonding process, the conversion of the formulation in the shadow region is desired to be high. In order to achieve this, the effect of decreasing oxygen concentration, which dissolves in the monomer resin, to prolong the lifetime of active centers for improved shadow cure was investigated. Next, shadow cure under conditions of visible-light cure with an electrode-embedded polyimide film was studied using visible-light-induced photoinitiator systems that were investigated in chapter CHAPTER 3. In the ACF bonding process, the short cure time is desired, as well as the high conversion in the shadow region. To achieve fast shadow cure using the photopolymerization process, various means including adding thiols or fluorescent additives, changing the process configuration, and increased light intensity were investigated.

5.2. Conversion Profiles under PET-FPC with UV Light

Using the common UV radical photoinitiator HCPK (IRG184, BASF), the photocuring potential in shadow regions was evaluated with a specially-designed film, polyethylene terephthalate – flexible printed circuit (PET-FPC), which is a transparent electrode-embedded PET film (see Figure 5-1). In order to evaluate the extent of the shadow cure, the depth and cross-sectional conversion profiles of the cured sample were measured using Raman microscopy.

5.2.1. Materials and Methods

Because the electrodes imbedded in the substrate are opaque, they serve to shade, or mask, alternating regions of the resulting photopolymer from the initiating light. The PET-FPC was provided by Bridgestone and Figure 5-1 shows the designed sample of the PET-FPC that was used as a substrate in this study through which the 2-hydroxyethyl acrylate (HEA, Sigma Aldrich) monomer resin was photopolymerized using UV light. The electrodes imbedded in the PET-FPC film have $100 \times 100 \mu\text{m}$ ($100 \mu\text{m}$ wide and spaced $100 \mu\text{m}$ apart), $100 \times 50 \mu\text{m}$, $50 \times 50 \mu\text{m}$, and $500 \times 500 \mu\text{m}$ line and space patterns, but only the $100 \times 100 \mu\text{m}$ and $500 \times 500 \mu\text{m}$ patterns were employed.

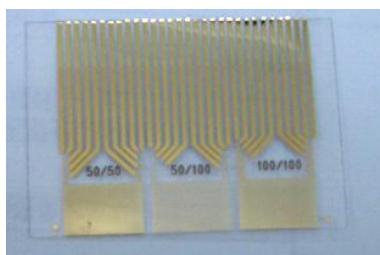


Figure 5-1: Designed PET-FPC film

HCPK was used to photopolymerize $100 \mu\text{m}$ thick HEA films. A droplet of HEA monomer containing 0.0484 M (1 per hundred resin (phr)) HCPK and a $100 \mu\text{m}$ thick spacer (PET film) were laminated between a PET-FPC film on the top surface and a quartz cover slip on the bottom surface. The laminated film was then placed on a polyimide film stage to prevent the reflection from the bottom and illuminated from the top-down using an electrodeless H-bulb UV lamp conveyor (Fusion UV systems). The sample was carried with 1 m/min on the conveyor during the UV exposure. The maximum light intensity and total light energy in the UVA region ($320 \text{ nm} - 390 \text{ nm}$) measured by a UV Power Puck (Electronic Instrumentation and Technology) were 1948 mW/cm^2 and 2.575 J/cm^2 .

The shadow regions behind the electrodes were investigated through the quartz cover slip. As shown in Figure 5-2a, the depth (Z-direction) and cross-sectional (X, Y-direction) conversion profiles of the cured sample were measured using Raman microscopy. This measurement method is described in detail in chapter CHAPTER 4.

5.2.2. Results and Discussion

First, the conversion profiles on the electrodes' surface at the $100 \times 100 \mu\text{m}$ line and space pattern were monitored for every $10 \mu\text{m}$ step in the X-direction using Raman microscopy. Figure 5-2 illustrates the scanned area on the PET-FPC film and its conversion profile. As shown in Figure 5-2b, these shadow regions on the electrodes were fully polymerized at the $100 \times 100 \mu\text{m}$ spacing.

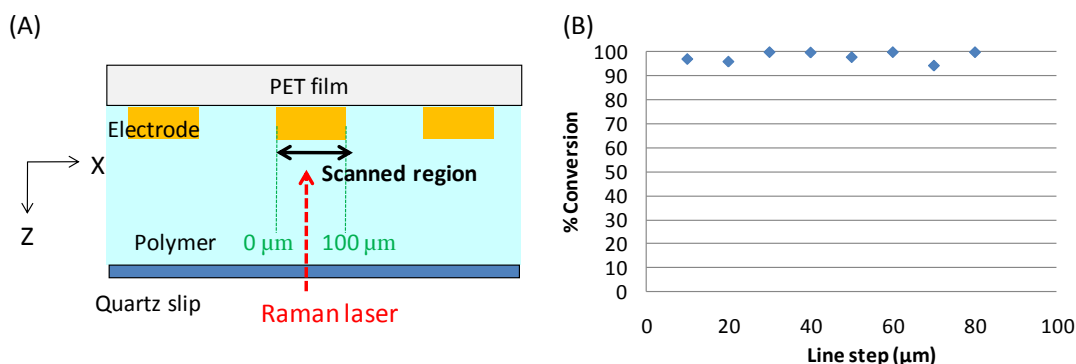


Figure 5-2: Measurement of shadow cure with PET-FPC in x-direction. (A) Scanned area behind an electrode and (B) its conversion profile (X-direction) for 1 phr HCPK at the electrode surface of the $100 \times 100 \mu\text{m}$ line and space PET-FPC film. Monomer: HEA, UV light intensity: 1948 mW/cm^2 , Total UV light energy: 2.575 J/cm^2 .

Then the conversion profiles at the $500 \times 500 \mu\text{m}$ line and space pattern were monitored. Figure 5-3 illustrates the conversion profile on the electrodes' surface that was monitored for every $10 \mu\text{m}$ step in the X-direction. As shown in the graph, unlike the $100 \times 100 \mu\text{m}$ profile, the conversion of the shadow regions has a gradient. As the

scanned position approaches the center of the electrode, its conversion decreases. Hence, although the conversion at the center is still high (higher than 90 %), the shadow regions under the 500 μm electrodes are not uniform and are not fully polymerized. The depth conversion profiles in shadow regions behind an electrode were also studied, as shown in Figure 5-4. The graph shows depth profiles behind an electrode at 50 μm , 100 μm , 150 μm , 200 μm , and 250 μm in the X-direction from the edge of the electrode. The depth profiles were measured every 2.5 μm distance. Corresponding to the result in Figure 5-3, as distance from the edge of the electrode in the X-direction increases, the conversion decreases. In addition, the conversions in the Z-direction are constant. Hence, the shadow regions' polymerization changes in the X-direction, but it does not depend on the depth direction (Z-direction) in these micro-meter scale experiments.

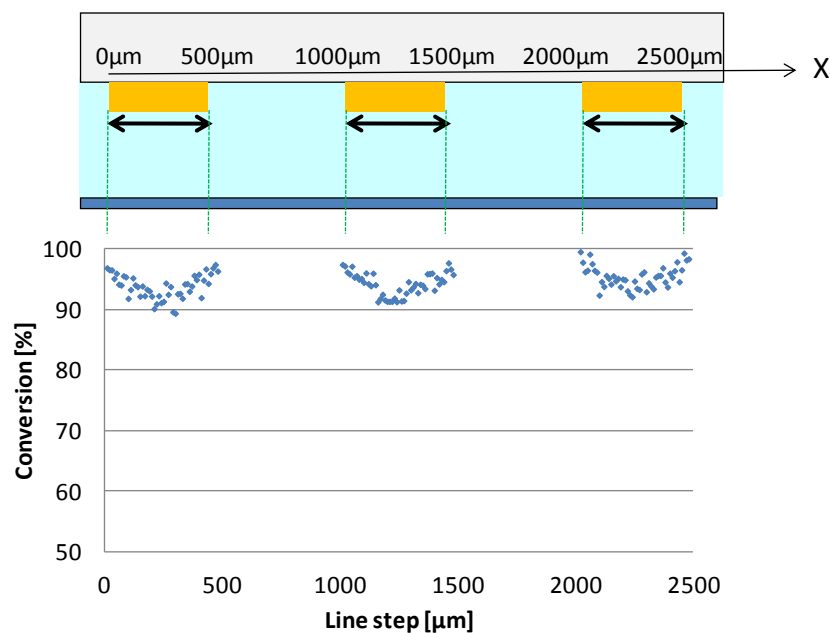


Figure 5-3: Conversion profile (X-direction) for 1 phr HCPK at electrodes' surface of the 500 \times 500 μm line and space PET-FPC film. Monomer: HEA, UV light intensity: 1948 mW/cm^2 , total UV light energy: 2.575 J/cm^2 .

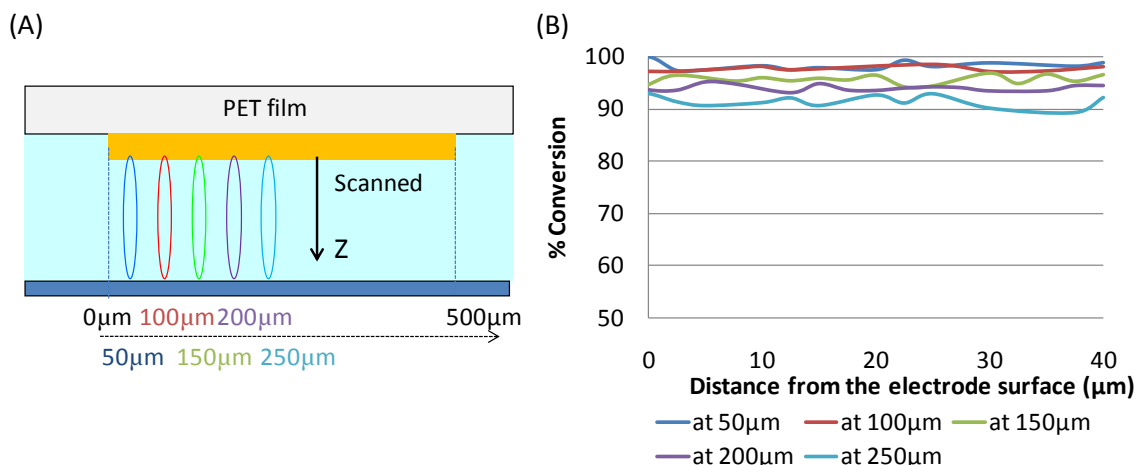


Figure 5-4: Measurement of shadow cure with PET-FPC in z-direction. (A) Scanned depth profiles behind an electrode and (B) depth profiles (Z-direction) for HCPK in the shadow region behind the electrode of the $500 \times 500 \mu\text{m}$ line and space PET-FPC film. Monomer: HEA, UV light intensity: 1948 mW/cm^2 , Total UV light energy: 2.575 J/cm^2 .

5.3. Effect of Decreasing Dissolved Oxygen in Shadow Cure for Type 1 Photoinitiator

In this section, to enhance shadow cure with UV light, the effect of decreasing oxygen to prolong the lifetime of active centers in the monomer was investigated. Gou *et al.*⁷ developed a photochemical method which efficiently consumed oxygen using specially designed additives which comprise of a singlet oxygen generator and a singlet oxygen trapper with a 670 nm light. In these experiments, the singlet oxygen generator was Zinc 2,9,16,23-tetra-tert-buty-29H,31H-phthalocyanine (Zn-ttp) and the singlet oxygen trapper was 9,10-dimethylantracene (DMA). The chemical structures of these additives are shown in Figure 5-5. In this method, molecular oxygen was effectively consumed photochemically before the photopolymerization took place, thereby allowing the reaction to proceed in an oxygen-free environment. The schematic in Figure 5-6 describes the generation of singlet oxygen ($^1\text{O}_2^*$) by reaction of the ground state oxygen with the excited triplet state of the singlet oxygen generator (Zn-ttp). The singlet oxygen

is then consumed by reaction with a second compound, the singlet oxygen trapper (DMA), to form an endoperoxide. This photochemical consumption of molecular oxygen in this manner was shown to significantly increase the polymerization rate for UV photopolymerization in acrylate systems containing photoinitiator 2, 2-dimethoxy-2-phcnylacetophenon.⁷

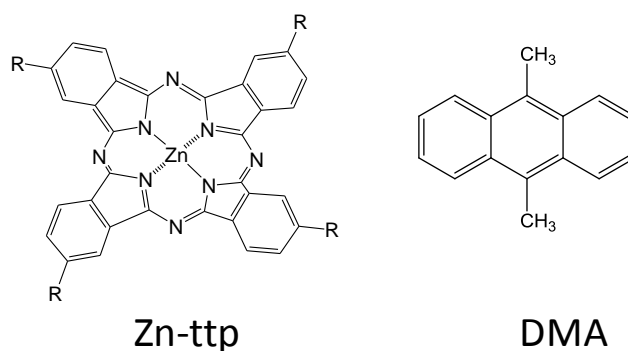


Figure 5-5: Chemical structure of Zinc 2,9,16,23-tetra-tert-butyl-29H,31H-phthalocyanine (Zn-ttp) and 9,10-dimethylanthracene (DMA)

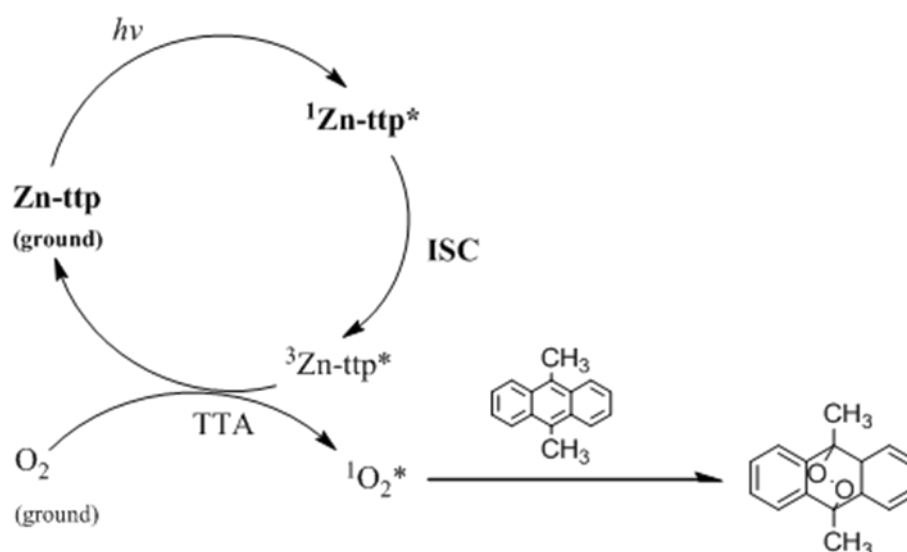


Figure 5-6: Proposed mechanism of the singlet oxygen generation and trapping process.

5.3.1. Materials and Methods

In order to act as the singlet oxygen generator and singlet oxygen trapper, 0.00002M Zn-ttp (Sigma Aldrich) and 0.002M DMA (Sigma Aldrich) respectively were added into the aforementioned HEA system containing 1 phr HCPK (section 5.2.1). In addition to the procedure described in section 5.2.1, a pre-irradiation process was performed using a 150W Xe lamp with a bandpass filter which emitted 670 nm light with a 19.6 mW/cm² light intensity before the UV exposure. The 670 nm light irradiated the sample for five minutes. Immediately afterwards, the sample was irradiated by the UV light (Fusion) and polymerized. Thus the effect of dissolved oxygen on shadow cure was studied. Again DMA, a polynuclear aromatic compound, should readily react with singlet oxygen and produces an endoperoxide in this system.

5.3.2. Results and Discussion

Figure 5-7 illustrates the comparison of the conversion profile (X-direction) for the system without additives and with additives (Zn-ttp and DMA) at the electrodes' surface of the 500 × 500 μm line and space PET-FPC film. As shown in the graph, compared to the system without additives, the system with additives achieves a higher and non-gradient conversion profiles in the shadow regions. Therefore, it is obvious that the procedure comprising of the addition of Zn-ttp, DMA and pre-irradiation is effective in enhancing the extent of shadow cure with UV-light. This indicates that quenching of dissolved oxygen is critical to enhance the polymerization in shadow regions to prolong the lifetime of active centers so that they can reach further into the shadow regions. In other words, the dissolved oxygen in the resin actually disturbs the diffusion of active centers in the shadow regions as oxygen inactivates these active centers. The depth conversion profiles in shadow regions behind an electrode were also studied as shown in Figure 5-8. The graph shows depth profiles behind an electrode at 50 μm, 100μm, 150μm, 200μm, and 250 μm in the X-direction from the edge of the electrode. The depth profiles

were measured every 2.5 μm distance. The graph shows that all of the conversions in the Z-direction are constant and high.

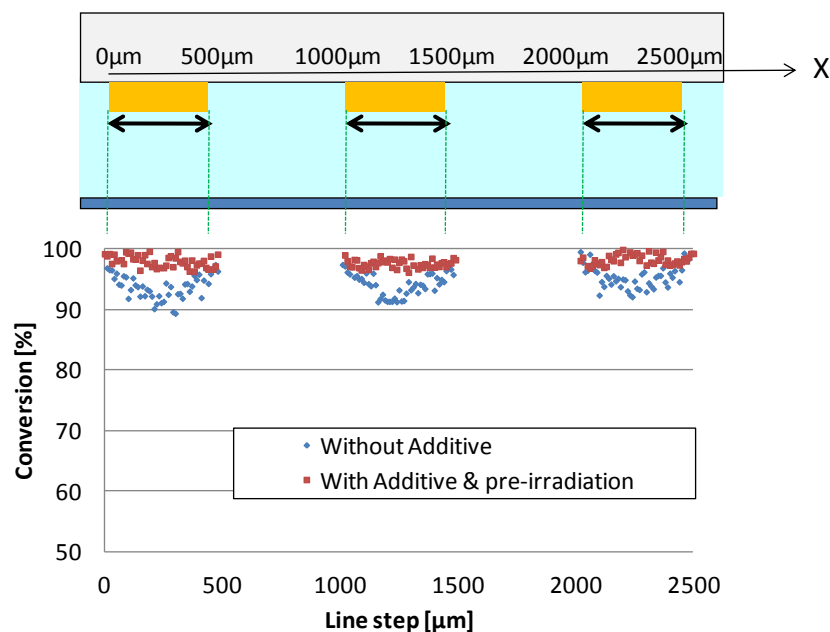


Figure 5-7: Comparison of conversion profile (X-direction) for the system without additives and with additives (0.00002M Zn-ttp and 0.002M DMA) at electrodes' surface of the $500 \times 500 \mu\text{m}$ line and space PET-FPC film. The system with the additives was pre-irradiated by a Xe lamp with 670 nm bandpass filter (light intensity: 19.6 mW/cm^2 , irradiation time 300 seconds). Monomer: HEA; UV light source: Fusion lamp; UV light intensity: 1948 mW/cm^2 , Total UV light energy: 2.575 J/cm^2 .

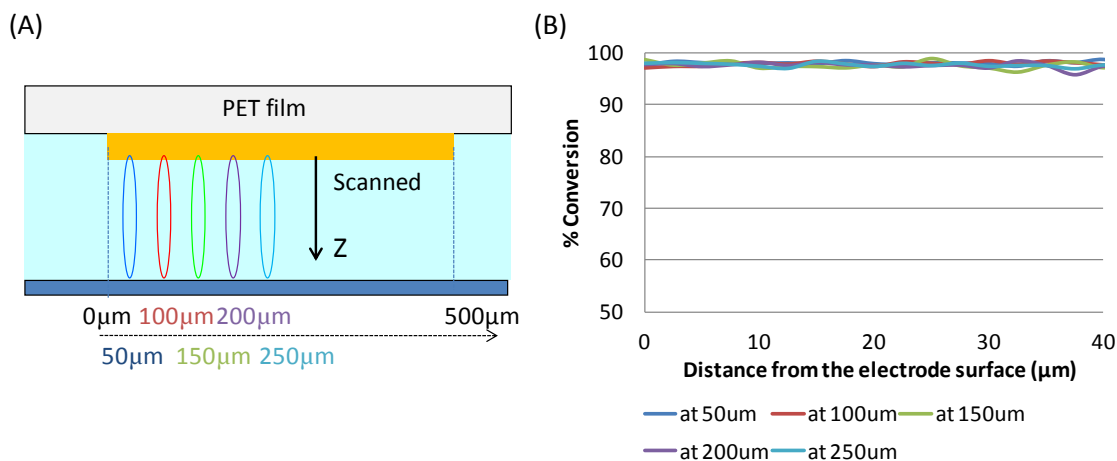


Figure 5-8: Measurement of shadow cure with PET-FPC in z-direction. (A) Scanned depth profiles behind an electrode and (B) depth profiles (Z-direction) for the system with additives (0.00002M Zn-ttp and 0.002M DMA) in the shadow region behind the electrode of the $500 \times 500 \mu\text{m}$ line and space PET-FPC film. The sample was pre-irradiated by a Xe lamp with 670 nm bandpass filter (light intensity: 19.6 mW/cm^2 , irradiation time 300 seconds). Monomer: HEA; UV light source: Fusion lamp, UV light intensity: 1948 mW/cm^2 , Total UV light energy: 2.575 J/cm^2 .

5.4. Conversion Profiles under PI-FPC with Visible Light

Using the EYss/MDEA (eosin Y spirit soluble/N-methyldiethanolamine) visible-light-induced photoinitiator system, the photocuring potential in shadow regions was evaluated with a specially-designed film, PI-FPC film, which is an electrode-embedded polyimide film (see Figure 5-9). Similar to section 5.2, the depth and cross-sectional conversion profiles of the cured sample were determined using Raman microscopy.

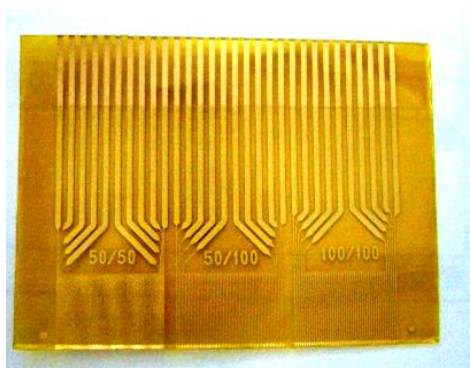


Figure 5-9: Designed PI-FPC film

5.4.1. Materials and Methods

A PI-FPC film with the same line and space patterns as the PET-FPC film used above was employed as a substrate in this study. Through the PI-FPC films, HEA resins were photopolymerized with visible light. An EYss/MDEA two-component photoinitiator system ($[EYss] = 0.00115 \text{ M}$, $[MDEA] = 0.32 \text{ M}$) was used to photopolymerize 100 μm thick HEA films. A droplet of HEA monomer containing EYss/MDEA and a 100 μm thick spacer (PET film) were laminated between a PI-FPC film on the top surface and a quartz cover slip on the bottom surface. The laminated film was then placed on a black stage to prevent the reflection from the bottom and illuminated from the top-down using a 150 W xenon (Xe) lamp (MAX-150, Asahi Spectra) for fifteen minutes. The light emitted a wide region of visible wavelength and its total light intensity was 89 mW/cm^2 . Note that the polyimide within PI-FPC filters light such that the light which actually irradiates the resin under the PI-FPC is attenuated (see Figure 3-6). The shadow regions behind the electrodes were investigated through the quartz cover slip. As shown in Figure 5-10a, the depth (Z-direction) and cross-sectional (X, Y-direction) conversion profiles of the cured sample were measured using Raman microscopy.

5.4.2. Results and Discussion

The conversion profiles on the electrodes' surface at the $500 \times 500 \mu\text{m}$ line and space pattern were monitored for every 10 μm step in the X-direction using Raman microscopy. Figure 5-10 illustrates the scanned area on the PI-FPC film and its conversion profile. As shown in Figure 5-10B, the conversions are uniform in this shadow region unlike the result of section 5.2 (see Figure 5-3). This trend is very similar to the phenomena observed in chapter CHAPTER 4, in which Type 2 photoinitiator systems containing fluorescent dyes polymerized a long distance in shadow regions, while photoinitiator systems that do not contain fluorescent dyes cured only short

distances in the shadow region. Therefore, the same consideration could apply to explain this uniformity.

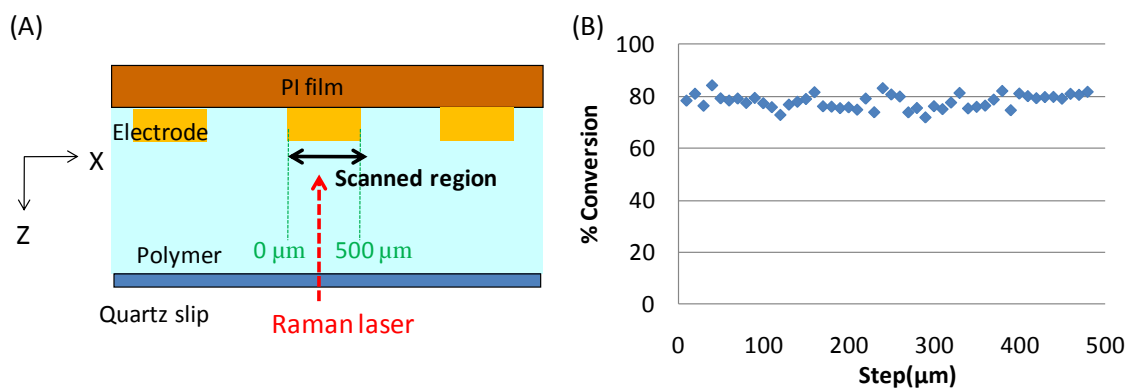


Figure 5-10: Measurement of shadow cure with PI-FPC in x-direction. (A) Scanned area behind an electrode and (B) its conversion profile (X-direction) for EYss/MDEA visible-light-induced photoinitiator system at the electrode surface of the $500 \times 500 \mu\text{m}$ line and space PI-FPC film. Monomer: HEA; Visible light source: a 150 W Xe lamp, visible light intensity: 89 mW/cm^2 , irradiation time: 900 seconds.

The depth conversion profiles in shadow regions behind an electrode were also determined as shown in Figure 5-11. The graph shows depth profiles behind an electrode at $50 \mu\text{m}$, $150 \mu\text{m}$, and $250 \mu\text{m}$ in the X-direction from the edge of the electrode. The depth profiles were measured every $2.5 \mu\text{m}$ distance. The conversions in the Z-direction are constant, and all values are similar. Therefore, no gradient was observed in Z-direction for this $100 \mu\text{m}$ thickness resin as in sections 5.2 and 5.3.

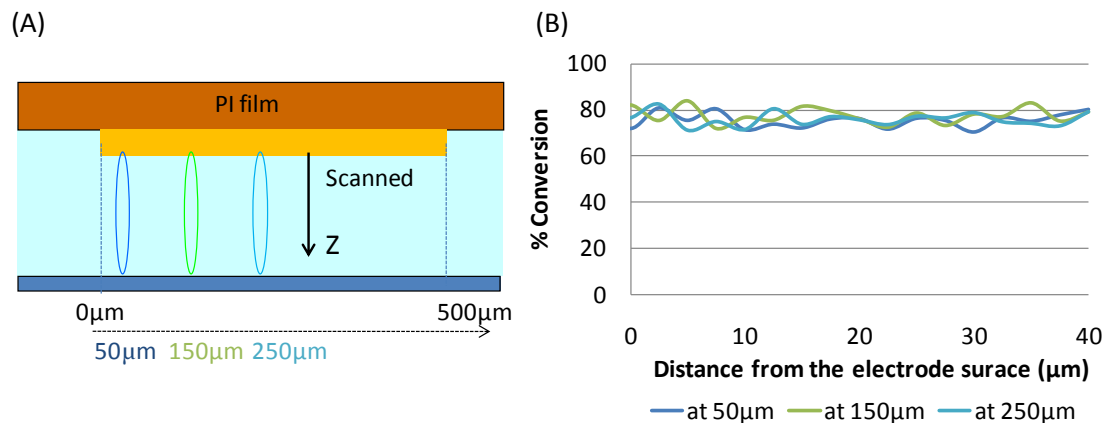


Figure 5-11: Measurement of shadow cure with PI-FPC in z-direction. (A) Scanned depth profiles behind an electrode and (B) depth profiles (Z-direction) for EYss/MDEA visible-light-induced photoinitiator system in the shadow region behind the electrode of the $500 \times 500 \mu\text{m}$ line and space PI-FPC film. Visible light source: a 150 W Xe lamp, visible light intensity: 89 mW/cm^2 , irradiation time: 900 seconds. $[\text{EYss}] = 0.00115 \text{ M}$, $[\text{MDEA}] = 0.32 \text{ M}$ in HEA monomer.

5.5. Optimization of Visible-Light Induced Photoinitiating Systems for Fast Shadow Cure

According to commercial catalogues about thermally cured ACF, a short cure time is required in the practical bonding process and its cure time is currently between 10 seconds and 30 seconds. Therefore, in order to apply the visible-light-induced photoinitiating systems to the ACF bonding process, it must possess fast cure ability indispensably. In this section, various means including adding additives, changing its process configuration, and increased light intensity to achieve faster cure times were investigated. In these experiments, the cure time was fixed as 10 seconds.

5.5.1. Effect of the Third Component, Diphenyliodonium Chloride (DPI)

First, the two-component photoinitiator system containing EYss and MDEA was studied using HEA monomer and PI-FPC. The sample is made in the same manner as described in section 5.4.1 but irradiated for only 10 seconds. The sample was slightly

cured and its conversion was only 3 % at the center of the electrode ($X= 250 \mu\text{m}$). Then, the conversion obtained by the three-component system (EYss/MDEA/DPI) was investigated in the same manner. As a result, the conversion at the center of the electrode was 62 % and was much higher than that of the EYss/MDEA two-component system as illustrated in Figure 5-12.

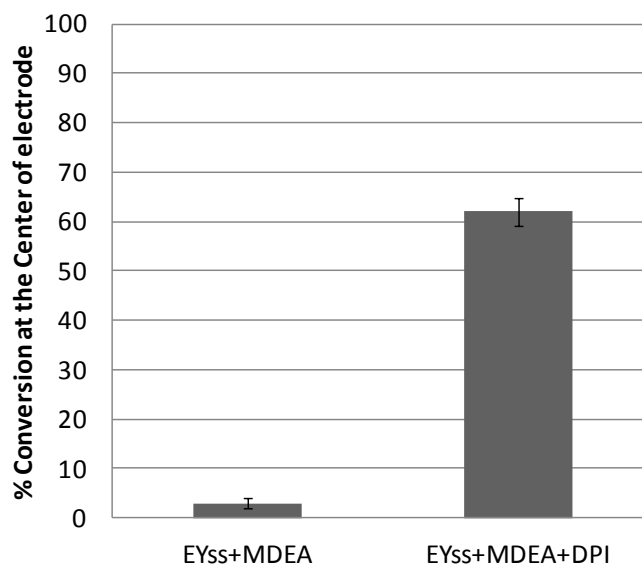


Figure 5-12: Comparison of conversion at the electrode's center surface of the $500 \times 500 \mu\text{m}$ line and space PI-FPC film between the EYss/MDEA two-component photoinitiator system and EYss/MDEA/DPI three-component photoinitiator system. The both samples are cured with a black stage. Monomer: HEA, Visible light source: a 150 W Xe lamp; visible light intensity: 89 mW/cm^2 , irradiation time: 10 seconds. $[\text{EYss}] = 0.00115 \text{ M}$, $[\text{MDEA}] = 0.32 \text{ M}$, $[\text{DPI}] = 0.0023 \text{ M}$.

5.5.2. Effect of Process Configuration: Two Types of Bottom Stage

The stage in this schematic configuration can affect the extent of shadow cure due to its reflection. Therefore, the effect of the stage was investigated. A white stage (white paper) was used instead of the black stage for the EYss/MDEA two-component system and EYss/MDEA/DPI three-component system using the same procedure described earlier (section 5.5.1). Figure 5-13 shows the comparison between the

conversion at the center of the electrode with the black substrate and the conversion with white substrate. As shown in the graph, for the both systems, the conversion with the white stage is higher than that with the black stage. Two reasons can be considered. First, the white stage reflects the irradiated light into the irradiated regions and generated active centers are increased, resulting in enhancing polymerization rate in shadow regions due to the increase of active centers which are diffused from the irradiated regions. Second, the reflected light from the white stage can scatter into the shadow region as well as the irradiated region. Therefore, this reflected light could cause polymerization in the shadow region via direct photoinitiation. Thus, the enhancement of shadow cure with the white stage was observed.

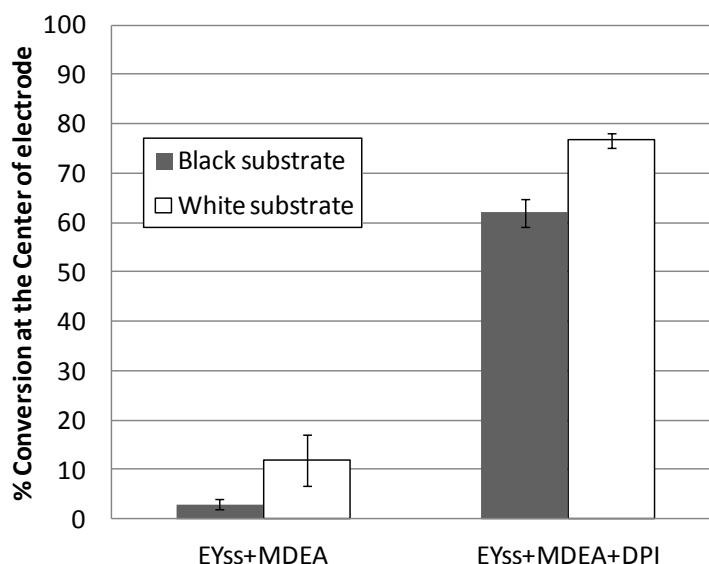


Figure 5-13: Comparison of conversion at the electrode's center surface of the 500×500 μm line and space PI-FPC film between black substrate and white substrate for the EYss/MDEA two-component photoinitiator system and EYss/MDEA/DPI three-component photoinitiator system. Monomer: HEA; Visible light source: a 150 W Xe lamp, visible light intensity: 89 mW/cm^2 , irradiation time: 10 seconds. $[\text{EYss}] = 0.00115 \text{ M}$, $[\text{MDEA}] = 0.32 \text{ M}$, $[\text{DPI}] = 0.0023 \text{ M}$.

5.5.3. Effect of Additives

Various additives including fluorescein (FL) (Sigma Aldrich), 9,10-dimethylanthracene (DMA), and pentaerythritol tetrakis(2-mercaptoacetate) (PEMP) (Sigma Aldrich) were tested in this study to enhance the fast shadow cure ability of the three-component system containing EYss, MDEA, and DPI using the same procedure in section 5.5.1 with a white stage. The addition of FL aimed at carrying photons into shadow regions using its fluorescence emission as described in chapter CHAPTER 4. The addition of DMA aims at consuming dissolved oxygen as described in section 5.3. PEMP is poly thiol chemical as shown in Figure 5-14. The ene (e.g. acrylate, vinyl ether, allyl ether, etc.)-thiol photopolymerization reaction has been investigated extensively this decade due to many advantages including rapid polymerization rate, lower shrinkage, and the ability to overcome oxygen inhibition.⁵⁷ However, the addition of thiol into acrylate system tends to change (mostly soften) its mechanical properties.¹⁰

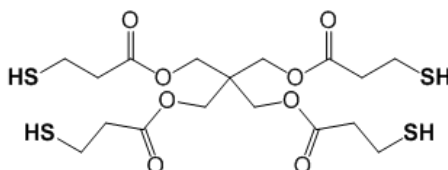


Figure 5-14: Chemical structure of pentaerythritol tetrakis(2-mercaptoacetate) (PEMP).

Figure 5-15 compares conversions at the center of an electrode for each additive with a white stage. As shown in the graph, FL and DMA do not enhance the conversion in shadow region or even worsens it compared to the system without additives (control). In fact, FL and DMA somehow hinder the EYss/MDEA/DPI reaction. Here, it is assumed that the excited EYss are quenched by DMA and/or FL before it encounters MDEA or DPI to generate active centers. On the other hand, PEMP enhances the shadow cure rate and achieves around 90% conversion when combined with a white substrate. Therefore, it

is confirmed that adding PEMP enhances the extent of shadow cure without interfering with the EYss/MDEA/DPI photoinitiation reaction. Again, the possibility of changes in mechanical properties must be considered due to the addition of thiols.

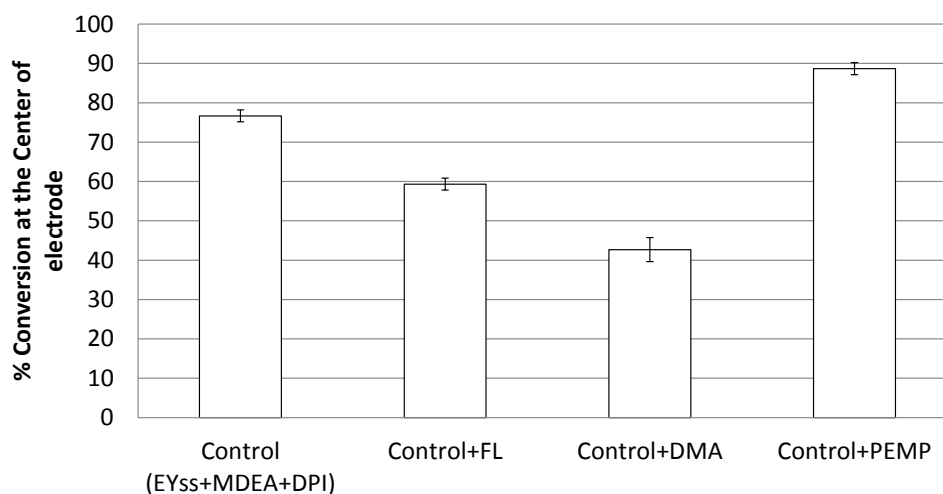


Figure 5-15: Effect of adding FL (0.00115 M), DMA (0.002 M) and PEMP (the thiol/acrylate ratio is 0.05, which is molar ratios of functional groups.) upon shadow cure conversion for the EYss/MDEA/DPI three-component photoinitiator system. Top substrate: PI-FPC, Measurement Point: the electrode's center surface of the $500 \times 500 \mu\text{m}$ line and space; Monomer: HEA; Visible light source: a 150 W Xe lamp, visible light intensity: 89 mW/cm^2 , irradiation time: 10 seconds. $[\text{EYss}] = 0.00115 \text{ M}$, $[\text{MDEA}] = 0.32 \text{ M}$, $[\text{DPI}] = 0.0023 \text{ M}$.

5.5.4. Effect of Light Intensity

Generally, the rate of production of active centers R_i , depends on its light intensity as expressed in an equation below.

$$R_i = \Phi I \quad \text{Equation 5-1}$$

Here, Φ is the photoinitiation quantum yield and I is the incident light intensity. Therefore, an increase in light intensity generates more active centers. Since the diffusion of active centers into the shadow regions depends on the concentration gradient, more active centers would diffuse into shadow regions by increased light intensity, and the polymerization rate in shadow regions can be enhanced.

As mentioned in chapter 4, the effect of fluorescence emitted from EYss into shadow region could be important in the EYss-containing photoinitiator systems for shadow cure. From this point, the increase of the light intensity can also enhance the extent of shadow cure because the fluorescence emission from EYss increases as well.

The effect of two different light intensities, 89 mW/cm² and 4950 mW/cm² upon shadow cure, were investigated for the EYss/MDEA two-component system, EYss/MDEA/DPI three-component system, and EYss/MDEA/DPI/FL four-component system using the same procedure described in section 5.5.1 with a white stage. Figure 5-16 illustrates the effect of light intensity on the conversion at the center of an electrode for these three photoinitiator systems. As shown in the graph, the increase of the light intensity is effective for the all photoinitiator systems and about 90 % conversion in the shadow region was achieved for the EYss/MDEA/DPI three-component system and EYss/MDEA/DPI/FL four component system. Therefore, it can be concluded that the increase of light intensity can enhance polymerization rate in shadow regions.

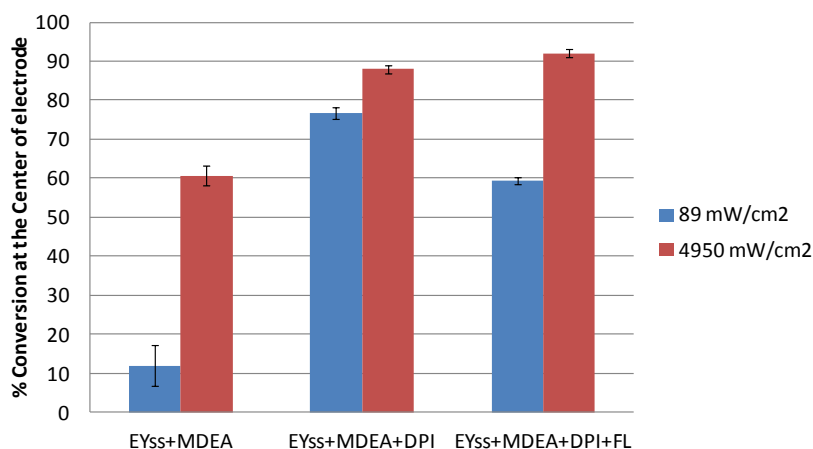


Figure 5-16: Effect of light intensity on the shadow cure conversion for photoinitiator systems: EYss/MDEA, EYss/MDEA/DPI, EYss/MDEA/DPI/FL. The all samples were cured with a white stage. Top substrate: PI-FPC; Measurement Point: the electrode's center surface of the 500 × 500 μm line and space, Monomer: HEA; Visible light source: a 150 W Xe lamp, irradiation time: 10 seconds. [EYss] = 0.00115 M, [MDEA] = 0.32 M, [DPI] = 0.0023M, [FL] = 0.00115 M.

5.6. Conclusion

Shadow cure with FPCs using free-radical photoinitiators was evaluated by Raman microscopy. First, the extent of shadow cure using photoinitiator systems including a common α -cleavage UV photoinitiator (HCPK) and visible-light-induced two-component system (EYss/MDEA) was investigated. All of the conversion profiles in shadow regions are uniform in z-direction. However, the HCPK system had a gradient in x-direction and the lowest conversion was at the center of the electrode due to oxygen inhibition. To eliminate this inhibition and to achieve a higher conversion, a photochemical method was attempted that used additives (Zn-ttp and DMA) and a pre-irradiation procedure with a 670 nm light source. As a result, higher and more uniform conversion profiles in the shadow regions were observed by this photochemical method.

In order to cure shadow regions with PI-FPC in a short time using visible-light-induced multi-component photoinitiator systems based on EYss/MDEA, various means were studied. Several methods to achieve faster shadow cure are listed below:

- add a third component such as DPI into the two-component photoinitiator systems,
- use a reflective (white) stage behind the cured sample,
- add thiol such as PEMP into systems,
- increase the intensity of incident light.

CHAPTER 6. EXTENT OF SHADOW CURE TO POLYMERIZE OLIGOMER-CONTAINING FORMULATION

6.1. Introduction

So far monomers have been used as the resin to study shadow cure. However, practical resins used in industry are mixtures of oligomers and monomers.¹ Oligomers control most mechanical properties of final products including glass transition temperature (T_g), stress-strain, adhesion, abrasion and hardness. Oligomers also influence formulation properties such as viscosity and wetting properties. Due to the importance of the photopolymerization process, it is of great value to understand the impact of oligomers on shadow cure as a means to design the process efficiently. It is reported that T_g and viscosity can affect the photopolymerization profiles.^{37, 58, 59}

In this chapter, T_g and viscosity impacts on photopolymerization were studied for two oligomers using Type I and Type II photoinitiator systems. Then, lower conversions in the shadow region for an oligomer-containing formulation with visible-light-induced Type II photoinitiator systems were observed compared to a Type I photoinitiator. To overcome this issue, a visible-light induced Type I photoinitiator, Bis(cyclopentadienyl) bis[2,6-difluoro-3-(1-pyrryl)phenyl]-titanium, was focused on and thoroughly characterized. Finally, high conversions in the shadow region were achieved using this photoinitiator with visible light.

6.2. Comparison of Photopolymerization between Type I and Type

II Photoinitiator for Oligomer-Containing Composition

6.2.1. Materials and Methods

A 2-hydroxyethyl acrylate (HEA) monomer (T_g -15 °C) and two aliphatic urethane diacrylate oligomers, CN9002 (T_g -52 °C) and CN9009 (T_g 40°C), were used as the monomer-oligomer mixture resin where monomer/oligomer mass ratios were 100/0,

70/30, 50/50, 30/70 and 0/100. The viscosity was measured by a digital viscometer (Brookfield). The mixtures were combined with four photoinitiator systems including bis(2,4,6-trimethylbenzoyl)-phenylphosphine oxide (BAPO), 1-hydroxycyclohexyl phenyl ketone (HCPK), Eosin Y spirit soluble/ N-methyldiethanolamine (EYss/ MDEA) two-component system, and EYss/MDEA/DPI (diphenyliodonium chloride) three-component system. BAPO and HCPK are conventional UV α -cleavage-type photoinitiators, Type I photoinitiators which decompose into free radicals via UV exposure. The chemical structure of BAPO and HCPK is shown in Figure 6-1. The oligomers were provided by Sartomer. HEA, EYss, MDEA and DPI were purchased from Sigma Aldrich. BAPO and HCPK were obtained from BASF. The studied compositions and light conditions are summarized in Table 6-1 where emitted wavelength and light intensities are indicated in nm and mW/cm² respectively. The overall conversion of the mixtures was measured using the RT-FTIR method introduced in section 3.2.1.

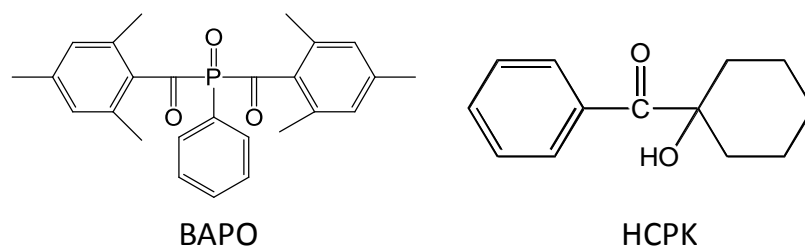


Figure 6-1: Chemical structure of BAPO and HCPK.

Table 6-1: Compositions of studied photoinitiator systems

		BAPO	HCPK	EYss/MDEA		EYss/MDEA/DPI		
				EYss	MDEA	EYss	MDEA	DPI
Concentration	(phr)*	0.720	0.345	0.0737	3.77	0.0737	3.77	0.0719
	[M]	0.0167	0.0167	0.00115	0.32	0.00115	0.32	0.0023
150 W Xe lamp	(nm)	400	365	520		520		
	(mW/cm ²)	1.0	1.0	2.1		2.1		

*phr: parts per hundred resin

6.2.2. Results and Discussion

The predicted T_g (mixture rule), measured viscosity, and final conversions for the monomer-oligomer mixtures are summarized in Table 6-2. The final conversions of the resins with the Type I photoinitiators, BAPO and HCPK, do not depend on the mixture viscosity but on the T_g as illustrated in Figure 6-2. This phenomenon is known as the glass or vitrification effect.⁵⁸ As polymerization proceeds in a mixture, the T_g of the reacting mixture increases. If the T_g exceeds the reaction temperature, its polymerization can stop short of full conversion. Hence, the final conversion of a monomer-oligomer mixture depends on its T_g and its reaction temperature; namely, the reaction is a T_g -controlled reaction. In this experiment, the reaction temperature is almost equal to room temperature because the sample is so thin (15 μ m) that the reaction heat and absorbed energy from the light are negligible. Therefore, if the predicted T_g of a monomer-oligomer mixture is higher than room temperature (23°C), the final conversion is low.

Table 6-2: T_g , viscosity and final conversions for four photoinitiator systems of monomer-oligomer mixtures

	T_g (°C)	Viscosity (mPa·s)	Final conversion			
			HCPK	BAPO	EYss/MDEA	EYss/MDEA/DPI
HEA/CN9002=100/0	-15	5	94.9	97.0	82.2	97.9
HEA/CN9002=70/30	-26.1	93	99.8	98.6	66.8	97.4
HEA/CN9002=50/50	-33.5	512	99.4	99.4	58.3	59.2
HEA/CN9002=30/70	-40.9	3504	99.4	99.8	49.8	43.1
HEA/CN9002=0/100	-52	66240	97.9	96.9	53.7	42.1
HEA/CN9009=100/0	-15	93	95.0	91.0	82.2	97.9
HEA/CN9009=70/30	1.5	87	94.0	98.0	78.5	96.2
HEA/CN9009=50/50	12.5	75	95.8	94.6	75.0	92.6
HEA/CN9009=30/70	23.5	543	91.6	91.9	66.5	69.2
HEA/CN9009=0/100	40	85547	68.1	55.9	44.7	41.5

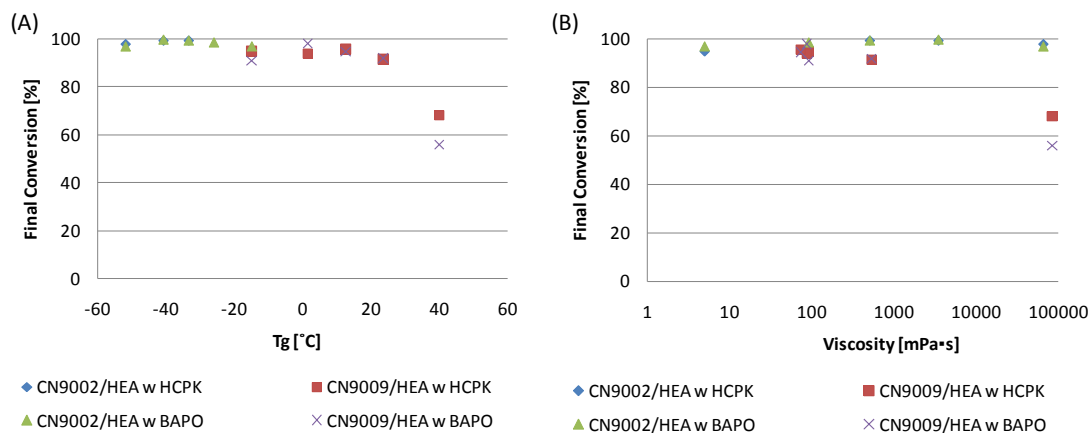


Figure 6-2: Correlation between UV-light-induced Type I photoinitiator systems' (HCPK, BAPO) final conversions and: (A) T_g, (B) viscosity.

In contrast to the results of the UV-light-induced Type I photoinitiators, the conversion profiles of the resins with the visible-light-induced Type II photoinitiators depend on viscosity as well as the mixture T_g, as illustrated in Figure 6-3. This trend implies that the mobility of the molecules in a formulation is more important to these multi-component Type II photoinitiators. While the unimolecular photoinitiators such as HCPK and BAPO are relatively insensitive to viscosity, the bimolecular electron transfer reactions tend to be diffusion-controlled reactions.^{59, 60} Therefore, the probability of an encounter of excited EYss with MDEA and/or DPI decreases with increasing viscosity.

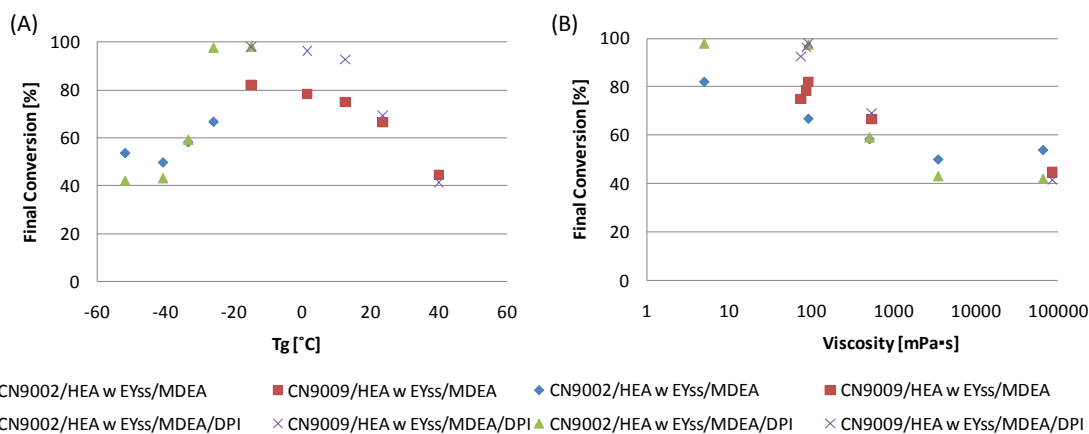


Figure 6-3: Correlation between visible-light-induced Type II photoinitiator systems' (EYss/MDEA, EYss/MDEA/DPI) final conversions and: (A) T_g, (B) viscosity.

6.3. Comparison of Shadow Cure between Type I and Type II Photoinitiator Systems for Oligomer-Containing Formulation

6.3.1. Methods

In this section, the extent of shadow cure for Type I and Type II photoinitiator systems, which are investigated above for oligomer-containing formulation, were studied using polyethylene terephthalate – flexible printed circuits (PET-FPCs). The samples were cured as described in section 5.2.1 and 5.4.1, where the used stages were polyimide for HCPK and black for Type II photoinitiators. Then the conversion profiles at the $500 \times 500 \mu\text{m}$ line and space pattern were monitored. The resin used here was a viscous HEA/CN9002 monomer-oligomer mixture in which the mass ratio was 30/70. The studied photoinitiator systems compositions and light conditions are summarized in Table 6-3, where the Fusion UV light conveyor speed was 1 m/sec, irradiation time with the Xe lamp was 900 seconds, and the respective accumulated light energies are indicated with J/cm^2 .

6.3.2. Results and discussion

Figure 6-4 illustrates the conversion profile on the electrodes' surface that was monitored for every $10 \mu\text{m}$ step in the X-direction by Raman microscope. As with the trends above (Figure 6-2b, Figure 6-3b), the Type II photoinitiators (EYss/MDEA and EYss/MDEA/DPI) do not achieve high conversion in shadow region due to the high viscosity of the resin while the Type I (HCPK) photoinitiator reached to 100 % conversion. Therefore, it can be concluded that the use of Type II photoinitiators is not ideal to achieve high conversion in the shadow region for viscous formulations.

Table 6-3: Compositions of studied photoinitiator systems and irradiated light conditions

		Type I	Type II				
		HCPK	EYss/MDEA		EYss/MDEA/DPI		
			EYss	MDEA	EYss	MDEA	DPI
Concentration	(phr)*	1.0	0.0737	3.77	0.0737	3.77	0.0719
	[M]	0.0484	0.00115	0.32	0.00115	0.32	0.0023
Light condition	Source	Fusion conveyor	150 Xe lamp				
	Wavelength	UV	Visible				
	(mW/cm ²)	1948	89				
	(m/min)	1	-				
	(sec)	-	900				
	(J/cm ²)	2.6	80.1				

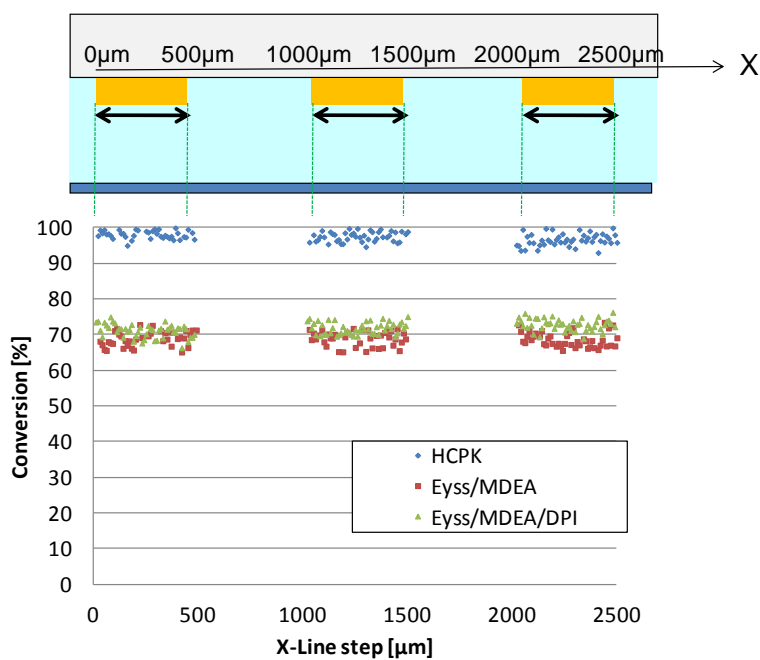


Figure 6-4: Conversion profile (X-direction) for three different photoinitiator systems at electrodes' surface of the 500 × 500 μm line and space PET-FPC film. Resin: HEA/CN9002 (30/70 in mass ratio).

6.4. Visible-Light-Induced Type I Photoinitiator:

Bis(cyclopentadienyl) bis[2,6-difluoro-3-(1-pyrryl)phenyl]titanium (Ti-PI)

As described above, conventional visible-light-induced Type II photoinitiators such as EYss/MDEA are not ideal to achieve high conversion in shadow regions with viscous oligomer-containing formulations. Therefore, a visible-light-induced Type I photoinitiator is desired to achieve shadow cure with a high conversion similar to that obtained by UV-light-induced Type I photoinitiators. Hence, a type I photoinitiator, Bis(cyclopentadienyl) bis[2,6-difluoro-3-(1-pyrryl)phenyl]titanium (henceforth referred to as Ti-PI), which absorbs up to 550 nm wavelength of light was focused on and investigated in this study. Figure 6-5 shows the chemical structure of Ti-PI and its Napierian molar absorptivity using methanol as a solvent. The absorption spectrum was measured by an 8453 UV-Visible spectrophotometer (Agilent Technologies). The photolysis absorptivity is also shown in the graph.

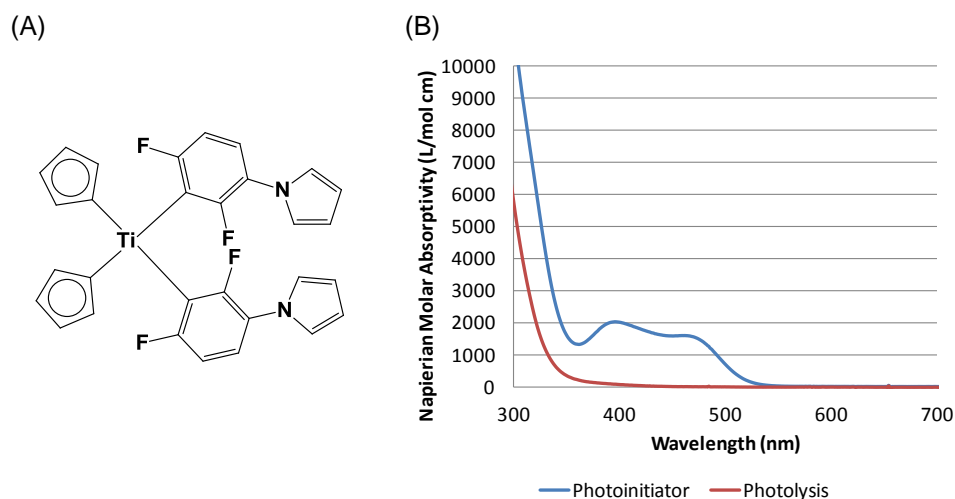


Figure 6-5: (A) Chemical structure of Ti-PI and (B) Napierian molar absorptivity of the photoinitiator and its photolysis product.

This photoinitiator was developed and commercialized with a commercial name Irgacure 784 in 1998 by Ciba Specialty Chemicals Inc. (now BASF). Several studies have been reported about photoinitiators containing titanocene.⁶¹⁻⁶⁵ However, the photoinitiation mechanism of this Ti-PI photoinitiator has not been clearly defined yet. A suggested mechanism about the photopolymerization reaction between this photoinitiator and the acrylate monomer is shown in Figure 6-6.⁶⁶ As shown in the figure, the reaction scheme for the titanocene initiator is very different from that of typical Type I photoinitiators where the active center adds to acrylate double bond directly. By absorbing a light, Ti-PI forms an isomer through an η^5 -to- η^1 cyclopentadienyl ring slippage. Because the isomer has a weaker bond between the titanium and cyclopentadienyl ring compared to the unirradiated Ti-PI, the isomer tends to generate radicals more easily. Thus, an active center in the form of a titanocene-containing radical is generated. Then, the titanocene radical is attacked by the carbonyl group of two molecules of the acrylate monomer. Finally, the resulting ketene acetal di-radical could initiate polymerization.

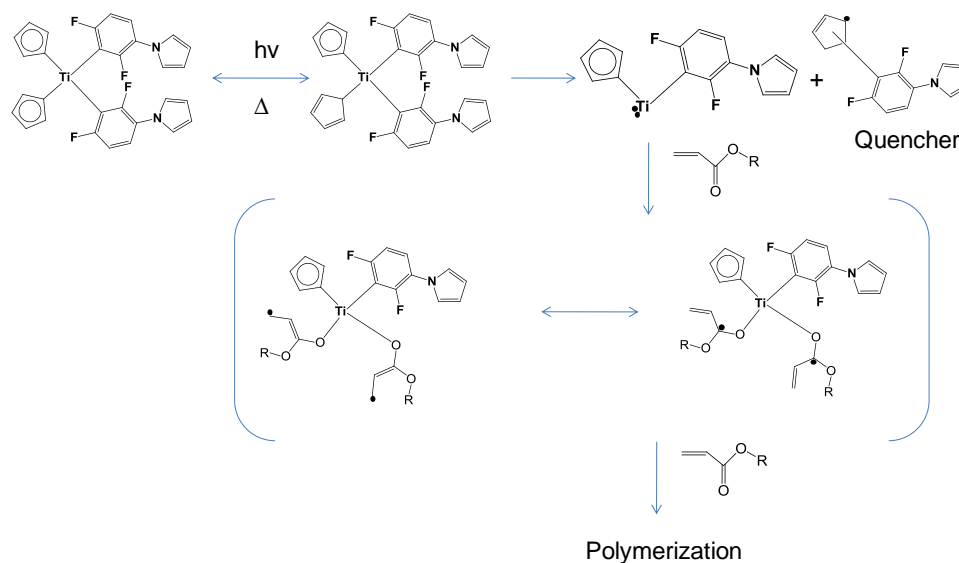


Figure 6-6: Suggested photoinitiation and photopolymerization mechanism for Ti-PI in acrylates.

6.4.1. Characteristics of Ti-PI Photopolymerization: Effect of Light

Intensity and Additives

The photopolymerization of Ti-PI in HEA monomer was investigated using the RT-FTIR method in this section. In an attempt to improve the photopolymerization capabilities of Ti-PI, the effect of light intensity (or light source) and additives ((meth)acrylate containing protonic acid) were studied.

The enhancement of photopolymerization by adding proton-acids including acryloyloxyethyl acid phosphate, 2-ethylhexyl acid phosphate, dodecylbenzenesulfonic acid, and citric acid into thick acrylates resin containing Ti-PI was reported by Seta⁶⁷. He hypothesized that the acids protonate the nitrogen atoms present on the pyrrole ring of Ti-PI. Due to this, the electron donating character of the phenyl ligands decreases (as the nitrogen atoms have no more free electrons) and the ratio of coordinative unsaturation increases. As a result, the titanium atom is more susceptible to attack by the acrylate monomer.

6.4.1.1. Materials and Methods

Two protonic-acids - 2-carboxyethyl acrylate (CEA) and phosphoric acid 2-hydroxyethyl methacrylate ester (PhMA) - were chosen for this study (Figure 6-7). Both acids were purchased from Sigma Aldrich, while Ti-PI was provided by BASF. The compositions of photoinitiator systems that were studied are summarized in Table 6-4. The overall HEA monomer conversion of the mixtures was measured using the RT-FTIR method introduced in section 3.2.1. Two light sources were used for this study: a 150W Xe lamp emitting a light intensity of 89 mW/cm² and the same Xe lamp with a 520 nm bandpass filter (520 nm light) emitting a light intensity of 2.4 mW/cm². The light spectra are illustrated previously (Figure 3-6).

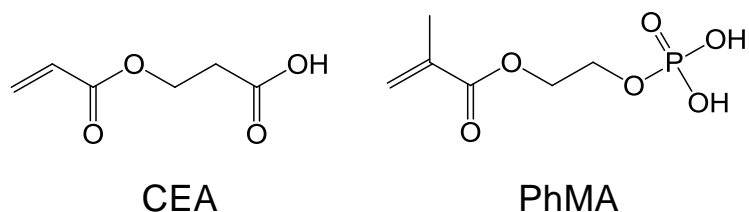


Figure 6-7: Chemical structure of 2-carboxyethyl acrylate (CEA) and phosphoric acid 2-hydroxyethyl methacrylate ester (PhMA).

Table 6-4: Compositions of studied photoinitiator systems

	unit	Ti-PI	Ti-PI+CEA	Ti-PI+PhMA
Ti-PI	(phr)	2.62	2.62	2.62
	[M]	0.0484	0.0484	0.0484
CEA	(phr)	-	1.50	-
	[M]	-	0.1029	-
PhMA	(phr)	-	-	1.50
	[M]	-	-	0.0650

6.4.1.2. Results and Discussion

RT-FTIR conversion profiles as a function of time for the three different photoinitiator systems are shown in Figure 6-8. For the Xe lamp (Figure 6-8A), all of the photoinitiator systems reach low conversions that are less than 10%. In particular, the sample containing Ti-PI without any additives (blue line) does not polymerize at all. On the other hand, if 520 nm light is used (Figure 6-8B), enhancement in photopolymerization is observed for the all of the three photoinitiator systems. This interesting trend, clarified later in chapter CHAPTER 8, was due to the unique dependency of these photoinitiator systems on the intensity of the incident light. If the light intensity is too strong, too many inactive (or slightly active) radicals (e.g. 2,6-difluoro-3(1H-pyrrol-1-yl)phenyl radical), which quench the active radicals, are generated, thus resulting in a very low final conversion. Therefore, the optimum light intensity for Ti-PI systems is relatively low in order to achieve a high final conversion.

Regarding the impact of proton-acid-containing additives, the addition of both CEA (red line) and PhMA (green line) shows much higher photopolymerization rates and

final conversions compared to the neat Ti-PI photoinitiator system in Figure 6-8B. Remarkably, the photoinitiator system containing Ti-PI and PhMA achieves a conversion of nearly 100% when illuminated by a 520 nm light source. The superiority of PhMA over CEA could be attributed to the stronger acidity of PhMA over CEA. PhMA would more readily protonate the nitrogen atoms present on the pyrrole group of Ti-PI, thereby increasing the ratio of generated active radicals. To verify this hypothesis, further studies were performed and have been reported in chapter CHAPTER 8. Thus, the addition of a proton-acid chemical and the use of a proper light intensity, which is relatively low for Ti-PI-containing photoinitiator systems, were determined to be critical in order to achieve a high final conversion.

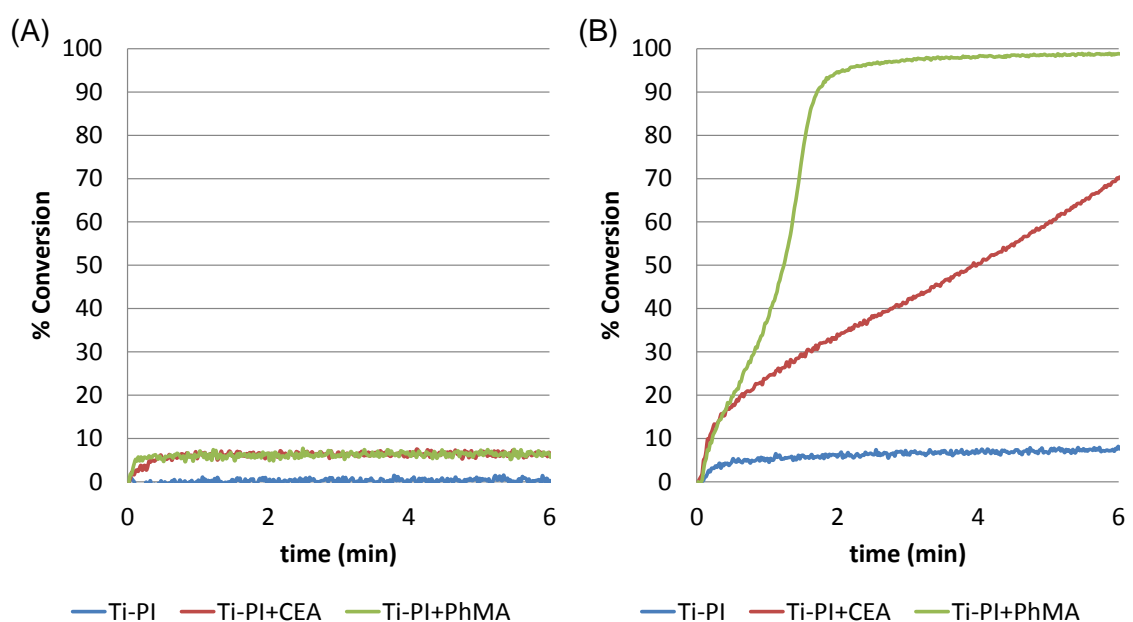


Figure 6-8: Comparison of the three different photoinitiator systems for photopolymerization conversion profiles. Monomer: HEA. (A) A 150W Xe lamp with 89 mW/cm² light intensity, (B) the Xe lamp attaching a 520 nm bandpass filter with 2.4 mW/cm² light intensity.

6.4.2. Comparison between Ti-PI (Type I) and Type II Photoinitiator Systems for Oligomer-Containing Composition Using Visible Light

Unlike Type II photoinitiator systems, including EYss/MDEA and EYss/MDEA/DPI, a Ti-PI-containing photoinitiator system can be classified as a Type I photoinitiator because it generates active centers via self-cleavage. Therefore, the Ti-PI-containing photoinitiator system has the potential to achieve high conversion in viscous oligomer-containing formulations. In this section, the superiority of the Ti-PI Type I photoinitiator system over Type II photoinitiator systems was confirmed using RT-FTIR spectroscopy.

6.4.2.1. Materials and Methods

The mixture of HEA/CN9002, in which the mass ratio was 30/70, was used as an oligomer-containing resin. The compositions of photoinitiator systems studied are summarized in Table 6-5. The overall conversion of the mixtures was measured using the RT-FTIR method introduced in section 3.2.1. The samples were irradiated by a Xe lamp with an attached 520 nm bandpass filter that emitted light with an intensity of 2.4 mW/cm².

Table 6-5: Compositions of studied photoinitiator systems

		Type I		Type II				
		Ti-PI/PhMA		EYss/MDEA		EYss/MDEA/DPI		
		Ti-PI	PhMA	EYss	MDEA	EYss	MDEA	DPI
Concentration	(phr)	2.62	1.50	0.0737	3.77	0.0737	3.77	0.0719
	[M]	0.0484	0.065	0.00115	0.32	0.00115	0.32	0.0023

6.4.2.2. Results and Discussion

RT-FTIR conversion profiles as a function of time for the three different photoinitiator systems are shown in Figure 6-9. As shown in the graph, the Type II

photoinitiators (red line and green line) are able to reach a conversion of about 50 % at the end of the experiment. In contrast, the Ti-PI/PhMA photoinitiator (blue line) achieves a high final conversion as expected. Thus, the potential of this Ti-PI-containing photoinitiator to achieve a high conversion in shadow region was verified.

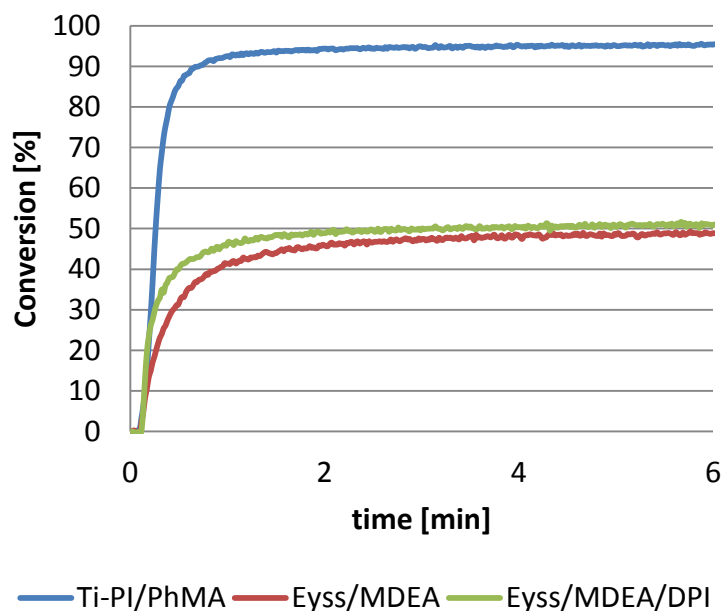


Figure 6-9: Comparison of the three different photoinitiator systems for photopolymerization conversion profiles. Resin: HEA/CN9002 (30/70 in mass ratio); Light source: a Xe lamp with a 520 nm bandpass filter, light intensity: 2.4 mW/cm².

6.5. Shadow Cure for Oligomer-Containing Formulation with Visible Light

As studied above, high conversion in the shadow region for viscous oligomer-containing formulations with a Ti-PI-containing photoinitiator system using visible light is expected. In this section, the extent of shadow cure for Ti-PI was investigated using polyimide-flexible printed circuits (PI-FPCs). The experiments were performed as described in section 5.4.1, where the used stage was black and the conversion profiles at

the $500 \times 500 \mu\text{m}$ line and space pattern were monitored. Here, the resin was HEA/CN9002 monomer-oligomer mixture in which the mass ratio was 30/70. The studied photoinitiator systems compositions and light conditions are summarized in Table 6-6. Note that polyimide film blocks light below 450 nm in wavelength (Figure 1-2). Therefore, the light sources used under this PI-FPC can emit only in the visible spectrum.

Figure 6-4 illustrates the conversion profile on the electrode's surface that was monitored for every $10 \mu\text{m}$ step in the x-direction using a Raman microscope. As was seen in the results in section 6.3, the Type II photoinitiators (EYss/MDEA and EYss/MDEA/DPI) do not achieve a high conversion in the shadow region due to the high viscosity of the resin. However, the Ti-PI/PhMA photoinitiator reached about 100 % conversion with the 520 nm light. Thus, the high conversion in shadow region for oligomer-containing formulation under visible light irradiation was finally achieved.

Table 6-6: Compositions of studied photoinitiator systems and irradiated light conditions

		Type I		Type II				
		Ti-PI/PhMA		EYss/MDEA		EYss/MDEA/DPI		
		Ti-PI	PhMA	EYss	MDEA	EYss	MDEA	DPI
Concentration	(phr)	2.62	1.50	0.0737	3.77	0.0737	3.77	0.0719
	[M]	0.0484	0.065	0.00115	0.32	0.00115	0.32	0.0023
Light condition	Source	520 nm light		150 Xe lamp				
	Wavelength	520 nm		Visible				
	(mW/cm ²)	2.2		89				
	(sec)	900		900				

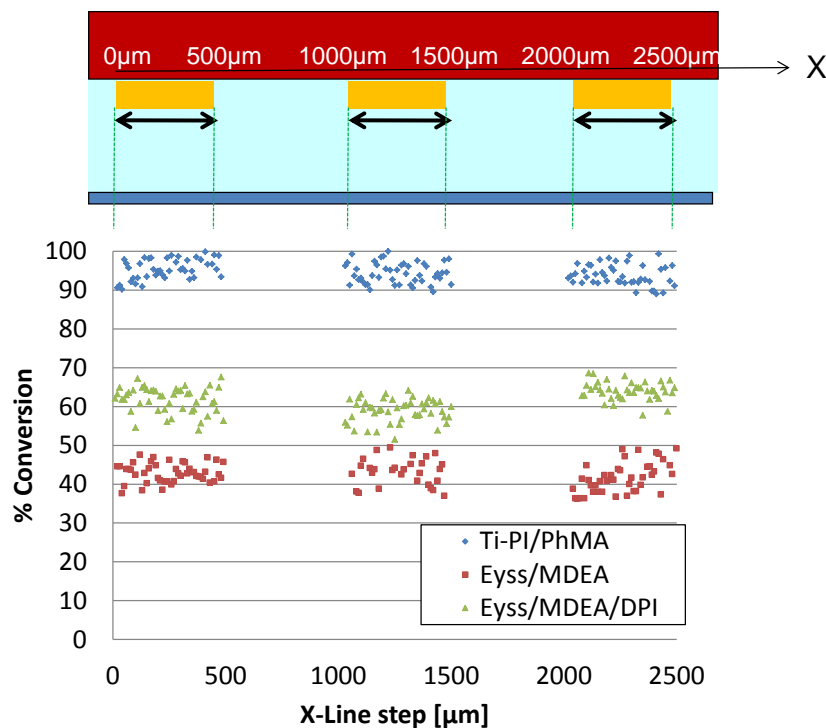


Figure 6-10: Conversion profile (X-direction) for three different photoinitiator systems at electrodes' surface of the $500 \times 500 \mu\text{m}$ line and space PI-FPC film. Resin: HEA/CN9002 (30/70 in mass ratio).

6.6. Conclusion

When considering industrially relevant viscous composition for ACF application, the viscosity becomes an impediment for achieving high conversion in shadow region using visible-light-induced Type II photoinitiators. To overcome this issue, Type I photoinitiators that can initiate polymerization with visible light are desired. Hence, a commercial visible-light-induced Type I photoinitiator, Ti-PI, was focused on and investigated. This research revealed that Ti-PI achieved high conversion in a viscous oligomer-containing formulation with the addition of a proton-acid-containing chemical and the selection of an optimal light intensity that is relatively low for this system. Using a proper combination of the proton acid and the intensity of a visible light source, the Ti-PI photoinitiator system was able to achieve a high conversion in shadow region under PI-FPC in viscous oligomer-containing resins as well.

CHAPTER 7. EXPERIMENTAL AND MODELING STUDIES OF PHOTOINITIATOR SYSTEMS FOR EFFECTIVE POLYMERIZATIONS WITH UV LEDS

7.1. Introduction

High intensity LED lamps are becoming increasingly available and offer many advantages over traditional broad-spectrum lamps. In addition to being highly efficient, LEDs can instantly be switched on and off, are ideal for heat sensitive materials (no stray IR emission), have long lifetimes (on the order of tens of thousands of hours of lamp life), do not contain hazardous vapors, and are light-weight/compact for customizable design and scaling. This aspect of the research will provide a comprehensive characterization (with both experimental and modeling studies) of the photopolymerization efficiency of commercially available photoinitiators illuminated with UV LED lamps.

Current characteristics of UV LED irradiation systems are illustrated in Figure 7-1, which is provided by Integration Technology, LTD (Oxford, UK).^{68, 69} The graph demonstrates spectral light intensities of 365, 375, 385, 395, and 405 nm wavelength LEDs and a conventional UV mercury lamp. As shown in the graph, while the conventional mercury lamp emits broad wavelengths, LEDs emit a monochromatic band of light that is centered at a specified peak wavelength. In the UV region, the figure also reveals that as the emitting wavelength of LEDs decreases, its light intensity also decreases. According to the company, only around 10 to 20 % of the electrical energy supplied to the LED system is actually converted into UV for longer wavelengths (395 and 405 nm) and less than 10 % for shorter wavelengths; whereas, visible and NIR LEDs efficiently use around 40 to 50 % of the electrical energy.

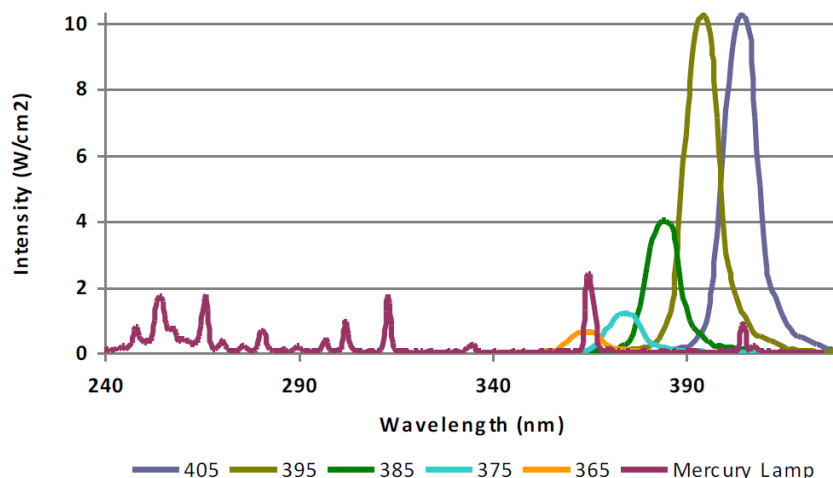


Figure 7-1: Spectral light intensities of LEDs and conventional UV light (provided by Integration Technology .LTD)⁶⁸

7.2. Investigation of a Commercial LED System

7.2.1. Light Emission Profiles

7.2.1.1. 400 nm LED

One commercial LED system emitting monochromatic band of light at 400 nm wavelength, Firefly (Phoseon Technology Inc.), was investigated to determine the uniformity of spectral light and light intensities using a spectrometer (Ocean Optics Inc.); this measures the spectral light intensity between 200 nm and 900 nm wavelengths. The light emission shape of Firefly is a 30.8 mm diameter circle that contains a 16.6 mm × 20.6 mm rectangle housing LED chip group, as shown in Figure 7-2. The measurements were taken at five positions (See Figure 7-2) and at varying distances between the spectrometer detector and Firefly.

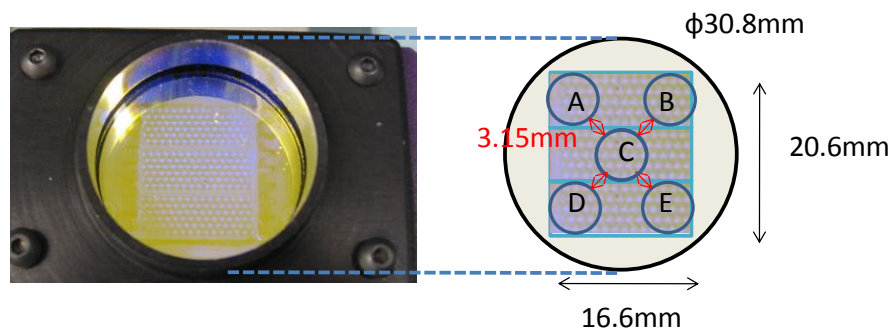


Figure 7-2: Shape of 400 nm LED light source (Firefly; Phoseon Technology, Inc.) indicating the five measurement points used for spectral light intensity.

The uniformity of the LED light spectral output was studied by comparing light spectral intensity at each of the five measurement positions. As shown in Figure 7-3, the uniformity of the LED chips was confirmed.

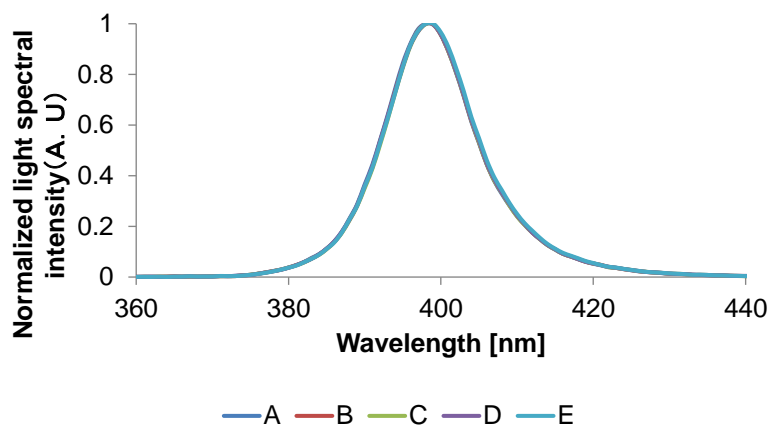


Figure 7-3: Normalized light spectral intensity of 400 nm LED at each of the five measurement positions.

Figure 7-4 shows the light intensity transition of each measurement position as a function of the measurement distance from the LED light source. The figure illustrates that if the distance from Firefly to the collection probe was less than 4 cm, the light intensity at the center position was higher than other locations because of the edge effect. On the other hand, light intensities at the five locations were uniform when the

measurement was taken at more than 4 cm. Therefore, in order to achieve uniform curing using Firefly in the LED chips area shown in Fig.1, the sample must be placed more than 4 cm from the LED light source.

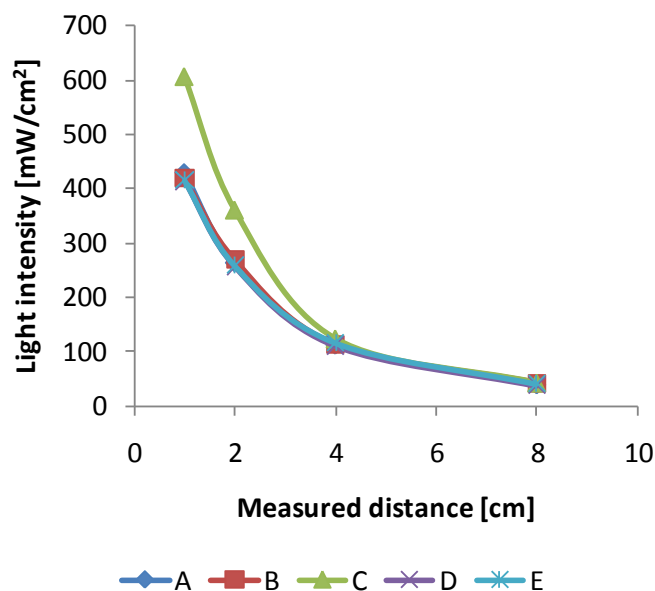


Figure 7-4: Correlation between light intensities at five measurement positions and measured distance.

7.2.1.2. 365 nm LED and 385 nm LED

Two commercial LED systems, supplied by Integration Technology, LTD., emitting monochromatic light at 365 nm (LEDZero Solidcure 365nm) and 385 nm (LEDZero Solidcure 385nm) wavelengths respectively were also investigated as in section 7.2.1.1. The light emission shape of these LEDs is a 35 mm × 20 mm rectangle containing two LED arrays, as shown in Figure 7-5. The measurements were taken at fifteen positions (See Figure 7-5) and at varying distances between the spectrometer detector and the LED systems.

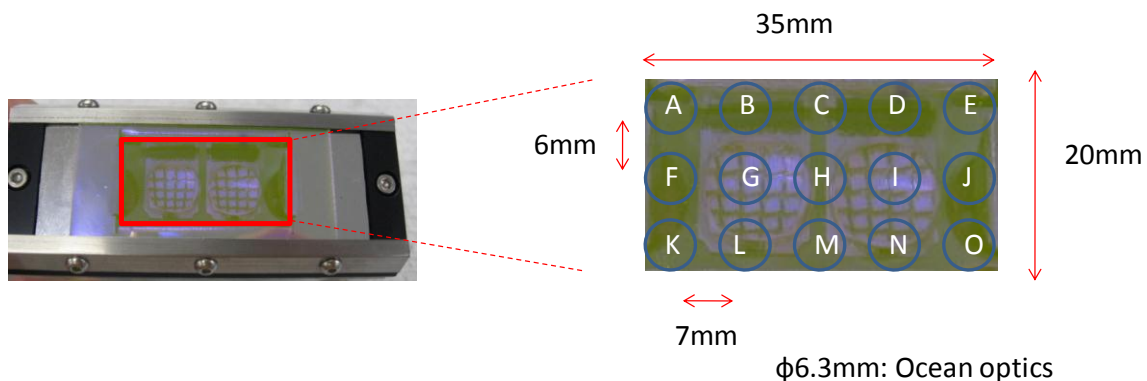


Figure 7-5: Shape of 365nm and 385 nm LED light sources (LED zero Solidcure; Integration Technology, LTD.) indicating the five measurement points used for spectral light intensity.

The uniformities of the LED light spectral output were studied and confirmed by comparing light spectral intensity at each of the five measurement positions as illustrated in Figure 7-6 (A), (B). Then, the light intensity transitions of each measurement position as a function of the measurement distance from the LED light sources were investigated, as shown in Figure 7-7. The light intensity profiles of both LEDs demonstrated similar trends in section 7.2.1.1; if the distance from the LED to the collection probe was higher than 4 cm, the light intensities at all measured positions were almost uniform.

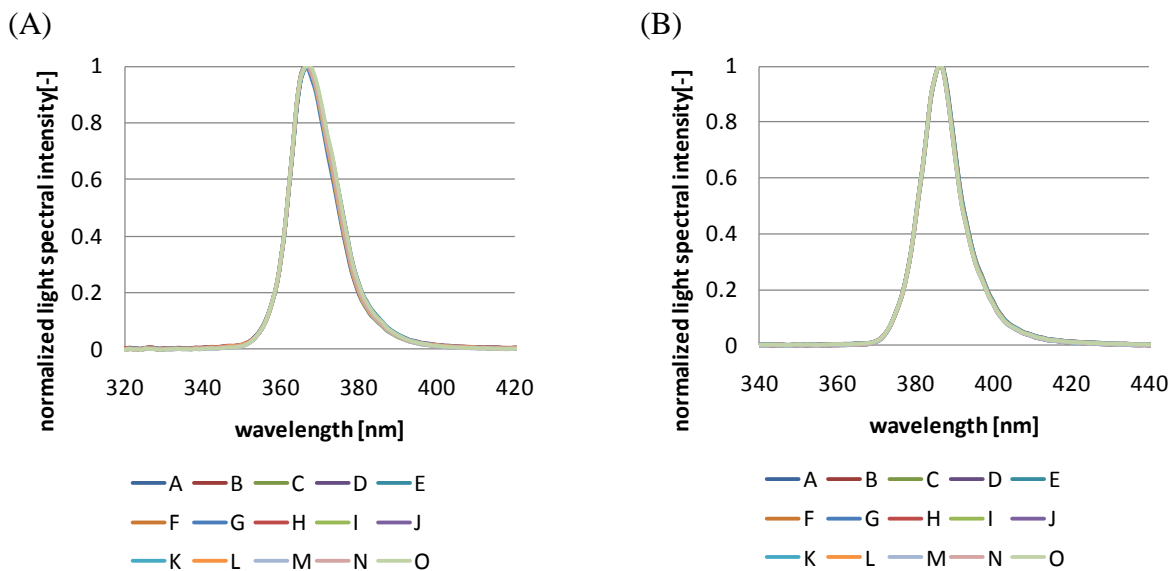


Figure 7-6: Normalized light spectral intensity LEDs at each of the fifteen measurement positions. (A) 365 nm LED, (B) 385 nm LED

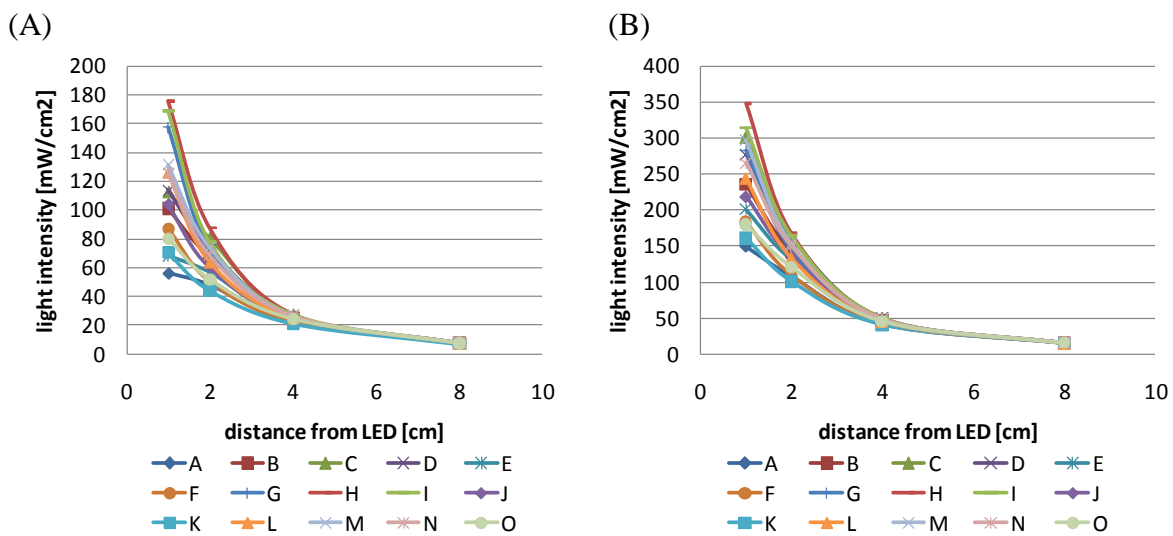


Figure 7-7: Correlation between light intensities at fifteen measurement positions and measured distance. (A) 365 nm LED, (B) 385 nm LED

7.2.1.3. Comparison of the Three LEDs

Figure 7-8 illustrates the comparison of the three LEDs investigated above. Since the total LED chips sizes of each system are similar (see Figure 7-2, Figure 7-5), it seems practical to compare the photopolymerization trends of these LEDs in order to determine optimal LED photocuring systems. The trend shown in the graph is identical to the current UV-LED situation that is explained in section 7.1. Namely, as the emitting wavelength of LEDs decrease, its light intensity also decreases.

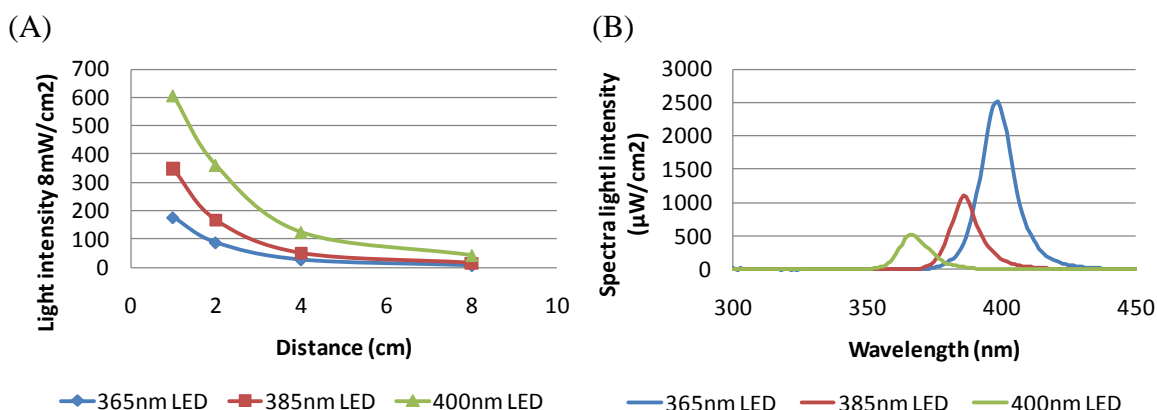


Figure 7-8: Comparison of 365 nm, 385 nm, and 400 nm LEDs; (A) Correlation between light intensities at center position and measured distance, (B) Spectral light intensities at 8cm distance, measured at center position

7.2.2. Comparison of the Energy Consumption and Irradiation of Light Sources

The energy efficiency of three types of light sources was compared by measuring both the light power emitted (W_{input}) and electrical power consumed (W_{output}) for each. The three light sources were: a 400 nm LED lamp (Firefly, Phoseon), a 100 W mercury (Hg) lamp (Acticure, EXFO), and a 150 W xenon (Xe) lamp (Max-150, Asahi). The apparent power consumed by each light source was measured using a wattage meter. The wattage meter was connected between the power source and the light source so that

the total energy used by lighting, cooling, displaying, *etc.* was measured. The light energy emitted from the light sources was characterized using a spectrometer (Ocean Optics, Inc.). Table 7-1 summarizes the measured power results and reveals that the 400 nm LED has the least power consumption at 97 W, but the highest power light emission (33 W) compared to the power of the Hg and Xe lamps. Figure 7-9 illustrates the energy efficiency, showing that the energy efficiency of the 400 nm LED is two orders of magnitude higher than the conventional lamps.

Table 7-1: Consumed electric power and emitted light power of a 400 nm LED (Firefly, Phoseon), 100 W mercury (Hg) lamp (Acticure, EXFO), and a 150 W xenon (Xe) lamp (Max-150, Asahi)

Light source	Power Consumption (W_{output})	Light Power Emitted (W_{input})
400 nm LED	97	33.0
100W Hg lamp	193	0.71
150W Xe lamp	290	1.01

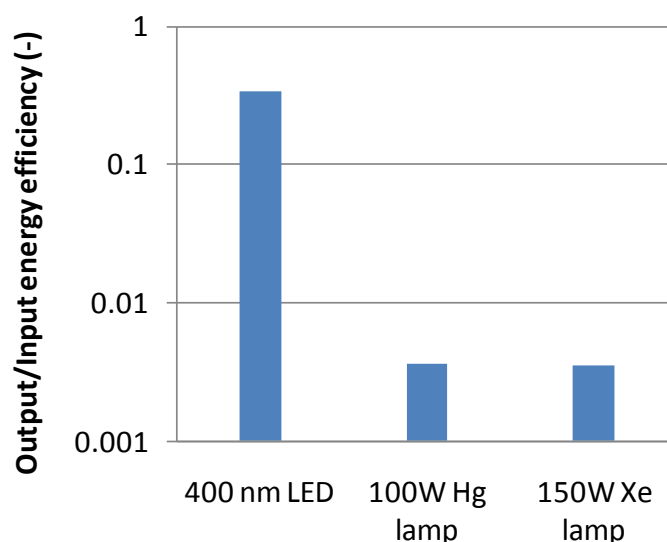


Figure 7-9 : Energy efficiency of 400 nm LED (Firefly, Phoseon), 100 W mercury (Hg) lamp (Acticure, EXFO), and a 150 W xenon (Xe) lamp (Max-150, Asahi).

7.3. Simulation Analysis and Experimental Studies for Thick Cure

To investigate photopolymerization using LEDs, a thick system in which the thickness is up to 3.5 cm was used in this section. Both experimental and modeling studies were performed.

7.3.1. Methods

7.3.1.1. Materials and Light Sources

In this aspect of the research, the monomer hexanediol diacrylate (HDDA) (SR238B, Sartomer, Exton, PA) was used with the following four α -cleavage type photoinitiators: BAPO (bis(2,4,6-trimethylbenzoyl)-phenylphosphine oxide), BDMB (2-benzyl-2-(dimethylamino)-1-[4-(4-morpholinyl)phenyl]-1-butanone), DMPA (2,2-dimethoxy-2-phenylacetophenone), and TPO (diphenyl(2,4,6-trimethylbenzoyl)-phosphine oxide). All photoinitiators are provided by BASF (Ludwigshafen, Germany). The structures of these photoinitiators are shown in Figure 7-10.

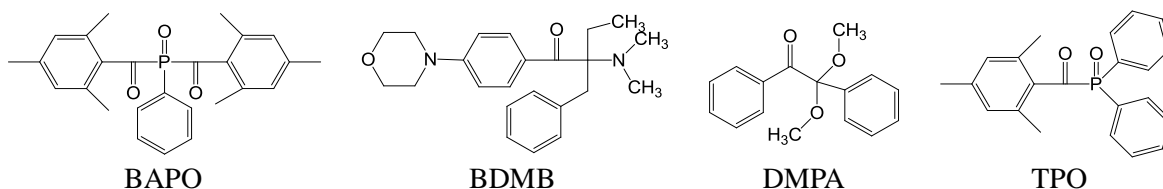


Figure 7-10: Chemical structure of the photoinitiators: BAPO (bis(2,4,6-trimethylbenzoyl)-phenylphosphine oxide), BDMB (2-benzyl-2-(dimethylamino)-1-[4-(4-morpholinyl)phenyl]-1-butanone), DMPA (2,2-dimethoxy-2-phenylacetophenone), and TPO (diphenyl(2,4,6-trimethylbenzoyl)-phosphine oxide).

Figure 7-11 shows the emission spectra for each lamp measured by an Ocean Optics USB 4000 fiber optic spectrometer of the lamps for the UV lamps (Hg-Xe lamps) and the 400 nm LED lamp (Firefly, Phoseon) used in this study.

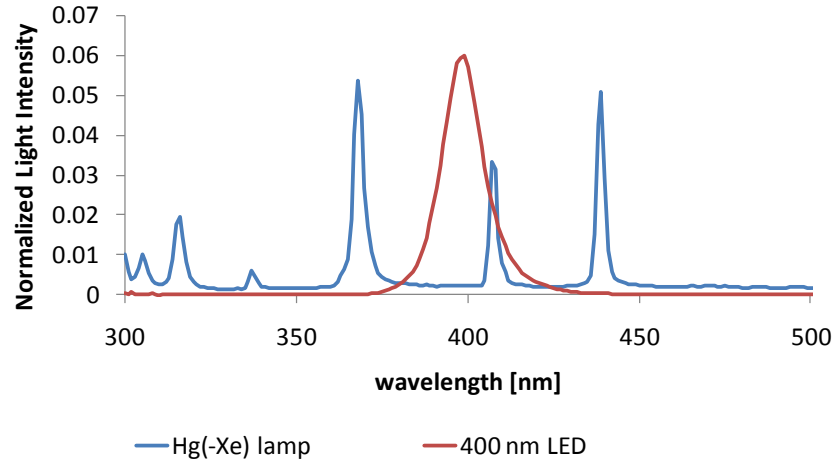


Figure 7-11 : Normalized spectral light intensities of a Hg(-Xe) lamp and a 400 nm LED lamp

7.3.1.2. Simulation Analysis

Simulation analysis was performed using a previously developed model⁵⁶ for multi-wavelength illumination. For a polymerization system with a rectangular cross-section subject to uniform polychromatic illumination normal to the top surface, the set of differential equations that govern the evolution of the light intensity gradient and initiator concentration gradient for polychromatic illumination are shown below.

$$\frac{\partial C_i(z,t)}{\partial t} = -\frac{C_i(z,t)}{N_A h} \sum_j \left(\frac{\varepsilon_{ij} \phi_j I_j(z,t)}{\nu_j} \right) + D_i \frac{\partial^2 C_i(z,t)}{\partial z^2} \quad \text{Equation 7-1}$$

$$\frac{\partial C_p(z,t)}{\partial t} = \frac{C_i(z,t)}{N_A h} \sum_j \left(\frac{\varepsilon_{ij} \phi_j I_j(z,t)}{\nu_j} \right) + D_p \frac{\partial^2 C_p(z,t)}{\partial z^2} \quad \text{Equation 7-2}$$

$$\frac{\partial I_j(z,t)}{\partial z} = -[\varepsilon_{ij} C_i(z,t) + \varepsilon_{pj} C_p(z,t) + a_{CBj} C_{CB} + A_m] I_j \quad \text{Equation 7-3}$$

Here, the subscript j is an index with a different value for each wavelength of light under consideration; $C_i(z,t)$ is the initiator molar concentration at depth z and time t ; $C_p(z,t)$ is the photolysis product molar concentration at depth z and time t ; $I_j(z,t)$ is the incident light intensity of a specific wavelength at depth z and time t with units of

energy/(area*time); ϵ_i is the initiator's Napierian molar absorptivity at a specific wavelength with units of volume/(length*mole); ϵ_p is the photolysis product Napierian molar absorptivity of a specific wavelength with units of volume/(length*mole); ϕ_i is the quantum yield of the initiator at a specific wavelength, defined as the fraction of absorbed photons that lead to fragmentation of the initiator; N_A is Avogadro's number; h is Planck's constant; ν is the frequency of light in units of inverse seconds; D_i is the diffusion coefficient of the initiator in units of length²/time; D_p is the diffusion coefficient of the photolysis products; and A_m is the absorption coefficient of the monomer and the polymer repeat unit with units of inverse length.

Note that this is the Napierian molar absorptivity because it is most natural for the differential version of the absorption equation (Equation 7-3). The measured Napierian molar absorptivity of the photoinitiators (BDMB, BAPO, TPO, and DMPA) and their photolysis products shown in Figure 7-12 are used in this simulation study. For each initiator, a typical value for the quantum yield of 0.2 was used. The following initial and boundary conditions apply to this reaction geometry:

$$C_i(z,0) = C_o \quad \text{Equation 7-4}$$

$$C_p(z,0) = 0 \quad \text{Equation 7-5}$$

$$\frac{\partial C_{i,p}}{\partial z} = 0 \text{ at } z = 0 \text{ and } z = z_{\max} \quad \text{Equation 7-6}$$

$$I(0,t) = I_o \quad \text{Equation 7-7}$$

Equation 7-4 states that the initial photoinitiator concentration is uniform throughout the depth of the sample. Similarly, Equation 7-5 indicates that the initial photolysis product concentration is zero. Equation 7-6 is the no-flux boundary condition indicating that there is no transport of initiator or photolysis product across the illuminated surface ($z=0$) or the substrate boundary ($z=z_{\max}$), and Equation 7-7 states that

at any time the intensity on the surface of the sample where the light enters is equal to the initial intensity of the light source.

The rate of production of free radicals as a function of depth was also considered in this study and is defined by Equation 7-8. Equation 7-8 defines the instantaneous local rate of production of free radicals, $R_i(z,t)$, if two active centers are produced upon fragmentation of the initiator.

$$R_i(z,t) = 2C_i(z,t) \sum [I(z,t)]_j \phi_j \epsilon_j \quad \text{Equation 7-8}$$

The solution to this set of equations provides detailed information regarding the time-evolution of the light intensity gradient, the initiator concentration gradient, and the photoinitiation rate profile (rate of active center generation as a function of time and location). For an accurate description of initiation with polychromatic illumination, the light intensity gradient at each incident wavelength must be individually described. As shown in Equation 7-3, the intensity of an individual wavelength is attenuated by absorption of the initiator, monomer, polymer repeat units, and the photolysis product. The time-evolution of all the light intensities are coupled to one another because the local initiator concentration depends upon all of the incident wavelengths and local light intensity of each wavelength depends upon the initiator concentration. Therefore, the complete set of differential equations must be solved simultaneously. Thus, the wavelength dependence of the intensity contributes considerably to the complexity of the model. For description of n wavelengths of incident light, $n+2$ equations must be solved simultaneously; typically, a 100 nm region of the spectrum is important, so in excess of 100 equations must be simultaneously solved. In this thick cure condition, the values of the diffusion terms occupied less than 10 % of total values in Equations 7-1 and 7-2. Hence, the diffusion terms were neglected.

One study utilizing this simulation has shown that illumination of TPO with the 400 nm LED lamp (Firefly) results in improved photoinitiation rates over the Hg(Xe) UV

lamp illumination for thick cure, as shown in Figure 7-13. Figure 7-13 contains a series of photoinitiation rate profiles for the Hg(Xe) and LED lamps for illumination times ranging from 30 seconds to 20 minutes. The figure illustrates that the LED source results in more symmetric photoinitiation rate profiles that exhibit a higher maximum and move through the sample faster than the corresponding profiles for the Hg(Xe) lamp. These trends are explained by the emission spectrum of the lamps and the absorption spectrum of the initiator. The LED emission spectrum is considerably narrower than the Hg(Xe) lamp and lies predominantly in the 390 – 410 nm range (see Figure 7-11). In this region of the spectrum, the TPO molar absorptivity is relatively constant (Figure 7-12), thereby leading to the symmetric photoinitiation rate profile. In contrast, there is a wide variation in photoinitiator molar absorptivity for the emission wavelengths emitted by the Hg(Xe) lamp. This leads to an asymmetric profile in which wavelengths of relatively low molar absorptivity create an enhanced photoinitiation rate on the leading edge of the photoinitiation front. This result suggests that selection of a photoinitiator system in conjunction with a given light source is a complex process, and optimum selection depends upon a number of variables in a manner that may not be anticipated based upon simple selection criteria.

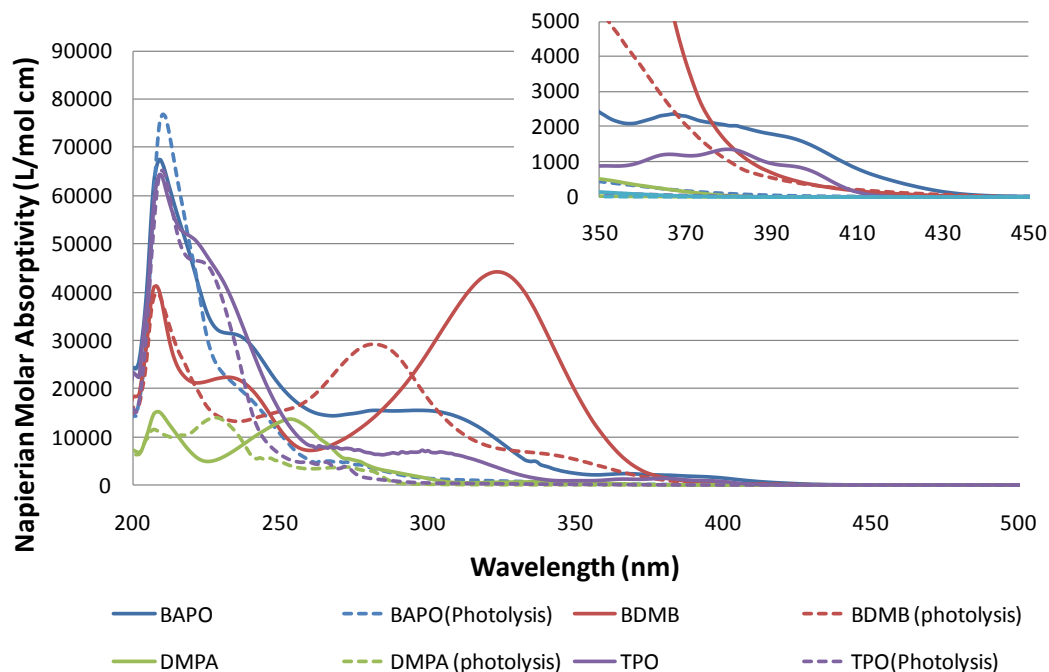


Figure 7-12: Napierian molar absorptivities of BAPO, DMPA, BDMP, and TPO and their photolysis products.

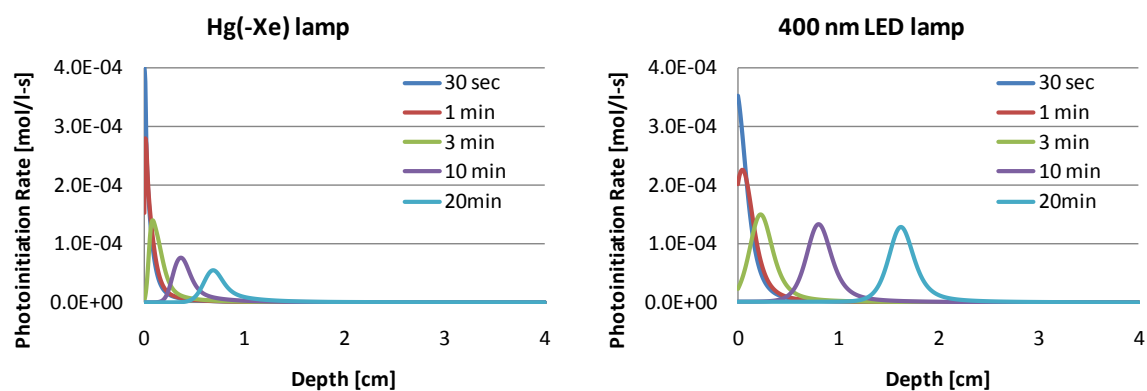


Figure 7-13: Calculated photoinitiation rates of a system initiated with TPO using either a Hg(-Xe) lamp or a 400 nm LED lamp over time (light intensity: 41 mW/cm^2 , photoinitiator concentration: 0.0167 M).

7.3.1.3. Experimental Studies:

Experiments for thick cure were performed using polymethyl methacrylate (PMMA) cuvettes. The 1 cm by 1 cm by 4 cm cuvettes were chosen because they were transparent to the wavelengths of interest and readily dissolved in a number of solvents,

thereby allowing the extent of polymerization to be easily determined. Again, these experiments were performed using HDDA monomer and the four α -cleavage type photoinitiators described in section 7.3.1.2. Each cuvette was filled with 3.5 cm of the monomer, and the cuvettes were placed on a quartz plate and illuminated with a light source from the bottom of the cuvette. In all samples, the concentration of the photoinitiator was 0.0167 M, and the total light intensity of the light sources was 41 mW/cm². Illumination from below avoided polymerization-induced convection or mixing because the density of the polymer was higher than that of the monomer. In each cuvette, the polymerization began at the bottom of the sample and moved as a polymerization front toward the top of the sample. The sample was placed in tetrahydrofuran (THF) to dissolve the cuvette and monomer from the uncured region of the sample. In these crosslinked systems, monomer became incorporated into the polymer matrix as it reacted with an active center; therefore, essentially no soluble polymer fractions existed. The insoluble crosslinked polymer matrix was washed again with pure THF to remove any remaining excess monomer. The polymer samples were dried thoroughly in a dry oven.

7.3.2. Results

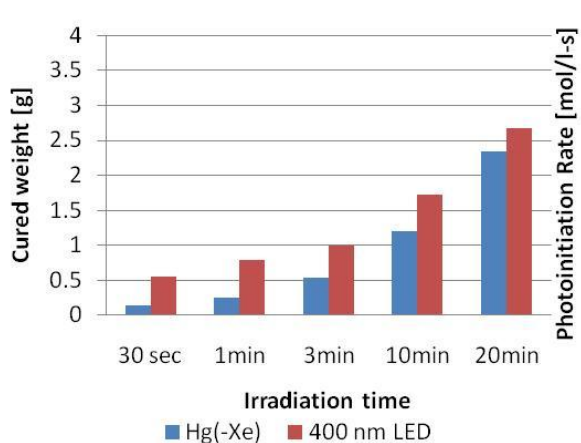
Figure 7-14 compares the experimental polymerized weight with modeled photoinitiation rates for photopolymerizations of thick HDDA systems containing four different initiators: BAPO (A), BDMB (B), DMPA (C), and TPO (D). For each initiator, the profile on the left side of the figure contains a plot of the weight of the polymerized samples as a function of time for both a Hg(-Xe) lamp and 400 nm LED lamp. The figure illustrates that for all four initiators the LED lamp is more effective for thick cure than the Hg(-Xe) lamp.

For each initiator, the profile on the right side of Figure 7-14 contains a plot of the calculated photoinitiation profiles at 0.5 cm depth as a function of time for the two

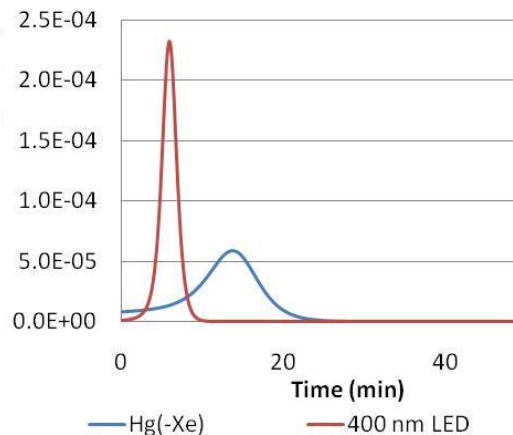
light sources. For the polymerization system containing BAPO (A) or TPO (D), the experimental and simulation results are in general agreement because the polymerization rate (left curve) and the photoinitiation rate (right curve) are both higher for the LED lamp. However, the calculated photoinitiation rates for the systems containing BDMB or DMPA do not match the experimental results. In Figure 7-14.B (a) and (b), the polymerized weight of the monomer containing BDMB is high whereas the calculated photoinitiation rate is quite small. For the system containing DMPA, the predicted photoinitiation rate profiles of the two lamps is inconsistent to the experimental result; Figure 7-14C (a) shows that the polymerized weight for the 400 nm LED is higher than the weight of a resin cured with the Hg(-Xe) lamp at all irradiation times, except for thirty seconds. On the other hand, Figure 7-14.C (b) shows that the calculated photoinitiation rate for the 400 nm LED is lower than that for the Hg(-Xe) lamp. A reason for this discrepancy between the experiment and simulation may be the effect of heat generated by the exothermic polymerization reaction. Because the system is thick, the total reaction energy is so high that the heat effect might not be negligible, unlike in “thin cure” which is described later.

A. BAPO

(a) Experimental result

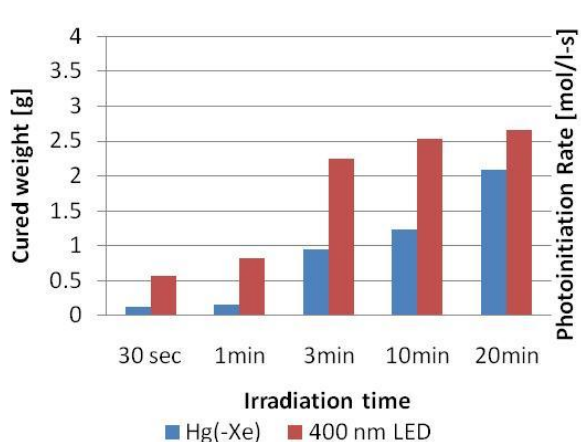


(b) Simulation result



B. BDMB

(a) Experimental result



(b) Simulation result

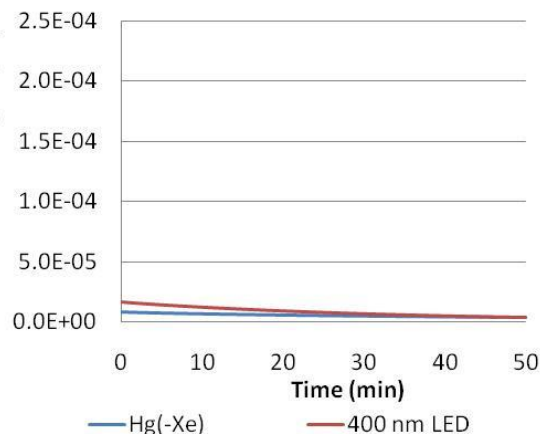
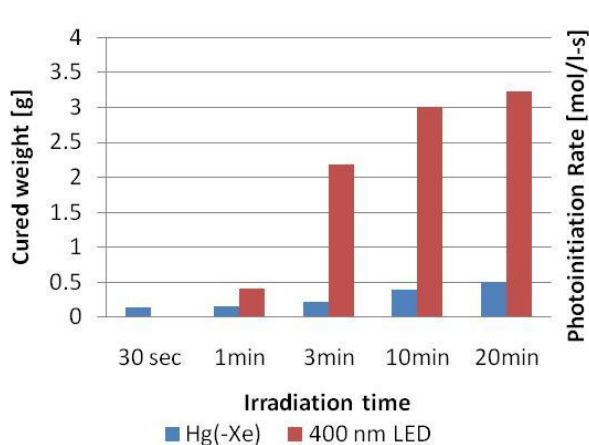


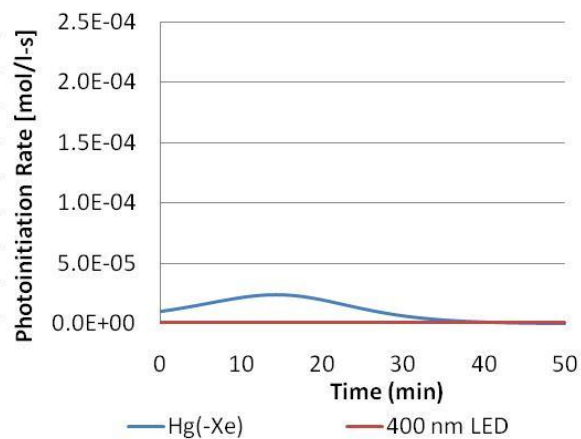
Figure 7-14: Comparison of two light sources for photopolymerizations of thick HDDA systems containing four different initiators: (A) BAPO, (B), BDMB, (C) DMPA, and (D) TPO. Light intensity: 41 mW/cm^2 ; Photoinitiator concentration: 0.0167 M . (a) Experimental conversion measured as a function of time, and (b) simulation results for photoinitiation rate at 0.5 cm depth as a function of time.

C. DMPA

(a) Experimental result

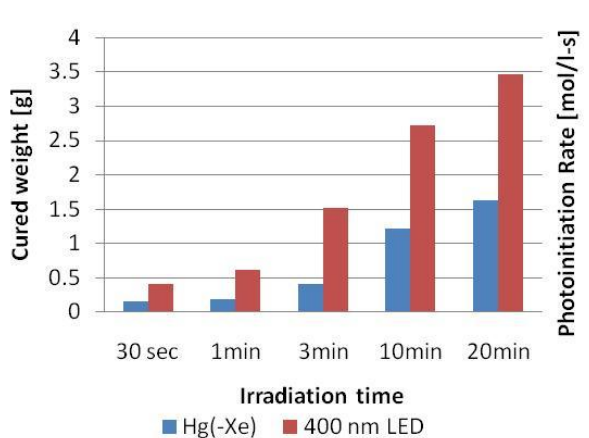


(b) Simulation result



D. TPO

(a) Experimental result



(b) Simulation result

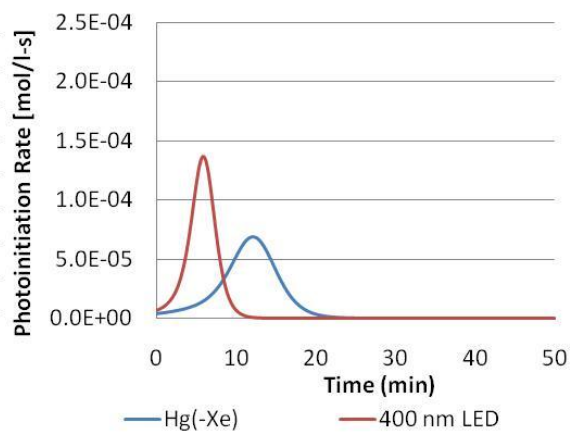


Figure 7-14 continued.

7.3.3. Heat Effect Analysis of Thick Cure

As described in section 7.3.2, heat generated by exothermic polymerization reactions may have an important role in thick cure. In this section, the influence of heat upon thick cure is investigated using different measurement techniques, including Raman

confocal microscopy, in-situ temperature measurement, Raman spectroscopy, and differential scanning calorimetry (DSC).

7.3.3.1. Evidence of Heat Effect

7.3.3.1.1. Conversion Profiles of Thick Cure Samples (Raman Confocal Microscopy)

Raman confocal microscopy was used to obtain conversion profiles of the thick cure polymerized samples. The middle of one of the four sides of the polymerized sample was chosen for the Raman measurement. The Raman confocal microscope was set to collect a Raman spectrum in 50 μm increments along the 3 cm length in the z-direction (from the irradiated bottom to top). Raman spectra of the samples were collected using a Leica DMLP optical microscope with confocal optics attached to the modular research Raman spectrograph (HoloLab 5000R, Kaiser Optical Systems, Inc) with a 785 nm laser.⁵² A combination of 785 nm single mode excitation fiber, 100 μm collection fiber, and long wide distance (LWD) 50 \times objective, with numerical aperture equal to 0.55, was used in the measurement. The laser beam intensity measured by a laser power meter through the LWD 50 \times lens was 8–15 mW/cm^2 . For each measurement step, the exposure time was set to 5 seconds with one accumulation to optimize the signal-noise ratio. The reactive C=C peak at 1640 cm^{-1} and an unchanging reference peak at 1720 cm^{-1} (attributed to the C=O carbonyl stretch) were monitored to determine the acrylate conversion. The conversion was calculated using the ratio of reactive (A_{rxn}) peak and internal reference (A_{ref}) peak areas:

$$\% \text{ Conversion} = \left[1 - \frac{A_{\text{rxn}}(\text{p})/A_{\text{ref}}(\text{p})}{A_{\text{rxn}}(\text{u})/A_{\text{ref}}(\text{u})} \right] \times 100 \quad \text{Equation 7-9}$$

where “u” refers to unpolymerized resin and “p” refers to polymerized resin.

Figure 7-15 shows the conversion profiles of HDDA thick systems containing four different photoinitiators (BAPO, BDMB, DMPA, and TPO) irradiated with the 400 nm LED for 20 minutes. As shown in Figure 7-15, the photoinitiators all have

approximately 95% conversion, which is much higher than the final conversion of approximately 80% observed in the thin cure study in section 7.4. This higher conversion in thick cure may be due to the high reaction heat occurring in thick cure. The heat increases the resin temperature higher than the glass transition temperature ($T_g = 105^\circ\text{C}$) during polymerization and results in overcoming the glass vitrification effect⁵⁸. Also, a high final conversion is achieved unlike in isothermal thin cure reactions. Figure 7-15 shows that the conversion of the sample containing BAPO or TPO decreases slightly and steadily away from the irradiated surface ($Z = 0$). The conversion gradient of the sample containing BDMB is high and the decay is not uniform compared to the profile of the sample containing BAPO or TPO. The sample containing DMPA profile has a unique trend. Contrary to the other three samples, the conversion decreases and then increases as the Z-step increases. These trends imply that the influence of heat on a resin containing BDMB or DMPA (especially DMPA) is greater than the influence on a resin containing BAPO or TPO.

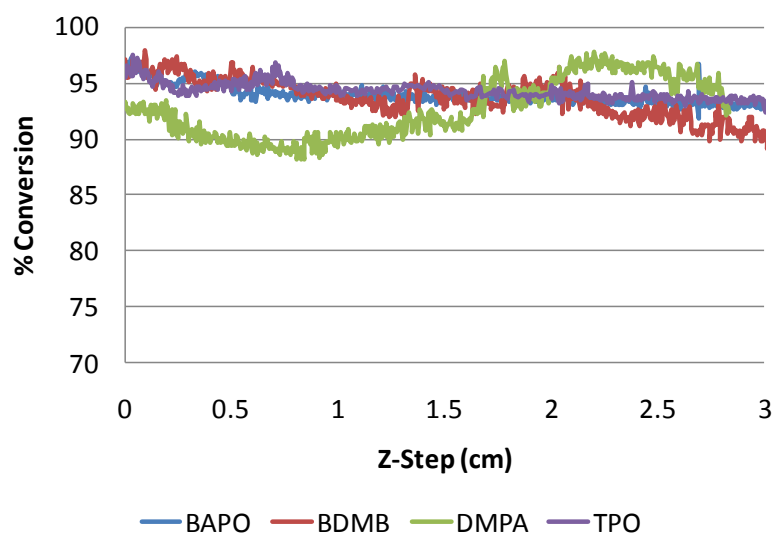


Figure 7-15: Final conversion profiles of thick cure samples with either BAPO, BDMB, DMPB, or TPO irradiated with a 400 nm LED (Firefly, Phoseon) for 20 minutes. Light intensity: 41 mW/cm^2 .

7.3.3.1.2. In-situ Temperature Measurement of Thick Cure

The actual temperature of the cuvette side was measured during thick cure irradiation using an IR thermometer (Extech 42560, INSTRUMENT). The thermometer was set at a specific height ($Z = 2, 5, 10, 15, 20, 35$ mm) and focused on the cuvette's side surface. The temperature was measured every 0.5 seconds. Figure 7-16 shows the cuvette temperature profiles for thick HDDA systems containing the four photoinitiators during irradiation with the 400 nm LED lamp. Note that this trend contains the conduction through the quartz at the bottom, convection to the surrounding air, and minor heat loss by radiation. Also note that the temperature profile is just for the cuvette surface. Therefore, the actual temperature inside is higher than the temperature measured. Below 10 mm, the temperature is almost constant due to conduction into the quartz from the cuvette bottom. However, above 10 mm, the temperature increases to a peak and then decreases as polymerization occurs. At some heights, the temperature rises above T_g (105 °C). For all the four thick systems, the temperature is above T_g at 35 mm, and for the system containing BDMB or TPO at 20 mm, the temperature is above T_g . In Figure 7-16 at a height of 35 mm (dark blue), the temperature profiles of the system containing BDMB or DMPA rise to a higher temperature compared to the profiles of the system containing BAPO or TPO. In addition, the increase of the temperature starts faster than that of the system containing BAPO or TPO. This implies that the effect of heat during polymerization occurs faster in the thick system containing BDMB or DMPA compared to in the system containing BAPO or TPO, because light irradiates thicker regions due to the low absorptivity and initiates polymerization in thick regions quickly.

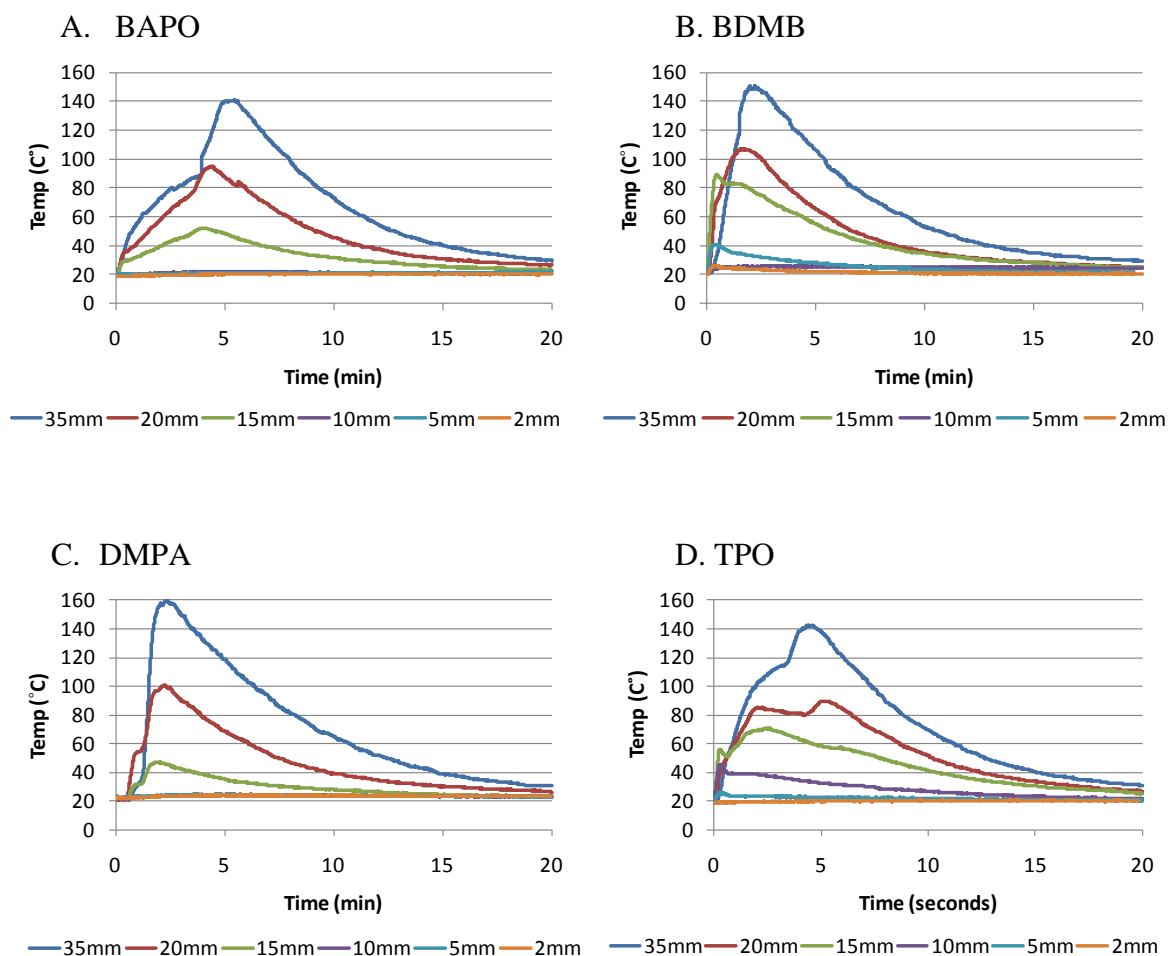


Figure 7-16: Temperature measured by an IR thermometer as a function of time at various heights of the cuvette during irradiation with a 400 nm LED (Firefly, Phoseon) for thick HDDA systems containing four different initiators: (A) BAPO, (B) BDMB, (C) DMPA, and (D) TPO. Light intensity: 41 mW/cm²; Photoinitiator concentration: 0.0167 M.

7.3.3.2. Study of effect of temperature on polymerization

7.3.3.2.1. Correlation between Photopolymerization and Temperature (Real-Time Raman Spectroscopy)

The dependence of photopolymerization kinetics on temperature was investigated using real-time Raman spectroscopy. Raman spectra were collected using a holographic fiber coupled stretch probehead (Mark II, Kaiser Optical Systems, Inc.) attached to a modular research Raman spectrograph. A sample containing HDDA

monomer with a photoinitiator (either BAPO, BDMP, DMPA, or TPO) was placed inside a 1 mm inner diameter (ID) quartz capillary tube and irradiated with the 400 nm LED (Firefly, Phoseon) at 6.8 mW/cm^2 . The sample temperature was controlled by a water jacket at 23°C , 50°C , or 80°C . A 785 nm laser through a 10x objective lens was directed into the sample to induce the Raman scattering effect. The conversions of the samples were calculated using the same analysis described in 7.3.3.1.1 with Equation 7-9.

Figure 7-17 illustrates the effect of temperature on conversion as a photopolymerization reaction occurs through time for the samples containing BAPO, BDMP, DMPA, and TPO. The conversion increases as the temperature increases due to a lower viscosity in higher temperature polymers that causes higher crosslinked densities. Figure 7-17 also shows that the higher temperature promotes a faster polymerization rate, because the accelerated propagation reaction occurs. The accelerated propagation rate is due to the higher possibility of the active centers and monomer (or dissolved oxygen) encountering each other.

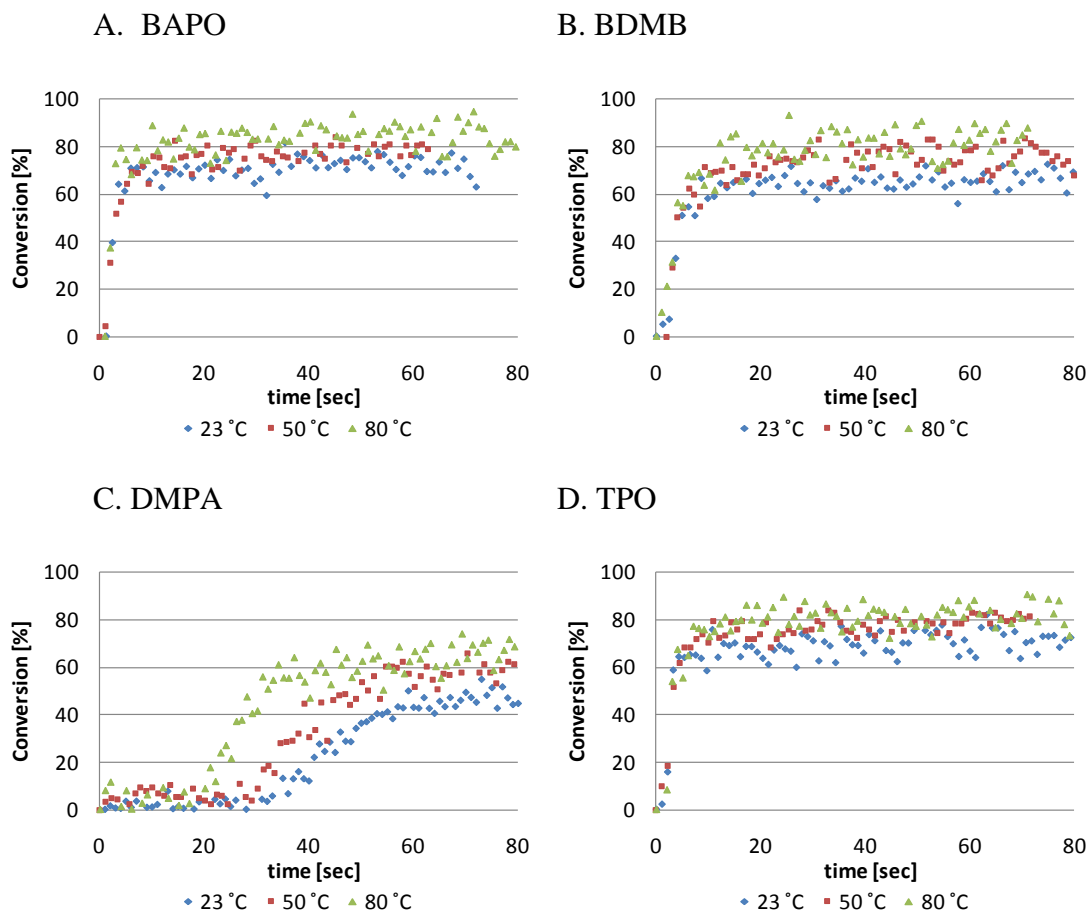


Figure 7-17: Percent conversion as a function of time at 23°C, 50°C, or 80°C for HDDA with (A) BAPO, (B) BDMB, (C) DMPA, and (D) TPO when cured with a 400 nm LED lamp (Firefly, Phoseon) (light intensity: 6.8 mW/cm²).

7.3.3.2.2. Thermal Stability of Monomer Systems in a Dark Condition

Differential scanning calorimetry (DSC) (DSC-7, PerkinElmer) was used to characterize the stability as a function of temperature for the HDDA monomer with and without a photoinitiator under dark conditions. The experimental heat flow program had a heating rate of 5°C/min over a temperature range of 50–220 °C, and two consecutive scans were obtained. For each system, a characteristic heat flow profile was obtained by subtracting the profile of the second run from the profile of the first run. In each case, the heat flow profile exhibits exothermic heat flow at the temperature at which thermally-induced polymerization begins to occur. Figure 7-18 shows the heat flow profiles as a

function of temperature for the HDDA monomer with the four photoinitiators and without a photoinitiator. Compared to neat HDDA without a photoinitiator (light blue line), the HDDA samples containing photoinitiators exhibit exothermic heat flow at lower temperatures (with the exception of DMPA (green line)). Therefore, it can be assumed that the photoinitiators act as thermal photoinitiators above 120°C, as shown in Figure 7-18. The threshold temperature of HDDA containing DMPA (160 °C in the graph) is higher than the other photoinitiators; however, the reaction is very rapid when the temperature is above the threshold temperature. This indicates that if the temperature rises to the threshold temperature during the (photo)polymerization reaction, the reaction accelerates because DMPA acts as a thermal initiator here.

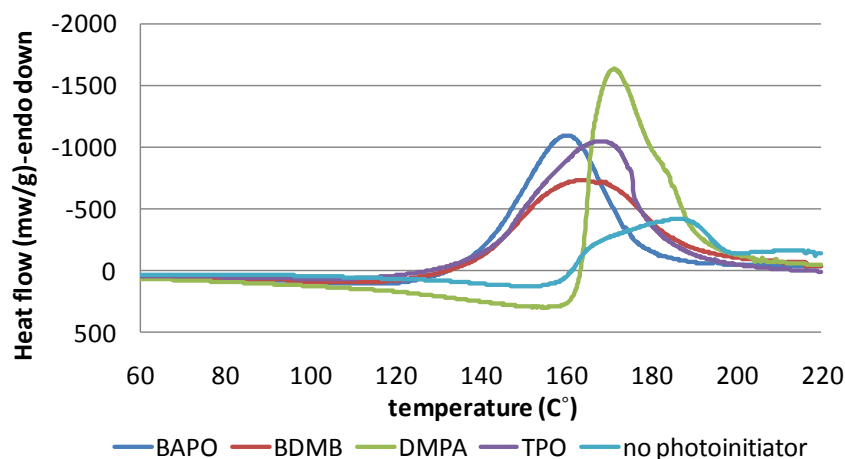


Figure 7-18: DSC heat flow (with the second run subtracted from the first run) as a function of temperature for HDDA with BAPO, BDMB, DMPA, TPO, or without photoinitiator.

7.3.3.3. Heat Effects in Thick Cure

The results shown in Section 7.3.3.1 and 7.3.3.2 provide information about the effect of temperature on the polymerization rate, and illustrate the possible effect of the heat of polymerization in thick systems. The Raman confocal microscopy as well as in-situ temperature measurements shown previously in Section 7.3.3.1 illustrate that the heat

released by the polymerization itself may lead to a significant temperature excursion and an increased ultimate conversion. The real-time Raman spectroscopy results from Section 7.3.3.2.1 further illustrate how the polymerization rate increases with increasing temperature. The DSC results indicate that thermally-induced polymerization will occur above the threshold temperature of approximately 120°C. To further consider the effect of heat on thick cure, the model was used to understand how light intensity and time vary as a function of depth and how the heat generated in thick cure relates to light intensity and depth.

The model was first used to represent a 4.0 cm thick system containing DMPA. Figure 7-19A illustrates the time and depth dependence of the light intensity in the system containing DMPA calculated by the model. As shown in Figure 7-19A, the light intensity is approximately the same as depth increases for both one minute and five minute illumination time, illustrating that light penetrates into thick regions. Therefore, the reaction heat generated in thick, wide regions enhances the photopolymerization propagation reaction. As heat is generated, the temperature increases to the threshold temperature and, thereby, induces the thermal initiation of DMPA. On the other hand, light illuminating a system containing TPO has light intensity that only penetrates the surface and allows a little light to pass into thick regions, as shown in Figure 7-19B. Therefore, the region that generates heat and the total exothermal energy are small, causing the polymerization enhancement by the effect of heat to perhaps be small compared with the system containing DMPA.

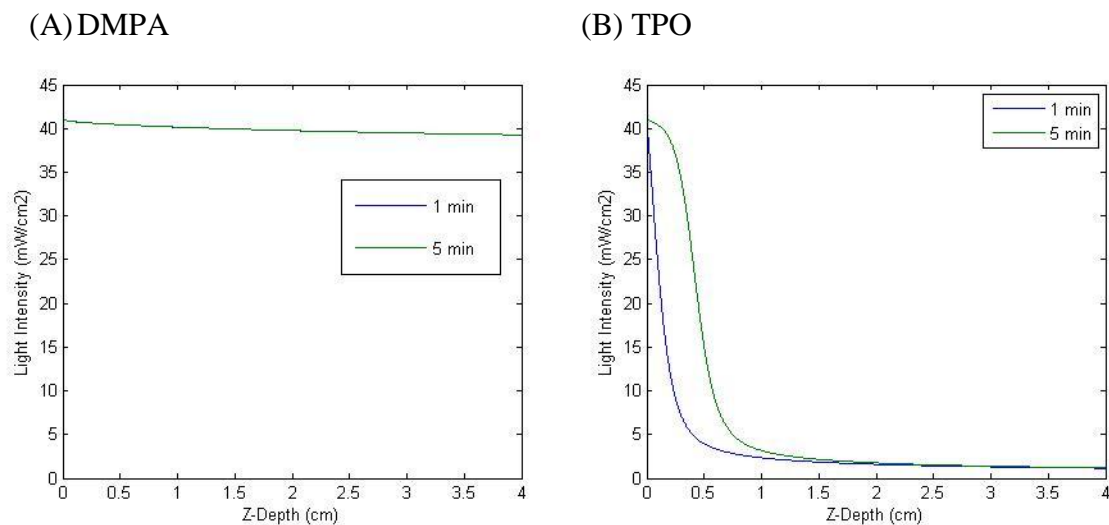


Figure 7-19: Calculated time and depth dependence of the light intensity for 4.0 cm thick systems containing different photoinitiators: (A) DMPA, (B) TPO. The systems were irradiated by the 400 nm LED (light intensity: 41 mW/cm², photoinitiator concentration: 0.0167 M).

7.4. Simulation Analysis and Experimental Studies for Thin Cure

In this section, photopolymerization of 15 μm thin system was investigated experimentally and numerically.

7.4.1. Methods

7.4.1.1. Materials and Light Sources

The same resin, HDDA, and same photoinitiators, BAPO, BDMB, DMPA, TPO, were used as with section 7.3. Conventional UV lamps (Hg or Hg-Xe lamps) and the 365 nm, 385 nm, and 400 nm LED lamps described above were employed as the light sources. In this study, two light conditions were investigated numerically and experimentally. The first condition was same total light intensity for all light sources. The second condition, which was focusing on only LEDs, was same distance between a light source and an irradiated sample.

7.4.1.2. Simulation Analysis

7.4.1.2.1. Expansion of the Model

To simulate conversion profiles in thin cure systems, in addition to the model described in section 7.3.1.2, further reaction mechanisms including propagation, termination, and oxygen inhibition were considered in this study using equations below.

$$\frac{\partial C_M(z,t)}{\partial t} = -2C_i(z,t)I(z,t)\epsilon_i\phi - k_p C_M(z,t)C_{M\bullet}(z,t) + D_M \frac{\partial^2 C_M(z,t)}{\partial z^2} \quad \text{Equation 7-10}$$

$$\frac{\partial C_{M\bullet}(z,t)}{\partial t} = 2C_i(z,t)I(z,t)\epsilon_i\phi - 2k_t C_{M\bullet}(z,t)^2 - k_q C_{M\bullet}(z,t)C_{O_2}(z,t) + D_{M\bullet} \frac{\partial^2 C_{M\bullet}(z,t)}{\partial z^2} \quad \text{Equation 7-11}$$

$$\frac{\partial C_{O_2}(z,t)}{\partial t} = -k_q C_{M\bullet}(z,t)C_{O_2}(z,t) + D_{O_2} \frac{\partial^2 C_{O_2}(z,t)}{\partial z^2} \quad \text{Equation 7-12}$$

These kinetic equations represent the decrease of monomer through polymerization, the generation and termination of monomer radicals, and the quench of dissolved oxygen. The gradient of the double bond concentration, C_M , is shown in Equation 7-10 where k_p is the propagation coefficient, $C_{M\bullet}$ is the concentration of growing macro-radical chains, and D_M is the diffusion coefficient of monomer. The macro-radical chains gradient is similarly illustrated in Equation 7-11, where k_t is the termination coefficient, k_q is the quenching coefficient, C_{O_2} is the dissolved oxygen concentration, and $D_{M\bullet}$ is the diffusion coefficient of macro-radical chains. The gradient of the dissolved oxygen concentration is indicated in Equation 7-12, where D_{O_2} is the diffusion coefficient of dissolved oxygen.

7.4.1.2.2. Parameter Setting

In the model for HDDA resin, based upon values reported in the literature, the propagation coefficient (k_p) was assumed as 2.5×10^4 L/mol-s at less than 80 % conversion.⁷⁰ At higher than 80 % conversion, k_p was hypothesized to decrease linearly

and become zero at 87 % due to vitrification effect. The termination coefficient (k_t) was 5.0×10^6 L/mol-s, which is estimated by fitting on the experimental data using fixed k_p value (2.5×10^4 L/mol-s). Initial concentration of oxygen and its quenching coefficient (k_q) were assumed 1.2×10^3 M⁷¹ and 5.0×10^8 L/mol-s⁶, respectively. In the condition used for thin cure, the diffusion terms were all slight due to the low gradients of concentrations. Therefore, all diffusion terms were neglected in this study.

7.4.1.3. Experimental Studies:

Experiments for thin cure (15 μ m films) were performed using Real-Time Fourier transform infrared spectroscopy (RT-FTIR). The thin film photopolymerizations were investigated using HDDA monomer and the four α -cleavage type photoinitiators described in section 7.4.1.1. In each experiment, the concentration of the photoinitiator was 0.0167 M. For each of these studies, a droplet of monomer was placed between two rectangular IR grade sodium chloride salt crystal slides with 15 μ m Teflon beads placed between both ends of the slides to serve as spacers. Infrared spectra were collected using a modified Bruker 88 FTIR spectrometer designed to accommodate a horizontal sample. The infrared absorption spectra were obtained during five minutes of lamp illumination. The carbon-carbon double bond absorbance peak at 812 cm^{-1} , associated with an out-of-plane vibration, was monitored to determine the acrylate conversion. The conversion was calculated using the ratio of peak height to peak height prior to polymerization.

7.4.2. Condition 1: Same Light Intensity

7.4.2.1. Light Sources

First, simulation and experimental study were performed using various light sources emitting the same total light intensity of 6.8 mW/cm². Figure 7-20 illustrates emission spectra for the used light sources including the conventional UV lamp and LEDs. In previous Industry University Cooperative Research Center (IUCRC) meetings,

industry representatives suggested that we perform a study to determine the effect of the wavelengths in the two “tails” of the LED emission on either side of the maximum peak. To create a narrower emission peak centered at 400 nm, the light from a lamp (Xe lamp) was passed through a bandpass filter (BPF) and used in experimental study. Figure 7-20 shows that the LED lamp with and without the bandpass filter are centered at 400 nm, but the LED has a wider distribution without the BPF than with the BPF.

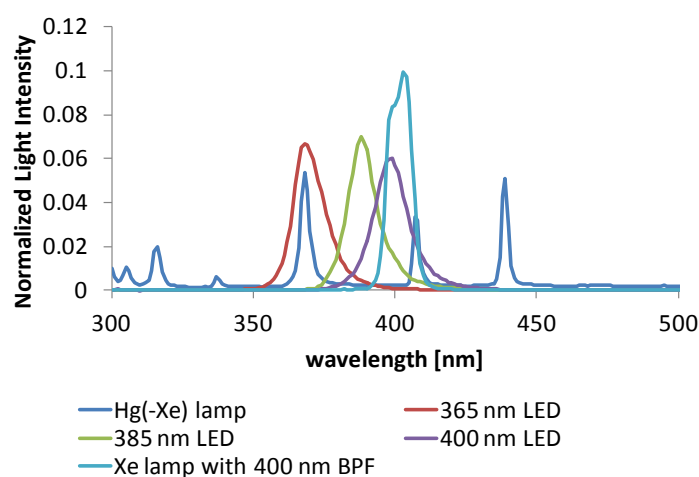


Figure 7-20: Normalized spectral light intensities of a Hg(-Xe) lamp, a 365 nm LED lamp, a 385 nm LED lamp, a 400 nm LED lamp, and a Xe lamp with a 400 nm bandpass filter (BPF).

7.4.2.2. Results

Figure 7-21 shows a comparison of five light sources for photopolymerization conversion profiles of thin HDDA systems containing four different initiators: (A) BAPO, (B), BDMB, (C) DMPA, and (D) TPO. The left-hand column of Figure 7-21(a) shows the experimental conversion profiles as a function of time for the Hg(-Xe) lamp, 365 nm LED lamp, 385 nm LED lamp, 400 nm LED lamp, and Xe lamp with the 400 nm bandpass filter. The graphs illustrate that the conventional Hg(-Xe) UV lamp (blue line) and 365 nm LED (red line) are more effective for the system containing BDMB (B) or

DMPA (C), because the conversion at a given time is always higher for the Hg(-Xe) lamp and 365 nm LED. However, for the system containing BAPO (A) or TPO (D), except the Xe lamp with 400 nm bandpass filter (sky blue line), all the lamps had approximately the same rapid polymerization. It appears that these trends are due to the different effective wavelength regions of the photoinitiators (See Figure 7-12). Specifically, BAPO and TPO exhibit higher absorbance around the 400 nm wavelength region than DMPA and BDMB. DMPA has relatively little absorbance above 370 nm. BDMB has high absorptivity around 400 nm wavelengths, but the total absorbed energy from the UV lamp and 365 nm LED is higher than that of the 400 nm LED due to the high absorbance below 370 nm. Compared to the Xe lamp with the 400 nm BPF, the 400 nm LED (purple line) is more effective for polymerization of thin regions for all four photoinitiators due to their higher absorption between 375–390 nm. As shown in Figure 7-20, the Xe lamp with the 400 nm BPF does not emit at wavelengths below 390 nm while the 400 nm LED does. The insert of Figure 7-12 shows that the photoinitiators have higher absorption at the wavelengths between 375–390 nm. Therefore, the 400 nm LED's lower wavelength region below 390 nm helps to achieve faster polymerization.

The right-hand column of Figure 7-21(b) shows calculated photoinitiation profiles at 15 μm depth as a function of time for the same five light sources as in part (a). For a specific photoinitiator, the light source exhibits similar trends for both the experimental conversion profile (left-hand column) and the simulated results (right-hand column). Then, comparing the same light source between the different photoinitiators, the calculated conversion profiles show the same general trends as the experimental results. For instance, using the 385 nm LED irradiation (green line), the system containing BAPO (A) is polymerized faster than the system containing BDMB (B) in both experimental (a) and calculated (b) results.

A. BAPO

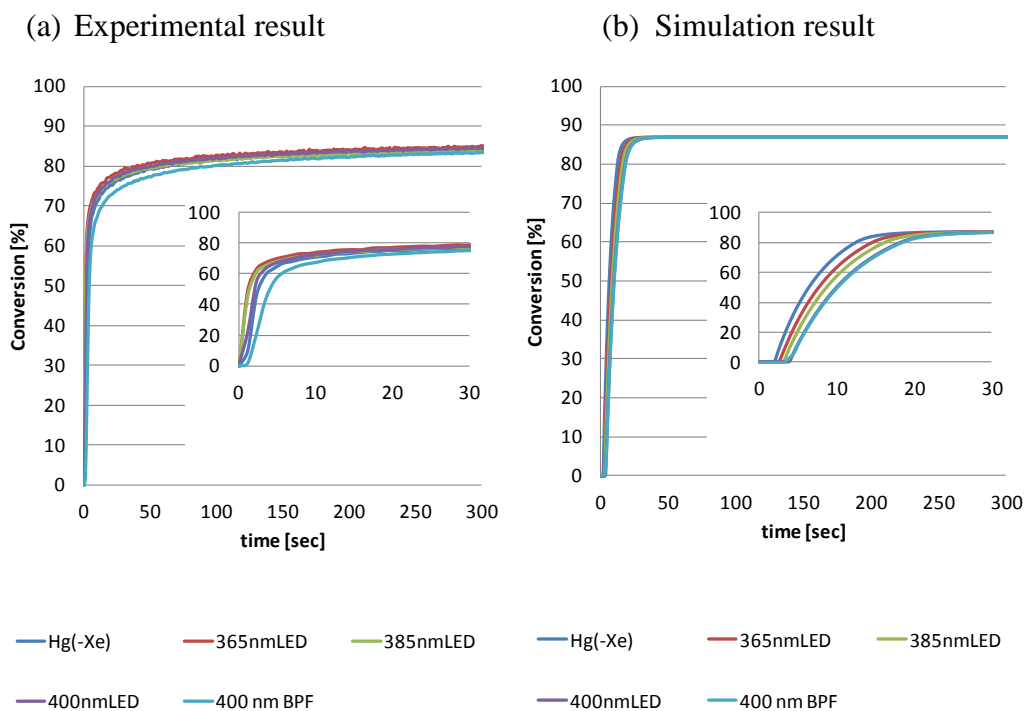
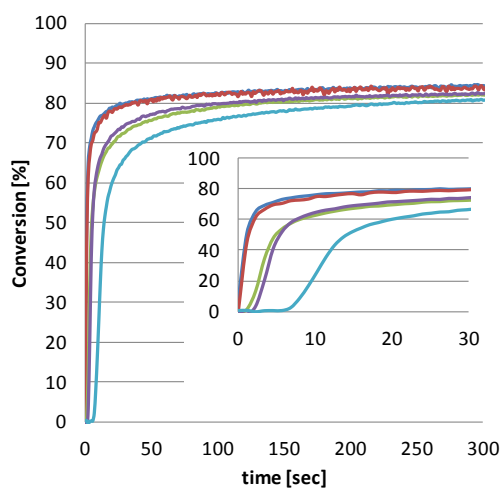


Figure 7-21: Comparison of five light sources for photopolymerization conversion profiles of thin HDDA systems containing four different initiators: (A) BAPO, (B), BDMB, (C) DMPA, and (D) TPO. Light intensity: 6.8 mW/cm^2 , photoinitiator concentration: 0.0167 M . (a) Experimental, (b) simulation.

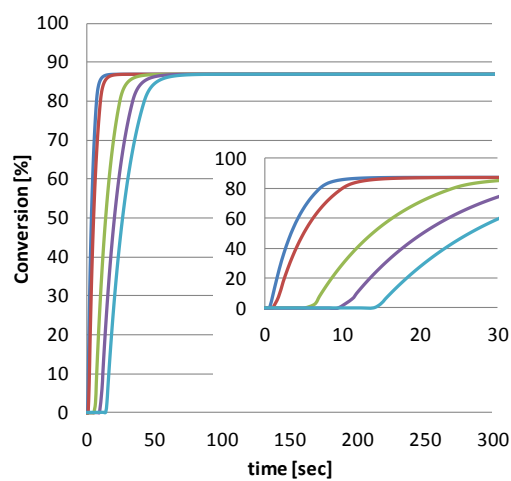
B. BDMB

(a) Experimental result



— Hg(-Xe) — 365nmLED — 385nmLED
 — 400nmLED — 400 nm BPF

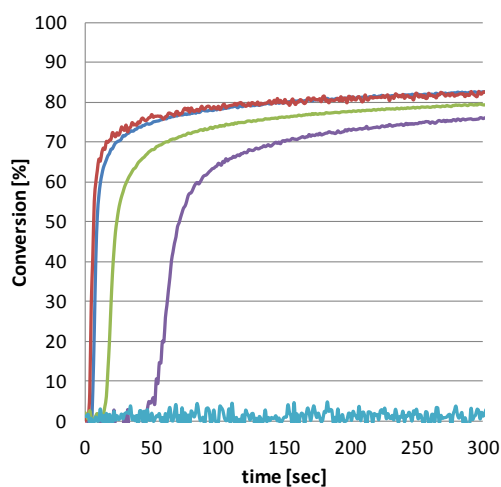
(b) Simulation result



— Hg(-Xe) — 365nmLED — 385nmLED
 — 400nmLED — 400 nm BPF

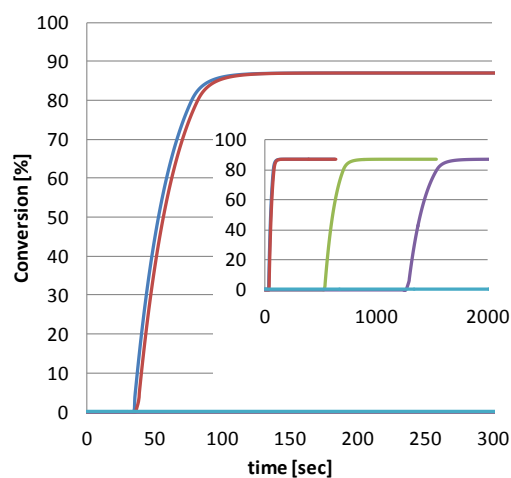
C. DMPA

(a) Experimental result



— Hg(-Xe) — 365nmLED — 385nmLED
 — 400nmLED — 400 nm BPF

(b) Simulation result



— Hg(-Xe) — 365nmLED — 385nmLED
 — 400nmLED — 400 nm BPF

Figure 7-21 continued.

D. TPO

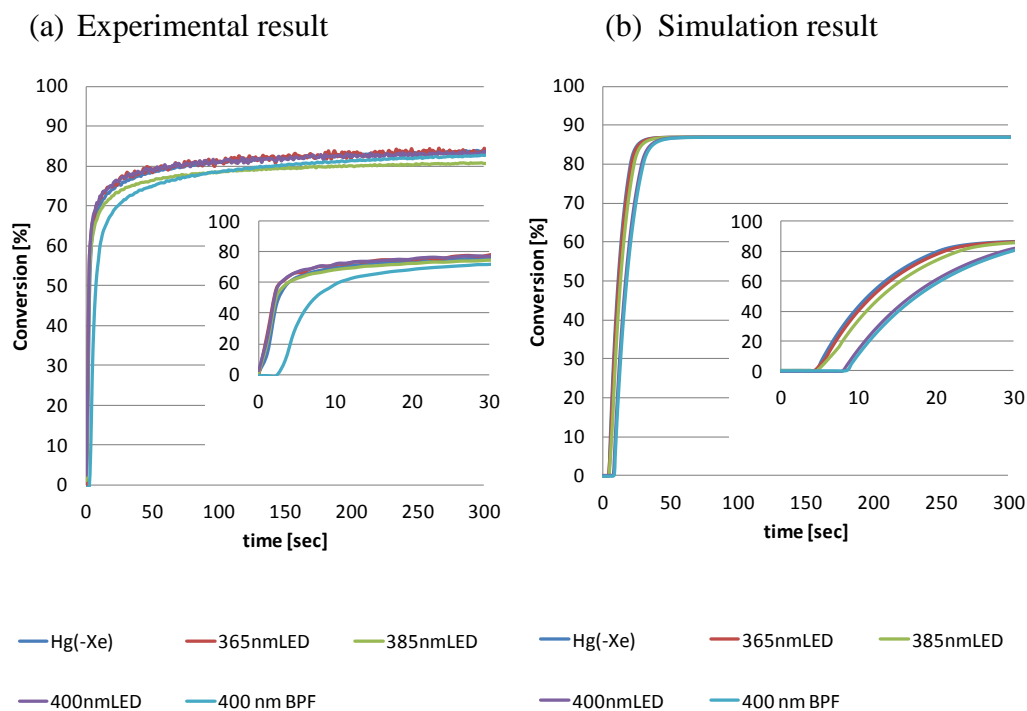


Figure 7-21 continued.

7.4.3. Condition 2: Same Configuration

In section 7.4.2, all light sources emit same light intensity; therefore, each distance between a light source and sample is basically different. In this section, the trends of the three LEDs (365 nm, 385 nm, 400 nm) with the same irradiation distance were studied.

7.4.3.1. Light Sources

The distance between the LED lamps and samples were fixed as 22.5 cm. The light spectral profiles are illustrated in Figure 7-22, and the total light intensity of the 365 nm LED, 385 nm LED and 400 nm LED was 1.3, 2.2 and 6.8 mW/cm² respectively.

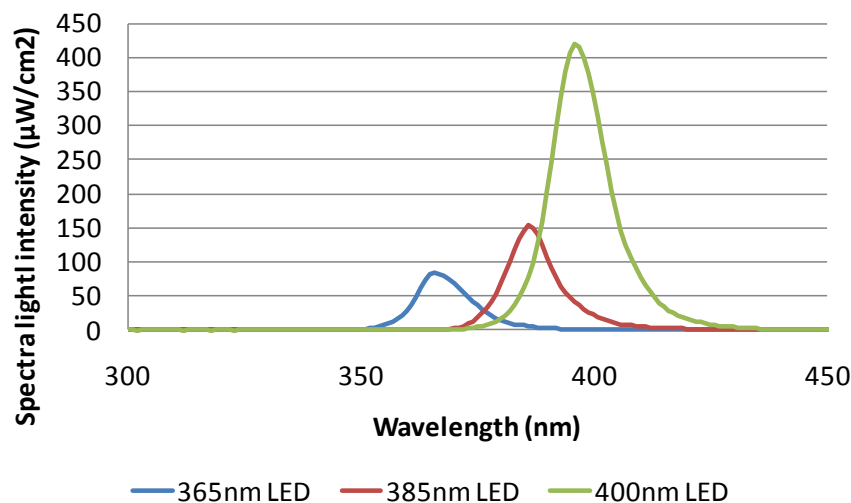


Figure 7-22: Spectral light intensities of a 365 nm LED lamp, a 385 nm LED lamp, and a 400 nm LED lamp, measured at 22.5 cm distance.

7.4.3.2. Results

As with section 7.4.2.2, Figure 7-23 shows a Comparison of three LEDs for photopolymerization conversion profiles of thin HDDA systems containing the four different initiators: (A) BAPO, (B), BDMB, (C) DMPA, and (D) TPO. The left-hand column of Figure 7-23(a) shows the experimental conversion profiles as a function of time whereas right-hand column Figure 7-23(b) demonstrates calculated one. Comparing the experimental results and simulation results, the trends are almost corresponding qualitatively. For instance, the most efficient lamp is the 400 nm LED and the second most is the 385 nm LED for both the experimental conversion profile (left-hand column) and the simulated results (right-hand column) for the system containing BAPO. For the system containing DMPA, the most effective LED was the 365 nm. Remarkably, the most effective lamp, provided by experimental study (left-hand column), was the 400 nm LED for the system containing BAPO, BDMB, or TPO. Although the lower wavelength regions of these photoinitiators show higher absorptivity (See Figure 7-12), the 400 nm LED, emitting the highest wavelength, is the most effective because the intensity of the

lamp is higher than the others. These results imply that to select the proper LED lamp practically both the wavelength and light intensity must be considered.

A. BAPO

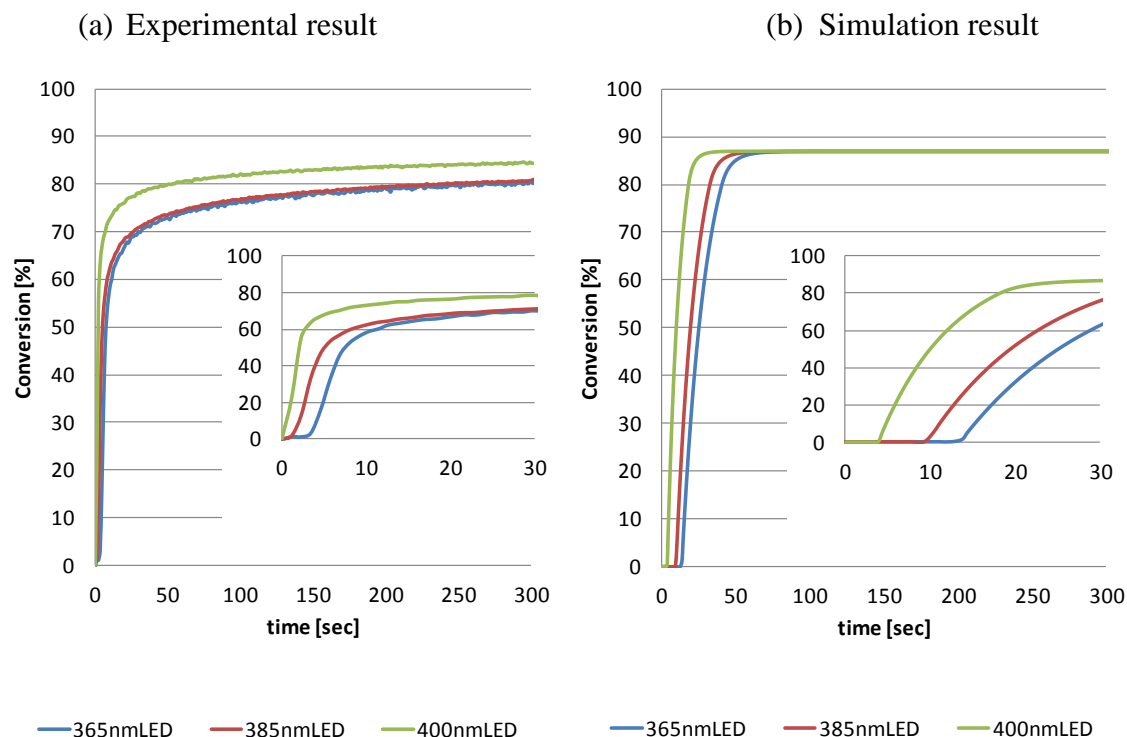
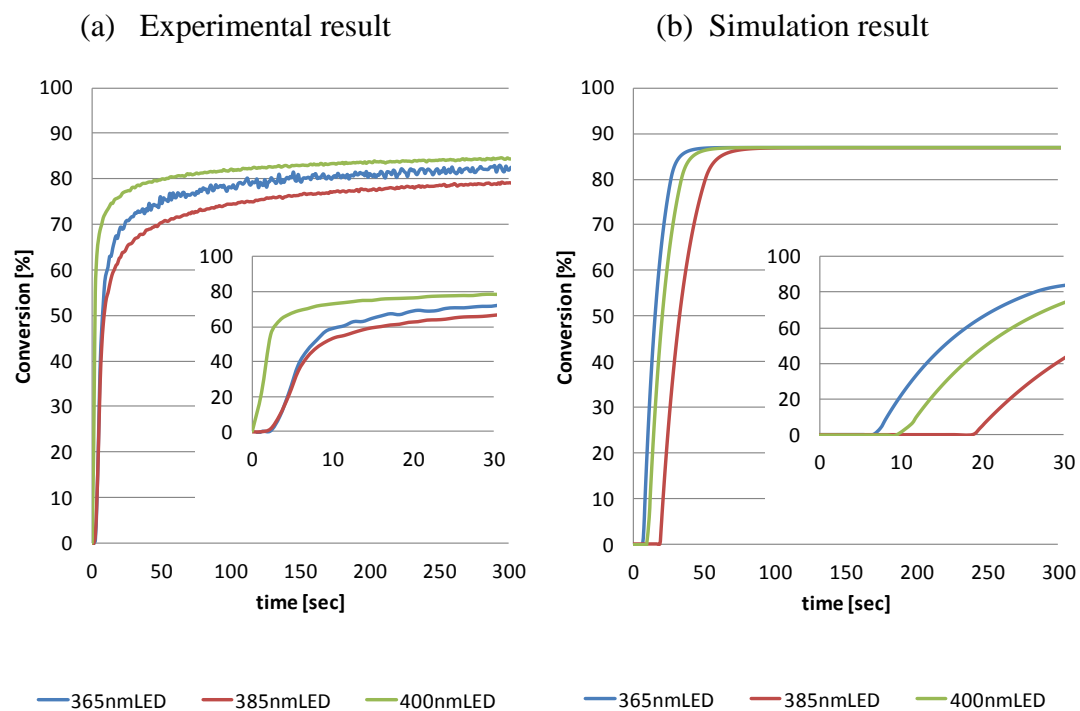


Figure 7-23: Comparison between a 365nm LED lamp (light intensity: 1.3 mW/cm^2), a 385 nm LED lamp (light intensity: 2.2 mW/cm^2) and a 400 nm LED lamp (light intensity: 6.8 mW/cm^2) for photopolymerization conversion profiles of thin HDDA systems containing four different initiators: (A) BAPO, (B) BDMB, (C) DMPA, and (D) TPO. Light intensity: 6.8 mW/cm^2 , photoinitiator concentration: 0.0167 M . (a) Experimental, (b) simulation. The irradiation distances are all set to 22.5 cm.

B. BDMB



C. DMPA

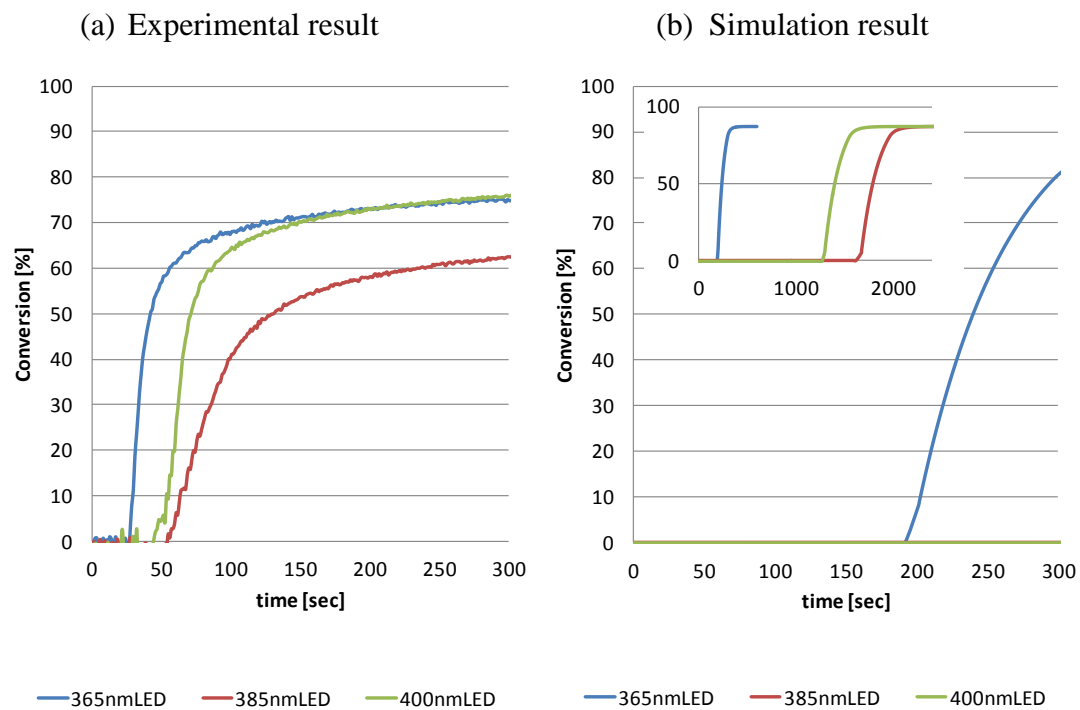


Figure 7-23 continued.

D. TPO

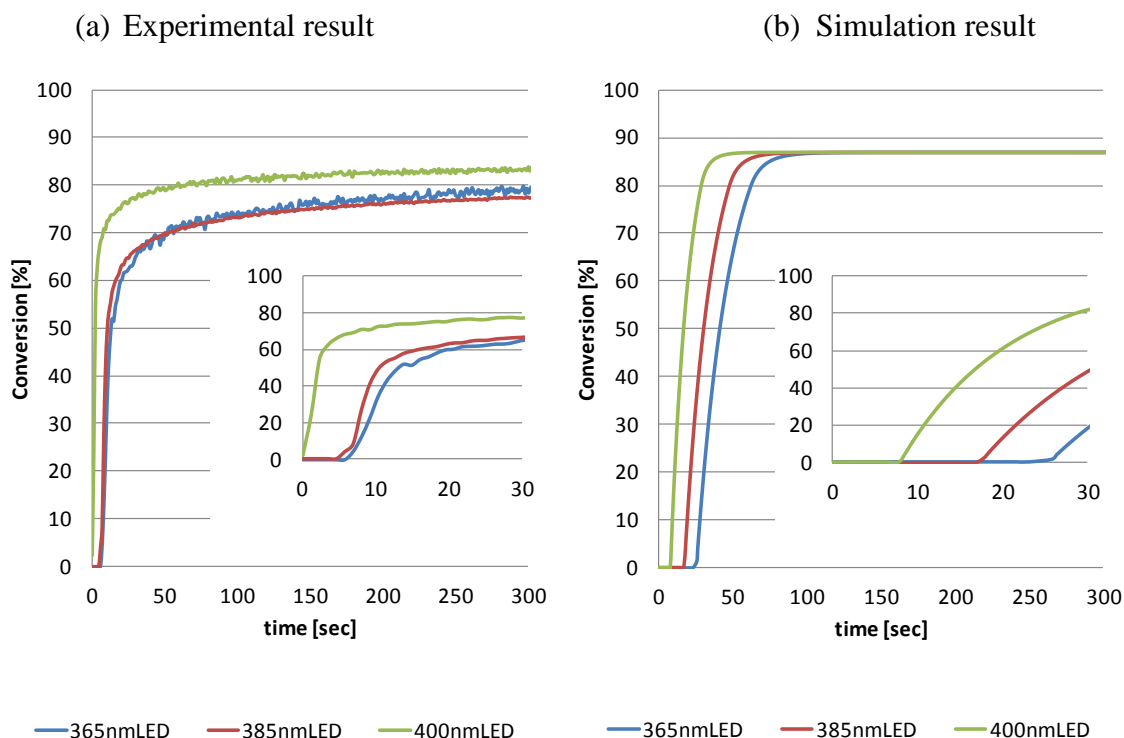


Figure 7-23 continued.

7.4.4. Validity of the Modeling for Thin Cure

In section 7.4.2 and 7.4.3, various combinations of photoinitiators and light sources were investigated experimentally and numerically. In this section, the validity of the model is considered. Figure 7-24 demonstrates the comparison between calculated conversion results and experimental ones at 40 seconds representatively. In the graph, at high conversion (more than 60 %) the correlation of simulation results and experimental results are almost in direct proportion. On the other hand, at low conversion (less than 60 %) which is the auto acceleration regime, the plots are not on the proportional line especially for the system containing DMPA. One of the reasons could be that the quantum yield of DMPA was estimated relatively low compared to actual phenomena.^{1,72} Although the parameters including quantum yield, k_p , k_t , k_q , and the initial dissolved oxygen concentration should be refined to achieve quantitative correspondence between

simulation and experiment, it can be concluded that the current model simulation is qualitatively corresponding to the experimental data especially in high conversion region. Therefore, the model can be applied to estimate the trends of thin cure for various photoinitiators and light sources.

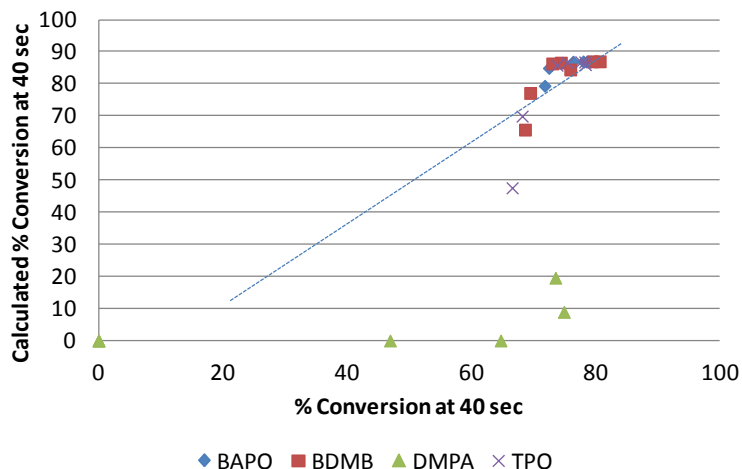


Figure 7-24: Calculated conversion vs. experimental conversion at 40 seconds

7.5. Numerical Calculation for Thin Cure with Various LEDs

As described above, it appears valid to apply the model to estimate the optimal combination of photoinitiators and light sources for thin cure. In this section, means to find the optimal combinations are demonstrated; namely, the estimation of thin cure trends using the model by combining with various LEDs and the four photoinitiators (BAPO, BDMB, DMPA, TPO), with 0.0167 M of each, is performed. The resin here is HDDA. However, the trends of the results in this research should be same with all kinds of common monomers and oligomers because those resins' absorbance is pretty low at focused wavelengths. As well as section 7.4 two conditions were considered: the same light intensity is used as condition 1 and same irradiation distance is used as condition 2.

7.5.1. Condition 1: Same Light Intensity

7.5.1.1. Light Sources

First, simulation study was performed using various light sources which emit LED-like spectra with same total light intensity of 6.8 mW/cm^2 , as shown in Figure 7-25. Since there are no commercial LED photocuring systems which emit less than 365 nm, the 335, 345, and 355 nm LEDs are not real but virtual light sources here.

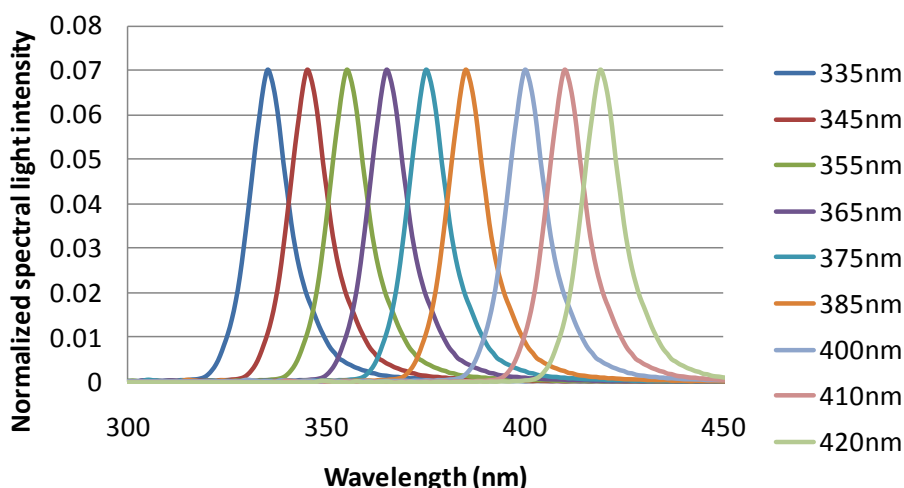


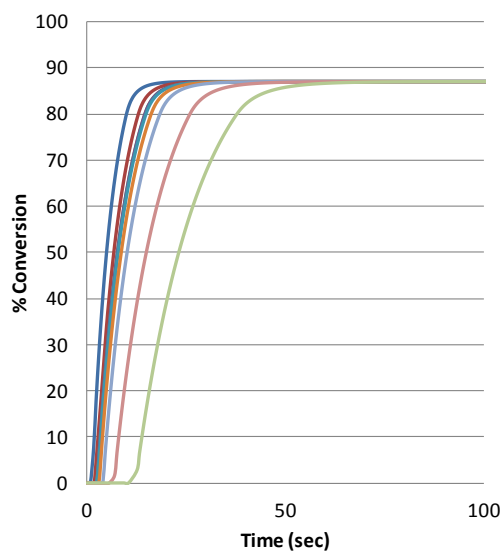
Figure 7-25: Spectral light intensities of 335, 345, 355, 365, 375, 385, 400, 410, and 420 nm LED lamps.

7.5.1.2. Results

Figure 7-26 shows calculated conversion results for the systems containing BAPO (A), BDMB (B), DMPA (C), and TPO (D). The graphs demonstrate the calculated conversion profiles as a function of time for the 335 nm, 345 nm, 355 nm, 365 nm, 385 nm, 400 nm, 410 nm, and 420 nm LED lamps. In the all four graphs, the lower wavelength LEDs are more effective than the higher wavelength LEDs due to the high absorptivity in lower wavelength region (see Figure 7-12).

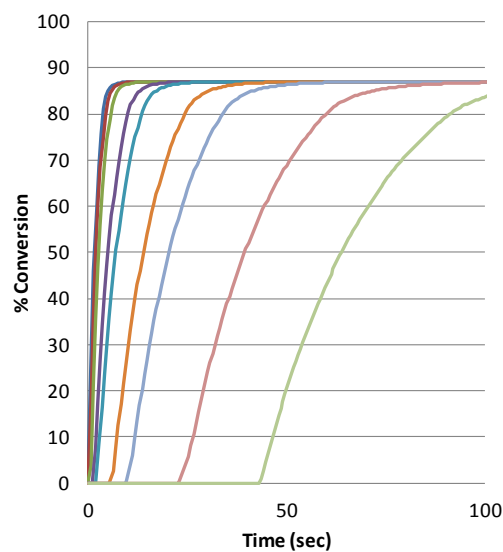
Next, Figure 7-27 illustrates the time required to attain 60% conversion as a function of the LED wavelength for the four different photoinitiators. Here the dotted lines demonstrate the time required for a conventional UV Hg(-Xe) lamp with 6.8 mW/cm² light intensity to achieve 60% conversion. As described in section 7.4.2, the time required with the Hg(-Xe) lamp is almost same as that of the LED lamps which emit less than 400 nm wavelength for the systems containing BAPO or TPO. However, the wavelength must be less than 365 nm for the system containing BDMB or DMPA to achieve the same efficiency with the Hg(-Xe) lamp. Regarding the LEDs, Figure 7-27 implies several interesting trends. First, for the LEDs which emit higher than 380 nm wavelength, BAPO is the most efficient photoinitiator. Second, for the LEDs which emit less than 380 nm wavelength, BDMB is the most efficient photoinitiator. Third, each photoinitiator exhibits a threshold wavelength, below which the photopolymerization efficiencies are not so different; the threshold wavelengths for BAPO, BDMA, DMPA, TPO are 400 nm, 360 nm, 350 nm, and 400 nm respectively. Finally, the combination of photoinitiator and light source that would provide the most rapid polymerization is BDMB with an LED emitted at 355 nm or below. Note that this 355 nm can also enhance the photopolymerization of the system containing DMPA dramatically.

A. BAPO



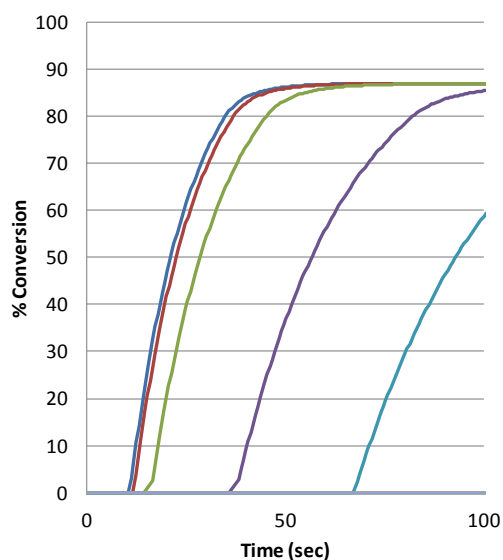
— 335nm — 345nm — 355nm — 365nm — 375nm
— 385nm — 400 nm — 410nm — 420nm

B. BDMB



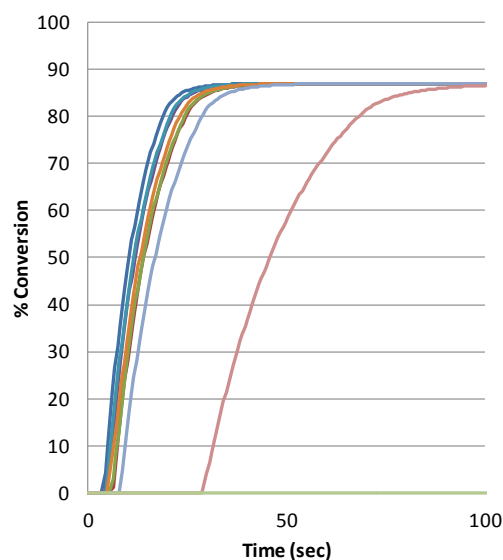
— 335nm — 345nm — 355nm — 365nm — 375nm
— 385nm — 400nm — 410nm — 420nm

C. DMPA



— 335nm — 345nm — 355nm — 365nm — 375nm
— 375nm — 385nm — 400nm

D. TPO



— 335nm — 345nm — 355nm — 365nm — 375nm
— 385nm — 400 nm — 410nm — 420nm

Figure 7-26: Comparison of seven LEDs for calculated photopolymerization conversion profiles of thin HDDA systems containing four different initiators: (A) BAPO, (B), BDMB, (C) DMPA, and (D) TPO. Light intensity: 6.8 mW/cm^2 , photoinitiator concentration: 0.0167 M .

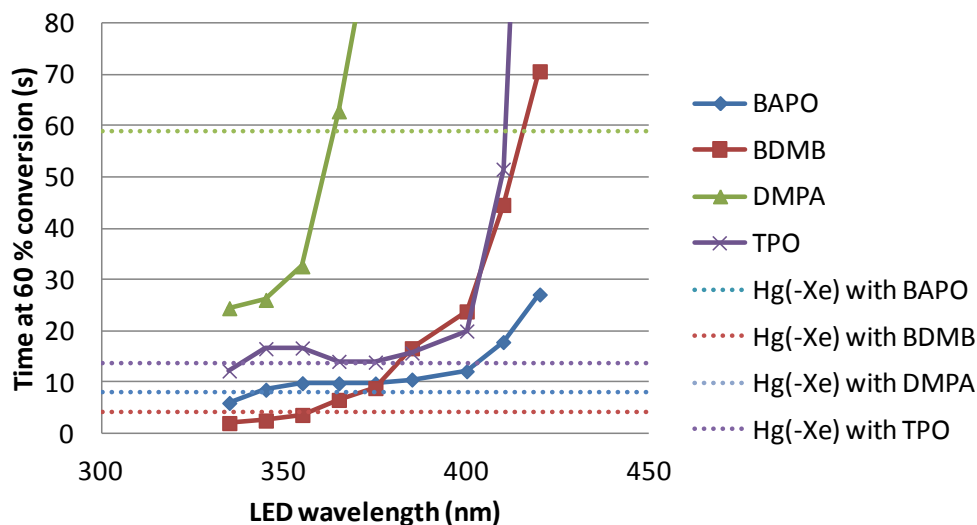


Figure 7-27: Calculated time required to attain 60% conversion as a function of the LED wavelength for four different photoinitiators. Light intensity: 6.8 mW/cm^2 , photoinitiator concentration: 0.0167 M . Dotted lines demonstrate the time required for a Hg(-Xe) lamp with 6.8 mW/cm^2 light intensity to achieve 60% conversion.

7.5.2. Condition 2: Same Configuration

7.5.2.1. Light Sources

Simulation study was also performed with thin cure using realistic LED light sources with same irradiation distance as shown in Figure 7-28, where the 365 nm LED light intensity is 1.3 mW/cm^2 , 385 nm LED light intensity is 2.2 mW/cm^2 , and other LEDs' light intensities are all 6.8 mW/cm^2 .

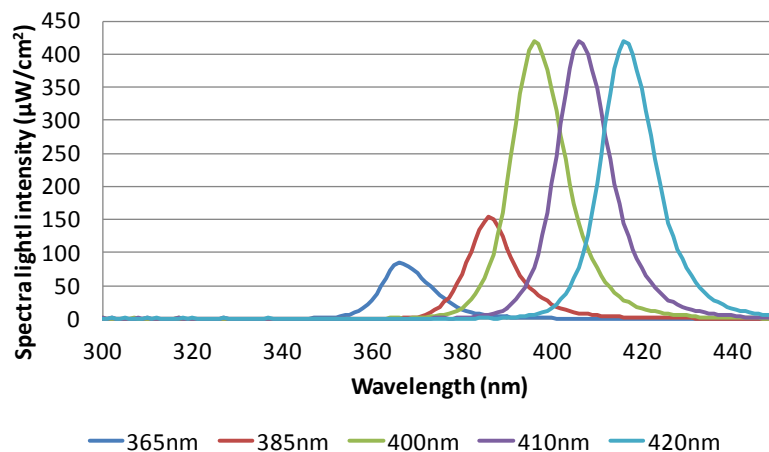


Figure 7-28: Spectral light intensities of 365, 375, 385, 400, 410, and 420 nm LED lamps.

7.5.2.2. Results

Figure 7-29 illustrates the time required to attain 60% conversion as a function of the LED wavelength for the four different photoinitiators. The trends of optimal combinations between photoinitiators and LEDs are different from the results in section 7.5.1. The best combination accomplishing the highest photopolymerization efficiency is BAPO with the 400 nm LED. In addition, the wavelength which achieves the highest photopolymerization efficiency depends on the photoinitiators; the 365 nm LED is the most effective for the system containing BDMB or DMPA while the 400 nm LED is the most effective for the system containing BAPO or TPO.

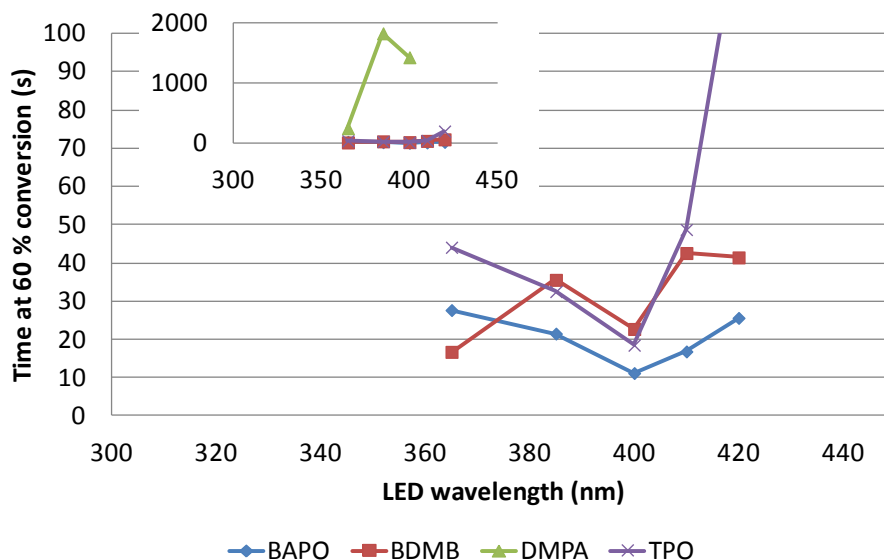


Figure 7-29: Calculated time required to attain 60% conversion as a function of the LED wavelength for four different photoinitiators. Photoinitiator concentration: 0.0167 M. Light intensities: 1.3 mW/cm² for a 365 nm LED, 2.2 mW/cm² for a 385 nm LED, 6.8 mW/cm² for 400 nm, 410 nm, and 420 nm LEDs. Here irradiation distances are assumed as same.

7.6. Conclusion

In this research, various LED photocuring systems including a 365nm LED, a 385 nm LED, and a 400 nm LED were investigated. First, representative commercial LED systems were characterized including the uniformity of emission spectra, relationship between light intensity and its irradiation distance, and energy consumption. This study clarified that the energy efficiency of a LED is much higher than conventional lamps. In addition, the trend that light intensities of LEDs became weak as those wavelength decreased was confirmed. Therefore, to design the practical process of LED curing the effect of both light intensity and emission spectra must be considered.

Then, thick cure was investigated using both experimental and modeling study to compare a 400 nm LED and a (Hg-)Xe lamp. For all of the photoinitiators, including BAPO, BDMB, DMPA, and TPO, the thick cure ability of the 400 nm LED was superior to that of the conventional UV lamp experimentally. However, some of the simulation

results did not correspond to the experimental results due to the effect of photopolymerization heat.

Thin cure was also investigated for the four photoinitiators using various LEDs and lamps experimentally and numerically. The effective light source was dependent on the photoinitiators respectively and several LEDs demonstrated high thin cure ability. Unlike thick cure, the calculated results corresponded to the experimental results qualitatively and the model was valid for thin cure system. Therefore, it was considered that this model could apply to the optimization of light sources and photoinitiators for thin cure.

Finally, various combinations of LEDs and photoinitiators in thin cure system were investigated to find optimal combination using this modeling. The results implied various interesting suggestion. For example, the commercialization of 355 nm LEDs might be able to achieve high photopolymerization efficiency for BDMB-containing resin besides the dramatic enhancement of photopolymerization efficiency for DMPA-containing resin.

CHAPTER 8. STUDIES OF PHOTOINITIATOR SYSTEMS FOR EFFECTIVE POLYMERIZATIONS WITH VISIBLE LEDS: CHARACTERIZATION OF VISIBLE-LIGHT-INDUCED PHOTOPOLYMERIZATION USING THE TITANOCENE PHOTOINITIATOR BIS(CYCLOPENTADIENYL) BIS[2,6-DIFLUORO-3-(1-PYRRYL)PHENYL]TITANIUM

8.1. Introduction

Photopolymerizations have become the state-of-the-art for rapid room-temperature cure of coatings, adhesives, and printed images.^{1, 66} In a typical photopolymerization a small amount of a light activated initiator is dissolved in a monomer. When this system is exposed to light with the right wavelength, the monomer is converted to polymer within seconds to minutes. Photopolymerizations are highly desired because the use of light affords great temporal and spatial control over the polymerization since light can be directed to a location of interest and shuttered at will. Photopolymerizations also offer environmental advantages such as low energy requirements, high polymerization rates, and solvent-free compositions which alleviates the need to remove solvent in a subsequent step. Because of these characteristics, photopolymerizations are attractive for new applications in medical devices including coatings for artificial implants and structural elements in bone and tissue restoration.⁷³⁻⁷⁵ Free radical photoinitiators have traditionally been based on the benzoyl chromophore, which absorbs light in the ultraviolet (UV) region of the spectrum. Some common classes of these photoinitiators include benzoin ethers, dialkoxyacetophenones, hydroxy alkyl ketones, benzoyl oxime esters, amino ketones, and morpholino ketones. When illuminated with UV light, these unimolecular photoinitiators produce active centers efficiently by the well-known α -cleavage process. However, ultraviolet light is undesirable for many applications. For instance, in biological, and medical applications, visible light is preferable due to the damaging effects of UV radiation. In addition, to

photopolymerize adhesives through a polyimide film (e.g. Kapton, Toray Co.), visible light whose wavelength is higher than 500 nm is required because this film absorbs light at wavelengths below 500 nm. Furthermore, visible-light-initiated cure is attractive because of the ready availability of inexpensive, reliable, mercury-free light sources such as light emitting diodes (LEDs).

A major challenge in this field is that although UV photoinitiators are unimolecular and their initiation is unaffected by viscosity of the monomer, visible-light induced photopolymerizations require multi-component photoinitiator systems. Visible light initiators are generally based upon electron-transfer processes due to the relatively low energy of a visible photon.^{3, 14, 16-20, 41-48} Because visible-light electron-transfer photoinitiator systems generally require two or more components, they rely upon bimolecular collisions during an excited state lifetime to facilitate the electron transfer process. While common unimolecular UV photoinitiators are relatively insensitive to viscosity, the bimolecular electron transfer reactions in the multi-component systems tend to be diffusion-controlled and are highly influenced by the viscosity of the solvent.^{60, 76} Hence, it can be difficult to achieve a complete cure in viscous formulations that contain oligomers for enhancement of mechanical properties.

Ganster et al.⁷⁷ reported a visible light photoinitiator, diacyldialkylgermanium compounds, which may be used, for example, in dental materials. These germanium compounds are highly efficient, cleavable photoinitiators for visible light curing and show an excellent bleaching behavior. However, these compounds absorb wavelengths less than 470 nm. Therefore, another photoinitiator which can be activated by higher than 500 nm light to polymerize the adhesive described above is still desired.

In this article we report the successful polymerizations of viscous acrylates at low intensities of visible light using a unimolecular titanocene compound. The photoinitiator is bis(cyclopentadienyl) bis[2,6-difluoro-3-(1-pyrryl)phenyl]titanium (henceforth referred to as Ti-PI, Figure 8-1A). This initiator is a commercially available

organometallic complex which absorbs light at wavelengths up to 550 nm and is known to produce radicals when exposed to visible light.^{61-64, 67, 78-81} Although the mechanism of decomposition of Ti-PI to yield radicals is not well understood, it is known that it decomposes by a unimolecular pathway and that the resulting polymerization rate is enhanced by the presence of acid.^{67, 82-85} In this contribution, we demonstrate that Ti-PI can rapidly polymerize monomers to high conversion with surprisingly low levels of visible light in the presence of acids. In this article we report a result that has not been seen by others: at relatively low light intensities, the rate of polymerization with Ti-PI increases as the intensity of light is increased; but for light intensities higher than an optimum value, the rate actually decreases as the intensity of light is further increased. The optimal intensity of light to quickly reach a high conversion was remarkably low for Ti-PI in the polymerization of acrylates ($\sim 8 \text{ mW/cm}^2$). This result was unexpected, and a detailed mechanism to explain it was explored.

In prior work by others^{67, 82}, it was shown that the presence of acids affect the polymerizations of acrylates using Ti-PI, but only the physical properties (i.e. gelation) of the resulting material was studied rather than the rate of polymerization or conversion. In this contribution, we have provided a more detailed investigation of the effect of a variety of acids on the rate and final conversion of the polymerization. Finally, we have demonstrated that Ti-PI is effective in viscous mediums where other visible light photoinitiators fail.

8.2. Experimental

8.2.1. Materials

The monomer 2-hydroxyethyl acrylate (HEA) (Figure 8-1B) (Sigma-Aldrich) was used as the base monomer in these experiments. A viscous urethane acrylate oligomer (CN9002, Sartomer) was mixed with 2-hydroxyethyl acrylate to prepare viscous reactive formulations. Ti-PI (commercial name Irgacure 784) was supplied by

BASF. Additives used in this study including 2-carboxyethyl acrylate (CEA) (Figure 8-1C), phosphoric acid 2-hydroxyethyl methacrylate ester (PhMA) (Figure 8-1D), p-toluenesulfonic acid (PTSA) (Figure 8-1E), and triethylamine (TEA) were purchased from Sigma-Aldrich. CEA and PhMA are polymerizable protonic acids. Eosin Y spirit soluble (EYss), *N*-methyldiethanolamine (MDEA), and diphenyl iodonium chloride (DPI), supplied by Sigma-Aldrich, were used to form a visible-light-induced multi-component photoinitiator system.¹⁷

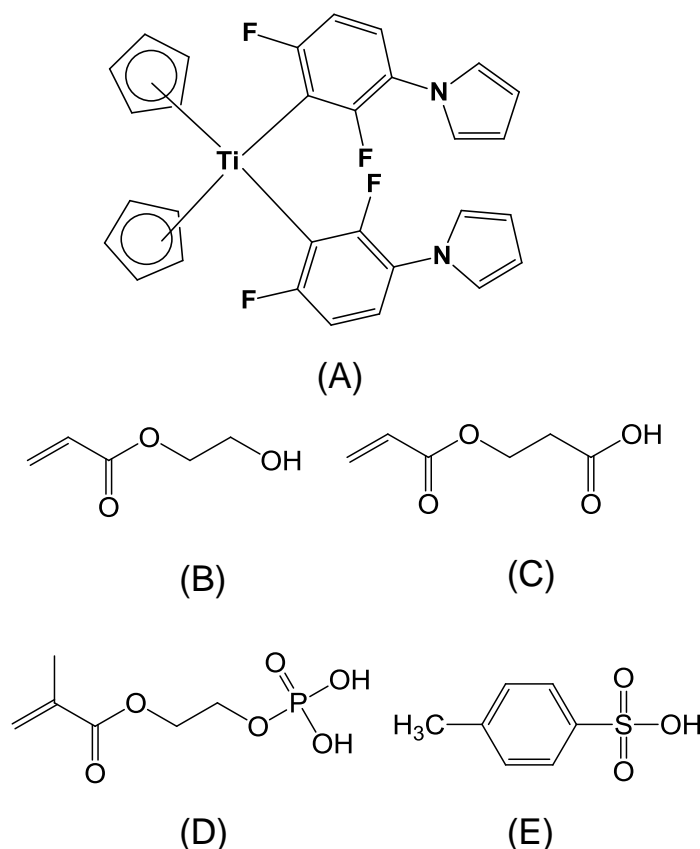


Figure 8-1: Chemical structures of the reaction components: (A) bis(cyclopentadienyl) bis[2,6-difluoro-3-(1-pyrryl)phenyl]titanium (Ti-PI), (B) 2-hydroxyethyl acrylate (HEA), (C) 2-carboxyethyl acrylate (CEA), (D) phosphoric acid 2-hydroxyethyl methacrylate ester (PhMA), and (E) p-toluenesulfonic acid (PTSA).

8.2.2. Methods

The photopolymerization rate was characterized using real-time Fourier transform infrared spectroscopy (RT-FTIR) at room temperature with a modified Bruker 88 FTIR spectrometer designed to accommodate a horizontal sample.⁸⁶ The RT-FTIR used a 520 nm LED lamp (UHP-MIC-LED-520, Prizmatix) or 150 W xenon lamp (MAX-150, Asahi Spectra) equipped with a 520 nm bandpass filter to illuminate the samples. The light spectrum of the lamp was measured using an Ocean Optics USB 4000 fiber optic spectrometer. The samples were prepared by placing a droplet of the monomer mixture between two rectangular IR grade sodium chloride salt crystals, with 15 μm Teflon beads placed between the salt plates to serve as spacers. The infrared absorption spectra during photopolymerization were collected *in situ* at 1.1 second intervals with four signal averaged scans for each spectrum. The carbon-carbon double bond infrared absorbance peak at 812 cm^{-1} associated with an out-of-plane vibration, was monitored during the reaction to determine the acrylate conversion. The conversion was calculated using the ratio of current peak height to peak height prior to polymerization. Since the reactive monomer or oligomer samples are confined between salt plates, they are initially saturated with dissolved oxygen, but the oxygen is consumed by free radicals and is not replenished from the atmosphere.

8.3. Results and Discussion

8.3.1. Effect of a Protonic Acid on the Photopolymerization Rate

Using Ti-PI as a Visible Light Initiator

Figure 8-2 shows the conversion profiles, as monitored by RT-FTIR spectroscopy, for HEA polymerizations photoinitiated using Ti-PI (2.6 wt %; 0.050 M) and mixtures of Ti-PI with four different protonic acid additives. The figure contains plots of the experimentally observed conversions as a function of time for neat HEA

monomer, and the monomer systems containing the protonic acids. For these experiments, the light intensity of the 520 nm light from the xenon lamp was 2 mW/cm².

Figure 8-2 clearly shows that the polymerization rate and conversions of monomer were strongly affected by the presence of acid. The photoinitiator system containing Ti-PI without any protonic acid (the curve labeled with solid diamonds) does not undergo appreciable polymerization. In contrast, the systems with acids present have significantly enhanced polymerization rates and ultimate conversions of monomer. Both values follow the trend: Ti-PI+CEA < Ti-PI+PhMA < Ti-PI+PTSA that correlate with the pKa of a carboxylic acid (approximate pKa of 4.0), phosphoric ester (pKa of phosphoric acid is 2.1), and PTSA (pKa of -2.8). This figure further illustrates that if a base (triethylamine) is added to the Ti-PI+PTSA system to quench the acid, the photopolymerization rate and ultimate conversion drop significantly and the conversion profile becomes similar to that of a photoinitiator system containing only Ti-PI. Therefore, it can be concluded that the presence of the protonic acid in the Ti-PI photoinitiator system is critical to achieve high overall photopolymerization and the enhancement in polymerization depends on the acidity of the protonic acid additive. It is important to note that this enhancement of photopolymerization by the addition of the acid is not observed in other photoinitiating systems including 1-hydroxy-cyclohexyl-phenyl-ketone, which is a common free-radical unimolecular photoinitiator. This enhancement is unique to Ti-PI.

Table 8-1 summarizes the ultimate conversions of the systems illustrated in Figure 8-2. The ultimate conversion is defined as the maximum or plateau conversion after six minutes of illumination. Importantly, the systems containing PTSA or PhMA reached ultimate conversions in excess of 95% which is highly desired for many applications of photopolymerizations.

The stability of solutions of HEA and Ti-PI with either PhMA or PTSA were investigated to learn if these solutions were stable in the absence of light. When the

solution containing PTSA was allowed to sit for one day in the dark and then exposed to light, the photopolymerization reached low monomer conversions. In contrast, the solution with PhMA showed a high photopolymerization reactivity and a long shelf life after a month of storage in the dark (see APPENDIX 6). Therefore, the protonic acid PhMA was used for the remainder of the work reported in this article.

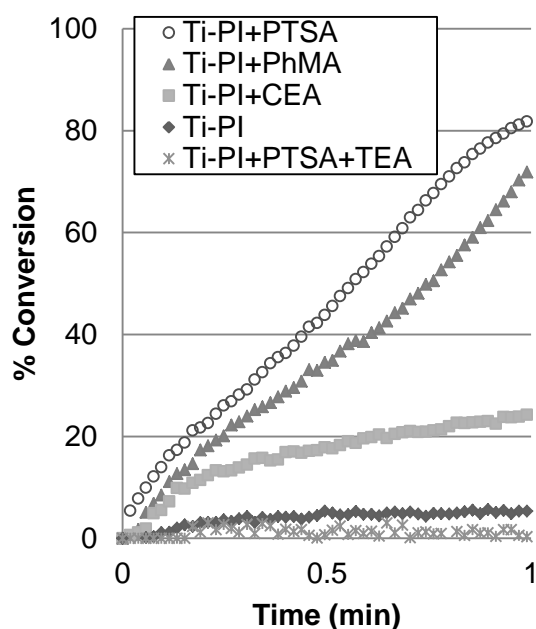


Figure 8-2: HEA photopolymerization conversion profiles in the presence of various additives: 1.0 wt % (0.053 M) PTSA (\circ); 1.5 wt % (0.067 M) PhMA (\blacktriangle); 1.5 wt % (0.105 M) CEA (\blacksquare); no additives (\blacklozenge); 1.0 wt % (0.053 M) PTSA plus 1.0 wt % (0.100 M) TEA ($*$). All samples contain 2.6 wt % (0.050 M) Ti-PI. Light intensity: 2 mW/cm².

Table 8-1: Ultimate conversions of photopolymerization profiles in Figure 8-2 after 6 minutes of illumination

	Ultimate conversion (%)
Ti-PI	8.2
Ti-PI+CEA	70.4
Ti-PI+PhMA	99.6
Ti-PI+PTSA	96.7
Ti-PI+PTSA+TEA	3.0

The effect of different concentrations of PhMA on the rates of polymerization and conversions of monomer were investigated to determine the optimal concentration of PhMA. Figure 8-3 contains profiles of the photopolymerization conversion as a function of time for HEA compositions containing 2.6 wt % (0.050 M) Ti-PI and various concentrations of PhMA ranging from 0 to 3.0 wt % (0 to 0.133 M). The rate of polymerization and conversion of monomer increase when the concentration of PhMA increases from 0 wt % to 0.5 wt %, but above a value of 0.5 wt % the rate and conversions are unchanged.

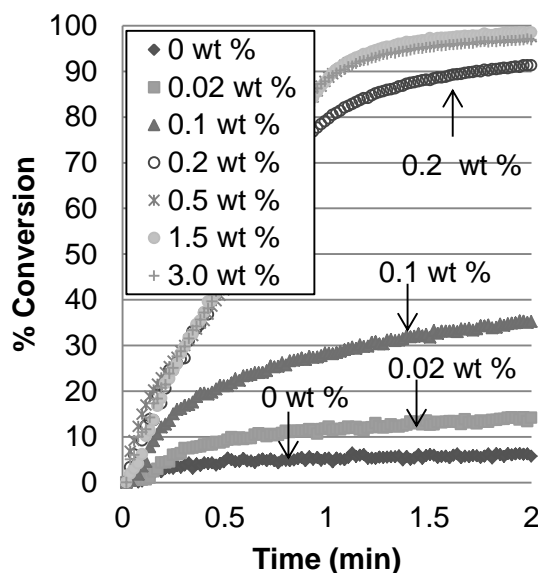


Figure 8-3: HEA photopolymerization conversion profiles for eight different concentrations of the protonic acid PhMA. All samples contain 2.6 wt % (0.050 M) Ti-PI. Light intensity: 2 mW/cm².

The enhancement in polymerization rate and conversion of monomer when an acid was added to a solution of monomer with Ti-PI was studied for other acrylate monomers including 1,6-hexandiol acrylate. The same enhancements were observed for this monomer. In contrast, for polymerizations of nonacrylate monomers, the effect of a

protonic acid on photopolymerization was negligible. For example, for styrene photopolymerizations initiated using Ti-PI, the addition of acid had no effect on the resulting conversion profiles (see APPENDIX 6).

8.3.2. Origin of the Effect of Acid on the Polymerization Rate

It was hypothesized that the rate of polymerization was increased when an acid was added to a solution of Ti-PI because the acid increased the absorption of Ti-PI. This hypothesis was investigated by collecting the UV-VIS absorbance spectrum of the Ti-PI photoinitiator as shown in Figure 8-4. The figure illustrates that the presence of the three different protonic acid additives had no measureable effect on the observed Ti-PI absorbance spectra. Therefore, the enhancement in the photopolymerization rate shown in Figure 8-2 did not result from enhanced absorbance of the incident light.

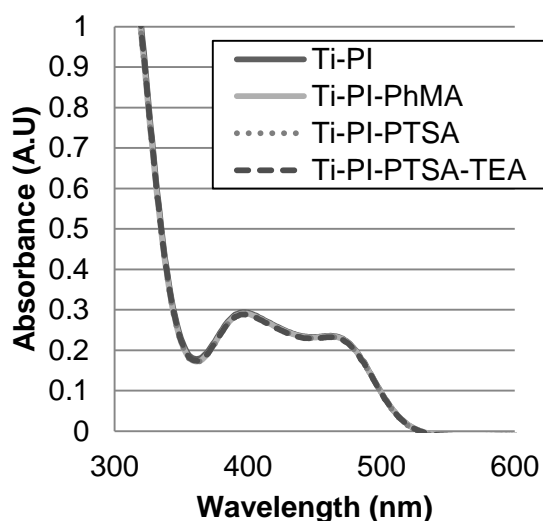


Figure 8-4: Absorbance spectra with and without the acid additives in ethyl acetate. For all samples, Ti-PI = 0.01 wt %, PhMA = 0.006 wt %, PTSA = 0.005 wt %, TEA = 0.01 wt %.

The effect of the protonic acid on the effectiveness of Ti-PI likely arises from a change in the photolysis products resulting from the presence of an acid. It is well known

that the identity of the chemical substituents on the aromatic ligands of a titanocene complex can have a marked effect of the photolysis products. For example, several investigators^{62, 63, 78, 79} have characterized the difference in photolysis products between diphenyltitanocene and perfluorodiphenyltitanocene (Figure 8-5). This comparison is interesting because the two titanocene complexes differ only in the substituents on the aromatic ligands, with the replacement of the hydrogen of the diphenyltitanocene with electronegative fluorine to yield perfluorodiphenyltitanocene. Previous work by others showed that the primary radicals (yields higher than 93%)^{62, 78} generated from photodecomposition of perfluorodiphenyltitanocene (structure 4) were titanium di-radicals containing both a cyclopentadienyl group and a perfluorophenyl group (structure 5), and pentafluorophenylcyclopentenyl (structure 6) which was not a radical. In contrast, the primary radicals (yields of higher than 80%)^{62, 78} generated from photodecomposition of diphenyltitanocene (structure 1) were phenyl radical (structure 2) and titanium mono-radical (structure 3). Roloff⁷⁸ and collaborators⁷⁹ reported that the titanium di-radical (structure 5) is the most effective initiating radical of the photolysis products shown in Figure 8-5, and this hypothesis is consistent with the observation that the perfluorodiphenyltitanocene is a more effective photoinitiator than diphenyltitanocene. As shown in Figure 8-3, protonic acid concentrations higher than 0.2 wt% appear to favor the production of the titanium di-radical, which produce propagating active centers upon reaction with the acrylate monomers to form a ketene acetal type di-radical capable of initiating polymerization.^{62, 79}

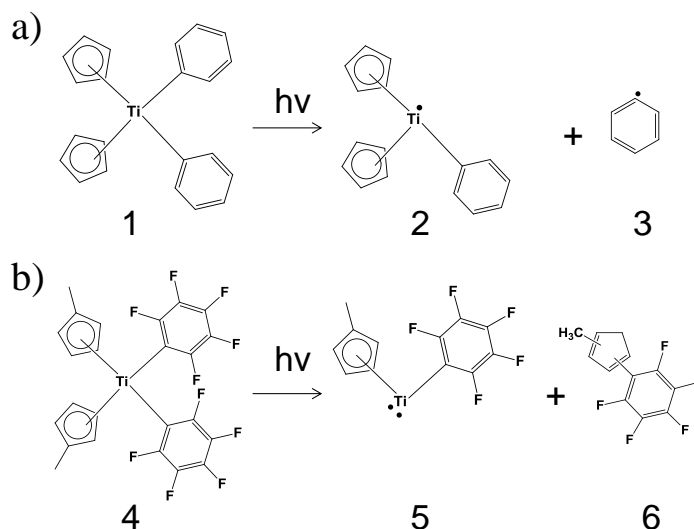


Figure 8-5: The products of the light activated decomposition of a) diphenyltitanocene differ from those of b) perfluorodiphenyltitanocene.

The literature studies on diphenyltitanocene and perfluorodiphenyltitanocene suggest that the addition of a protonic acid increases the effectiveness of Ti-PI is by shifting the distribution of photolysis products. In the absence of added acid, the unprotonated Ti-PI is likely to have a photolysis product distribution resembling that of diphenyltitanocene (Figure 8-6a). In this state, the pyrrole groups of the 2,6-difluoro-3(1H-pyrrol-1-yl)phenyl side chains are electron donating and the molecule most closely resembles diphenyltitanocene. In the presence of acid, the nitrogen in the pyrrole functional group can be reversibly protonated which will make the pyrrole ring strongly electron withdrawing (Figure 8-6b). When the protonated Ti-PI was illuminated with light, the photolysis product distribution was similar to that of perfluorodiphenyltitanocene (with five electron-withdrawing fluorines). Thus, in the presence of acid Ti-PI would favor generation of highly active titanium di-radicals.

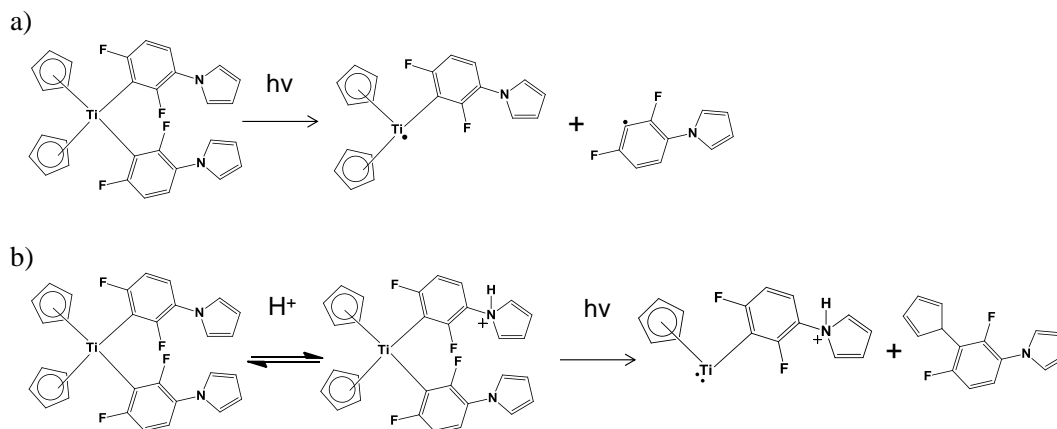


Figure 8-6: Photodecomposition reactions of Ti-PI. a) When Ti-PI is not protonated by external acid, the degradation products resemble those from diphenyltitanocene. b) In the presence of an acid to protonate the nitrogen on Ti-PI, the degradation products change and resemble those of perfluorodiphenyltitanocene.

8.3.3. Effect of Light Intensity and Photoinitiator Concentration on the Photopolymerization Rate and Conversion of Monomer

A series of experiments were performed to investigate the effect of light intensity on the observed photopolymerization rate and ultimate conversion. Figure 8-7 contains RT-FTIR conversion profiles as a function of time in HEA monomer for a photoinitiator system composed of 2.6 wt % (0.050 M) Ti-PI and 1.5 wt % (0.067 M) PhMA when irradiated by 520 nm light of different light intensities. The data in Figure 8-7 illustrate a surprising trend. The lowest polymerization rate is observed for the highest light intensities investigated, and there is a light intensity threshold above which higher light intensities result in poor polymerization. Specifically, if the light intensity is higher than 30 mW/cm^2 , the photopolymerization rates are relatively low, and the observed ultimate conversions are less than 30% (see Table 8-2). In contrast, for light intensities below 18 mW/cm^2 a high ultimate conversion of $>99\%$ is observed, and the photopolymerization rate is relatively high. The data in Figure 8-7 illustrate that the

maximum photopolymerization rate was observed for a light intensity of 8 mW/cm² and the rate is lower for light intensities above or below this value.

The low polymerization rate and ultimate conversion for light intensities above 18 mW/cm² is surprising, and the reason for this effect is not obvious. One possible explanation is that the rapid photodegradation of the Ti-PI leads a lower concentration of propagating radicals due to an increase in the rate of radical-radical combination reactions. At the relatively high light intensities, radical combination reactions could dominate thereby preventing effective polymerization. At low light intensities, the rate of formation of radicals from Ti-PI is reduced, thereby leading to lower radical concentrations, and a reduction in the rate of the radical combination reactions. Therefore, the concentration of propagating radicals may actually increase with decreasing light intensity due to a shift in the probability of propagation relative to radical combination before propagation can occur. The optimal polymerization rate at a low terminate rate was found at approximately 8 mW/cm². It should be noted that the surprising effect of increasing light intensity on the ultimate conversion was also observed for photopolymerizations initiated using other light sources including a xenon lamp which emits a broad wavelength spectrum (see Appendix 6).

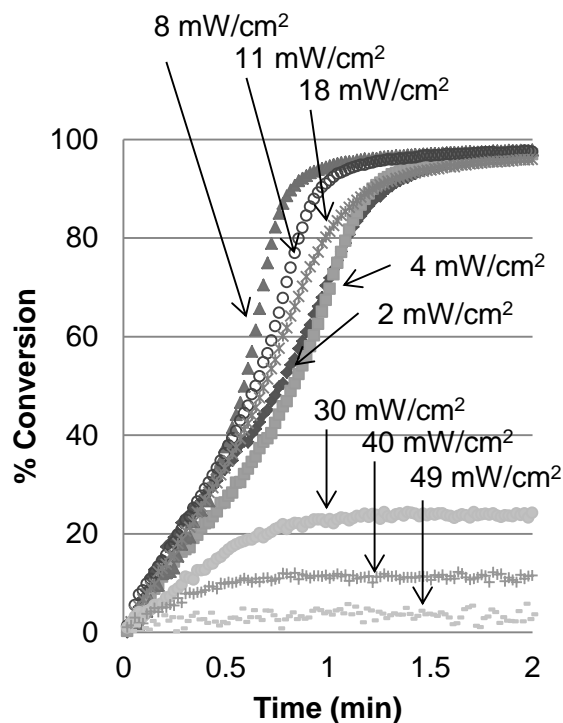


Figure 8-7: HEA photopolymerization conversion profiles for seven different light intensities: 2 mW/cm² (◆), 4 mW/cm² (■), 8 mW/cm² (▲), 11 mW/cm² (○), 18 mW/cm² (*), 30 mW/cm² (●), 40 mW/cm² (+), 49 mW/cm² (-). For all systems Ti-PI = 2.6 wt % (0.050 M), PhMA = 1.5 wt % (0.067 M).

Table 8-2: Ultimate conversions of photopolymerization profiles in Figure 8-7

	Ultimate conversion	
	%	
2 mW/cm ²	99.2	
4 mW/cm ²	99.2	
8 mW/cm ²	99.1	
11 mW/cm ²	99.0	
18 mW/cm ²	97.9	
30 mW/cm ²	23.9	
40 mW/cm ²	12.5	
49 mW/cm ²	5.3	

The general trends of an enhancement in photopolymerization with the addition of the acid and the decrease in ultimate conversion with an increase in light intensity were observed in other (meth)acrylates including 1,6-hexandiol acrylate, 2-hydroxyethyl methacrylate and a HEA/urethane acrylate mixture (see APPENDIX 6). In addition, reports in the literature⁸⁷ have illustrated that photopolymerization profiles of 1,6-hexandiol acrylate initiated using 2,2-dimethoxy-2-phenylacetophenone were not affected by addition of a strong acid. Therefore, the phenomena shown in Table 8-2 and Figure 8-7 are not limited to any particular acrylic monomer but are instead associated with the Ti-PI photoinitiator.

A series of experiments were completed to investigate the effect of the photoinitiator concentration on the observed polymerization rate and ultimate conversion. These studies were completed using PhMA as the protonic acid, and the molar ratio of the PhMA to Ti-PI was maintained at a value of 1.4 to 1. Figure 8-8 contains profiles for the conversion as a function of time for three different photoinitiator concentrations (0.1, 0.5, and 2.6 wt % Ti-PI) and two different light intensities (8 and 30 mW/cm²). The data in the figure illustrate that, for both light intensities, the observed profiles for conversion vs. time depend strongly upon the photoinitiator concentration, however the nature of the dependence is very different at the low light intensity than at the high light intensity. Specifically, Figure 8-8a illustrates that at the low light intensity of 8 mW/cm² the most rapid photopolymerization is observed for the highest photoinitiator concentration (2.6 wt % Ti-PI, solid line in the figure), and a significant inhibition period (due to oxygen) is observed for the lowest photoinitiator concentration (0.1 wt %, dotted line in the figure). The intermediate photoinitiator concentration (0.5 wt %, dashed line) shows no appreciable inhibition period, but a relatively sluggish polymerization. All three photoinitiator concentrations resulted in the same ultimate limiting conversion of over 91% after 6 minutes illumination.

Figure 8-8b illustrates that a very different trend is observed for the higher light intensity of 30 mW/cm^2 . Here, the lowest Ti-PI concentration (0.1 wt %, dotted line) shows a small inhibition period followed by a relatively high polymerization rate, and the two higher photoinitiator concentrations lead to ineffective polymerization. The ultimate limiting conversions after 6 minutes illumination for the samples containing 0.1, 0.5, and 2.6 wt % Ti-PI were 24%, 49%, and 79%, respectively .

The trends described in the previous paragraphs are consistent with the postulate that the photolysis of Ti-PI leads to the production of high concentration of radical species that leads to fast termination reactions at high light intensities. Therefore, the highest polymerization rates and highest ultimate limiting conversions are observed for the combination of low light intensity and relatively high initiator concentration. At higher light intensities, lower photoinitiator concentrations are required to achieve appreciable polymerization.

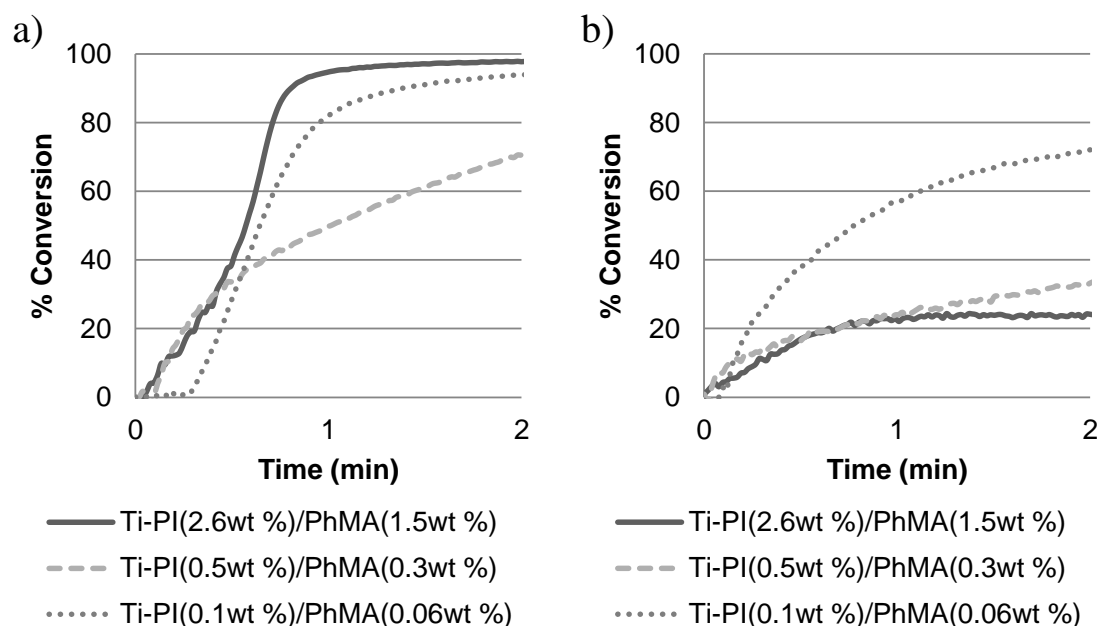


Figure 8-8: HEA photopolymerization conversion profiles for three different Ti-PI/PhMA concentrations and two different light intensities: (a) 8 mW/cm^2 and (b) 30 mW/cm^2 .

8.3.4. Comparison of Ti-PI to a 3-Component Visible Light

Photoinitiator system

A series of experiments were conducted to compare the performance of the Ti-PI photoinitiator to a 3-component visible light photoinitiator. Multi-component photoinitiator systems are commonly employed for visible-light-induced photopolymerization. The energy of a visible photon is generally lower than the bond dissociation energy of most organic molecules, therefore visible-light-induced photoinitiator systems are primarily two-component photoinitiator systems in which the active centers are produced via an electron transfer followed by a proton transfer from the electron donor (typically an amine) to the excited light-absorbing component. The polymerization rate is further enhanced by the addition of a third component such as diphenyl iodonium chloride (DPI) into the two-component photoinitiator systems, as described by a number of investigators^{3, 16-20, 46-48}.

The polymerization observed for the Ti-PI/PhMA photoinitiator system is compared to that observed for the EYss/MDEA/DPI three-component photoinitiator system for monomer mixtures of two different viscosities (Figure 8-9). Figure 8-9a corresponds to photopolymerization of the neat HEA monomer which exhibits a relatively low viscosity of 0.005 Pa-sec (measure with a Brookfield digital viscometer). In this case, both photoinitiators resulted in a high ultimate limiting conversion of 98%, however the 3-component initiator system reached this limiting conversion more rapidly. Figure 8-9b corresponds to a high viscosity mixture of the HEA monomer with a urethane acrylate oligomer (30 wt % HEA, 70 wt % oligomer) which exhibits a viscosity of 3.5 Pa-sec. For this high viscosity system, the Ti-PI/PhMA photoinitiator is more effective, and leads to an ultimate limiting conversion of more than 95%, while the 3-component photoinitiator EYss/MDEA/DPI leads to a final conversion of only ~50%. The sensitivity of multicomponent photoinitiator systems to the monomer viscosity is well known and arises from the fact that the electron transfer process that leads to the

production of active centers is diffusion controlled and becomes less efficient as the viscosity is increased. For the EYss/MDEA/DPI photoinitiator system requires diffusion-controlled bimolecular encounters to occur between the excited EYss and MDEA or DPI during the lifetime of the EYss excited state.¹⁷ The probability of this encounter decreases as the viscosity is increased. In contrast, the photolysis reaction of Ti-PI is unimolecular, and will be relatively insensitive to the system viscosity. In fact, comparison of the solid line in Figure 8-9a to the solid line in Figure 8-9b reveals that the TI-PI photoinitiator is more effective at the higher viscosity, perhaps due to a decrease in the fraction of active centers which participate in radical combination reactions upon photolysis.

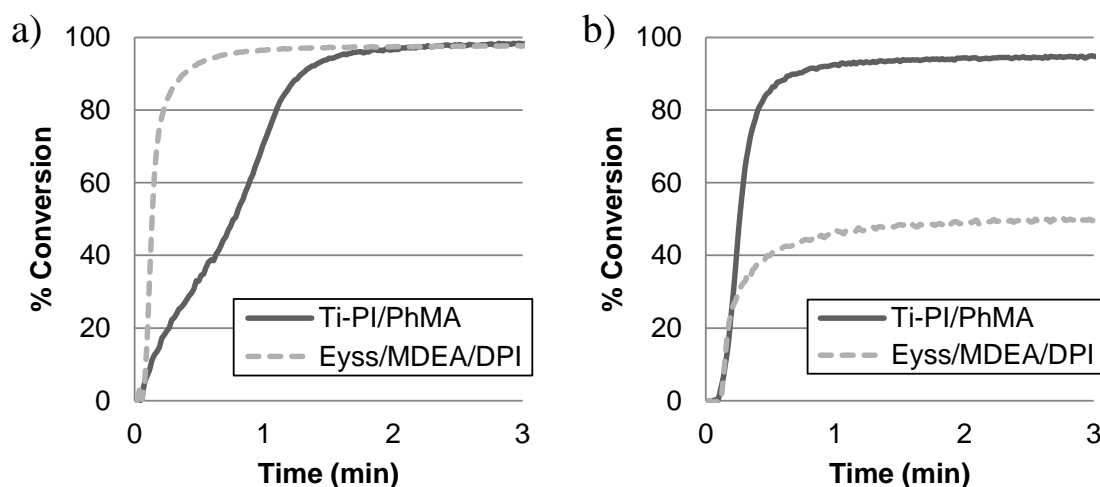


Figure 8-9: Photopolymerization conversion profiles for Ti-PI/PhMA photoinitiator system (Ti-PI = 2.6 wt %, PhMA = 1.5 wt %) and EYss/MDEA/DPI photoinitiator system (EYss = 0.074 wt %, MDEA = 3.77 wt %, DPI = 0.072 wt %) for two different monomer systems: (a) neat HEA monomer, (b) high viscosity urethane acrylate/HEA mixture (urethane acrylate = 70 wt %, HEA = 30 wt %). Light intensity: 2 mW/cm².

8.4. Conclusion

This contribution has provided a characterization of the photopolymerization effectiveness of the visible-light-photoinitiator Ti-PI for a variety of reaction

compositions and conditions. The experimental results demonstrate that a carefully selected combination of a protonic acid additive and light intensity is important to achieve effective photopolymerization using the Ti-PI photoinitiator system. As the acidity of the additive increases, the overall photopolymerization achieved by the Ti-PI-containing photoinitiator system increased accordingly, and the protonic acid phosphoric acid 2-hydroxyethyl methacrylate ester provided an excellent combination of reactivity and shelf life. For a given concentration of the initiator and the acid, a relatively low optimal light intensity for effective polymerization was observed, and light intensities above a threshold yield no effective polymerization at all. This implies that, although careful light intensity control is required to reach a high conversion, this photoinitiator system has great potential to realize safe and low energy photopolymerization using visible-light sources including visible LEDs. Furthermore, with careful selection of the light intensity gradient within the sample, some interesting cure scenarios could be created. For example, in thick systems such as adhesives and sealants, the deep regions (where the intensity is lower), might undergo more rapid polymerization than the shallow regions. As a result, low shrinkage stress of the thick system may be achieved. Finally, this initiator is very promising for visible-light-induced polymerizations of viscous systems. Most visible-light photoinitiators are based upon electron transfer processes and are comprised of two or more components. These initiators can lose effectiveness in viscous systems because the underlying reactions are diffusion controlled. In contrast, the Ti-PI containing photoinitiator systems achieved high conversion in viscous oligomer-containing compositions, and the polymerization effectiveness actually increased with increasing viscosity.

CHAPTER 9. CONCLUSIONS AND RECOMMENDATIONS

9.1. Part I: Shadow Cure in Free Radical Photopolymerizations

9.1.1. Summary of Research

In this aspect of the research, the extent of shadow cure in visible-light-induced free radical photopolymerization has been investigated. Using a dye/amine, EYss/MDEA, two-component Type II photoinitiator system as a basic visible-light-induced photoinitiator system, it was demonstrated that shadow cure in free radical photopolymerization of masked systems can be enhanced with the use of fluorescent additives in two- or three-component initiator systems. The addition of DPI to the two-component system led to a significant enhancement in the observed shadow cure. This result was attributed to the fact that DPI will increase both the number of active centers and the mobility of the active centers as a result of the electron transfer reactions in which it participates.

ACF is being considered as one of the representative shadow cure applications which tend to require short cure time. Therefore, a series of shadow cure experiments with PI-FPC using visible-light-induced free-radical photoinitiators were evaluated by Raman microscopy. In order to cure the shadow regions in a short time, various means were studied using photoinitiator systems based on EYss/MDEA and several effective methods including adding DPI and/or thiols, utilizing a reflective stage, and increased light intensity were investigated.

When considering industrially relevant resins for an ACF application, which are generally mixtures of oligomers and monomers, the viscosity was the major impediment that had to be overcome in order to achieve high conversion in shadow region using visible-light-induced Type II photoinitiators. Hence, a commercial visible-light-induced Type I photoinitiator Ti-PI was investigated. As a result, the proper combination of Ti-PI, with a protonic acid and an optimal light intensity was able to achieve a high conversion

in shadow region (under PI-FPC) of the viscous oligomer containing resin, when illuminated by a visible light source.

9.1.2. Recommendations for Future Work

In this contribution, shadow cure for various photoinitiator systems was investigated as a fundamental study. However, the effect of the resin on shadow cure ability has not been studied except for specific cases in ACF applications. Therefore, the extent of the shadow cure in various formulations, including oligomer-containing formulations, is an interesting topic to be studied as industries are using oligomer-monomer mixtures as their basic resins. The photopolymerization rate of any resin depends on the values of the propagation coefficient k_p and termination coefficient k_t and is in fact proportional to $k_p/k_t^{0.5}$.^{58, 88} Therefore, as the properties of the resins determine the values of k_p and k_t , they have a significant impact on the photopolymerization rate. This implies that properties of the resin such as viscosity, function number, molecular weight, glass transition temperature, and chemical structure can have a big impact on the extent of shadow cure.

Figure 9-1 shows the comparison of shadow cure conversion profiles (x-direction) between HEA(50)/HDDA(50) monomer mixture and CN9002(70)/HEA(30) oligomer-monomer mixture using the Ti-PI/PhMA photoinitiator system (see chapter CHAPTER 6). The measurement procedure is same as what was described in chapter CHAPTER 4. In the graph, the oligomer-monomer mixture demonstrates much higher shadow cure ability than the monomer mixture. This big difference in conversion profiles can be attributed to the lower termination rate in the oligomer-monomer mixture due to its higher initial viscosity, a property that results in higher photopolymerization rate. Thus, the resin can have a big impact on the extent of shadow cure and its impact should be further investigated.

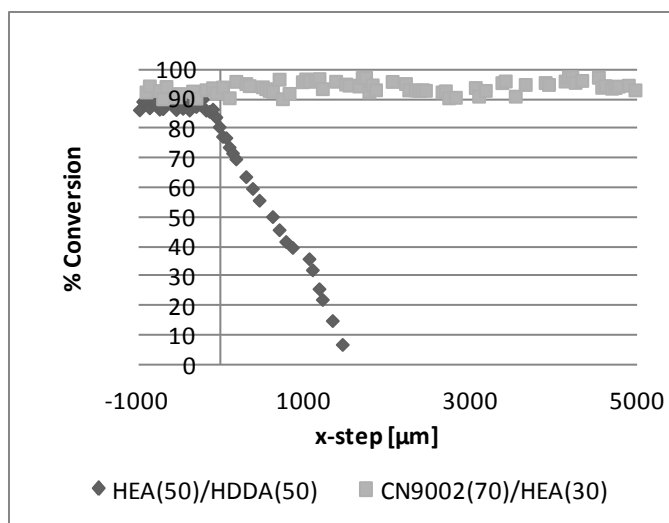


Figure 9-1: Comparison of shadow cure conversion profiles (x-direction) between HEA(50)/HDDA(50) monomer mixture and CN9002(70)/HEA(30) oligomer-monomer mixture. Negative values of x correspond to the illuminated region, while positive values of x correspond to the masked region. Photoinitiator system: Ti-PI 2.7 wt%, PhMA; 1.5 wt %. Light source: a 150 W xenon lamp with 520 nm bandpass filter, light intensity: 24 mW/cm², irradiation time: 15 minutes.

9.2. Part II: Experimental and Modeling Studies of Photoinitiator

Systems for Effective Polymerizations with LEDs

9.2.1. Summary of Research

In this aspect of the research, various LED photocuring systems including a 365nm LED, a 385 nm LED and a 400 nm LED were investigated. First, representative commercial LED systems were characterized for the uniformity of emission spectra, the relationship between light intensity and its irradiation distance, and its energy consumption. This study clarified that the energy efficiency of a LED is much higher than that of conventional lamps. In addition, the trend that light intensities of LEDs become weaker as their peak emission wavelengths decrease was also confirmed. Therefore, to design the practical process of LED curing, the effect of both the light intensity and the emission spectra of the lamp must be considered.

Thin cure was investigated for four photoinitiators using various LEDs and lamps using experimental and simulation studies. The effective light source was dependent on the photoinitiators and several LEDs demonstrated high thin cure ability. The calculated results from the model displayed good qualitative correspondence with the experimental results – thus, making the model a valid and reliable platform to study thin cure systems. Therefore, it was concluded that this model could be applied for the optimization of light sources and photoinitiators for thin cure.

9.2.2. Recommendations for Future Work

In this research, single LED wavelengths were employed to investigate photopolymerization with various photoinitiator systems. As a result, different LED light sources were characterized and then used in the model to predict photopolymerization conversion profiles for various combinations of light sources and photoinitiators. It is assumed that this research can be expanded to design various LED photopolymerization systems including the design of multi-wavelength LED lamps to provide an optimal light source to attain high photopolymerization. One of the considerable systems is the combination of two LEDs in which a LED performs quenching dissolved oxygen while the other initiate photopolymerization reaction using the photochemical method described in section 5.3. A few examples of this expansion are demonstrated below.

9.2.2.1. Combination1: Green LED and UV LED

In this demonstration, 5,10,15,20-Tetraphenyl-21H23H-porphine zinc (Zn-tp) was used as singlet oxygen generator with dimethylantracene (DMA) as a singlet oxygen scavenger. To excite this singlet oxygen generator, a 520 nm LED (Prizemax) was used with 322 mW/cm^2 light intensity. In HDDA monomer, the dissolved oxygen is quenched as shown in Figure 9-2, where the measurement was performed using UV-Vis spectroscopy by following a procedure described in previous study⁷¹.

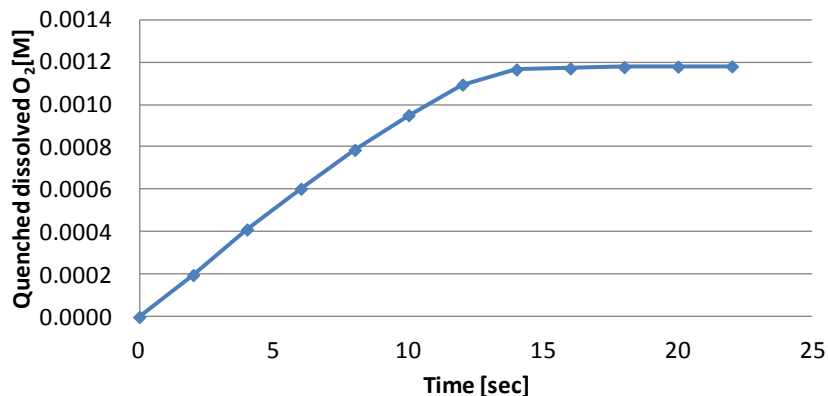


Figure 9-2: .Quenched dissolved oxygen as a function of illumination time. Monomer: HDDA. $[Zntpp] = 2 \times 10^{-3}$ M, $[DMA] = 2 \times 10^{-3}$ M. Light source: a 520 nm LED, light intensity 322 mW/cm^2 .

A series of experiments was performed with RT-FTIR. DMPA was employed as a photoinitiator to photopolymerize the HDDA monomer. 365 nm LED (Integration technology) and 400 nm LED (Phoseon) lamps were used to initiate photopolymerization with a light intensity of 6.8 mW/cm^2 . Figure 9-3 illustrates the comparison of RT-FTIR conversion profiles as a function of time in HDDA monomer using four different combinations of photoinitiator systems and irradiation conditions - (A) 365 nm LED and (B) 400 nm LED. In each of these systems, the photoinitiator DMPA has the same concentration of 0.0167 M. Here, pre-irradiation with the 520 nm LED was performed for 30 seconds before the sample was irradiated for photopolymerization by the 365nm and 400nm LED lamps. It was assumed that the pre-irradiation time was enough to quench the dissolved oxygen as shown in Figure 9-2. Figure 9-3-A and B show that the photopolymerization rate follows these trends: DMPA with irradiation by the photoinitiating LED (365 nm or 400 nm LED) < Zntpp/DMA/DMPA with irradiation by the photoinitiating LED < Zntpp/DMA/DMPA with simultaneous irradiation by the 520 nm LED, and the photoinitiating LED < Zntpp/DMA/DMPA with pre-irradiation by the 520 nm LED and irradiation by the photoinitiating LED.

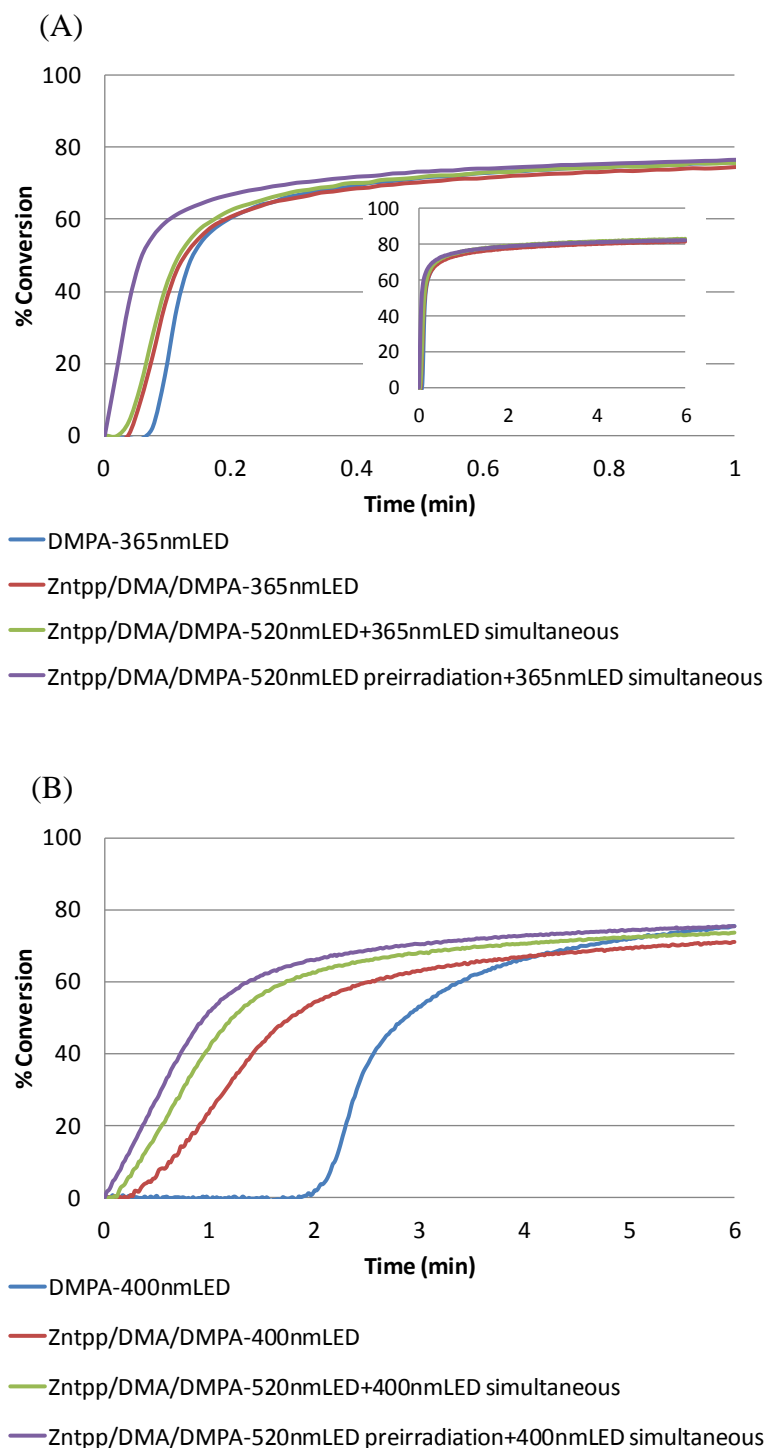


Figure 9-3: Comparison of RT-FTIR conversion profiles as a function of time in HDDA monomer in four different combinations of initiator, SG/ST, and light sources. Irradiation conditions: (A) 365 nm LED with 6.8 mW/cm^2 light intensity, (B) 400 nm LED with 6.8 mW/cm^2 light intensity. $[\text{DMPA}] = 0.0167 \text{ M}$, $[\text{Zntpp}] = 2 \times 10^{-5} \text{ M}$, $[\text{DMA}] = 2 \times 10^{-3} \text{ M}$. A 520 nm LED with 322 mW/cm^2 light intensity was used to scavenge dissolved oxygen.

9.2.2.2. Combination2: Red LED and UV LED

In this demonstration, Zn-tpa was used as a singlet oxygen generator with DMA as a singlet oxygen scavenger. To excite this singlet oxygen generator, a Xe lamp with a polyimide film (see Figure 3-6) was used at a 54 mW/cm^2 light intensity instead of using a red LED (e.g. 680 nm LED). In this condition, the dissolved oxygen in HDDA monomer is quenched as shown in Figure 9-4.

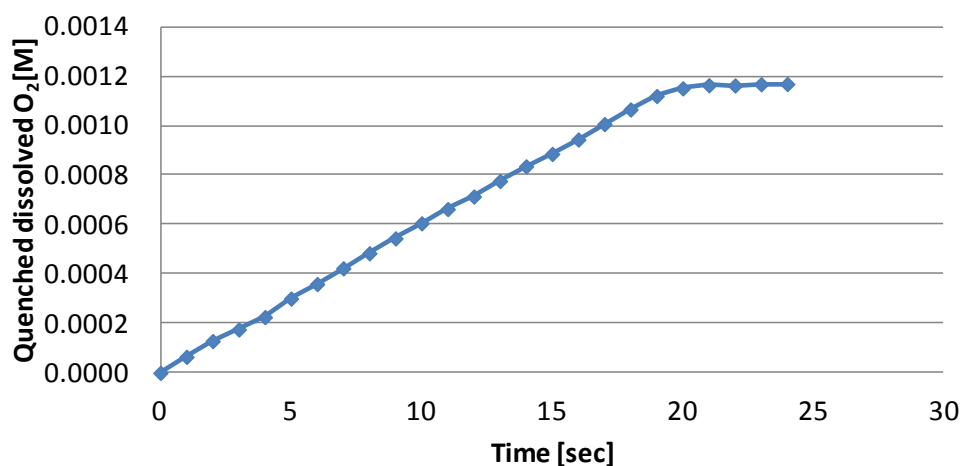


Figure 9-4: Quenched dissolved oxygen as a function of illumination time. Monomer: HDDA. $[\text{DMA}] = 1 \times 10^{-4} \text{ M}$, $[\text{Zn-tpa}] = 2 \times 10^{-5} \text{ M}$. Light source: a Xe lamp with a polyimide film, light intensity 322 mW/cm^2 .

A series of experiments was performed with the same methods as described in section 9.2.2.1. Figure 9-5 illustrates the comparison of RT-FTIR conversion profiles as a function of time in HDDA monomer in the four different combinations of photoinitiator systems and irradiation conditions with (A) 365 nm LED and (B) 400 nm LED, in which the photoinitiator DMPA has the same concentration of 0.0167 M. Pre-irradiation is performed with the Xe lamp (with a polyimide film attached to the light guide) for 30 seconds before the sample is irradiated by the photoinitiating LED lamps. It was assumed that the pre-irradiation time was enough to quench the dissolved oxygen as shown in

Figure 9-4. Figure 9-5 shows the same photopolymerization rate trends: DMPA with irradiation by the photoinitiating LED (365 nm or 400 nm LED) < Zntpp/DMA/DMPA with irradiation by the photoinitiating LED < Zntpp/DMA/DMPA with simultaneous irradiation by the Xe lamp and the photoinitiating LED < Zntpp/DMA/DMPA with pre-irradiation by the Xe lamp and irradiation by the photoinitiating LED.

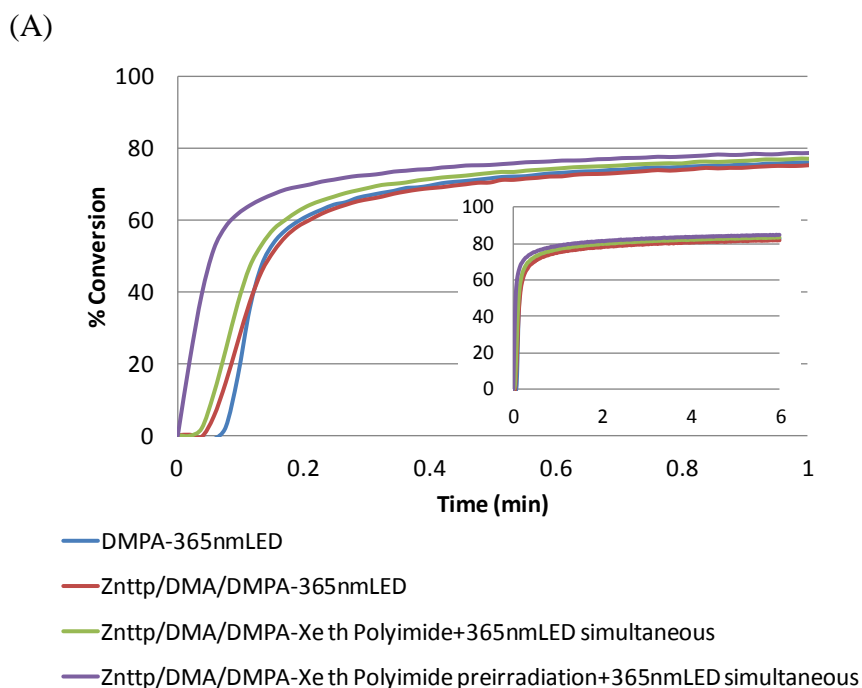


Figure 9-5: Comparison of RT-FTIR conversion profiles as a function of time in HDDA monomer in four different combinations of initiator, SG/ST, and light sources. Irradiation conditions: (A) 365 nm LED with 6.8 mW/cm^2 light intensity, (B) 400 nm LED with 6.8 mW/cm^2 light intensity. $[\text{DMPA}] = 0.0167 \text{ M}$, $[\text{Zntpp}] = 2 \times 10^{-5} \text{ M}$, $[\text{DMA}] = 2 \times 10^{-3} \text{ M}$. A Xe lamp with a polyimide film (54 mW/cm^2 light intensity) was used to scavenge dissolved oxygen.

(B)

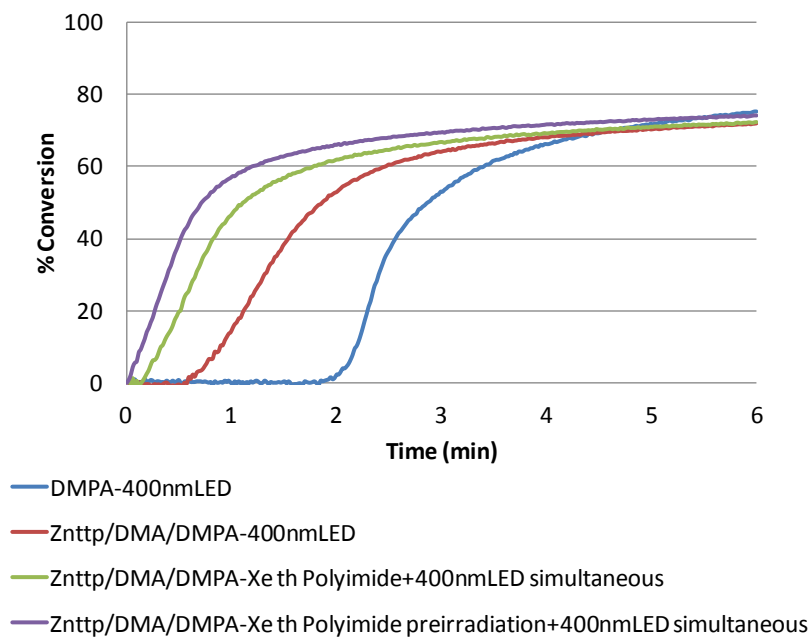


Figure 9-5 continued.

9.2.2.3. Summary

As demonstrated above, the combination of multi-wavelength LEDs has a lot of potential to achieve high photopolymerization. Therefore, modeling studies and experimental characterizations of LEDs performed in this contribution can be used for the design of new multi-wavelength LED photopolymerization systems.

APPENDIX A. FEASIBILITY STUDY FOR THE CANDIDATES
OF VISIBLE-LIGHT-INDUCED PHOTOINITIATOR SYSTEM
WITH FLUORESCENT ADDITIVE

As mentioned in chapter CHAPTER 4, photoinitiation within the shadow regions by photons emitted from a fluorescent additive should have been investigated. In this method, the molecular absorption of light by the fluorescent additive leads to the emission of another photon at a longer wavelength. This fluorescent emission is multidirectional, potentially resulting in illumination within shadow regions behind the electrodes (trivial mechanism³⁷). Regarding the EYss system as a basic visible light-induced photoinitiator system, the candidates for dyes to be combined with the EYss system are FL and MB (methylene blue). FL is excited between 400–500 nm wavelengths without the absorption by EYss and generates active centers through the reaction with MDEA. At the same time, the FL fluorescence around 520 nm might irradiate shadow regions and activate the EYss photoinitiator system. In the case of MB, EYss is excited around 520 nm wavelength without the MB absorption and begins to polymerize. In the shadow region, photons around 600 nm may be carried by EYss fluorescence emission and excite MB, resulting in photoinitiation.

In this contribution, combinations of EYss/MB/MDEA and EYss/FL/MDEA were chosen as plausible candidates to apply illumination within shadow regions by emission from fluorescent additives. Their chemical structures are shown in Figure A- 1. In the EYss/MB/MDEA system, EYss is excited around 520 nm wavelength without the MB absorption and begins to polymerize. In the shadow region, photons around 600 nm may be carried by EYss fluorescence emission and excite MB resulting in photoinitiation. In the EYss/FL/MDEA system, FL is excited around 450 nm wavelength without absorption by EYss and generates active centers through the reaction with MDEA. At the same time, FL fluorescence around 520 nm might irradiate

shadow regions and activate the EYss photoinitiator system. The characteristics of these systems and their potential to enhance shadow cure using these dye combinations are investigated in this study using RT-FTIR.

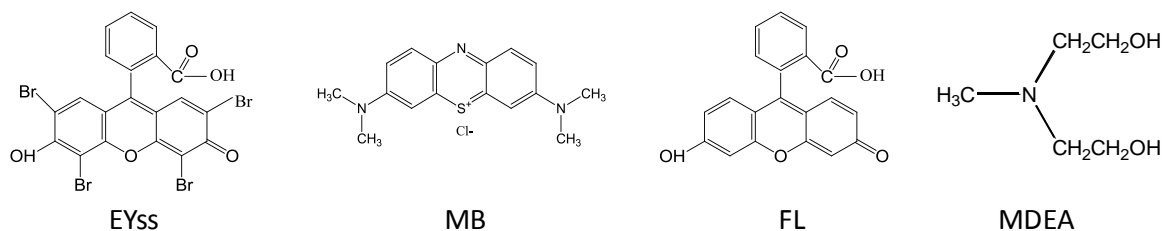


Figure A- 1: Chemical structures of EYss, MB, FL, and MDEA.

A-1. Materials and Methods

HEA monomer was used as the resin. The studied compositions and light conditions are summarized in Table A- 1 and Table A- 2. A 150 W xenon lamp equipped with 450 nm, 520 nm, or 650 nm bandpass filters (MAX-150, Asahi Spectra) was used. The overall conversion of HEA films was measured using RT-FTIR with the method described in section 3.2.1.

Table A- 1: Studied compositions and light conditions for EYss/MB/MDEA.

		EYss/MDEA		MB/MDEA		EYss/MB/MDEA		
		EYss	MDEA	MB	MDEA	EYss	MB	MDEA
Concentration	[M]	0.00115	0.32	0.00115	0.32	0.00115	0.00115	0.32
150 W Xe lamp	(nm)	520		520		520		650
	(mW/cm ²)	2.1		2.1		1.3		2.1

Table A- 2: Studied compositions and light conditions for EYss/FL/MDEA

		EYss/MDEA		FL/MB		EYss/FL/MDEA		
		EYss	MDEA	MB	MDEA	EYss	FL	MDEA
Concentration	[M]	0.00115	0.32	0.00115	0.32	0.00115	0.00115	0.32
150 W Xe lamp	(nm)	450		450		450		520
	(mW/cm ²)	1.3		1.3		1.3		2.1

A-2. Results and Discussions

RT-FTIR conversion profiles as a function of time for the EYss/MB/MDEA combination are shown in Figure A- 2. The solid lines represent EYss/MDEA, MB/MDEA, and EYss/MB/MDEA conversions in illuminated regions irradiated by 520 nm wavelength light. The dotted line represents EYss/MB/MDEA conversion irradiated by 650 nm light to imitate the shadow region. In EYss/MB/MDEA system, both 520 nm (from the lamp) and 650 nm (from the EYss fluorescence) light exists in the illuminated region. However, only the 650 nm light extend into to the shadow regions. Therefore, the EYss/MB/MDEA solid line in the graph expresses the typical tendency at the illuminated region and the EYss/MB/MDEA dotted line states the trend at the shadow regions. From the graph, it can be concluded that the EYss/MB/MDEA system is not effective for shadow cure. In shadow regions, the polymerization caused by 650 nm wavelength fluorescence is not so efficient. Furthermore, adding MB into EYss/MDEA system decreases the polymerization efficiency compared to EYss/MDEA system. One of the reasons of this poor efficiency in illuminated regions could be the static interaction between MB and EYss. As shown in Figure A- 3, EYss generates a negative charge radical, $EYss^{\bullet-}$, during its photoinitiating reaction. On the other hand, MB is a positive charge molecular, MB^+ , originally. Hence the static interaction between $EYss^{\bullet-}$ and MB^+ can interfere the photoinitiating reactions.

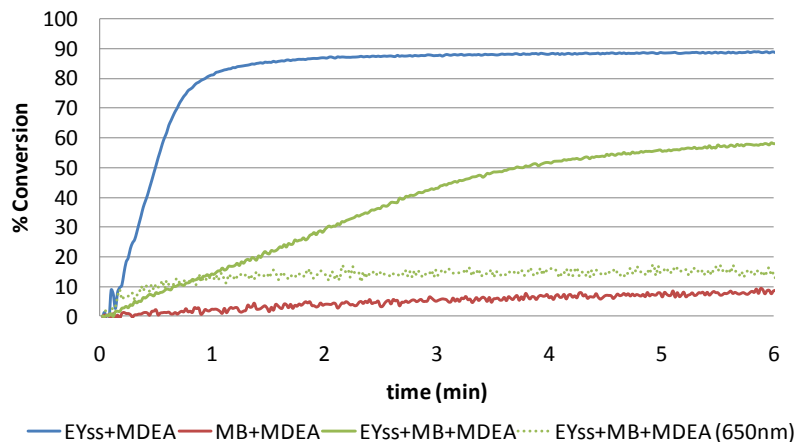


Figure A- 2: Conversion vs. time of HEA monomer with EYss, MB, MDEA irradiated by 520 nm wavelength light

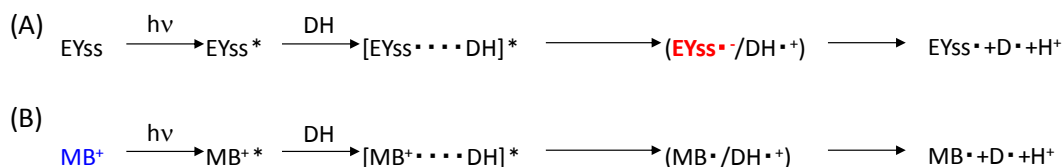


Figure A- 3: Reaction schemes of (A) EYss/MDEA and (B) MB/MDEA photoinitiator systems

RT-FTIR conversion profiles as a function of time for the EYss/FL/MDEA combination are shown in Figure A- 4. The solid lines represent EYss/MDEA, FL/MDEA, and EYss/FL/MDEA conversions in illuminated regions irradiated by 450 nm wavelength light. The dotted line represents EYss/FL/MDEA conversion irradiated by 520 nm fluorescent light to imitate the shadow region. In the EYss/FL/MDEA system, light of both wavelengths exists in the illuminated region. However, only the 520 nm fluorescent light can be extended into the shadow region. Therefore, the solid EYss/FL/MDEA line in the graph can be considered as the illuminated_regions' reaction and the dotted EYss/MB/MDEA line can be considered as the shadow regions' reaction. From the graph, it can be assumed that the EYss/FL/MDEA system is effective for shadow cure. In the shadow region, the 520 nm wavelength fluorescence

emitted from FL can polymerize the HEA resin. With respect to the illuminated region, EYss/FL/MDEA system can polymerize the resin more efficiently compared to the EYss/MDEA system. Unlike the EYss/MB/MDEA system, the reaction of EYss-MDEA and FL-MDEA can be assumed to be independent of each other due to no static charge interactions between them (see Figure A- 5). Thus, adding FL into the EYss/MDEA may be effective for shadow cure.

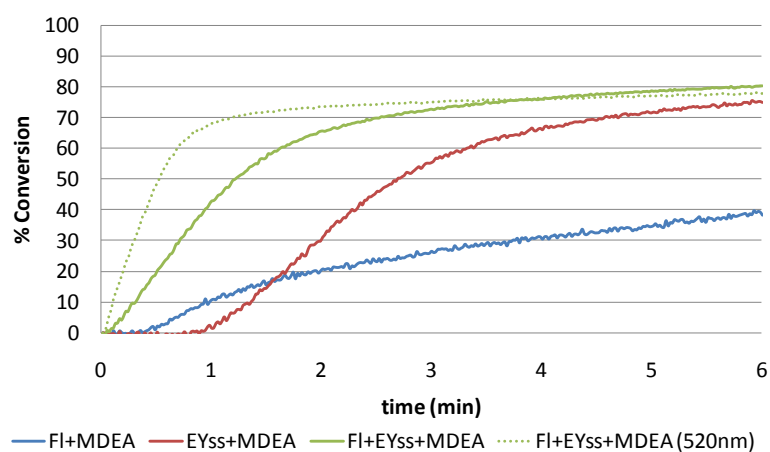


Figure A- 4: Conversion vs. time of HEA monomer with EYss, FL, MDEA irradiated by 450 nm wavelength light

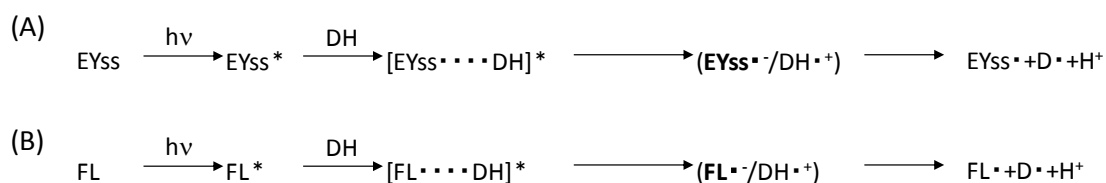


Figure A- 5: Reaction schemes of (A) EYss/MDEA and (B) FL/MDEA photoinitiator systems

APPENDIX B. CHARACTERIZATION OF EYSS/DABCO/DPI
AND EYSS/EDMAB/DPI THREE-COMPONENT SYSTEMS

As mentioned in section 3.3.1, the use of an electron donor 1, 4-diazabicyclo [2.2.2] octane, 1-azabicyclo [2.2.2] octane (DABCO) was suggested as an effective chemical in extending the shelf life of methylenblue (MB)/amine/DPI three-component systems.³⁸ In addition, ethyl 4-(dimethylamino)benzoate (EDMAB), which is commercially used for dental materials, is also being considered as amine in three-component photoinitiators^{89, 90} for lengthening their shelf lives. To investigate the effect of using DABCO or EDMAB instead of MDEA in an EYss/amine/DPI system, EYss/DABCO/DPI and EYss/EDMAB/DPI three-component photoinitiator systems were investigated.

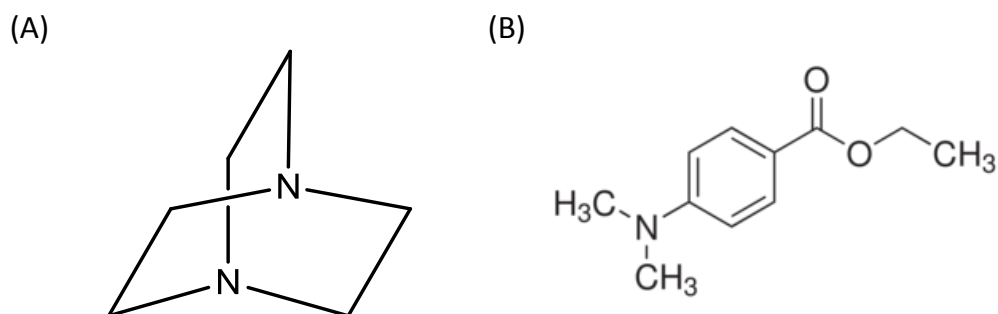


Figure B- 1 Chemical structures of 1, 4-diazabicyclo [2.2.2] octane, 1-azabicyclo [2.2.2] octane (DABCO) and ethyl 4-(dimethylamino)benzoate (EDMAB)

B-1. Photopolymerization of EYSS/DABCO/DPI Three-Component System

HEA monomer was used as the resin. The formulations of two types of two-component systems (EYss/DABCO, EYss/DPI) and a three-component system (EYss/DABCO/DPI) that were studied are shown in Table B- 1. The overall conversion of HEA films was measured using RT-FTIR. The sample was irradiated through a

polyimide film by a 150 W Xe lamp with no filter emitting the full spectrum and a through 520 nm bandpass filter as well. Normally, the xenon lamp emits a total light intensity of 89 mW/cm² with a broad wavelength. However, with the polyimide film it emitted 39 mW/cm² total light intensity due to the attenuation of light, especially in the low wavelength regions. With the bandpass filter, the lamp emitted 2.4 mW/cm² total light intensity with 520 nm single wavelength.

Table B- 1: Two-component system and three-component system formulas studied for EYss/DABCO/DPI system.

		Two-component system		Three-component system
		EYss/DABCO	EYss/DPI	EYss/DABCO/DPI
EYss	[M]	0.00115	0.00115	0.00115
DABCO	[M]	0.32	-	0.32
DPI	[M]	-	0.0023	0.0023

Figure B- 2 illustrates conversion as a function of time for the two-component and three-component systems. As expected, the final conversions of the two-component systems are not high in the all of the light conditions (Figure B- 2A, B). In particular, overall conversions in the EYss/DABCO two-component systems are very low. However, when all of the three components are combined, the final conversions become higher than 80% in the all of the light conditions.

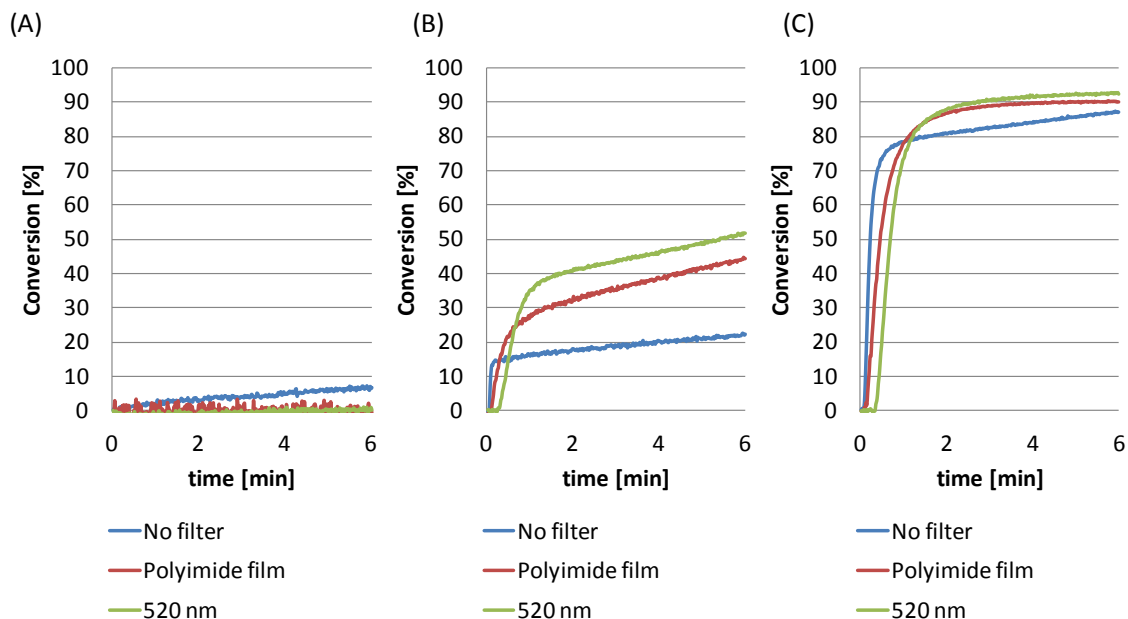
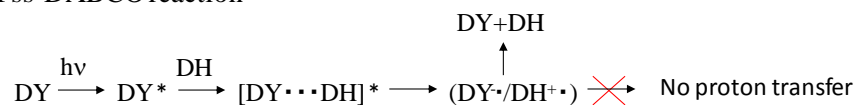


Figure B- 2: Conversion vs. time of two-component systems and a three-component system for three different incident lights: (A) EYss/DABCO two-component system, (B) EYss/DPI two-component system, (C) EYss/DABCO/DPI three-component system. Monomer: HEA. Incident lights: a 150 W xenon lamp with no filter (89 mW/cm^2), a polyimide film (39 mW/cm^2) and a 520 nm bandpass filter (2.4 mW/cm^2).

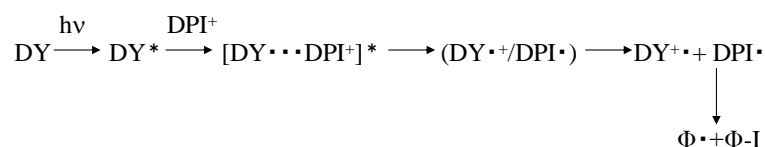
The reaction mechanism of the two-component systems (EYss/DABCO, EYss/DPI) and the three-component system (EYss/DABCO/DPI) are shown in Figure B- 3 and Figure B- 4. As shown in Figure B- 3A, unlike the EYss/MDEA two-component system, the electron-transfer/proton-transfer reaction between EYss and DABCO does not occur due to the stereoelectronic effect of DABCO even though the electron-transfer/proton-transfer reaction may occur.³⁸ However, in the three-component system, DPI can produce an active phenyl radical (Φ^\bullet) from the amine/dye reactions by irreversibly oxidizing the DY^\bullet radical, and thereby preventing the back-electron transfer reaction shown in Figure B- 4C. DPI also oxidizes an excited dye molecule in a reaction that produces a phenyl radical in both the two-component (Figure B- 3B) and three-component systems (Figure B- 4D). Hence, the three-

component photoinitiator system is more effective in photopolymerization than the two-component photoinitiator systems as demonstrated in Figure B- 2.

(A) EYss-DABCO reaction



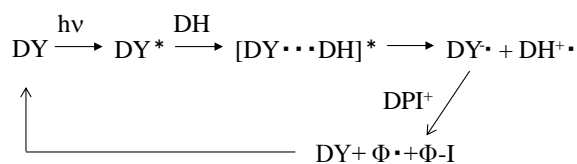
(B) EYss-DPI reaction



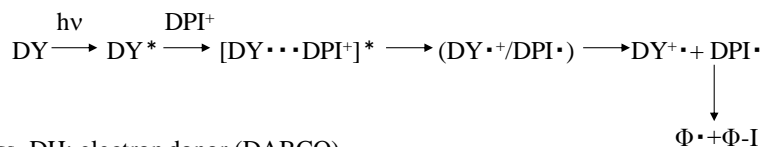
DY: EYss, DH: electron donor (DABCO),
DPI⁺: iodonium salt, $\Phi\cdot$: phenyl radical, $\Phi\text{-I}$: phenyl iodide

Figure B- 3: Reaction mechanism of two-component systems. (A) EYss/DABCO (B) EYss/DPI.

(C) EYss-DABCO-DPI reaction



(D) EYss-DPI reaction



DY: EYss, DH: electron donor (DABCO),
DPI⁺: iodonium salt, $\Phi\cdot$: phenyl radical, $\Phi\text{-I}$: phenyl iodide

Figure B- 4: Reaction mechanism in an EYss/DABCO/DPI three-component system. (C) photo-reduction of EYss by DABCO and (D) photo-oxidation of EYss by DPI.

B-2. Shelf Life of EYss/DABCO/DPI Three-Component System

The shelf lives of EYss/MDEA/DPI and EYss/DABCO/DPI three-component systems in HEA monomer were compared. The compositions of the samples are illustrated in Table B- 2. These samples were made on day zero. Then they were stored in a dark environment at room temperature and their polymerization was studied on successive days using RT-FTIR spectroscopy to investigate their shelf life. The samples were irradiated by a Xe lamp with a 520 nm bandpass filter emitting a light intensity of 2.4 mW/cm². Figure B- 5 shows the comparison between the time dependent conversion profiles of the EYss/MDEA/DPI and EYss/DABCO/DPI systems. The initial conversions (at t=0) of both components increase with the passage of time due to the thermal reaction that takes place even during storage. On the contrary to expected results, the shelf life of the EYss/DABCO/DPI is shorter than that of the EYss/MDEA/DPI system. The EYss/MDEA/DPI system can maintain its photopolymerization trend for at least four days. However, the photopolymerization capability of the EYss/DABCO/DPI system begins to fall at day 1 and continues to worsen with the passage of time, thus resulting in no photopolymerization reaction at day 10.

Table B- 2: Three-component systems' formulas studied.

		EYss/MDEA/DPI	EYss/DABCO/DPI
EYss	[M]	0.00115	0.00115
MDEA	[M]	0.32	-
DABCO	[M]	-	0.32
DPI	[M]	0.0023	0.0023

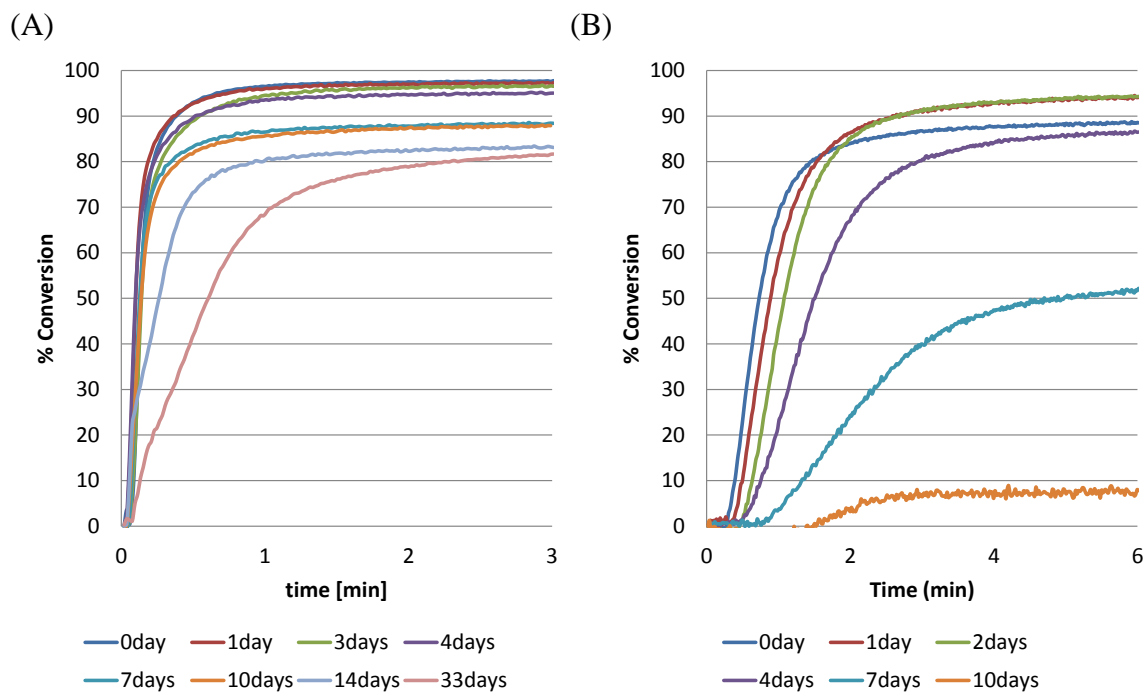


Figure B- 5: The comparison of time dependence for conversion profiles. (A) EYss/MDEA/DPI three-component system and (B) EYss/DABCO/DPI three-component system. Light source: a Xe lamp with a 520 nm bandpass filter (light intensity: 2.4 mW/cm^2). Monomer: HEA.

To investigate the reactions under the dark condition that result in a shorter shelf life time for the EYss/DABCO/DPI three-component system, differential scanning calorimetry (DSC) (DSC-7, PerkinElmer) was used to characterize the stability as a function of temperature for the HEA monomer with and without the components under dark conditions. Using an experimental heat flow program that had a heating rate of $2^\circ\text{C}/\text{min}$ over a temperature range of $25\text{--}100^\circ\text{C}$, two consecutive DSC scans were obtained for each sample. For each measurement, a characteristic heat flow profile was obtained by subtracting the profile of the second run from the profile of the first run. If thermally-induced polymerization begins to occur, the heat flow profile exhibits exothermic heat flow as a function of temperature.

Figure B- 6 shows the heat flow profiles as a function of temperature for the HEA monomer with zero-, single-, two-, and three-component systems respectively. Based on the DSC results, it can be concluded that DABCO-DPI containing components (orange and gray lines) cause polymerization in this temperature range because other species demonstrate a similar trend that results in no reaction. Therefore, it can be assumed that the combination of DABCO and DPI in the three-component system causes a reaction under dark conditions. This trend is similar to that of the EYss/MDEA/DPI three-component system.

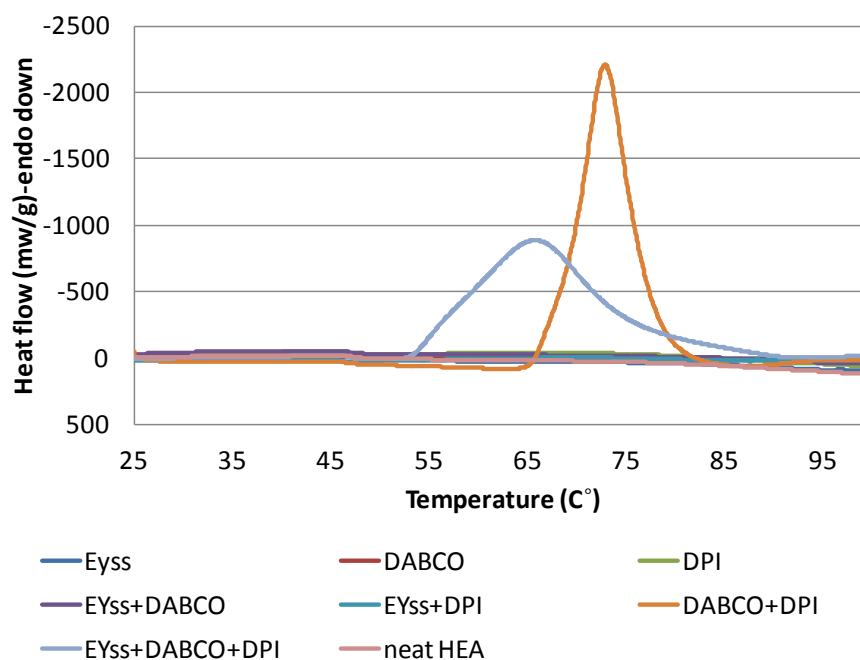


Figure B- 6: DSC heat flow (with the second run subtracted from the first run) as a function of temperature for HEA with EYss, DABCO, DPI, EYss-DABCO, EYss-DPI, DABCO-DPI, EYss-DABCO-DPI, or without species. $[EYss] = 0.00115 \text{ M}$, $[DABCO] = 0.32 \text{ M}$, $[DPI] = 0.0023 \text{ M}$.

Figure B- 7 compares the heat flow profiles between MDEA/DPI and DABCO/DPI (or EYss/MDEA/DPI and EYss/DABCO/DPI). Because the DABCO-containing systems start reacting faster than the MDEA-containing systems, it can be

assumed that DABCO-DPI thermal reaction is more likely to occur compared to that of MDEA-DPI. This result corresponds to the result demonstrated in Figure B- 7. Thus it can be concluded that systems containing DABCO and DPI are not stable due to their redox reaction illustrated in Figure B- 8.

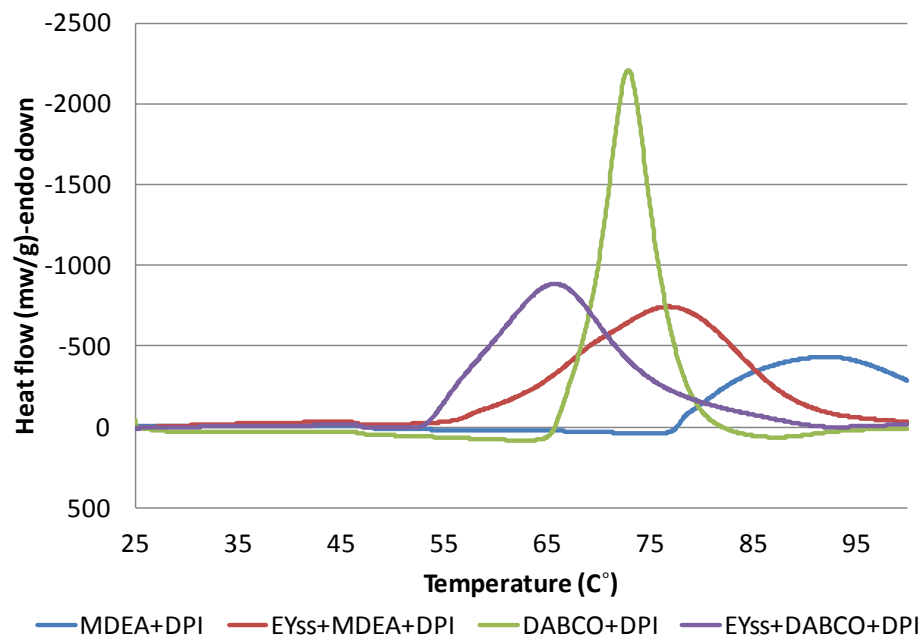


Figure B- 7: DSC heat flow (with the second run subtracted from the first run) as a function of temperature for HEA with MDEA-DPI, EY_{ss}-MDEA-DPI, DABCO-DPI, EY_{ss}-DABCO-DPI. [EY_{ss}] = 0.00115 M, [MDEA] = 0.32 M, [DABCO] = 0.32 M, [DPI] = 0.0023 M.

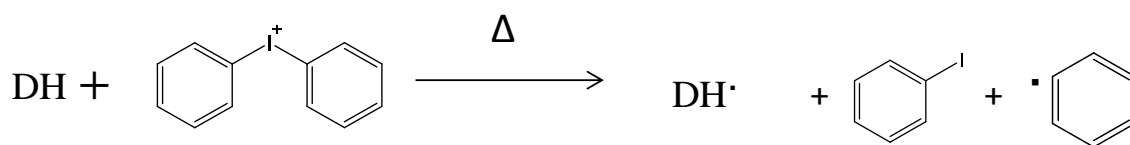


Figure B- 8: Suggested reaction scheme between DABCO (DH) and DPI.

B-3. Photopolymerization of EYSS/EDMAB/DPI Three-Component System

HEA monomer was used as the resin. The formulations of two types of two-component systems (EYss/EDMAB, EYss/DPI) and a three-component system (EYss/EDMAB/DPI) studied are shown in Table B- 3. The overall conversion of HEA films was measured using RT-FTIR. The sample was irradiated by a 520 nm LED emitting light at an intensity of 4 mW/cm².

Table B- 3: Two-component system and three-component system formulas studied.

		Two-component system		Three-component system
		EYss/EDMAB	EYss/DPI	EYss/EDMAB/DPI
EYss	[M]	0.00115	0.00115	0.00115
EDMAB	[M]	0.16	-	0.16
DPI	[M]	-	0.0023	0.0023

Figure B- 9 illustrates conversion as a function of time for the two-component and three-component systems. The three-component system shows higher photopolymerization compared to two-component systems.

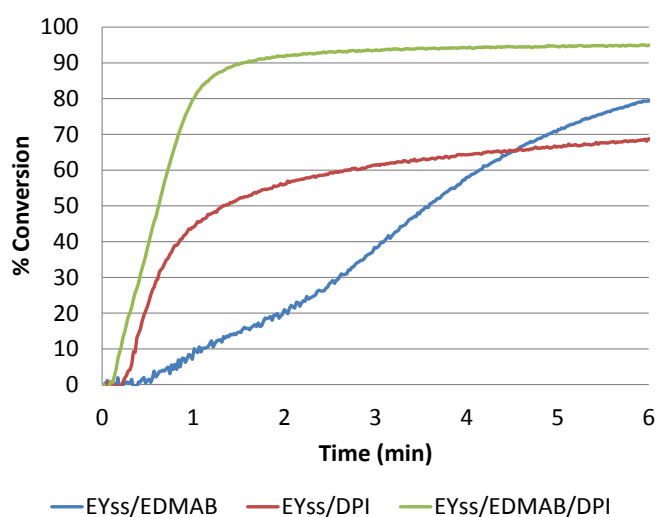


Figure B- 9: Conversion vs. time of two-component systems and a three-component system. Monomer: HEA. Incident lights: a 520 nm LED (4 mW/cm²).

Figure B- 10 illustrates the effect of light intensity on the EYss/EDMAB/DPI three-component system. As the light intensity increases, photopolymerization is enhanced. However, compared to the photopolymerization profile of EYss/MDEA/DPI, the photopolymerization rates of EYss/EDMAB/DPI are relatively slow.

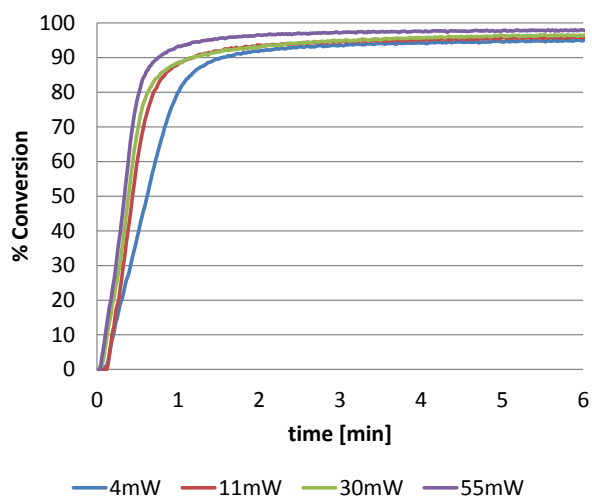


Figure B- 10: HEA photopolymerization conversion profiles for seven different light intensities. For all systems EYss = 0.00115 M, EDMAB = 0.16 M, DPI = 0.0023 M. Light source: 520 nm LED.

B-4. Shelf Life of EYss/EDMAB/DPI Three-Component System

The shelf lives of EYss/EDMAB/DPI three-component system for three different concentration combinations in HEA monomer were studied. The compositions of the samples are illustrated in Table B- 4. These samples were made on day zero. Then, they were stored in a dark environment at room temperature and their polymerization was studied on successive days using RT-FTIR spectroscopy to investigate their shelf lives.

Table B- 4: EY_{ss}/EDMAB/DPI three-component systems' formulas studied.

		Formula 1	Formula 3	Formula 2
EY _{ss}	[M]	0.00115	0.00115	0.00115
DABCO	[M]	0.16-	0.16	0.04
DPI	[M]	0.0023	0.0115	0.0115

Figure B- 11 illustrates the photopolymerization profiles of three different concentration combinations for EY_{ss}/EDMAB/DPI three-component systems (formula 1-3) measured at various days. Inconsistent photopolymerization rates in each graph are observed here. One of the considerable reasons is the change of sensitivity to the light intensity as the passage of days, but the mechanism is still not clear. Regarding ultimate conversions of the photopolymerization profiles, unlike EY_{ss}/MDEA/DPI system (Figure B- 7A) or EY_{ss}/DABCO/DPI system (Figure B- 7B), the ultimate conversions of EY_{ss}/EDMAB/DPI systems are stable and high (more than 95 %). Therefore, the use of EDMAB as an electron donor could be effective to prolong shelf life for three-component systems.

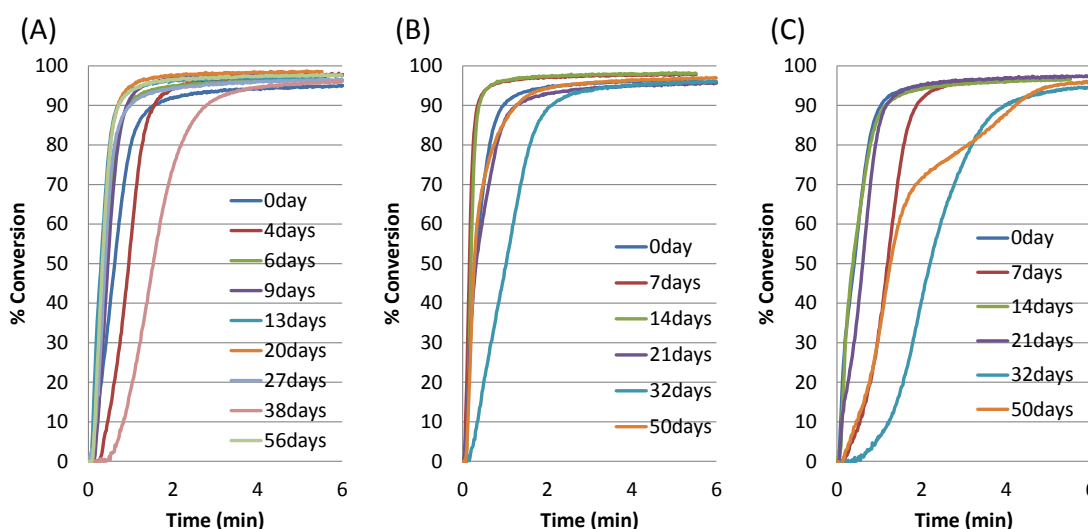


Figure B- 11: The comparison of time dependence for conversion profiles. (A) EY_{ss}/MDEA/DPI three-component system and (B) EY_{ss}/DABCO/DPI three-component system. Light source: a Xe lamp with a 520 nm bandpass filter (light intensity: 2.4 mW/cm²). Monomer: HEA.

B-5. Summary of Shelf Lives Study for Various Amines in Three-Component System

Figure B- 12 demonstrates conversion at 3 minutes irradiation as a function of time (in days) for EYss/amine/DPI three-component systems, where amine is MDEA, DABCO, or EDMAB. This graph illustrate that the stability of three-component systems depends on the amine and the observed trend (in order to increase shelf life) is DABCO < MDEA < EDMAB. However, this does not correlate well with the pKa of the amines, DABCO (pKa of 2.97), MDEA (pKa of 8.82), and EDMAB (approximate pKa of 4.0). This implies that factors other than pKa including steric hindrance, nucleophilicity, and redox potential of amines (or electron donors) must be considered to design three-component systems to achieve long shelf life.

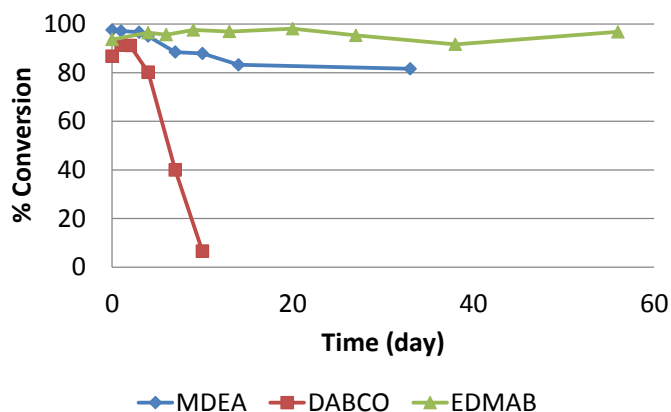


Figure B- 12: Conversion at 3 minutes irradiation vs. time. Light source: 520 nm lamp. Light intensity: 2~4 mW/cm². EYss = 0.00115 M, DPI = 0.0023 M for all systems. MDEA = DABCO = 0.32 M, EDMAB = 0.16 M.

APPENDIX C. DEPENDENCY OF ABSORBANCE ON XHANTENE DYE CONCENTRATIONS

As described in section 4.3, at dye concentrations higher than 10^{-5} M, the dyes (fluorescein (FL) and eosin Y spirit soluble (EYss)) exist primarily as dimers⁴⁹⁻⁵¹. In this contribution, the dependency of absorbance on concentration was investigated for each dye.

The absorbance profiles of the dyes were monitored using an 8453 UV-Visible spectrophotometer (Agilent Technologies) for different concentrations. In these measurements, methanol was used as the solvent. Figure C- 1 and Figure C- 2 show the dependence of absorption on the concentration of the dyes in methanol. At dye concentrations higher than 10^{-5} M, the dyes exist primarily as dimers, and the dimer formation is evident from the results in Figure C- 1A and Figure C- 2A because a decrease in the absorptivities are observed. In the normalized absorptivity spectrum of FL (Figure C- 1B), the unassociated dye exhibits its maximum absorbance at a wavelength of 480 nm, and the formation of the associated dye (dimer) leads to a blue-shift in the absorption spectra with a maximum absorbance at 451 nm. Similarly, in the spectrum of EYss (Figure C- 2B), the unassociated dye exhibits its maximum absorbance at a wavelength of 533 nm, and the associated dye (dimer) has a minor blue-shifted peak absorption at 495 nm.

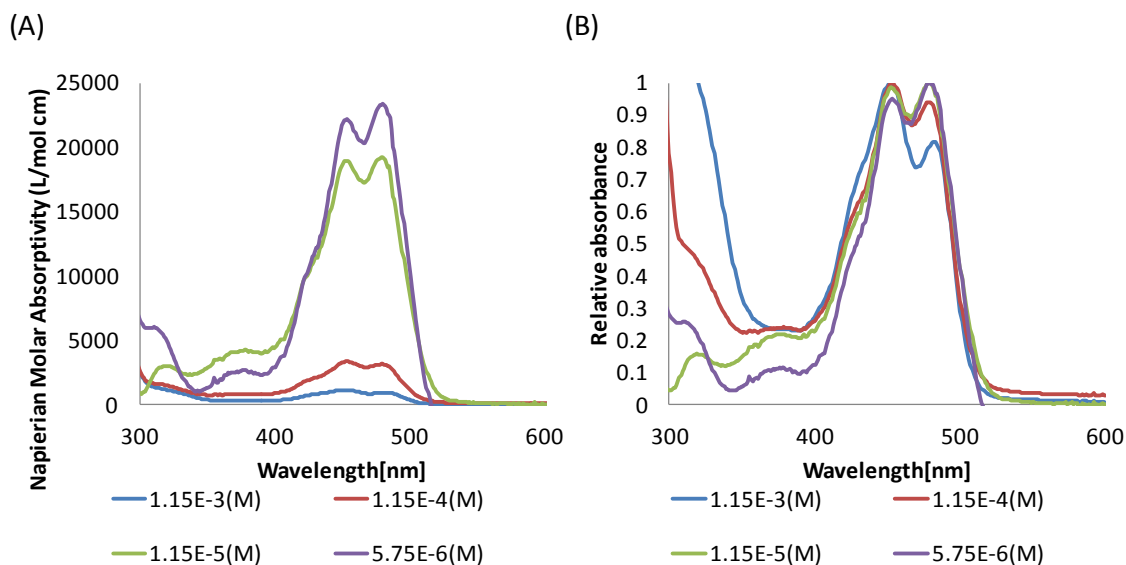


Figure C- 1: Dependence of absorption on fluorescein (FL) concentration in methanol. (A) Napierian molar absorptivities (B) Normalized absorption.

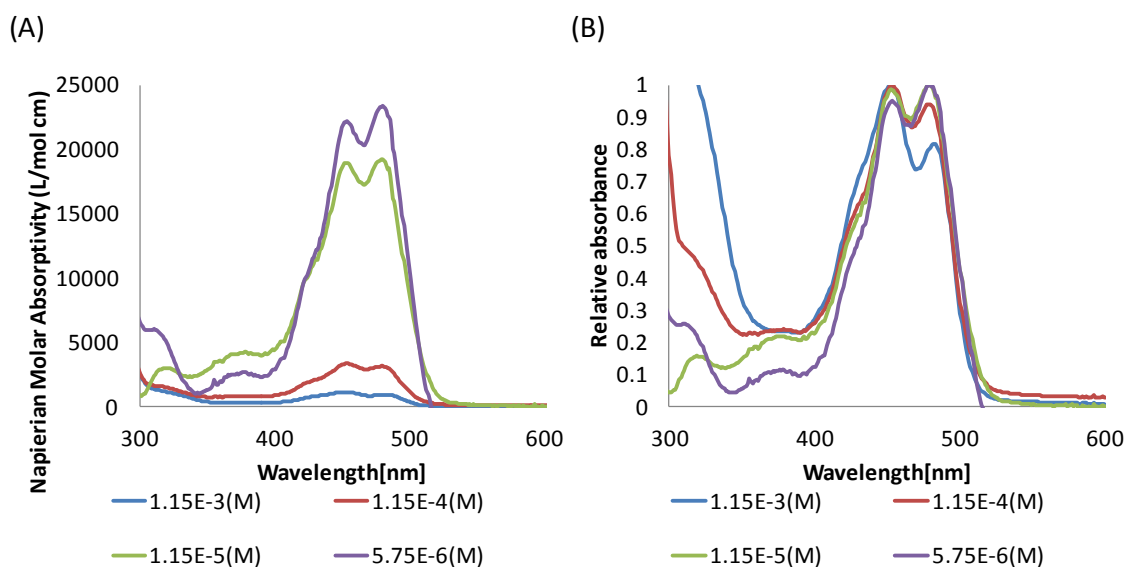


Figure C- 2: Dependence of absorption on eosin Y spirit soluble (EYss) concentration in methanol. (A) Napierian molar absorptivities (B) Normalized absorption.

APPENDIX D. IMPACT OF STAGE REFLECTION ON SHADOW CURE

In this contribution, the impact of reflection from the stage on shadow cure was investigated. The system used was an EYss/MDEA two-component photoinitiating system in a monomer mixture of 50 wt % HEA and 50 wt % HDDA. The procedure for this method has been described in section 4.2.2, where four different stages (Figure D-1), a black foam plate, a white sheet of paper, a steel plate (Q-panel) with a rough iron surface, and a mirror were employed to investigate their effect on shadow cure.

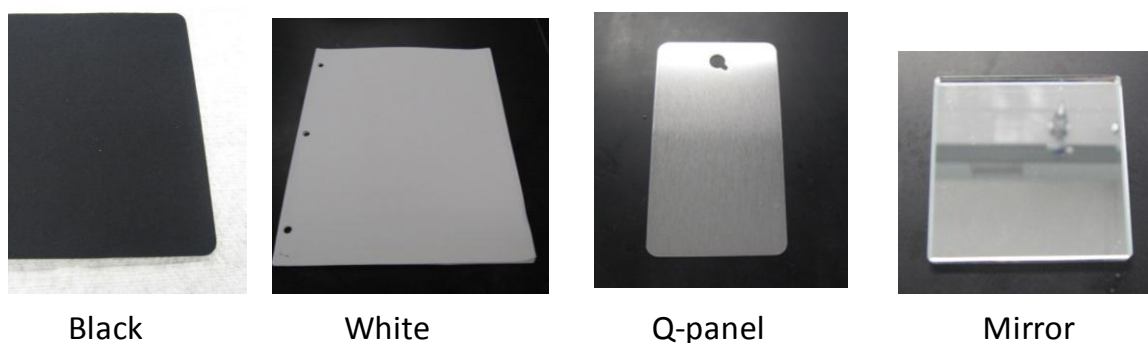


Figure D- 1: Four different stage substrates

Figure D- 2 contains plots of the conversion profiles in the x-direction, perpendicular to the edge of the illuminated region for the four different substrates. For all four substrates, the conversion in the illuminated region is above 70%. The data in Figure D- 2 illustrate that the reflective substrates including white paper, Q-panel, and mirror used for the experiment have a marked effect on the observed degree of shadow cure in which the conversions in shadow regions are higher than those of the black substrate, and that the reflective substrates exhibit the same trend. Thus, it is confirmed that the substrate of this shadow cure system influences shadow cure profiles due to reflection. This reflection increases the number of photons derived from the light source

in the irradiated region and in the shadow region. In addition, the fluorescence and diffraction in the shadow region are also enhanced by this reflection. As a result, the photopolymerization reaction is more likely to occur in both irradiated and shadow regions.

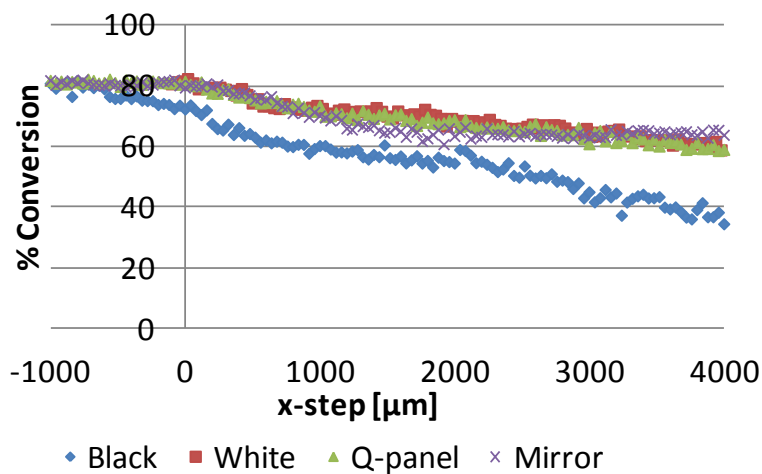


Figure D- 2: The effect of the bottom substrate on the conversion profiles (x-direction) observed for EYss/MDEA₂ system. Light source: a 150 W xenon lamp, light intensity: 89 mW/cm², irradiation time: 15 minutes.

APPENDIX E. SUPPLEMENTAL STUDY ABOUT SINGLET-
OXYGEN-GENERATOR/SINGLET-OXYGEN-TRAPPER
SYSTEMS

In this contribution, various studies relating with singlet oxygen generator (SG)/singlet oxygen trapper (ST) systems, described in section 5.3 and 9.2, were performed. Zinc 2,9,16,23-tetra-tert-butyl-29H,31H-phthalocyanine (Zn-ttp) or 5,10,15,20-tetraphenyl-21H23H-porphine zinc (Zn-tpp) was used as a SG and 9,10-dimethylantracene (DMA) was used as a ST. Their chemical structures are shown in Figure F- 1. All the chemicals were purchased from Sigma-Aldrich.

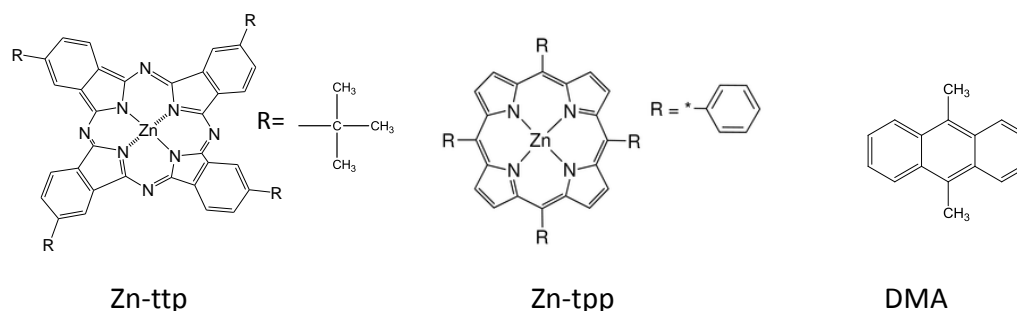


Figure E- 1: Chemical structures of zinc 2,9,16,23-tetra-tert-butyl-29H,31H-phthalocyanine (Zn-ttp), 5,10,15,20-Tetraphenyl-21H23H-porphine zinc (Zn-tpp), and 9,10-dimethylantracene (DMA).

E-1. Measurement of Dissolved Oxygen Concentration in Various

Formulations

The dissolved oxygen was determined using Zn-ttp as a SG and DMA as a ST. The concentrations of the SG and ST used in the measurement are illustrated in Table E- 1. The measurement procedure is described in previous paper⁷¹. A 150 W xenon lamp with a 670 nm bandpass filter was used as the light source to excite the SG. Using UV-Vis spectroscopy, the change in the 380 nm peak absorption wavelength of DMA

was measured. The decreased 380nm peak absorbance for DMA (from UV-Vis spectroscopy) was then used to calculate the dissolved oxygen concentration using the equation below⁷¹.

$$[DO_2] = 890 \times (\text{Change in the 380 nm peak absorption wavelength of DMA})$$

Here, [DO₂] is the molarity of the dissolved oxygen concentration, and the *change in the 380 nm peak absorption wavelength of DMA* unit is in absolute units. The determined oxygen concentrations for each formulation are illustrated in Table E- 1 as well.

Table E- 1: Dissolved Oxygen Concentration in different formulations

Monomer	SG conc. (10 ⁻⁵ mol/L)	DMA conc. (10 ⁻³ mol/L)	DO ₂ conc. (10 ⁻³ mol/L)
HEA	2.00	2.00	0.78
HDDA	2.00	2.00	1.09
HEA(50)/HDDA(50)	2.00	2.00	0.98
CN9002(70)/HEA(30)	2.00	2.00	0.77

E-2. Light Intensity Effect

The effect of light intensity on quenching dissolved oxygen was investigated using a HDDA monomer comprising 0.00002M Zn-ttp (SG) and 0.002M DMA (ST). The sample was irradiated by a 150 W Xe lamp with no filter and a 670 nm bandpass filter. The xenon lamp emitted a light intensity of 89 mW/cm² with a broad wavelength. With the bandpass filter, the lamp emitted a light intensity of 2.4 mW/cm² with a 670 nm single wavelength.

Figure E- 2 illustrates the dependence of quenched dissolved oxygen on light intensities as a function of illumination time. It is obvious that time to quench dissolved

oxygen becomes shorter as the light intensity increases. As the number of excited singlet oxygen generator molecules increase as the number of photons increase, the possibility of having a greater number of excited singlet oxygen trapper molecules increases as well. As a result, more dissolved oxygen is likely to be trapped by the excited singlet oxygen trapper.

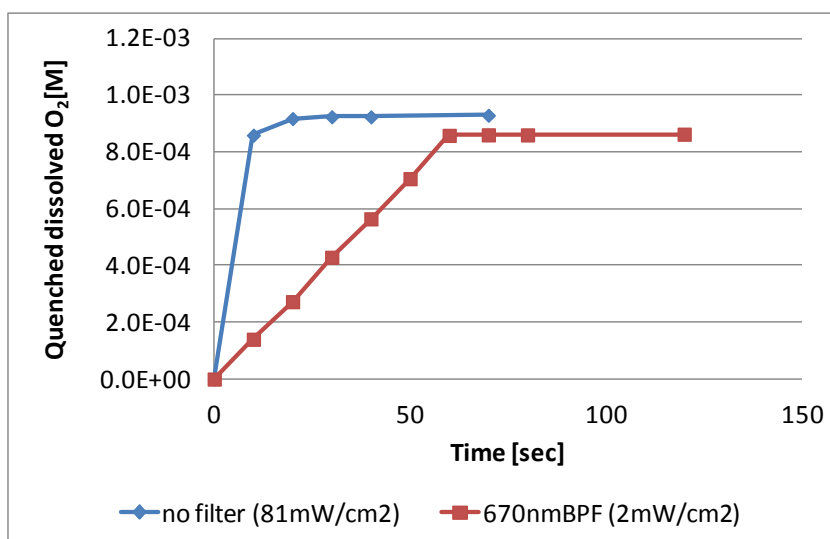


Figure E- 2: Quenched dissolved oxygen as a function of illumination time for different light intensities. Monomer: HDDA. $[Zntpp] = 2 \times 10^{-5}$ M, $[DMA] = 2 \times 10^{-3}$ M.

E-3. Shelf life of ST in formulations

The stability of DMA (ST) in HDDA monomer was investigated. A sample containing DMA in HDDA and a sample containing DMA and Zn-ttp (SG) in HDDA were monitored to investigate their stability. The compositions of the samples are illustrated in Table E- 2. These samples were made on day zero. Then they were stored in a dark environment at room temperature and the DMA concentrations were measured using UV-Visible spectroscopy to investigate their shelf lives.

Table E- 2: Compositions of studied samples

Systems	SG (Zn-ttp) conc. (10^{-5} mol/L)	ST (DMA) Conc. (10^{-3} mol/L)
DMA	-	2.00
DMA/Zn-ttp	2.00	2.00

Figure E- 3 shows the time dependence study of the DMA/Zn-ttp system. The peak heights at 361 nm, 380 nm and 401 nm, which are characteristic of a DMA absorbance spectrum, decrease with the passage of time. On the other hand, the values of peak height at 680 nm, which originate from Zn-ttp absorbance, are constant. This means that the concentration of Zn-ttp in the systems is constant (at least during five days) while that of DMA decreases. It is assumed that DMA in the system was quenched by ground state oxygen due to its triplet state activity, thus resulting in the decrease of DMA concentration.

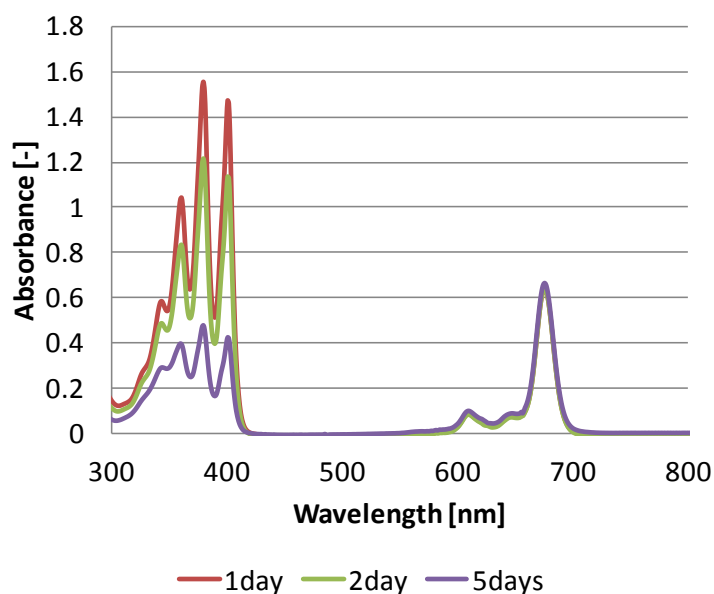


Figure E- 3: Time dependence of the DMA/Zn-ttp UV-Visible spectrum profiles. Monomer: HDDA.

Figure E- 4 illustrates the time dependence of DMA concentrations for the DMA and DMA/Zn-ttp containing samples. In both cases, DMA concentration decreases with the passage of time because DMA is quenched by dissolved ground-state oxygen. This trend must be noted when designing systems containing DMA as a singlet oxygen trapper.

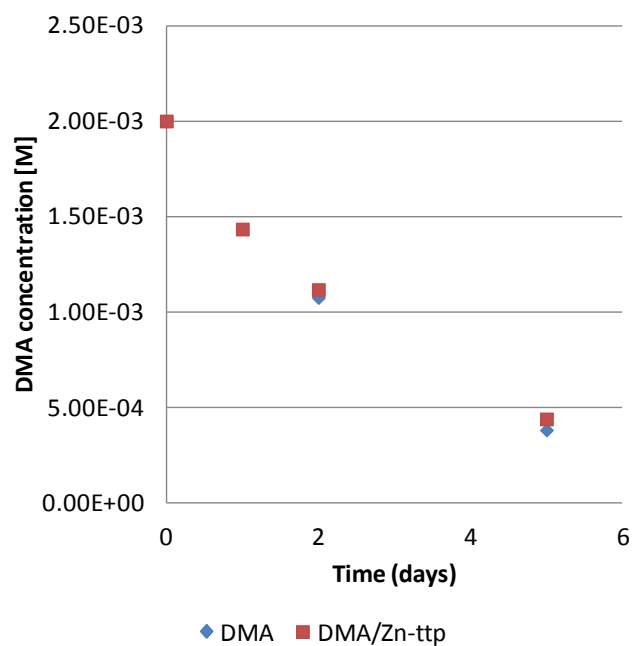


Figure E- 4: Time dependence of DMA concentrations for DMA and DMA/Zn-ttp. Monomer: HDDA.

APPENDIX F. SUPPLEMENTAL STUDY OF
PHOTOPOLYMERIZATION WITH TI-PI

In chapter CHAPTER 8, a self-cleavable photoinitiator bis(cyclopentadienyl) bis[2,6-difluoro-3-(1-pyrryl)phenyl]titanium (Ti-PI) was investigated. In this contribution, further and/or supplemental studies of this photoinitiator have been performed.

F-1. Effect of Light Intensity and Photoinitiator Concentration on the Photopolymerization Rate and Conversion with a Xenon Lamp

In chapter 8, a series of experiments was performed to investigate the effect of light intensity on the observed photopolymerization rate and ultimate conversion using a 520 nm light source. A similar series of experiments was performed using a 150 W Xe lamp in this section. Figure F- 1 contains RT-FTIR conversion profiles as a function of time in HEA monomer for three different concentration combinations of Ti-PI and phosphoric acid 2-hydroxyethyl methacrylate ester (PhMA) when irradiated by a 150 W xenon lamp at different light intensities. Figure F- 2 illustrates the ultimate conversion values (obtained from photopolymerization profiles in Figure F- 1) as a function of light intensity. The lowest ultimate conversion is observed at the highest light intensity and there is a light intensity threshold above which higher light intensities result in poor ultimate conversions for each concentration combination. Figure F- 3 shows the time to reach 90% of ultimate conversion (defined as T90 here) as a function of light intensity, the data for which was obtained from Figure F- 1. The figure implies the existence of an optimal light intensity for each concentration combination. The trends described above are very similar to results shown in chapter 8 with the 520 nm light source.

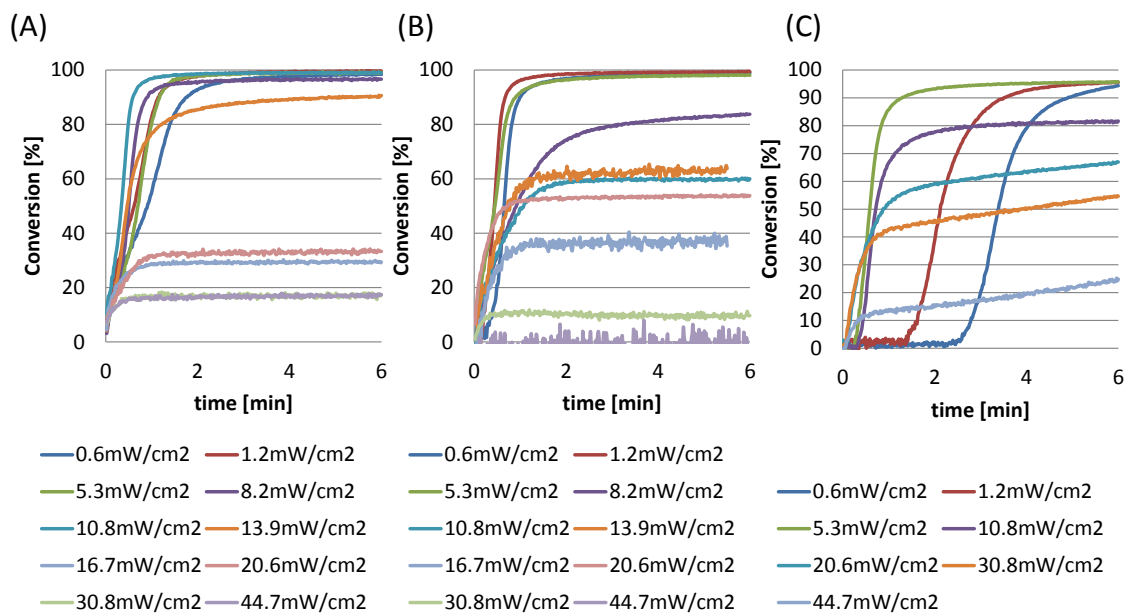


Figure F- 1: HEA photopolymerization conversion profiles for seven different light intensities: (A) Ti-PI = 2.6 wt % (0.050 M), PhMA = 1.5 wt % (0.067 M), (B) Ti-PI = 0.5 wt % (0.0095 M), PhMA = 0.3 wt % (0.0133 M), (C) Ti-PI = 0.1 wt % (0.00019 M), PhMA = 0.06 wt % (0.00027 M).

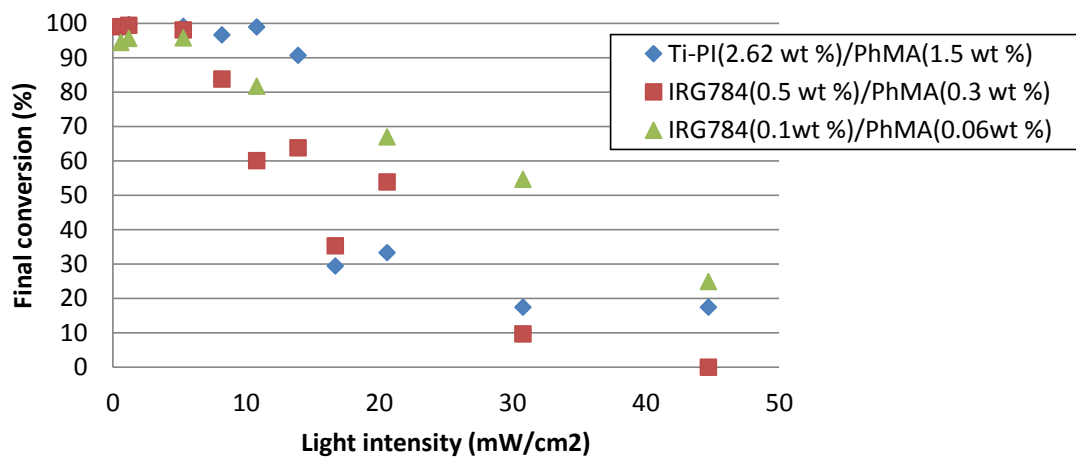


Figure F- 2: Ultimate conversions of photopolymerization profiles in Figure F- 1.

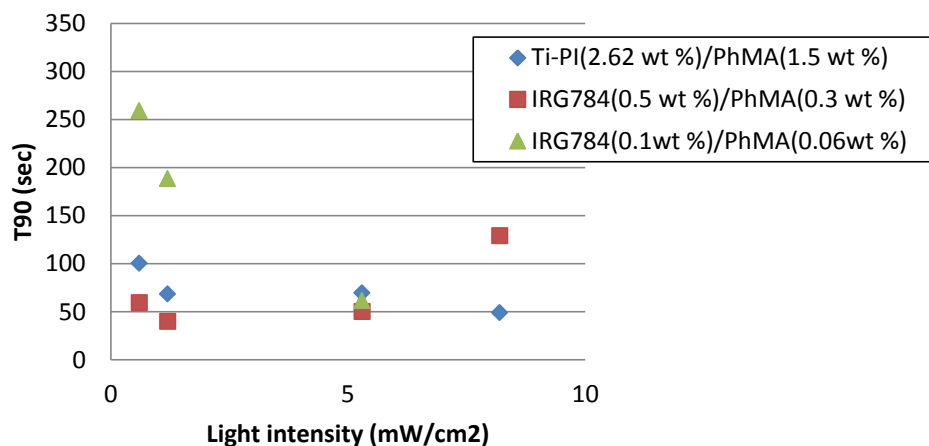


Figure F- 3: Time to reach 90 % of its ultimate conversion (T90) in Figure F- 1.

F-2. Shelf Life of HEA Monomer Containing Ti-PI and a Protonic Acid Additive

The shelf lives of Ti-PI/ p-toluenesulfonic acid (PTSA) and Ti-PI/PhMA in HEA monomer were compared. These samples were made on day zero. Then they were stored in a dark environment at room temperature and their polymerization was studied on successive days using RT-FTIR spectroscopy to investigate their shelf life. The samples were irradiated by a Xe lamp with a 520 nm bandpass filter emitting light at an intensity of 2.4 mW/cm². Figure F- 4 shows a comparison between the time dependent conversion profiles of Ti-PI/PTSA and Ti-PI/PhMA, where both photoinitiator systems contain the same concentration, 2.6 wt % (0.050 M), of Ti-PI with a protonic acid additive. As described in section 8.3.1, the monomer system containing PTSA exhibits a shelf life of less than one day. In contrast, the protonic acid PhMA demonstrates the desirable combination of high photopolymerization reactivity and a long shelf life of at least one month.

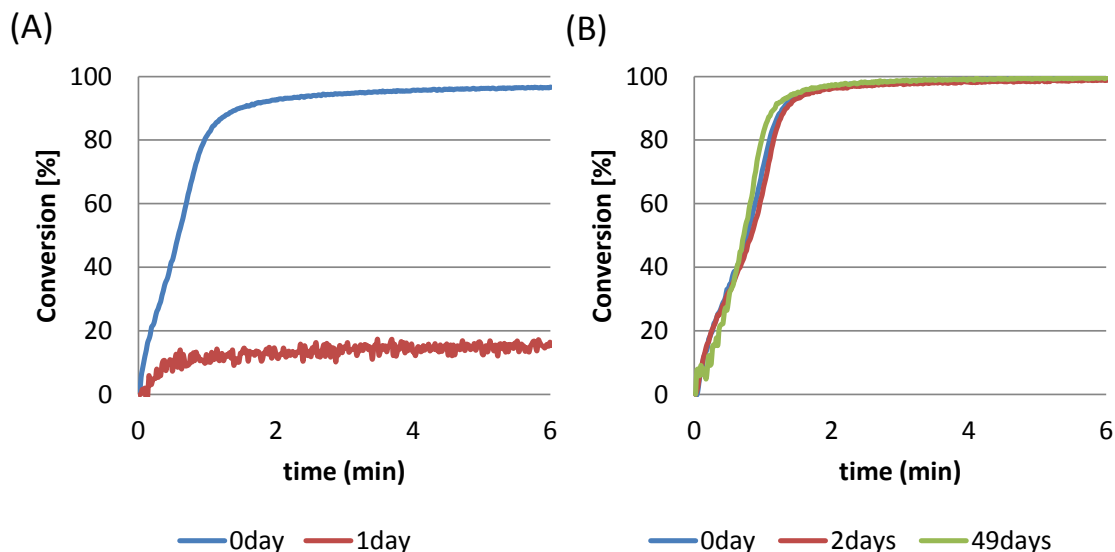


Figure F- 4: The comparison of time dependence for conversion profiles: (A) 1.0 wt % (0.053 M) PTSA; (B) 1.5 wt % (0.067 M) PhMA. All samples contain 2.6 wt % (0.050 M) Ti-PI. Light source: a Xe lamp with a 520 nm bandpass filter (light intensity: 2.4 mW/cm^2). Monomer: HEA.

F-3. Investigation of Ti-PI Photoinitiation Reaction Mechanism

Using Styrene Monomer

As described in chapter CHAPTER 6 and CHAPTER 8 , it is hypothesized that the titanium di-radical produces propagating active centers upon reaction with the carbonyl groups of the acrylate monomer to form a ketene acetal type di-radical capable of initiating polymerization in an acrylate system containing Ti-PI (see Figure 6-6 in section 6.4). In an attempt to validate this hypothesis, a non-acrylate monomer (that does not contain any carbonyl groups) will be photopolymerized using Ti-PI. If the photopolymerization of styrene using Ti-Pi fails and if it succeeds with a control photoinitiator, this experiment could lend possible credit to our hypothesis regarding the Ti-Pi reaction mechanism.

The photopolymerization profiles of styrene monomers with various photoinitiating systems at high temperature (70 C°) were investigated using real-time Raman spectroscopy. As styrene barely photopolymerizes at room temperature, higher

temperatures were used to overcome the energy of activation barrier and make the polymerization more favorable. The measurement procedure is described in section 7.3.3.2.1. Table F- 1 illustrates the photoinitiating systems that were studied including photoinitiator concentrations, light sources, and light intensities. A common unimolecular photoinitiator bis(2,4,6-trimethylbenzoyl)-phenylphosphine oxide (BAPO) was used as a control photoinitiator (to compare it with Ti-PI photoinitiator systems) as BAPO forms radicals by self-cleavage and reacts with the carbon double bonds of styrene. In other words, the photopolymerization with BAPO does not rely on interactions with carbonyl groups of the monomer to initiate polymerization. Figure F- 5 demonstrates photopolymerization profiles of styrene with four different initiation conditions listed in Table F- 1. The figure illustrates that both the values of polymerization rate and the ultimate conversion follow the trend: neat styrene < Ti-PI = Ti-PI/PTSA < BAPO.

Table F- 1: Studied photoinitiator compositions and light conditions in styrene monomer

			BAPO	Ti-PI	Ti-PI/PTSA	Neat Styrene
Photoinitiator	Ti-PI	phr	-	2.6150	2.6150	-
		M	-	0.0495	0.0495	-
	PTSA	phr	-	-	1.5000	-
		M	-	-	0.0531	-
	BAPO	phr	2.1	-	-	-
		M	0.0495	-	-	-
Temperature		C°	70	70	70	70
Light	400 nm LED	mW/cm ²	41	-	-	-
	520 nm LED	mW/cm ²	-	7.9	7.9	-

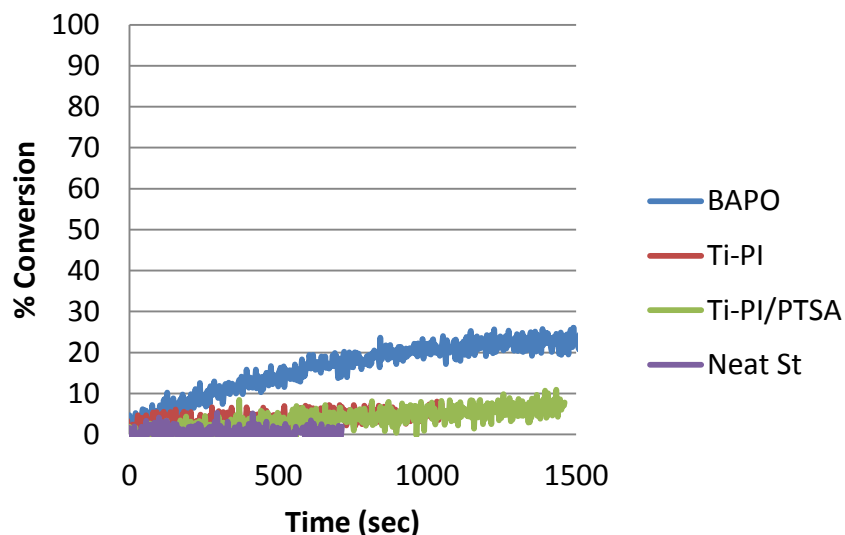


Figure F- 5: Percent conversion as a function of time at 70°C for styrene with four different photoinitiating systems.

The photopolymerization profiles of the styrene monomer with four photoinitiating systems were investigated at 40 C° using photo-DSC as well. The measurement procedure is described in a previous paper¹⁶. Table F- 2 illustrates photoinitiating systems studied including photoinitiator concentrations, light sources, and light intensities. Figure F- 6 demonstrates photopolymerization profiles of styrene with four different initiating conditions listed in Table F- 2. Table F- 3 summarizes the total exothermic energies and styrene monomer conversions observed in Figure F- 6. The figure and table illustrate that the both values of polymerization rate and the ultimate conversion follow the trend: neat styrene < Ti-PI = Ti-PI/PTSA < BAPO. This trend is nearly identical to the one obtained from real-time Raman microscopy described above.

In acrylate monomer systems, both BAPO and Ti-PI/PTSA photoinitiators achieved high ultimate conversion in previous studies. On the contrary, although its polymerization rate is relatively low, BAPO is twice as effective in polymerizing styrene compared to the Ti-PI/PTSA system. When comparing Ti-PI and Ti-PI/PTSA,

the both systems achieve slight polymerization and no significant differences in the photopolymerization trends were observed. These phenomena are very different from those demonstrated in acrylate monomers (see chapter 8, APPENDIX 6-4). It is reasonable to assume that 2,6-difluoro-3(1H-pyrrol-1-yl)phenyl radical is the only active radical and that the titanium di-radical is not active for styrene when using Ti-PI or Ti-PI/PTSA. Although its reactivity is relatively weak, this phenyl radical could react with the carbon double bond of styrene and initiate polymerization as BAPO does. However, the titanium di-radical could not react with styrene since it does not contain carbonyl function. As a result, Ti-PI and Ti-PI/PTSA cannot polymerize styrene to the extent that BAPO does. In addition, Ti-PI and Ti-PI/PTSA do not show any difference of photopolymerization profiles since the generation of the primary active radical for acrylate systems – the titanium di-radical, is unable to react with the styrene monomer and propagate polymerization due to the absence of carbon double bonds. Therefore, it can be concluded that the Ti-Pi system is only effective with monomers containing carbonyl functional groups (acrylates) as the titanium di-radical does not react with carbon double bonds but carbonyl bonds.

Table F- 2: Studied photoinitiator compositions and light conditions in styrene monomer

			BAPO	Ti-PI	Ti-PI/PTSA	Neat Styrene
Photoinitiator	Ti-PI	phr	-	2.6150	2.6150	-
		M	-	0.0495	0.0495	-
	PTSA	phr	-	-	1.5000	-
		M	-	-	0.0531	-
	BAPO	phr	2.1	-	-	-
		M	0.0495	-	-	-
Temperature		C°	40	40	40	40
Light	400 nm LED	mW/cm ²	41	-	-	41
	520 nm LED	mW/cm ²	-	7.9	7.9	-

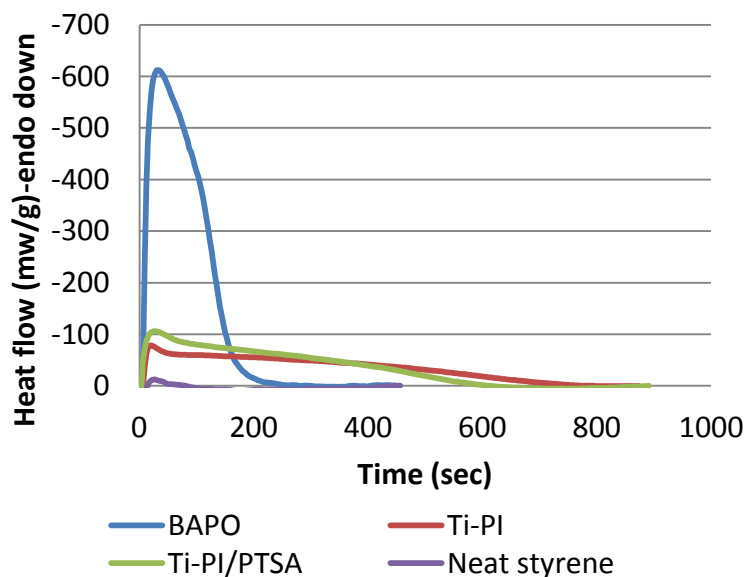


Figure F- 6: Heat flow profiles for the photopolymerizations of styrene for four different photoinitiating systems at 40 °C.

Table F- 3: Total exothermic energies and conversions in Figure F- 6

	BAPO	Ti-PI	Ti-PI/PTSA	Neat St
Total exothermic energy (mJ/g)	64087	29474	28925	373
% Conversion	7.7	3.6	3.5	0.0

F-4. Investigation of Photopolymerization with Ti-PI for Various Monomers and Oligomers

In this section, photopolymerization of various resins including HEA, 1,6-hexandiol acrylate (HDDA), 2-hydroxyethyl methacrylate (HEMA) and a HEA/urethane acrylate mixture (HEA(30)/CN9002(70)) using Ti-PI and Ti-PI + PhMA as photoinitiators is investigated. Here, the photoinitiating system was composed of 2.6 wt % (0.050 M) Ti-PI and/or 1.5 wt % (0.067 M) PhMA in each resin. The overall conversion of the mixtures was measured using the RT-FTIR method.

Figure F- 7, Figure F- 8, and Figure F- 9 compare the conversion profiles of the monomer resins obtained upon illumination from two different light sources (Figure F- 7: HEA, Figure F- 8: HDDA, Figure F- 9: HEMA) containing Ti-PI with and without PhMA. Two light sources were used for this study: a 150W Xe lamp emitting a light intensity of 89 mW/cm^2 and the same Xe lamp with a 520 nm bandpass filter (520 nm light) emitting a light intensity of 2 mW/cm^2 . The emission spectra of the two light sources have been displayed earlier (Figure 3-6). As shown in the figures below, the same trends are observed. Without a protonic acid PhMA, photopolymerization is poor for the both light sources. The enhancement of photopolymerization is achieved by adding PhMA and using a lower light intensity (520 nm light).

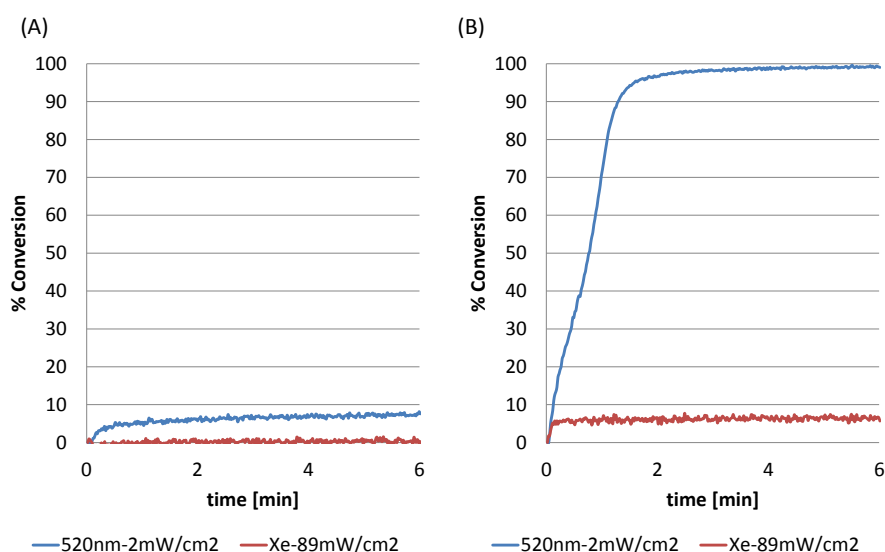


Figure F- 7: Comparison of two light sources, a 150W Xe lamp with 89 mW/cm^2 light intensity (blue line) and the Xe lamp attaching a 520 nm bandpass filter with 2 mW/cm^2 light intensity (red line), for photopolymerization conversion profiles. Monomer: HEA. Photoinitiator: (A) Ti-PI, (B) Ti-PI + PhMA.

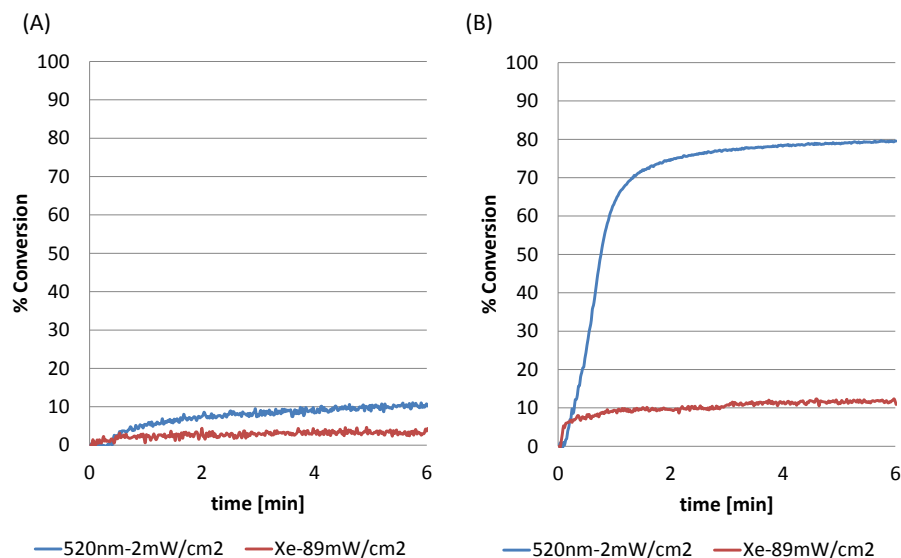


Figure F- 8: Comparison of two light sources, a 150W Xe lamp with 89 mW/cm² light intensity (blue line) and the Xe lamp attaching a 520 nm bandpass filter with 2 mW/cm² light intensity (red line), for photopolymerization conversion profiles. Monomer: HDDA. Photoinitiator: (A) Ti-PI, (B)Ti-PI + PhMA.

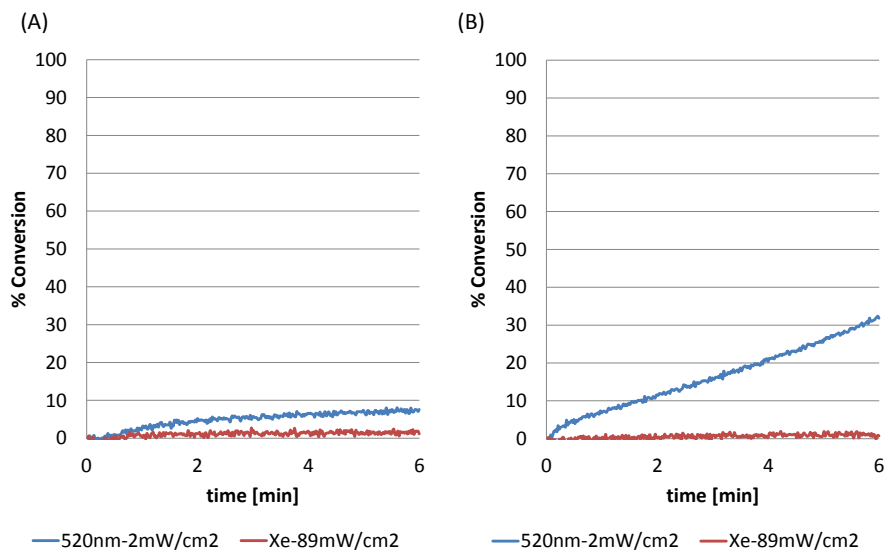


Figure F- 9: Comparison of two light sources, a 150W Xe lamp with 89 mW/cm² light intensity (blue line) and the Xe lamp attaching a 520 nm bandpass filter with 2 mW/cm² light intensity (red line), for photopolymerization conversion profiles. Monomer: HEMA. Photoinitiator: (A) Ti-PI, (B)Ti-PI + PhMA.

Figure F- 10 illustrates RT-FTIR conversion profiles as a function of time in the monomer/oligomer mixture, HEA(30)/CN9002(70) (see chapter 6), containing Ti-PI with and without PhMA, when irradiated by a 520 nm LED at different light intensities. The trends observed with the monomer/oligomer mixture are very similar with those obtained for pure HEA monomer that was discussed in chapter 8. The addition of a protonic acid into Ti-PI and the use of a low light intensity results in high photopolymerization. It is worth noting that 50% final conversion is achieved with Ti-PI photoinitiator for the HEA/CN9002 mixture with an intensity of 2 mW/cm² while the final conversions of HEA or HDDA are less than 10% (see Figure F- 7, Figure F- 8). This higher photopolymerization is due to the high initial viscosity of the monomer/oligomer mixture because termination reactions are reduced in viscous systems. As compared to low viscosity systems (pure HEA or HDDA), the higher viscosity of the HEA/CN9002 system favors the initial propagation reaction that results in higher photopolymerization rate and final conversion that is observed in Figure F- 10.

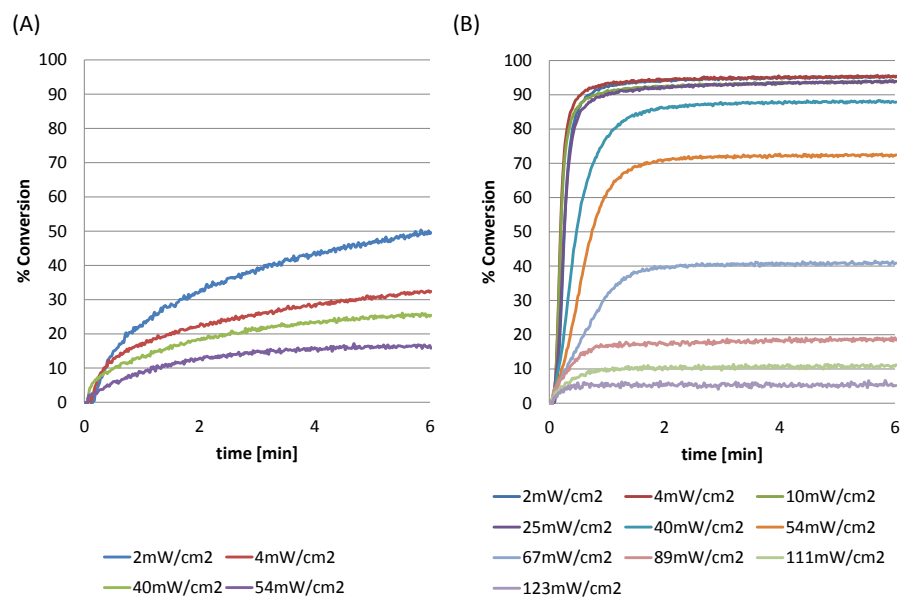


Figure F- 10: Photopolymerization conversion profiles for different light intensities. Monomer/oligomer mixture: HEA(30)/CN9002(70). Light source: a 520 nm LED. Photoinitiator: (A) Ti-PI, (B) Ti-PI + PhMA.

REFERENCES

- (1) Fouassier, J. P. In *Photoinitiation, photopolymerization, and photocuring*; Hanser Publishers, Munich Vienna New York: 1995; .
- (2) Catilaz-Simonin, L.; Fouassier, J. P. Investigation of a system capable of photoinitiating radical polymerizations in thick pigmented media. *J Appl Polym Sci* **2001**, *79*, 1911-1923.
- (3) Fouassier, J. P.; Allonas, X.; Burget, D. Photopolymerization reactions under visible lights: principle, mechanisms and examples of applications. *Progress in Organic Coatings* **2003**, *47*, 16-36.
- (4) Arikawa, H.; Takahashi, H.; Kanie, T.; Ban, S. Effect of various visible light photoinitiators on the polymerization and color of light-activated resins. *Dent. Mater. J.* **2009**, *28*, 454-460.
- (5) Horie, K.; Kishi, K.; Okayama, T.; Maeda, M. US Patent 6146789, 2000.
- (6) Decker, C.; Jenkins, A. D. Kinetic approach of oxygen inhibition in ultraviolet-and laser-induced polymerizations. *Macromolecules* **1985**, *18*, 1241-1244.
- (7) Gou, L.; Opheim, B.; Coretsopoulos, C.; Scranton, A. B. Consumption of the molecular oxygen in polymerization systems using photosensitized oxidation of dimethylantracene. *Chem. Eng. Comm.* **2006**, *193*, 620-627.
- (8) O'Brien, A. K.; Bowman, C. N. Impact of oxygen on photopolymerization kinetics and polymer structure. *Macromolecules* **2006**, *39*, 2501-2506.
- (9) Padon, K. S.; Scranton, A. B. The effect of oxygen on the three-component radical photoinitiator system: Methylene blue, N-methyldiethanolamine, and diphenyliodonium chloride. *J Polym Sci A: Polym Chem* **2000**, *38*, 3336-3346.
- (10) O'Brien, A. K.; Cramer, N. B.; Bowman, C. N. Oxygen inhibition in thiol-acrylate photopolymerizations. *Journal of Polymer Science Part A: Polymer Chemistry* **2006**, *44*, 2007-2014.
- (11) Tsukagoshi, I. Development History of the Anisotropic Conductive Film ANISOLM. *Hitachi Chemical Technical Report* **2003**, *41*, 7-18.
- (12) Tsukagoshi, I.; Yamaguchi, Y.; Nakayama, T. US Patent 4731282, 1988.
- (13) Tsukagoshi, I.; Yamaguchi, Y.; Nakajima, A.; Mikami, Y.; Muto, K.; Ikezoe, Y. US Patent 4740657, 1988.
- (14) Oxman, J. D.; Ubel III, F. A.; Larson, E. G. U.S. Patent 4735632.
- (15) Padon, K. S.; Scranton, A. B. Recent Advances in Three Component Photoinitiator Systems. *Recent Research Developments in Polymer Science* **1999**, *3*, 369-385.
- (16) Padon, K. S.; Scranton, A. B. A mechanistic investigation of a three-component radical photoinitiator system comprising methylene blue, N-methyldiethanolamine, and diphenyliodonium chloride. *J Polym Sci A: Polym Chem* **2000**, *38*, 2057-2066.

- (17) Padon, K. S.; Scranton, A. B. A mechanistic investigation of the three-component radical photoinitiator system Eosin Y spirit soluble, N-methyldiethanolamine, and diphenyliodonium chloride. *J Polym Sci A: Polym Chem* **2001**, *39*, 715-723.
- (18) Kim, D.; Scranton, A. B. The role of diphenyl iodonium salt(DPI) in three-component photoinitiator systems containing methylene blue(MB) and an electron donor. *J Polym Sci A: Polym Chem* **2004**, *42*, 5863-5871.
- (19) Kim, D.; Scranton, A. B.; Stansbury, J. W. Analysis of association constant for ground-state dye-electron acceptor complex of photoinitiator systems and the association constant effect on the kinetics of visible-light-induced polymerizations. *J Polym Sci A: Polym Chem* **2009**, *47*, 1429-1439.
- (20) Kim, D.; Stansbury, J. W. A Photo-Oxidizable Kinetic Pathway of Three-Component Photoinitiator Systems Containing Porphyrin Dye (Zn-tpa), an Electron Donor and Diphenyl Iodonium Salt. *J Polym Sci A: Polym Chem* **2009**, *47*, 3131-3141.
- (21) Sato, N. Applications of pre-irradiation system. *Three Bond Technical News* **1994**, *42*, 1-7.
- (22) Shinya, Y.; Kamiya, K.; Kamata, Y. US Patent US2009/0186552A1, 2009.
- (23) Gregory, S. US Patent 6245827, 2001.
- (24) Hayashi, S.; Tasaka, Y.; Hayashi, N.; Akita, Y. Development of smart polymer materials and its various applications. *MITSUBISHI JUKO GIHO* **2004**, *41*, 62-64.
- (25) Ficek, B. A.; Thiesen, A. M.; Scranton, A. B. Cationic photopolymerizations of thick polymer systems: Active center lifetime and mobility. *Eur. Polym. J.* **2008**, *44*, 98-105.
- (26) Schubert, E. F.; Kim, J. K. Solid-state light sources getting smart. *Science* **2005**, *308*, 1274.
- (27) Taguchi, T. Developing white LED lighting systems and its technological roadmap in Japan. *Journal of Light & Visual Environment* **2006**, *30*, 177-182.
- (28) ARIKAWA, H.; TAKAHASHI, H.; KANIE, T.; BAN, S. Effect of various visible light photoinitiators on the polymerization and color of light-activated resins. *Dent. Mater. J.* **2009**, *28*, 454-460.
- (29) Leonard, D. L.; Charlton, D. G.; Roberts, H. W.; Cohen, M. E. Polymerization efficiency of LED curing lights. *Journal of Esthetic and Restorative Dentistry* **2002**, *14*, 286-295.
- (30) Nalcaci, A.; Kucukesmen, C.; Uludag, B. Effect of high-powered LED polymerization on the shear bond strength of a light-polymerized resin luting agent to ceramic and dentin. *J. Prosthet. Dent.* **2005**, *94*, 140-145.
- (31) Price, R. B. T.; Felix, C. A.; Andreou, P. Evaluation of a second-generation LED curing light. *Journal-Canadian Dental Association* **2003**, *69*, 666-666.

- (32) Teshima, W.; Nomura, Y.; Tanaka, N.; Urabe, H.; Okazaki, M.; Nahara, Y. ESR study of camphorquinone/amine photoinitiator systems using blue light-emitting diodes. *Biomaterials* **2003**, *24*, 2097-2103.
- (33) Zonca, M. R.; Falk, B.; Crivello, J. V. LED-induced thiol-ene photopolymerizations. *Journal of Macromolecular Science-Pure and Applied Chemistry* **2004**, *A41*, 741-756.
- (34) McDermott, S. L.; Walsh, J. E.; Howard, R. G. A comparison of the emission characteristics of UV-LEDs and fluorescent lamps for polymerisation applications. *Opt. Laser Technol.* **2008**, *40*, 487-493.
- (35) Anyaogu, K. C.; Ermoshkin, A. A.; Neckers, D. C.; Mejiritski, A.; Grinevich, O.; Fedorov, A. V. Performance of the light emitting diodes versus conventional light sources in the UV light cured formulations. *J Appl Polym Sci* **2007**, *105*, 803-808.
- (36) Padon, K. S.; Scranton, A. B. Mechanistic studies of the three-component, photoinitiator-system methylene blue, N-methyldiethanolamine, and diphenyliodonium chloride. *Abstracts of Papers of the American Chemical Society* **2000**, *219*, 20-PMSE.
- (37) Inoue, H.; Sasaki, M.; Takagi, K.; Shou, S. In *Photochemistry I*; Maruzen corporation: 1999; .
- (38) Kim, D.; Scranton, A. B.; Stansbury, J. W. Effect of the electron donor structure on the shelf - lifetime of visible - light activated three - component initiator systems. *J Appl Polym Sci* **2009**, *114*, 1535-1542.
- (39) Goodner, M. D.; Bowman, C. N. Development of a comprehensive free radical photopolymerization model incorporating heat and mass transfer effects in thick films. *Chemical Engineering Science* **2002**, *57*, 887-900.
- (40) Takimoto, Y. In *Photopolymer surface fabrication material*; The Technical Association of Photopolymers, Japan, Ed.; Bunshin corporation: 2001; , pp 175.
- (41) Kawabata, M.; Kimoto, K.; Takimoto, Y. US Patent 4766055.
- (42) Fouassier, J. P.; Chesneau, E. Polymerization induced by irradiation with a visible laser, 4. The system eosin UV-photoinitiator amine. *Makromol. Chem.* **1991**, *192*, 245-260.
- (43) Fouassier, J.; Wu, S. Visible laser lights in photoinduced polymerization. VI. Thioxanthenes and ketocoumarins as photoinitiators. *J Appl Polym Sci* **1992**, *44*, 1779-1786.
- (44) Davidson, R. The chemistry of photoinitiators--some recent developments. *J. Photochem. Photobiol. A.* **1993**, *73*, 81-96.
- (45) Jockusch, S.; Timpe, H. J.; Schnabel, W.; Turro, N. Photoreduction of organic dyes in ketone amine systems. *J. Photochem. Photobiol. A.* **1996**, *96*, 129-136.
- (46) Fouassier, J. P.; Ruhlmann, D.; Graff, B.; Takimoto, Y.; Kawabata, M.; Harada, M. A new three-component system in visible laser light photo-induced polymerization. *J. Imaging Sci. Technol.* **1993**, *37*, 208-210.

- (47) Erddalane, A.; Fouassier, J. P.; Morlet - Savary, F.; Takimoto, Y. Efficiency and excited state processes in a three - component system, based on thioxanthene derived dye/amine/additive, usable in photopolymer plates. *J Polym Sci A: Polym Chem* **1996**, *34*, 633-642.
- (48) Ibrahim, A.; Ley, C.; Tarzi, O. I.; Fouassier, J. P.; Allonas, X. Visible Light Photoinitiating Systems: Toward a Good Control of the Photopolymerization Efficiency. *J. Photopolym. Sci. Technol.* **2010**, *23*, 101-108.
- (49) Speiser, S.; Chisena, F. Optical bistability in fluorescein dyes. *Appl. Phys. B* **1988**, *45*, 137-144.
- (50) Chambers, R. W.; Kajiwarra, T.; Kearns, D. R. Effect of dimer formation on the electronic absorption and emission spectra of ionic dyes. Rhodamines and other common dyes. *J. Phys. Chem.* **1974**, *78*, 380-387.
- (51) Fornasiero, D.; Kurucsev, T. Vibronic exciton bands. Absorption spectra of Eosin Y dimers. *J.Chem.Soc., Faraday Trans.2* **1986**, *82*, 15-19.
- (52) Cai, Y.; Jessop, J. L. P. Decreased oxygen inhibition in photopolymerized acrylate/epoxide hybrid polymer coatings as demonstrated by Raman spectroscopy. *Polymer* **2006**, *47*, 6560-6566.
- (53) Zou, Y.; Armstrong, S. R.; Jessop, J. L. P. Apparent conversion of adhesive resin in the hybrid layer, Part 1: Identification of an internal reference for Raman spectroscopy and the effects of water storage. *Journal of Biomedical Materials Research-Part A* **2008**, *86*, 883-891.
- (54) Zou, Y.; Jessop, J. L. P.; Armstrong, S. R. Apparent conversion of adhesive resin in the hybrid layer, Part II: In situ studies of the resin-dentin bond. *Journal of Biomedical Materials Research Part a* **2009**, *89A*, 355-362.
- (55) Forster, L. S.; Dudley, D. THE LUMINESCENCE OF FLUORESCHEIN DYES1. *J. Phys. Chem.* **1962**, *66*, 838-840.
- (56) Kenning, N. S.; Ficek, B. A.; Hoppe, C. C.; Scranton, A. B. Spatial and temporal evolution of the photoinitiation rate for thick polymer systems illuminated by polychromatic light: selection of efficient photoinitiators for LED or mercury lamps. *Polym. Int.* **2008**, *57*, 1134-1140.
- (57) Hoyle, C. E.; Lee, T. Y.; Roper, T. Thiol-enes: Chemistry of the past with promise for the future. *Journal of Polymer Science Part A: Polymer Chemistry* **2004**, *42*, 5301-5338.
- (58) Odian, G. G. In *Principles of polymerization*; Fourth Edition; Wiley-Interscience: A John Wiley & Sons, Inc., 2004; .
- (59) Moorjani, S. K.; Rangarajan, B.; Scranton, A. B. Effect of Viscosity on the Rate of Photosensitization of Diaryliodonium Salts by Anthracene. *POLYMERIC MATERIALS SCIENCE AND ENGINEERING-WASHINGTON-* **1996**, *74*, 315-316.
- (60) Nelson, E. W.; Carter, T. P.; Scranton, A. B. The role of the triplet state in the photosensitization of cationic polymerizations by anthracene. *J Polym Sci A: Polym Chem* **1995**, *33*, 247-256.

- (61) Klingert, B.; Roloff, A.; Urwyler, B.; Wirz, J. Photochemical Ring Slippage of Bis (pentafluorophenyl) titanocene: Reaction kinetics and matrix isolation of the primary photoproduct. *Helv. Chim. Acta* **1988**, *71*, 1858-1867.
- (62) Finter, J.; Riediker, M.; Rohde, O.; Rotzinger, B. Photosensitive Systems for Microlithography Based on Organometallic Photoinitiators. *Makromolekulare Chemie-Macromolecular Symposia* **1989**, *24*, 177-187.
- (63) Roloff, A. In *Light-Sensitive Organometallic Compounds in Photopolymerization*; Kutal, C., Serpone, N., Eds.; Photosensitive Metal—Organic Systems; ACS Publications: 1993; Vol. 238, pp 399-409.
- (64) Lin, S.; Hsiao, Y.; Hsu, K. Preparation and characterization of Irgacure 784 doped photopolymers for holographic data storage at 532 nm. *Pure Appl. Opt.* **2009**, *11*, 024012.
- (65) Sabol, D.; Gleeson, M. R.; Liu, S.; Sheridan, J. T. Photoinitiation study of Irgacure 784 in an epoxy resin photopolymer. *J. Appl. Phys.* **2010**, *107*, 053113-053113-8.
- (66) Yamaoka, A. In *Optical Application Technology, Material Encyclopedia*; Yamaoka, A., Ed.; Sangyo Cijutsu Service Center corporation: 2006; .
- (67) Seta, T. Visible Light Curable Coating System. *TECHNO COSMOS* **2002**, *15*, 15-20.
- (68) Heathcote, J. UV-LED Overview Part I—. *JULY/AUGUST 2010 RADTECH REPORT* **2010**, 23-33.
- (69) Heathcote, J. UV-LED Overview Part II—. *SEPTEMBER/OCTOBER 2010 RADTECH REPORT* **2010**, 31-41.
- (70) Cramer, N. B.; Davies, T.; O'Brien, A. K.; Bowman, C. N. Mechanism and Modeling of a Thiol–Ene Photopolymerization. *Macromolecules* **2003**, *36*, 4631-4636.
- (71) Gou, L.; Coretsopoulos, C. N.; Scranton, A. B. Measurement of the dissolved oxygen concentration in acrylate monomers with a novel photochemical method. *Journal of Polymer Science Part A: Polymer Chemistry* **2004**, *42*, 1285-1292.
- (72) Goodner, M. D.; Bowman, C. N. In *In Modeling and experimental investigation of light intensity and initiator effects on solvent-free photopolymerizations*; ACS SYMPOSIUM SERIES; ACS Publications: 1998; Vol. 713, pp 220-231.
- (73) Anseth, K. S.; Burdick, J. A. New directions in photopolymerizable biomaterials. *MRS Bull.* **2002**, *27*, 130-138.
- (74) Ifkovits, J. L.; Burdick, J. A. Review: photopolymerizable and degradable biomaterials for tissue engineering applications. *Tissue Eng.* **2007**, *13*, 2369-2385.
- (75) Giannatsis, J.; Dedoussis, V. Additive fabrication technologies applied to medicine and health care: a review. *Int J Adv Manuf Technol* **2009**, *40*, 116-127.

- (76) Moorjani, S. K.; Rangarajan, B.; Scranton, A. B. In *Effect of viscosity on the rate of photosensitization of diaryliodonium salts by anthracene*; Scranton, A. B., Bowman, C. N. and Peiffer, R. W., Eds.; Photopolymerization Fundamentals and Applications; ACS Publications: 1997; Vol. 673, pp 95-106.
- (77) Ganster, B.; Fischer, U. K.; Moszner, N.; Liska, R. New photocleavable structures. Diacylgermane-based photoinitiators for visible light curing. *Macromolecules* **2008**, *41*, 2394-2400.
- (78) Roloff, A.; Meier, K.; Riediker, M. Synthetic and metal organic photochemistry in industry. *Pure Appl. Chem.* **1986**, *58*, 1267-1272.
- (79) Angerer, H.; Desobry, M.; Riediker, M.; Spahni, H.; Rembold, M. A new class of photoinitiators for radical polymerization with UV and Visible light. *Proc. Conf. on Radiation Curing Asia* **1988**, 461.
- (80) Criqui, A.; Lalevée, J.; Allonas, X.; Fouassier, J. P. Electron spin resonance spin trapping technique: Application to the cleavage process of photoinitiators. *Macromol. Chem. Phys.* **2008**, *209*, 2223-2231.
- (81) Tehfe, M. A.; Blanchard, N.; Fries, C.; Lalevée, J.; Allonas, X.; Fouassier, J. P. Bis (germyl) ketones: Toward a New Class of Type I Photoinitiating Systems Sensitive Above 500 nm? *Macromol. Rapid. Commun.* **2010**, *31*, 473-478.
- (82) Doba, T.; Watanabe, B. US Patent 5445918.
- (83) Dhar, L.; Katz, H. E. US Patent 6124076.
- (84) Bauman, H.; Strehmel, B.; Dwars, U.; Muller, U. US Patent .
- (85) Forray, D. D.; Liu, P.; delos Santos, B. US Patent 7851254.
- (86) Lee, T. Y.; Roper, T. M.; Jonsson, E. S.; Kudyakov, I.; Viswanathan, K.; Nason, C.; Guymon, C. A.; Hoyle, C. E. The kinetics of vinyl acrylate photopolymerization. *Polymer* **2003**, *44*, 2859-2865.
- (87) Beckel, E. R.; Stansbury, J. W.; Bowman, C. N. Evaluation of a potential ionic contribution to the polymerization of highly reactive (meth) acrylate monomers. *Macromolecules* **2005**, *38*, 9474-9481.
- (88) Scranton, A. B.; Bowman, C. N.; Klier, J.; Peppas, N. A. Polymerization reaction dynamics of ethylene glycol methacrylates and dimethacrylates by calorimetry. *Polymer* **1992**, *33*, 1683-1689.
- (89) Cramer, N.; Stansbury, J.; Bowman, C. Recent advances and developments in composite dental restorative materials. *J. Dent. Res.* **2011**, *90*, 402-416.
- (90) Brennan, J. V.; Kalgutkar, R. S.; Perez, M. A.; Mahoney, W. S.; Stark, P. A.; Oxman, J. D.; James, D. S. US Patent 7896650, 2011.